MEASUREMENT-BASED CHARACTERIZATION OF LARGE-SCALE NETWORKED SYSTEMS

by

REZA MOTAMEDI

A DISSERTATION

Presented to the Department of Computer and Information Science
and the Graduate School of the University of Oregon
in partial fulfillment of the requirements
for the degree of
Doctor of Philosophy

December 2016

DISSERTATION APPROVAL PAGE

Student: Reza Motamedi

Title: Measurement-Based Characterization of Large-Scale Networked Systems

This dissertation has been accepted and approved in partial fulfillment of the requirements for the Doctor of Philosophy degree in the Department of Computer and Information Science by:

Reza Rejaie	Chair
Allen Malony	Core Member
Jun Li	Core Member
Walter Willinger	Core Member
David Levin	Institutional Representative

and

Scott L. Pratt	Dean of the Graduate School

Original approval signatures are on file with the University of Oregon Graduate School.

Degree awarded December 2016

DISSERTATION ABSTRACT

Reza Motamedi

Doctor of Philosophy

Department of Computer and Information Science

December 2016

Title: Measurement-Based Characterization of Large-Scale Networked Systems

As the Internet has grown to represent arguably the largest "engineered" system on earth, network researchers have shown increasing interest in measuring this large-scale networked system. In the process, structures such as the physical Internet or the many different (logical) overlay networks that this physical infrastructure enables have been the focus of numerous studies. Many of these studies have been fueled by the ease of access to "big data". Moreover, they benefited from advances in the study of complex networks.

However, an important missing aspect in typical applications of complex network theory to the study of real-world distributed systems has been a general lack of attention to *domain knowledge*. On the one hand, missing or superficial domain knowledge can negatively affect the studies "input"; that is, limitations or idiosyncrasies of the measurement methods can render the resulting graphs difficult to interpret if not meaningless. On the other hand, lacking or insufficient domain knowledge can result in specious "output"; that is, popular graph abstractions of real-world systems are incapable of accounting for "details" that are important from an engineering perspective.

In this thesis, we take a closer look at measurement-based characterization of a few real-world large-scale networked systems and focus on the role that domain knowledge plays in gaining a thorough understanding of these systems key properties and behavior.

More specifically, we use domain knowledge to *(i)* design context-aware measurement strategies that capture the relevant information about the system of interest, *(ii)* analyze the captured view of the networked system baring in mind the abstraction imposed by the chosen graph representation, and *(iii)* scrutinize the results derived from the analysis of the graph-based representations by investigating the root causes underlying these findings. The main technical contribution of our work is twofolds. First, we establish concrete connections between the amount and level of domain knowledge needed and the quality of the measurements collected from networked systems. Second, we also provide concrete evidence for the role that domain knowledge plays in the analysis of views inferred from measurements collected from large-scale networked systems.

CURRICULUM VITAE

NAME OF AUTHOR: Reza Motamedi

GRADUATE AND UNDERGRADUATE SCHOOLS ATTENDED:

University of Oregon, Eugene, OR
Sharif University of Technology, Tehran, Iran
Iran University of Science & Technology, Tehran, Iran

DEGREES AWARDED:

Doctor of Philosophy in Computer and Information Science,
2016, University of Oregon
Master of Science in Information Technology,
2010, Sharif University of Technology
Bachelor of Engineering in Computer Software Engineering,
2007, Iran University of Science & Technology

AREAS OF SPECIAL INTEREST:

Distributed Systems, Computer Networks, Measurement, Data Science

PROFESSIONAL EXPERIENCE:

Graduate Research Fellow, Department of Computer and Information Science, University of Oregon, 2010 - present

Research Intern, Department of Computer Science, Duke University, Feb 2015 - May 2015

Network Analyst and Designer, Advanced Information & Communication Technology Center, 2009

Chief Information Officer, SIEMENS SSK, 2006 - 2007

GRANTS, AWARDS AND HONORS:

Student Travel Grant
CAIDA's BGP Hackaton (San Diego) - 2016

Student Travel Grant
ACM Conference on Online Social Networks (San Fransisco) - 2015

Julie and Rocky Dixon Graduate Innovation Award
University of Oregon - 2014

Gurdeep Pall Scholarship Award
University of Oregon - 2013

Clarence and Lucille Dunbar Scholarship Award
University of Oregon - 2012

Student Travel Grant
ACM Internet Measurement Conference (Boston) - 2012

Student Travel Grant
IPAM Workshop on Multi Resolution Analysis (Lake Arrowhead) - 2011

Juilf Scholarship Award
University of Oregon - 2011

PUBLICATIONS:

R. Gonzalez, R. Cuevas, R. Motamedi, R. Rejaie, and Á. Cuevas. Assessing the Evolution of Google+ in its First Two Years. *IEEE/ACM Transactions on Networking (ToN)*, 24(3):1813–1826, 2016.

R. Motamedi, R. Rejaie, and W. Willinger. A Survey of Techniques for Internet Topology Discovery. *IEEE Communications Surveys & Tutorials*, 17(2):1044–1065, 2014.

R. Gonzalez, R. Cuevas, R. Motamedi, R. Rejaie, and A. Cuevas. Google+ or google-?: Dissecting The Evolution of the New OSN in its First Year. In *Proceedings of the 22nd International Conference on World Wide Web*, pages 483–494. ACM, 2013.

R. Motamedi, R. Rejaie, W. Willinger, D. Lowd, and R. Gonzalez. Inferring coarse views of connectivity in very large graphs. In *Proceedings of the second ACM conference on Online social networks, COSN 2014, Dublin, Ireland, October 1-2, 2014*, pages 191–202. ACM, 2014.

R. Motamedi. WalkAbout – a Random Walk Based Framework to Characterize OSNs. In *Proceedings of the Second Internet Multi-Resolution Analysis Workshop*, Lake Arrowhead, IPAM, July 2011.

M. Moshref, R. Motamedi, and H. R. Rabiee. LayeredCast – A Hybrid Peer-to-Peer Live Layered Video Streaming Protocol. In *Proceedings of the fifth international symposium of telecommunication*, Kish, Iran, Dec, IST 2010.

ACKNOWLEDGEMENTS

None of my accomplishments during the course of this eventful journey through the years of my PhD, no matter how feeble, would have been possible without the help and support of many. I would like to acknowledge them for their support along the way. Above all I would like to acknowledge the tremendous sacrifices that my parents made to ensure that I had an excellent education. Although their physical presence was lacking from my life in the past six year, their love, devotion and support always guided me forward. For this and much more, I am forever in their debt.

I am very grateful to my advisor Reza Rejaie who guided my research, shared his insights and ideas, encouraged me continually and provided me with opportunities in any possible way during the course of my time in Eugene. Working with him taught me far more than research skills and helped me handle fasts and slows of the life of a graduate student.

I had the privilege of having some of the most extraordinary research mentors. I would like to thank Walter Willinger for sharing his time and invaluable experience in research and non-research matters. His advice and recommendations were crucial to my progress on numerous occasions. I would also like to express my gratitude to Bruce Maggs for his mentorship and the opportunity he provided me as an intern at Duke University. Many thanks to Ruben Cuevas for his counsel in research and genuine friendship. I would also like to explicitly thank my committee members, Prof. Allen Malony, Prof. Jun Li, Prof. David Levin, and Prof. Walter Willinger for taking the time to review my dissertation and giving valuable suggestions and feedback.

Working closely with Bahador Yeganeh, Bala Chandrasekaran, and Roberto Gonzales were some of the highlights of my life during my PhD, and the hours spent

together at white boards and at lunch created friendships which I hope to keep for many years to come. I owe special thanks to my friends and colleagues in the ONRG Lab and other research groups at University of Oregon, including Saed Rezaei, Soheil Jamshidi, and Pedram Rooshenas for their invaluable support and suggestions throughout my PhD study. They were wonderful group-mates and friends and made my last few years of PhD an enjoyable and memorable journey.

The truth is that I have had an incredible team to work with and be inspired by throughout the course of my PhD. Each of you has contributed to my academic success in a meaningful way, and I am sincerely grateful for your support.

To my dearest parents, my beloved Brandi, and all my teachers.

TABLE OF CONTENTS

LIST OF FIGURES

Figure Page

LIST OF TABLES

CHAPTER I

INTRODUCTION

In different information and technological distributed systems, there exists the need for a monitoring and measurement of processes to analyze the health of the platform, incorporate proper controlling mechanisms, and identify the most desired new features of the system. In computer science research, these distributed systems cover a wide variety of interconnected systems. Examples of such systems include but are not limited to electric power grids, the world wide web, social networking sites, and the Internet. The traditional approach in the research of distributed systems is to present the relationships/interactions between the individual parts of the system as (large scale) complex networks. The analysis, characterization, and distinction of such a complex network in return yields insight about the distributed system that the network represents.

Recent popularity of complex networks stems from their generality and flexibility in representing systems limited not only to man-crafted structure, but including natural and biological systems as well. As a result, the ease of access to big data produced an abundance of publications in this area. These studies mostly involve representing the structure of interest as a network, followed by an analysis of the topological features of the obtained representation performed in terms of a set of measurements. One important missing element in the research on distributed systems casted as complex networks is the lack of attention to *domain knowledge* and how the shortcomings of the measurement approach and limitations of complex networks may affect the captured view. The extent to which calculated measures are informative has also not been at the center of attention.

In this thesis, we take a closer look at measurement-based analysis of a few large scale distributed systems. The emphasis on the role of domain knowledge lies at the heart

of this thesis. More specifically we use domain knowledge in: *(i)* designing a context aware measurement strategy, *(ii)* analyzing the captured view of the networked system, and *(iii)* investigating the root causes that lead to certain properties of the system. Our target systems include various online social networks and the physical interconnections of the Internet.

Challenges and Foci in Studying Distributed Systems

The Measurement and characterization of distributed systems is not without is challenges. The most relevant challenges in this domain include:

Scale: Distributed systems are often very large. Social networks have millions of active accounts and billions of relationships. There are approximately 40K networks in the Internet and it is approximated that each has up to a few thousand routers. While complex networks provide a flexible platform for the representation of these large systems, capturing, characterizing, and analyzing these systems at scale is an open problem.

Heterogeneity: Heterogeneity of entities and subsystem proposes an additional challenge in the study of distributed systems. For instance, in social network studies not all user accounts are similar, as some belong to individuals and others belong to corporations. These heterogeneities in turn effect the measurement and influence the findings.

Data: The availability and quality of data is yet another challenging aspect. Needless to say, the study of some distributed system data is in fact considered a well-kept secret for confidentiality and privacy reasons. While publicly available data has proven to be a valuable source of information for researchers, more elaborate data collection tools and techniques are often necessary to collect the most relevant information from the system. These active data collection efforts are often limited by the API thresholds. The

heterogeneity of the system also imposes additional obstacles as each subsystem offers a different API, which in turn complicates the data collection process.

Domain Knowledge: The knowledge of the context and domain governing the system is not only necessary to the design of a proper data collection methodology, but is also critical in characterizing and analyzing the captured view of the distributed system and drawing informative and meaningful conclusions from the analysis. For instance, the insight on the limitation of data collection techniques in general, the rules and attributes of an online social network, and common practices of network operators are of great importance in the measurement-based studies of distributed systems that we target in this dissertation. The overall challenge is therefore the need for an extra level of "care" to ensure the correctness of the findings inferred from the views of the distributed system that are captured using techniques with many limitations. Indeed this level of assurance is impossible without a sufficient amount of domain knowledge.

Over Arching Themes of the Thesis

Although we target various kinds distributed systems in our research, the design of the measurement methodologies and analysis frameworks have many similarities.

Complex Network Analysis

Our research studies mainly fall in the category of complex network measurement and analysis. In our analysis we often present the target system as a network (or a graph) and aim to draw inference using this graph structure from the underlying system. We often use graph partitioning and clustering (in Chapters III and V) to identify groups of nodes that are tightly connected within the group and are less interconnected between different groups. In all cases we use these groups to explain some aspect of the network

by analyzing the root cause for the formation of such highly knit groups. When graph partitioning falls short, we utilize more sophisticated machine learning methods for drawing inference over networks (in Chapter VII).

Big Data; Is More Always Better?

Another recurring theme in our research on distributed systems regards the usage of "big data". We argue that more data is not necessarily better and in many ways controlled measurements can help arrive at more meaningful findings. To this end, we often take a *targeted* approach to collect data from the most relevant and informative parts of any target distributed system. Examples of such methods can be found in Chapters IV and V where our measurement methodology allow us to find great wealth of information about a small yet important set of users of OSNs. Similarly, in Chapter VII we demonstrate how domain knowledge can help devise a traceroute-based campaign to uncover details of network interconnection in a specific geographical area among a set of target networks.

Scope & Contributions

The main technical contribution of our work is the established connections between the domain knowledge and the measurement of networked systems, and the analysis of the views captured from complex networked systems. The following projects represent our proposed solutions to the aforementioned problems.

Inferring Coarse Views of Connectivity in Very Large Graphs

In this research, we present a simple framework, called WalkAbout, to infer a coarse view of connectivity in very large graphs by identifying well-connected "regions" with different edge densities and determining the corresponding inter- and intra-region

connectivity. We leverage the transient behavior of many short random walks (RW) on a large graph that is assumed to have regions of varying edge density, but whose structure is otherwise unknown. The key idea is that as RWs approach the mixing time of a region, the ratio of the number of visits by all RWs to the degree for nodes in that region converges to a value proportional to the average node degree in that region. Leveraging this indirect sign of connectivity enables our proposed framework to effectively scale with graph size.

We demonstrate the capabilities of WalkAbout by applying it to three major OSNs (i.e. Flickr, Twitter, and Google+) and obtaining a coarse view of their connectivity structure. For comparison, we illustrate how the communities that are obtained by running a popular community detection method on these OSNs stack up against the WalkAbout-discovered regions. Finally, we examine the "meaning" of the regions obtained by WalkAbout, and demonstrate that users in the identified regions exhibit common social attributes.

Characterisation and Comparison of Group-level User Behavior in Major Online Social Networks

In a detailed measurement-based study to characterize and compare the behavior of users in Facebook, Twitter, and Google+, our solution involves a "group-level" analysis. We focus on *Popular*, *Cross* (with account in three OSNs) and *Regular* groups of users in each OSN since they offer complementary views. We capture user behavior with the following metrics: user connectivity, user activity and user reactions. Our group level methodology enables us to capture major trends in the behavior of small but important groups of users, and to conduct inter- and intra-OSN comparisons of user behavior. Furthermore, we conduct temporal analysis on different aspects of user behavior for all

groups over a two-year period. Our analysis leads to a set of useful insights including: *(i)* The more likely reaction by Facebook and Google+ users is to express their opinion whereas Twitter users tend to relay a received post to other users and thus facilitate its propagation. Despite the culture of reshare among Twitter users, a post by a Popular Facebook user receives more Reshares than a post by a Popular Twitter user. *(ii)* Added features in an OSN can significantly boost the rate of action and reaction among its users.

Dissecting Twitter Elite Power Network

Highest degree nodes in Online Social Networks (OSNs) such as Twitter can be viewed as "social elites" or "connectivity hubs" as they are followed by many users and therefore have influence over their followers. All these elites along with their pairwise friendship relations form a structure that we refer to as "The Elite Network". The Elite Network serves as the backbone of the OSN structure and thus its characteristics offer valuable insights about the core of any OSN. Despite their importance, the characterization of elite networks has received little attention among computer scientists. Our research presents a detailed analysis of the macro- and micro-level structure of the Twitter elite network. Using PageRank of elites in the elite network, we show that the Twitter elite network has an "onion-like" structure where the more popular elites are in the center and adding less popular elites only adds to this structure's outer layers. Furthermore, this network is composed of a number of "communities" that exhibit strong social cohesion. The examination of pairwise tightness between these communities reveals the coarse structure (and level of interest) among these communities. Finally, by exploring the aggregate influence of individual elites on other elites based on various measures, we demonstrate that no single measure can capture all the aspects of influence.

Mapping X-Connects Inside a Colocation

A significant fraction of the Internet's physical infrastructure (e.g. routers, switches, and related equipment) is hosted at a relatively small number of physical building complexes such as colocation facilities (or carrier hotels) and Internet eXchange Points (IXPs). More importantly, these facilities have generally known street addresses and thus can be accurately geo-located. Companies like Equinix, CoreSite, and Telx manage and operate these carrier-neutral colocation facilities (also called colos) where they provide, among other offerings, interconnection services. These facilities supply the infrastructure (e.g. rack space, cabling, power, and physical security) necessary for network operators to colocate their routers for easy interconnection.

This observation motivated our new methodology that is specifically designed to map a given colo facility. This methodology relies on targeted active measurements to identify not only all the PoPs of all the ASes present in that colo facility, but also the corresponding inter-AS connectivity that is visible to active probing at that location. In turn, this methodology defines a very promising, widely applicable, and highly accurate approach for geo-locating potentially hundreds or thousands of IP addresses (i.e. all the discovered IPs of the interfaces on the routers in the co-located PoPs) to the street address of that facility.

This work focuses on identifying interconnections of the "x-connect" (read cross connect) type, i.e. dedicated point-to-point private peering links (which might be used to carry transit traffic or peer-to-peer traffic) that the network operators can buy from the colo providers so that their networks can exchange traffic within the confines of these facilities. In particular, our goal is to infer who is interconnecting with whom in which colos and in which cities. Precisely locating the private peering links between two networks is a prerequisite for studying, for example, the root causes of the peering

disputes between large content and eyeball providers in recent years. We illustrate the approach with case studies of colos in Los Angles, Chicago, and Miami. These studies demonstrate the promise as well as the challenges inherent in such a mapping effort.

Dissertation Outline

This dissertation is organized in two parts. Part I covers the material related to the analysis of social networks and Part II focuses on discovering the topology of the Internet. Part I is organized as follows. In Chapter II, we briefly discuss the background and the related work on analytical measurement-based characterization of social networks used as foundation of our own projects in Part I. Chapter III presents WalkAbout, our proposed tool for coarsening large graphs and its application represented by three OSNs. In Chapter IV, we present a new methodology to characterize and compare OSNs by focusing on the behavior of diverse "groups" of users. We then show that such a group-level cross comparison allows us to compare various aspects of the underlying OSNs without the need for exhaustive crawls of the systems. We discuss the importance of "Elite Power Networks" and present our methodology to effectively collect the elite network of Twitter in Chapter V. Our detailed characterization of this network reveals interconnection between communities of elites and allows us to identify key elite users.

Part II is composed of two chapters. Chapter VI covers a rather detailed survey on tools and techniques for Internet topology discovery. In Chapter VII, we propose a methodology for capturing interconnections between networks that participate in one colocation facility to recover PoP-level maps of the topology of the Internet. We demonstrate the applicability of our method by mapping interconnections inside three colocation facilities. Finally, we present concluding remarks and future possible directions for research in Chapter VIII.

Part I

Online Social Networks

CHAPTER II

ONLINE SOCIAL NETWORKS; BACKGROUND

Introduction

In the past decade, the increasing popularity of Online Social Networks (OSNs) has led to a growing public fascination with new forms of digital connectedness. Examples of such networks cover a variety of systems such as Email lists, discussion groups, chat and instant messaging, audio and video conferencing, networks of financial interactions, collaborative systems, virtual worlds and games, micro-blogging and multimedia-blogging, and general-purpose social sharing networks. An in depth understating of an OSN, often facilitated through complex network analysis on its social graph structure, is essential for the evaluation of the state of the current system for social and economical purposes. The identification of the network's shortcomings and most critical new features are also important. This comprehensive understanding allows researchers to synthesize artificially crafted graphs that capture the most important features of an OSN which are most useful for modeling purposes. For instance, the analysis on the structure of an OSN leads to the identification of most influential and trusted users [31, 59, 43], understanding how information diffuses over the social system [90, 154, 193, 218], designing defense mechanisms for the system against tampering by fake users [262], or even providing services such as web search that are not the main mission of OSNs [15, 14].

This Chapter lists the most relevant work to our studies on Online Social Networks. After providing a brief background and context in Section 2.2, we cover a few studies on general characterization and comparison of connectivity features, user behavior, and temporal evolution of various OSNs in Section 2.3. In Section 2.4, we provide an

overview of graph clustering and community detection techniques. We then cover work related to the identification of key users and the estimation of their influence on online social networks in Section 2.5.

Online Social Network as a Graph

In their simplest form, online social networking sites allow (registered) users to publish and read posts by other users. Most sites also encourage users to form friendships, therefore allowing "friends" to automatically receive updates on the content posted by their friends. A user can also repost others' contents or engage in an interaction by commenting on or replying to another user's post. The common denominator in the studies of OSNs is to represent the systems as graphs. These *social graphs* encode relationships (e.g. friendship, repost, reply) as edges between nodes that often represent user accounts. Depending on the OSN, social graphs can be either directed or undirected. For instance, in Twitter many relationships are asymmetric, therefore the graph that captures the relationship is a directed one. In order to capture a friend-follower relationship between two users (represented by two vertex in the graph), in which u_{fol} follows u_{fri}, a common encoding is to assume an edge from u_{fri} to u_{fol}. In this case, messages travel along the direction of the edges on this *follow graph*. On the other hand, in Facebook friendships are symmetric, therefore the social graph of Facebook can be represented as an undirected graph. These social graphs are often referred to as the *connectivity* graphs since they represent the most trivial type of relationship in the social network.

Similar to the friendships, the interaction between users can be encoded as graphs. As an example, in Twitter if u_{rt} retweets u_{orig}, one can encode this relationship as a

directed edge from u_{orig} to u_{rt}. Therefore, many different graph-based representations can be derived from an OSN, each capturing one aspect of the underlying system.

Comparing Online Social Networks Through Measurement

The public popularity of OSNs spawned great interest among social and computer scientists to monitor and characterize different aspects of these social systems [163, 254, 258, 270, 191, 190, 119]. A significant number of studies examine an OSN individually (e.g. Twitter [163], Facebook [197], and Google+ [119]) by devising sophisticated measurement tools for capturing (commonly referred to as crawlers) and characterizing various aspects of the OSN. Numerous metrics have been proposed to help quantify specific properties of these networks. Such quantitative characterization inherently facilitates comparison between these social systems. Moreover, the growing number of alternative social networking websites that provide similar functionalities to the most popular OSNs motivated researchers to directly compare properties of various OSNs. The conducted studies in this field can be broadly classified into three classes:

Social Graph & Connectivity Properties

The earliest studies on OSNs focused on characterizing their social graphs. The commonly reported properties in all such networked systems include *power law degree distribution*[1] [74], *high clustering coefficient* [266], and *small-world* properties [21]. Power law degree distribution means the fraction of nodes in the graph that have k relationships to other nodes is proportional to $k^{-\alpha}$, in which α is the parameter of the distribution ($\alpha > 0$). Figure 2.1 demonstrates the empirical degree distribution of four real social graphs [191] and the fitted power law distributions. As seen in the OSN graphs

[1]Graphs whose node degrees follows power law distribution are commonly referred to as *scale-free*.

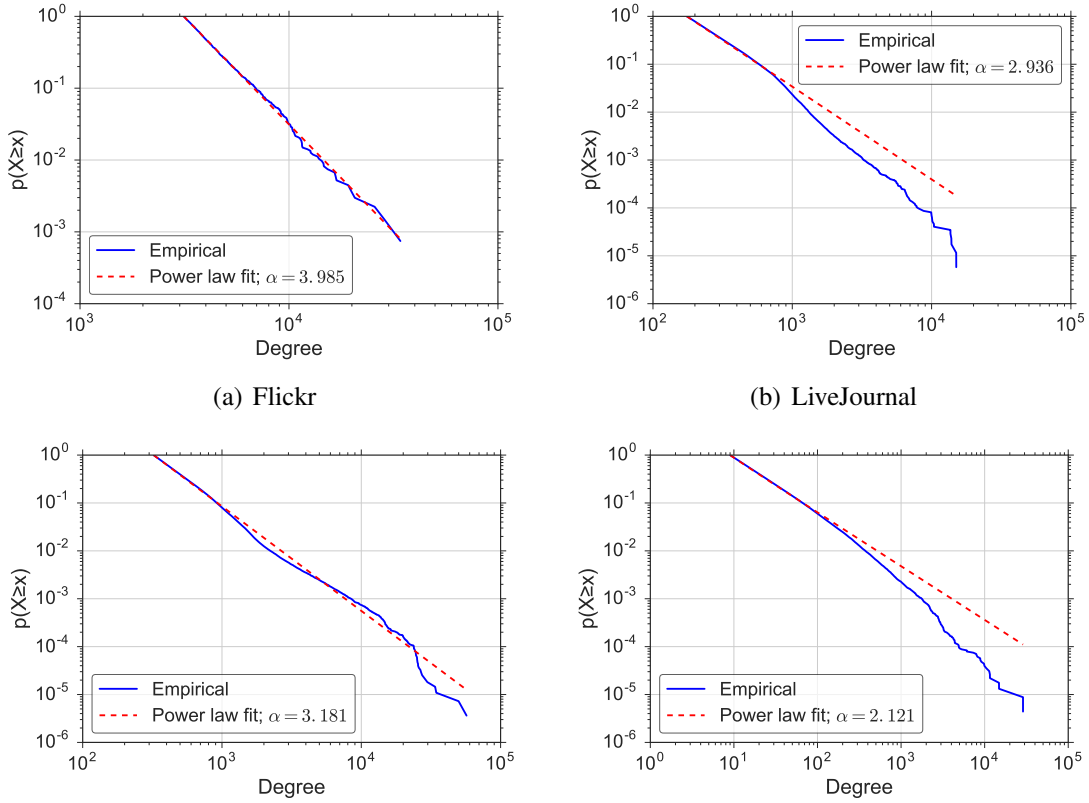

(a) Flickr (b) LiveJournal

(c) Orkut (d) YouTube

FIGURE 2.1. Empirical degree distribution of four real OSN graphs and the fitted power law distribution.

in Figure 2.1, the value of α is reported to be within the range of 2 to 3 in many OSN graphs. Power law degree distribution suggests that it is qualitatively possible to have very large values of k, i.e. users with extremely high popularity. While the results in more recent studies present non-power law degree distribution [163, 257], this property is still among the most accepted features of OSN social graphs. Clustering coefficient is closely is related to triadic closures. Triadic closure is an intuitive feature of many social systems and alludes to the potential of friends of a specific user to be or become friends [200, 266]. Specifically, the clustering coefficient of a user u is defined as the probability that two randomly selected users that are friends of u are indeed friends with each other. A common definition of clustering coefficient in a graph is the average

of clustering coefficient of all users in the social graph. Alternatively, global clustering coefficient of a graph can be defined as follows:

$$\text{global clustering coefficient} = \frac{3 \times \textit{No. of triple nodes connected by 3 edges}}{\textit{No. of triple nodes connected by at least 2 edges}}$$

Finally, a graph is considered small-world if its average local clustering coefficient is higher than the randomized version of the graph, and if the graph has approximately the same mean-shortest path length as its corresponding randomized graph (so called "six degrees of separation") [266]. Figures 2.2 and 2.3 present two real sample social graphs [198, 168] and their randomized counterparts. We applied a commonly used rewiring technique in which each endpoint of each edge can be rewired with a constant probability to randomize the graphs. Within the graphs, we set the rewiring probability to 0.5. We also used forced-based layouts to visualize them [109]. We observe clear topological structures in the form of closed triangles (three vertices that are fully connected) and groups of well-connected vertices in the original graph. These structures are, however, not visible in the randomized graphs. Figures also report on two metrics in these graphs, namely clustering coefficient and average path length. We observe in both examples that randomization clearly reduces the clustering coefficient but does not affect the average path length. Therefore, these social graphs are examples of small-world graphs.

The existence of these properties (or lack there of) in real social graphs has been the focus of many studies. The connectivity properties of the social graph for Facebook [257, 29, 117], Twitter [163, 59], Google+ [178, 227, 119] and other less popular OSNs [70, 128] have been carefully analyzed recently. The results presented in these studies reveal the social properties of the underlying system and the extent to which they resemble each other and other social systems by comparing the quantitative metrics representing each

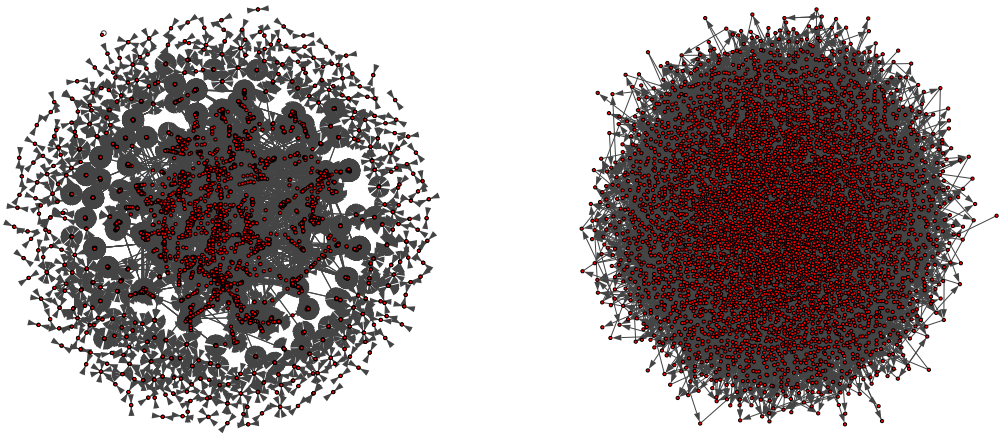

(a) Original social graph;
Clustering Coefficient $= 0.62$;
Average path length $= 2.51$;

(b) Degree preserving randomization;
Clustering Coefficient $= 0.03$;
Average path length $= 2.14$;

FIGURE 2.2. Collaboration network from the e-print arXiv and the corresponding randomized graph.

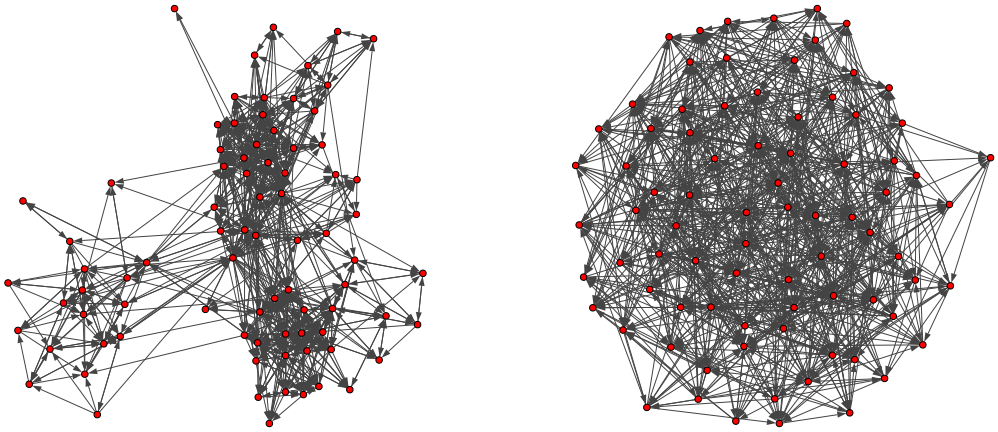

(a) Original social graph;
Clustering Coefficient $= 0.47$;
Average path length $= 6.04$;

(b) Degree preserving randomization;
Clustering Coefficient $= 0.25$;
Average path length $= 4.92$;

FIGURE 2.3. Friendship network of a UK university faculty members and the corresponding randomized graph.

social system. Some studies explicitly focus on comparing the social graphs of different OSNs. Mislove et al. [191] analyze the graph properties for Orkut, Flickr, LiveJournal, and YouTube. Their results confirmed the power-law and small-world properties in all OSNs. In the same year, Ahn et al. [16] compared the topological structures of Cyworld, MySpace, and Orkut by reporting the degree distribution, clustering property, and degree correlation. Magno et al. [178] performed an early analysis on Google+ and identified its main similarities and differences with other OSNs like Facebook and Twitter. Gonzalez et al. [119] also compared the connectivity properties of the social graph of Google+, Facebook, and Twitter. Although all the social graph of these OSNs seem to have similar topological attributes, the small differences in them seem to render some networks more suitable for specific purposes. For instance, it is widely accepted that Twitter is used as a message propagation network, but Facebook is mostly used for social biding.

Users' Behavior in Online Social Networks

Users' behavior can also to be characterized based on real data collected from OSNs. In particular, previous studies have used two different strategies: Passive measurements [38, 228] and active measurements [275, 127, 119]. The former captures traces of traffic or click streams that allow user interaction with the OSN to be reconstructed, whereas the latter uses crawling techniques to tell *"who does what"* in the system.

Gyarmati et al. [127] used active measurements to characterize user activity in the not so popular OSNs of Bebo, MySpace, Netlog, and Tagged. They defined activity as the time a user stays online in the system. Alternatively, a recent study by Gonzalez et al. [120, 119] actively collected the posts contributed to Google+ by its users to characterize the level of their interaction with the system. Another important feature of many OSNs

is user reaction to posts, for instance, in the form of liking or resharing a post created by other users. In the same study, Gonzales et al. measured the amount of reaction that posts receive. In a recent study on Pinterest, Han et al. [128] focused on the difference between the acts of posting and reposting by considering user gender and post topics. Their results show that in their target OSN, there is a significant variance between the frequency of posting and reposting across topics. They also show that gender is an important factor in the level of user engagement with the system.

These studies also commonly reported a high level of skewness withing user activity and reaction [146]. Skewness refers to the measurement of asymmetry within a probability distribution. Large skewness means that the mean value of the distribution poorly captures the outliers. For instance, it has been reported that 1% of Google+ users receive more than 80% of reactions in the system [120]. Similarly, the duration of OSN users' online sessions exhibit high skewness and show power law distribution characteristics. These commonly reported skewed distributions of user properties pose additional challenges when sampling techniques are used in the characterization of social systems.

Evolution of Online Social Networks

The evolution of OSNs has also been the focus of research in the past. The objective of these studies is not to capture the OSN social graph as a single snapshot at a certain point in time, but to characterize the OSN as an evolving distributed social system, in which new user accounts are created, new friendships are formed or removed, and content is shared through the media. The analysis of the evolution of the social graph properties [119, 190, 16, 284, 110, 114, 217], the evolution of the interactions between

users [145], and the evolution of users' availability (time spent online) over time [44] are a few examples of such studies.

The evolution of Flickr and Yahoo! with respect to their number of users, friendships, and the structure of their connected components was studied by Kumar et al. [162]. Rejaie et al. [217] studied the evolution of the network size and the user activity in MySpace and Twitter. Gonzalez et al. [119, 120] studied the growth in the number of users and their daily activity in Google+ by capturing and monitoring the network's main component over the course of two years.

While studies on the evolution of OSNs primarily focus on capturing the dynamics of the system, they also provide great insight for modeling and predicting their growth and decline. For example, Garcia et al. [113] used snapshots of Friendster to create a model that identifies growth patterns that result in social graph structures that are more resilient to users' departure.

Graph Clustering & Community Detection

One of the commonly studied aspects of graphs that represent real social systems is detecting clusters in them or their community structure. This involves organizing vertices in clusters (also referred to as communities, partitions, or modules) with many edges connecting vertices of the same cluster and comparatively few edges connecting vertices of different clusters. Finding such clusters is considered to be very important, since each one can be considered as a fairly independent segment of a graph. In social graphs, each community is often formed as a result of common interests of a group of users (i.e. homophily) [186].

In the analysis of clusters in graph, one important question is how to evaluate the "goodness" of the resulting clusters. This evaluation allows researchers to compare

clusters as well as the techniques that identified them. Two commonly used goodness indexes are conductance [41] and modularity [201]. Conductance, which is a value in $[0, 1]$ measures how well a certain bipartition of nodes splits the graph. Therefore, for each cut through the edges in the graph a single conductance value can be computed. For a given cut that splits the graph into S and $\bar{S}$, conductance (φ) is defined as:

$$\varphi(S, \bar{S}) = \frac{\sum_{i \in S} \sum_{j \in \bar{S}} a_{i,j}}{\min(\sum_{i \in S} \sum_{j \in V} a_{i,j}, \sum_{i \in \bar{S}} \sum_{j \in V} a_{i,j})} \tag{2.1}$$

in which $a_{ij} = 1$ if an edge exists between vertex i and j. A small conductance index means few edges are cut in order to split the graph into two halves (i.e. the community and the rest of the graph).

On the other hand, modularity measures how well a graph divides into clusters. In other words, a graph with high modularity computed for a certain grouping of nodes into clusters have dense connections between the nodes within modules, but sparse connections between nodes in different modules. Modularity (Q) of the graph G over grouping $\mathcal{C}$ is defined as follows:

$$Q(G, \mathcal{C}) = \sum_{i=1}^{k} (e_{ii} - a_i^2) \tag{2.2}$$

in which k is the number of communities in $\mathcal{C}$, e_{ii} is fraction of edges in community i, and a_i is the fraction of edges with at least one side in community i. Using the above definition, modularity essentially measures the fraction of the edges in the network that connect vertices in the same cluster minus the expected value of the same quantity in the randomized version of the graph. Therefore, for each graph partitioning into communities

a single modularity index is computed, and a higher modularity index indicate a better splitting into clusters.

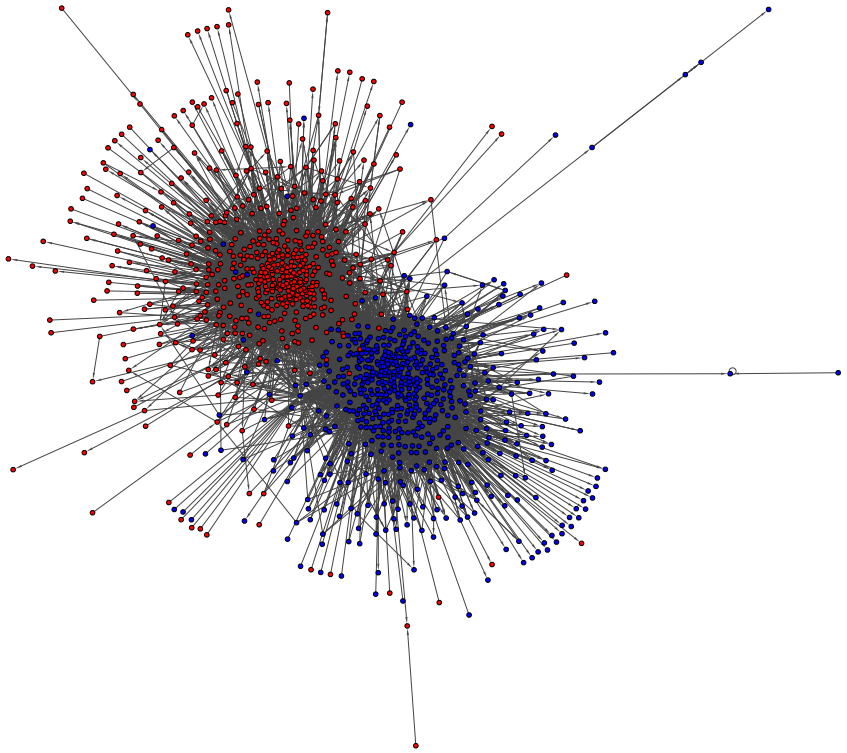

FIGURE 2.4. Visualizing two clusters of well connected nodes in the graph of hyperlinks between weblogs on US politics [11].

Figure 2.4 presents the graph of hyperlinks between weblogs on US politics [11]. In this example, we use ground truth data in terms of association with Democratic and Republican to cluster vertices. In the figure, we used colors to encode Democrats and Republicans and a forced based layout to compute the position of each vertex. Conductance of this slicing is 0.091 and the resulting modularity is 0.41.

While the problem of finding good clusters in graphs was the focus of a large interdisciplinary community of scientists, it has not been solved yet and different proposed methods tend to fit the problem of clustering specific graphs. Identifying

clusters in graphs can be broadly categorized into two categories. In a *global* clustering, each vertex of the input graph is assigned a cluster in the output, whereas in a *local* clustering, the cluster assignments are performed with respect to a certain subset of vertices in the graph to create a bi-partitioning of the input graph.

Local Graph Clustering: Local clustering methods aim to detect a tightly interconnected partition around a given seed vertex. The time complexity of most algorithms that fill in this category are proportional to the size of the local cluster and not the entire graph. Local graph partitioning using PageRank [22] is one of the most popular approaches in this domain. In this method, first a localized PageRank vector is used to rank vertices based on their distance (similarity) to the seed vertex. Then a sweep over this ordering is used to find a set of vertices that minimizes the normalized cut (conductance) and therefore results in a good bi-partitioning.

A few prior studies have used RWs to distinguish local clusters. For instance, to distinguish sybil from trusted accounts in an OSN, random walks are used to measure accounts' relative connectivity from trusted vertices [58, 263]. Therefore the algorithm divides users into two groups; a group that falls within the local cluster and the rest of vertices that do not.

Global Graph Clustering: The general goal underlying global clustering methods is to produce a grouping of nodes into modules (also referred to as clusters, communities, partitions) that is optimal (or close to optimal) with respect to a given cluster quality measure [107, 164, 129]. Uncovering the community structure exhibited by networks is a crucial step in understanding the complex systems. Many algorithms have been proposed that show great potential in detecting communities within small to mid-size networks that are sometimes artificially generated and therefore have known community structures. The two main classes of approaches in this field are community detection and graph

partitioning. While community detection methods perform bottom-up clustering, graph partitioning methods typically perform in a top-down fashion by splitting the graph into sets of nodes with low interconnections [149, 41].

Most methods work by optimizing an objective function. Since this is typically NP-hard, greedy or heuristic methods are usually necessary. One of the most popular metrics for community detection is *modularity*, which relates the number of edges within clusters to the expected number for a random graph. Louvain method [40] is one of the most scalable and effective algorithms that aims at optimizing modularity. It greedily assigns nodes to communities based on their local connectivity, then coarsens the graph by replacing each community with a single node. This procedure repeats until it reaches a local optimum of modularity. However, in most real-world graphs, modularity tends to favor smaller communities of around 100 nodes [169]. Other measures such as conductance also tend to favor small clusters in real-world graphs, limiting their effectiveness at describing high-level structure.

Graph partitioning techniques [150, 151] adopt a top-down approach. These techniques divide the vertices in groups of predefined size, such that the number of edges lying between the groups is minimal. These methods optionally recurse within each partition to obtain the desired granularity [88, 150, 151]. While this does discover larger regions than the bottom-up approaches, these regions may or may not faithfully represent the overall graph structure. For example, methods that optimize the popular normalized cut criterion tend to produce regions of approximately equal size, even when this leads to poorly separated regions. Furthermore, some approaches require specifying seed instances for each partition [22] or the total number of partitions, both of which can be difficult to determine a priori. Finally, many of these techniques, including spectral

clustering [149], do not scale with graph size and often require a complete snapshot of the target graph or its adjacency matrix.

Spectral clustering techniques attempt to partition a graph into dense groups of nodes, for instance by minimizing the normalized cut. These techniques typically involve finding eigenvectors of the adjacency matrix of a graph or one of its derivatives. This transforms the initial set of vertices into points in the space whose coordinates are elements are eigenvectors. Classical clustering techniques such as K-means [170] can then be used to cluster vertices. The main complexity of these techniques lies in the calculation of eigenvectors which is computationally expensive ($O(n^3)$). There are more scalable alternatives which do not use eigenvectors (Graclus [84]) or approximate them instead by using techniques such as power method. However, methods based on the normalized cut tend to create clusters whose sizes are known a priori (often time balanced), which may lead to clusters that are not well-separated since the provided sizes are not correct.

The Markov clustering algorithm (MCL) [260] has proven particularly effective for finding structure in biological networks. It works by defining and iteratively refining a stochastic flow until each node has a non-zero flow to just one other node. Nodes with the same target are grouped into the same community. The main limitation of MCL is its poor scalability with the graph size. MLR-MCL [225] is a multi-level, regularized variant of MCL that improves the scalability and quality of MCL.

Some proposed algorithms use random walks and "flows" [259, 213, 225, 130] for community detection. The random walk or the associated transition matrix are used to compute a measure of distance between all pairs of nodes. This distance measure is in turn used to cluster groups of nodes that are closer to each other, and hence find

communities in the graph. However, the computational and storage overhead for pairwise information is usually too expensive on large graphs with millions of nodes.

Identifying Key Users; Importance and Influence

Identifying key user accounts by measuring centrality and importance in a social network has also been studied in the past. These studies either use the characteristics of users in the social graph (e.g. total number of followers) or metrics that capture the historical success of the user to attract other users' attention (e.g. number of retweets in Twitter or number of views in YouTube) to identify most influential in an OSN. From the perspective of analysis on directed social graphs, the problem of identifying key users in an OSN is closely related to the problem of searching in WWW. Therefore, PageRank and its derivatives [47, 165], which have been proposed to facilitate the search for key webpages in the graph of WWW, are also used to identify users that can potentially be very influential on other users. Models that capture information cascade have been used to identify key users as well [43]. The objective in these models is to find vertices in the graph that can result in the largest *cascade* of events or *diffusion* tree [221, 247]. Various measures of centrality such as betweenness centrality [108], closeness centrality [220] and eigenvector centrality [20] have been proposed to identify entities that have a prime topological situation within the OSN. The goal of these methods is to rank the location of vertices based on their level of access to other parts of the network. Therefore, the concepts of *market access* in *viral marketing* are closely related to the measurement of influence and importance in OSN graphs. In addition to measures that are based on the structure of the social graph, researchers have also used metrics provided by some OSNs that measure the popularity of contents. To this end, the influence of a user can be estimated by the popularity of the content that she shares [75, 272].

Since influence and importance have many aspects, many studies used multiple metrics to capture them. Kwak et al. [163] ranked Twitter users by *(i)* their number of followers, *(ii)* PageRank computed over the social graph and, *(iii)* their number of retweets to identify the most influential users. They reported a higher correlation between the number of followers and PageRank metrics compared to the correlations among other pairs of metrics[2]. Welch et al. [267] computed PageRank over both graph and social graphs, and then compared the resulting rankings. They concluded that PageRank over the social graph reveals the popularity of a user and PageRank over the retweet graph demonstrates user influence. However, since their retweet graph has a direct edge from the original sender to each retweeting user (essentially a collection of a number of star-graphs), it does not capture the diffusion of the tweet and thus the resulting PageRank on the retweet graph does not reveal a correct measure of influence. To overcome this issue, some studies tried to heuristically reconstruct the diffusion tree using the timing of the reposts and the friendships among users that are invalided in the diffusion [30, 60]. Backshy et al. [30] tried to predict individual influence by predicting how an individual can start a cascade event of a certain size and depth. To do so, they first proposed a technique to reconstruct the retweet diffusion tree using the entire social graph. However, due to the limited data collection capacity, they used an old snapshot of the social graph that was captured approximately 10 months prior to the retweet events. This timing gap potentially leads to error in retweet tree reconstruction. Cogan et al. [75] studied user interactions on Twitter. They designed an algorithm to reconstruct the conversational graphs (mentions, retweets, replies). Their goal was to reconstruct cascade trees that capture interactions between individual users, and measure the influence of a user based on the cascades that started from each user. Deng et al. [81] argued that past history is

[2]This higher level of correlation seems inherent since PageRank centrality and degree centrality are greatly correlated.

not sufficient when measuring influence. Instead, they assume that users are primarily influenced by their friends. Using the social graph of Weibo (Chinese Twitter) and retweet information, they used a Baysian method to estimate the pairwise influence of users (influence over each edge) and therefore predict the properties of new diffusion trees. Wu et al. [272] also studied the influence on Twitter. However, their main focus is to capture "who listens to whom on Twitter" and report that conventional media sources with large number of followers play a different role in message propagation to regular users compared to other online celebrities.

CHAPTER III

WALKABOUT; INFERRING COARSE VIEWS OF VERY LARGE GRAPHS USING RANDOM WALKS

This chapter presents a simple framework, called WalkAbout, to infer a coarse view of connectivity in very large graphs; that is, identify well-connected "regions" with different edge densities and determine the corresponding inter- and intra-region connectivity. We leverage the transient behavior of many short random walks (RW) on a large graph that is assumed to have regions of varying edge density but whose structure is otherwise unknown. The key idea is that as RWs approach the mixing time of a region, the ratio of the number of visits by all RWs to the degree for nodes in that region converges to a value proportional to the average node degree in that region. Utilizing this indirect sign of regional connectivity enables our proposed framework to effectively scale with graph size.

After describing the design of WalkAbout, we demonstrate the capabilities of WalkAbout by applying it to three major OSNs (i.e. Flickr, Twitter, and Google+) and obtaining a coarse view of their connectivity structure. In addition, we illustrate how the communities that are obtained by running a popular community detection method on these OSNs stack up against the WalkAbout-discovered regions. Finally, we examine the "meaning" of the regions obtained by WalkAbout, and demonstrate that users in the identified regions exhibit common social attributes.

WalkAbout is different from the prior approaches in graph clustering as it is not optimizing a single metric or objective function. Rather, it is a heuristic approach that relies on an interesting transient phenomenon to explore the coarse view of structure in very large graphs. More specifically, WalkAbout does not only produce a single coarse

view of connectivity, but also its parameters allow a user to explore the connectivity structure to identify proper view at the desired resolution.

Introduction

Large-scale, networked systems such as the World Wide Web or Online Social Networks (OSNs) can be represented as graphs where nodes represent individual entities, such as web pages or user accounts, and directed or undirected edges represent relations between these entities, such as interaction or friendship between users [159, 191, 249]. Characterizing the connectivity structure of such a graph, in particular at scale, often provides deeper insight into the corresponding networked system and has motivated many researchers to analyze graph representations of large networked systems (e.g. [16]).

It is often very useful to obtain a coarse view of the connectivity structure of a huge graph that shows a few major tightly connected components or *regions* of the graph along with the inter- and intra-region connectivity. Such a regional view also enables a natural top-down approach to the analysis of large graphs, where one first examines the regional connectivity of a huge graph and then zooms in to individual regions to explore their structure in further detail. However, capturing a regional view of a huge graph is a non-trivial task that existing tools and techniques are not able to achieve. While many techniques exist for graph clustering [268, 83], graph partitioning [150], and community detection [40, 213, 107], these approaches do not work well for discovering coarse regional views in very large graphs. These methods usually scale poorly, force regions to have similar size, or find communities that are too small. For example, existing techniques (e.g. Louvain [40]) are likely to identify tens of thousands of communities in the structure of a large OSN that is still too complex for high-level analysis to determine the full picture of inter-community connectivity.

This chapter presents a simple top-down framework, called WalkAbout, to identify tightly connected regions in a large unknown graph and subsequently characterize the regional view of its connectivity structure. The main idea is to leverage the behavior of an army of short random walks (RW) on a graph to identify nodes that are located in the same region. When the random walks are longer than the mixing time of an individual region and shorter than the mixing time of the overall graph, the ratio of node degree to expected number of visits is proportional to the edge density of that region. We refer to this quantity as the degree/visit ratio (*dvr*). If individual regions in a graph have different edge densities and shorter mixing times than the entire graph, we can leverage the *dvr* "signal" to identify the regions, their corresponding nodes and their intra- and inter-region connectivity. The main novelty of WalkAbout is to leverage this indirect sign of connectivity to identify tightly connected nodes in a region. This leads to a very scalable method: in a graph with $|V|$ nodes, $|E|$ edges, and a regional mixing time of wl, WalkAbout requires only $O(wl \times |E|)$ time and $O(|V|)$ space. A few parameters in WalkAbout enable one to explore different aspects of the regional connectivity in order to produce the outcome with the desired resolution.

In our empirical evaluation, we apply WalkAbout to three major OSNs: Flickr, Twitter and Google+. Compared to Louvain [40], the gold standard for scalable community detection, WalkAbout runs faster and finds larger, coarser regions. Most communities discovered by Louvain can be mapped to a single one of WalkAbout's regions, suggesting that WalkAbout is providing a higher-level view of the network than Louvain. Finally, we analyze the regions in Flickr and show that different regions discovered by WalkAbout correspond to different interest groups, providing a meaningful coarse view of this OSN.

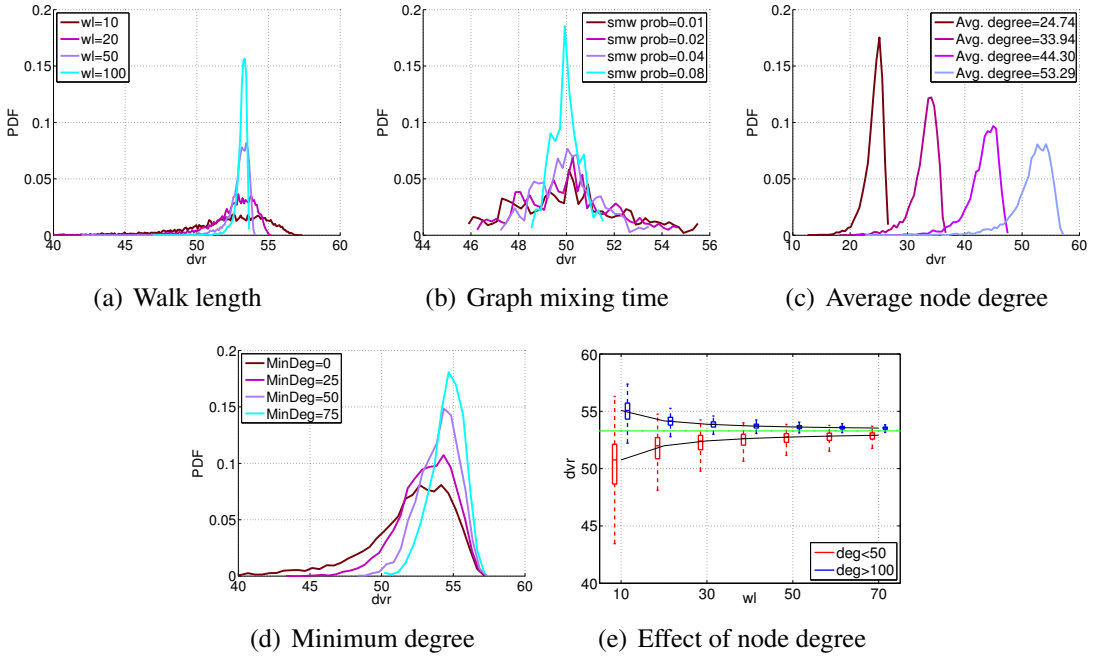

(a) Walk length (b) Graph mixing time (c) Average node degree

(d) Minimum degree (e) Effect of node degree

FIGURE 3.5. The effect of main parameters on the shape of the *dvr* histogram

The remainder of this chapter is organized as follows. Section 3.2 explores the behavior of short random walks and *dvr* on graphs with a single region. Section 3.3 extends this analysis to multiple region graphs and motivates using *dvr* for region identification. In Section 3.4, we present the full details of WalkAbout, our step-by-step framework for identifying regions in large graphs. To demonstrate and evaluate WalkAbout, we apply it to three major OSNs in Section 3.5. In Section 3.6, we compare the characteristics of Louvain communities with WalkAbout regions. We show that the regions discovered by WalkAbout are indeed meaningful in Section 3.7. We conclude the chapter in Section 3.8 and summarize our future plans.

The Behavior of Many Short RWs

Random Walks (RW) are a well-known technique for sampling graphs. A RW on a graph starts from an arbitrary node and at each step moves to a randomly chosen

neighbor of the current node. Consider a graph $G = [V, E]$ where V and E denote the set of graph vertices and edges, respectively. In an undirected, connected, and non-bipartite graph, the probability that a sufficiently long RW would be at a particular node x converges to $\frac{deg(x)}{2\times|E|}$ [173]. The *mixing time* $T_G(\epsilon)$ of a graph G is the walk length at which the probability of being at each node is within ϵ of the stationary distribution. In this chapter, we will use this term somewhat informally, without specifying a particular value of ϵ.

Suppose we run $|V|$ RWs in parallel, one starting at each node. Let $V(x, wl)$ denote the expected number of RWs that are at a particular node x after wl number of steps (e.g., *walk length* of wl). Since one RW is started at each node, $V(x, 0) = 1$. For other values of wl, we can define $V(x, k)$ inductively:

$$\begin{aligned} V(x,0) &= 1 \\ V(x,wl) &= \sum_{n\in\text{Neighbors}(x)} \frac{V(n,wl-1)}{\deg(n)} \qquad \text{for } wl > 0 \end{aligned} \tag{3.1}$$

This function can be computed iteratively with complexity $O(|E|wl)$. As wl reaches the *mixing time*, $V(x, wl)$ converges to $|V|\frac{deg(x)}{2\times|E|}$. Hence, when wl is sufficiently long, the following holds for all nodes:

$$\frac{deg(x)}{V(x,wl)} \approx \frac{2\times|E|}{|V|} \tag{3.2}$$

We refer to the fraction $\frac{deg(x)}{V(x,wl)}$ as the *degree/visit ratio* or *dvr*. Equation (2) indicates that the *dvr* converges to the average degree of the graph.

In practice, estimating the mixing time for an arbitrary graph is a known hard problem. In this section, we will explore the dependency of *dvr* on wl through

simulations on different synthetically-generated graphs. The graphs are generated by selecting the range of node degrees, the distribution of node degrees across this range, and then randomly connecting the nodes until all half-edges are connected. For each simulation, we show a normalized histogram of *dvr* values across all nodes, which represents the empirical distribution of *dvr* values for that simulation.

Effect of Walk Length: Figure 3.5(a) shows the evolution of the *dvr* histogram as we increase walk length over a generic random graph. As the walk length increases, the variation in *dvr* across different nodes decreases, leading to the formation of a narrower peak in the histogram. As wl reaches the mixing time, the probability of visiting each node becomes approximately proportional to its degree.

Effect of Mixing Time: To explore the effect of mixing time on the *dvr* histogram, we show in Figure 3.5(b) the evolution of the *dvr* histogram for a small-world graph as we increase the level of clustering (and thus the mixing time) for a particular walk length ($wl = 20$). As the mixing time becomes longer, the variation in *dvr* values increases because the RWs are farther from convergence.

Effect of Average Node Degree (E): Figure 3.5(c) presents the effect of average node degree (i.e. changing $|E|$ when $|V|$ is fixed) on the shape of the *dvr* histogram at a given walk length ($wl = 20$). Increasing the average node degree shifts the corresponding peak to higher *dvr* values. It is worth noting that the placement of each peak is in perfect agreement with the average degree of each graph.

Effect of Minimum Node Degree: Figure 3.5(d) shows the contribution of low degree nodes to the shape of the *dvr* histogram by plotting the histogram only for nodes whose degree is larger than a threshold D_{min}. We find that higher degree nodes show less variation in *dvr* than low degree nodes, i.e. filtering low degree nodes leads to a sharper peak in the histogram. Figure 3.5(e) depicts the evolution of summary distribution of *dvr*

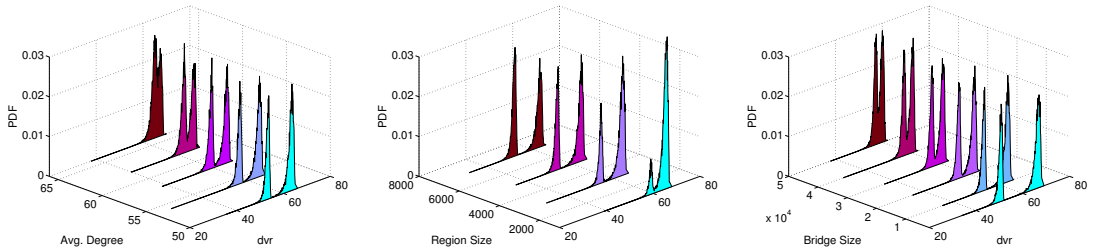

(a) Changing edge density of one region (b) Changing the size of one region (c) Changing the num. of bridge connections

FIGURE 3.6. The effect of connectivity features of a two-region graph on the *dvr* histogram ($wl = 20$)

across two groups of nodes with different degrees which shows that the range of *dvr* is inversely proportional with node degree and rapidly decreases with the walk length. This property is due to the fact that higher degree nodes are averaging over more neighbors in each update of $V(x, wl)$, thus reducing the variation.

Detecting Regions in a Graph

To infer a coarse view of graph connectivity, we assume that each graph consists of a number of weakly inter-connected regions, where individual regions have varying edge density. We use the term "region" instead of "community" to emphasize the fact that regions are often much larger in size than typical communities, and are identified based on a heuristic rather than optimizing an objective function or a metric.

We have no a priori knowledge of either the number of regions or their relative size and make no assumptions about the precise nature of the inter-region connectivity or intra-region connections.

The Key Idea

Our approach is to leverage the behavior of RWs that are shorter than the mixing time of the graph to identify nodes in each region of the graph. To this end, consider RWs that start from randomly selected nodes of a graph $G = [V, E]$ that has multiple regions. Based on our discussion in Section 3.2, the fraction of RWs that start in region i ($G_i = [V_i, E_i]$) of the graph is equal to the fraction of nodes in that region (i.e. $\frac{|V_i|}{|V|}$). If the length of those RWs is approximately equal to the mixing time of regions G_i, a majority of RWs will remain within that starting region, and for all practical purposes, we can view the different regions of the graph as disconnected partitions. Thus, we can use Equation (3.2) to determine the value of the *dvr* ratio to which node x in region i converges to as follows:

$$dvr_i(x) = \frac{deg(x)}{E[V(x, wl)]} = \frac{(2 \times |E_i|)}{|V_i|}, \tag{3.3}$$

Equation 3.3 shows that the degree-to-visit ratio for nodes x in region i equals $\frac{2\times|E_i|}{|V_i|}$ which is the average node degree for region i. Therefore, if regions of the graph have different average node degrees, the $dvr_i(x)$ values for nodes in each region converge to a different *dvr* value, i.e. form a peak at a different location in the *dvr* histogram across all nodes. We can represent each region with its associated non-overlapping range of *dvr* values and then map visited nodes to a region based on their *dvr* values. Furthermore, as discussed earlier, other key connectivity features of a region i (e.g. mixing time and size) affect the shape of the corresponding peak.

As the length of the RWs increases beyond the mixing time of individual regions, the RWs are likely to leave their starting regions and contribute to the number of visits for nodes in other regions of the graph. This in turn decreases the gap in the

$dvr_i(x)$ values for different regions and the *dvr* values for all nodes converge to a single value (determined by Equation (3.2)) as soon as the walk length of the RWs agrees approximately with the mixing time of the entire graph. Therefore, the separation between peaks in the *dvr* histogram that are associated with different regions of a graph is a *transient* phenomenon that occurs for RWs whose walk lengths are between region-specific mixing times and the mixing time for the entire graph. The more pronounced the regions, the larger the gaps between the mixing times of individual regions and the entire graph, which in turn translates to a longer transient phase and simplifies the detection of different regions. *In a nutshell, the similarity in dvr value serves as a promising indirect signal that reveals a tight connectivity among a group of nodes in a graph. The indirect nature of the dvr signal coupled with the ability to efficiently obtain dvr values using short random walks enables our approach to scale with graph size.*

Validation with Synthetic Graphs

Next we use synthetic graphs to demonstrate how our basic idea can reveal (or decode) the regional connectivity features within a graph. To this end, we consider a graph G with two regions, R_0 and R_1, both with 4K nodes and random connectivity and an average degree of 70 and 60, respectively. We connect these two regions with b bridge connections, where each bridge connection is between a pair of random nodes from these regions, and its default value is b=10k. In essence, the value of b controls the inter-region connectivity and thus the mixing time of the entire graph. To illustrate the effect of regional connectivity features on the shape of the *dvr* histogram, we keep region R_0 fixed and systematically change features of R_1 and the value of b.

Figure 3.6(a) shows the evolution of the *dvr* histogram as we vary the average node degree in R_1 between 50 and 66. We observe that as the average degree of $R1$ increases,

the corresponding peak gradually moves to higher *dvr* values and blends into the peak for R_0 until individual peaks are no longer distinguishable. Figure 3.6(b) shows how varying the size of R_1 from 1K to 8K nodes affects the shape of the *dvr* histogram when all other parameters remain constant. Increasing the size of a region proportionally increases the number of RWs that start from that region which in turn leads to a proportionally larger peak. Since we normalize *dvr* and plot the PDF, the peak corresponding to R_0 decreases in size. Finally, Figure 3.6(c) illustrates the effect of increasing the number of bridge edges (or bridge width) between the two regions from 5K to 50k. We note that as the bridge width increases, the two peaks gradually merge and become less and less distinguishable. This is due to the fact that increasing bridge width decreases the mixing time of the entire graph and thus shrinks the transition phase where the peaks for two regions can be clearly identified.

In summary, these examples illustrate that the behavior of many short RWs on a single graph can be extended to multi-region graphs as long as the mixing time of the entire graph is sufficiently larger than the the mixing time of individual regions.

WalkAbout

In this section, we present WalkAbout, our proposed method for inferring and exploring a regional (i.e. coarse) view of connectivity for large graphs. We first discuss some of the basic challenges in designing such a methodology and then describe our approach and how it addresses these challenges.

Basic Challenges

The behavior of many short RWs on a large graph motivates the idea of using the similarity of *dvr* values to identify individual regions of a graph where regions

are represented as a collection of nodes with non-overlapping ranges of *dvr* values. To implement this idea in practice, a number of challenges arise. First, we recall that the variation of *dvr* values across nodes with degree d in a given region decreases monotonically while the median value converges towards the average node degree of the region. More importantly, the degree of variation and its rate of convergence is inversely proportional to the node degree d, i.e. *dvr* values of higher degree nodes exhibit smaller variations and convergence faster than lower degree nodes. The typically large fraction of low degree nodes in big graphs coupled with the wider variation and slower convergence rate of their *dvr* values make it difficult to accurately associate a set of nodes with their corresponding region. This problem is further exacerbated by the fact that different regions may have a different mixing time and overlapping ra nges of *dvr* values.

Main Steps of WalkAbout

Given a large graph $G[V, E]$, the goal of WalkAbout is to identify the number of regions, map all nodes to their corresponding region, and determine the inter- and intra-region connectivity (i.e. fraction of edges that are connecting nodes in different regions or the same region). We call such a representation of a large graph a *regional (or coarse) view* of the graph. To overcome the above-mentioned challenges, WalkAbout identifies individual regions in two steps. First, it identifies a "core" component for each region. Such a component consists of a collection of high degree nodes in that region based on the similarity of their *dvr* values. Second, it considers each of these core components, views their elements as "anchors" and maps the remaining low degree nodes to the various regions based on the nodes' relative reachability to each core. This approach can effectively cope with the variations of the *dvr* values for low degree nodes and is less sensitive to the walk length. The WalkAbout technique comes with a set of

parameters/options that enable the exploration of the regional connectivity of a graph and support experimentation with different coarse views of a graph. In the following, we describe the five main steps of the WalkAbout technique.

1) Determining *dvr* Values for Individual Nodes: We emulate the behavior of $|V|$ short RWs starting from individual nodes in the graph and derive the probability of visits and use that probability to determine the degree-to-visit ratio for individual nodes at walk length wl, similar to Equation (1).

2) Creating the *dvr* Histogram: Given the *dvr* values of different nodes , our goal is to group nodes with similar *dvr* values and use them as the core elements for the corresponding region. To this end, we bin the nodes based on their *dvr* values and generate a histogram to identify the most common values (i.e. "peaks") which in turn suggest the existence of different regions. To reduce the noise that the wide variation of *dvr* values for low degree nodes introduces, we first filter out all nodes whose degree is smaller than a threshold D_{min}. In fact D_{min} is a parameter that can be used to control the visibility of nodes that are under possible consideration for being selected as core elements. It provides a knob for examining the trade-offs that result from increasing the level of noise caused by a larger number of low degree nodes (i.e. small D_{min} values) – allowing for more noise typically results in the identification of a larger number of less reliable core elements and hence regions. Next, while the *dvr* values for higher degree nodes are significantly more reliable, these nodes may not have a profound impact on the shape of the histogram due to the often small fraction of high degree nodes. We deal with this issue by introducing a bias towards the *dvr* v alues of high degree nodes. In particular, for each high degree node, we multiply its *dvr* value by its node degree. In effect, we simply increase the frequency of the *dvr* values of the high degree nodes proportional to their node degree. The resulting *conditioned* histogram is in general more

amenable to reveal the presence of reliable regions since it has more pronounced peaks that are less sensitive to the value of D_{min} parameter.

3) Identifying Core of a Region From the Histogram: Identifying regions from a *dvr* histogram requires *(i)* determining a proper walk length that generates the best histogram, and *(ii)* detecting the regions from the resulting histogram. To deal with item *(i)*, we progressively increase the walk length and repeat steps (1) and (2) to generate the resulting histogram. We carefully examine the evolution of the histogram as a function of walk length and select the histogram where the peaks are most pronounced and most separated. By definition, such a histogram should be formed when the walk length is close to the mixing time of individual regions. In such a histogram, each peak (i.e. a local maximum that is surrounded by two local minimum values) represents a region's core whose range of *dvr* values is specified by the *dvr* values corresponding to the two minimum values. This heuristic can be viewed as a naive one-dimensional clustering technique. We examine the connectivity among nodes that are part of each core to ensure that they form a connected component[1]. This check also reveals whether the cores of two separate regions with overlapping *dvr* ranges appear as a single peak which makes it difficult to distinguish them from the histogram in the first place. At the end of this step, we have the number of regions and the list of high degree nodes that form the core of each region.

4) Mapping Low-Degree Nodes to Cores: We use the relative reachability of low degree nodes to identified cores in order to map them. To this end, we start N RWs from each node where each RW walk continues until it hits a node in one of the cores. Each walk provides a sample of reachability for this node. The node is mapped to the core with the

[1]It is not a required condition that core nodes form a connected component. However, forming a connected component does indicate that the core is coherent.

highest reachability. The fraction of RWs that hit the most reachable core indicates our confidence in mapping a node to that region.

5) Producing the Regional View: Once nodes in each region of the graph are identified, we determine the edges that are within each region or connecting two different regions. Then we produce a diagram that incorporates all the information about regional connectivity of a graph including *(i)* a circle represents a region with the area logarithmically proportional to the size of the region, *(ii)* arrows between two regions indicate the inter-region connectivity and their width as well as color is proportional with the relative fraction of directed half-edges between two regions. Intra region half-edges are represented with the modularity of a region and thus are not shown in the regional view to keep this less crowded.

Inferring vs. Exploring Regions

The design of WalkAbout provides several parameters or knobs that can be tuned to explore different coarse views of a given graph. These parameters include the walk length, the D_{min} threshold, and the precise nature of determining how low degree nodes get mapped to regions (core anchors). In essence, examining the effect of these parameters on the resulting regional views facilitates studying the quality of a given regional view in terms of its robustness to the choices WalkAbout offers to its users. In this sense, WalkAbout can be viewed as a framework for exploring regional connectivity in an interactive manner rather than a technique for producing a single regional view.

It is also important to emphasize that since WalkAbout is not trying to optimize an explicit objective function (e.g. modularity [201], the regional view that results from running WalkAbout for a given graph is not unique. Instead, by harvesting a transient phenomenon, we face a new challenge in the form of deciding on a proper walk length.

TABLE 1. Characteristics of LCC snapshots of target OSNs

	FL	TW	G+
Nodes	1.6M	41.6M	51.7M
Edges	31.1M	1,468M	869.4M
Louvain Communities	28K	24K	39.2K

Our approach to deal with this challenge is to gain an understanding of the sensitivity of a resulting regional view to the choice of the walk length to minimize potential mistakes at each step.

By varying the D_{min} parameter, we are able to explore the trade-off between level of coarsening and the accuracy of the regional view. Large values of this parameter typically result in few but reliable regions (i.e. coarse and stable view), while smaller values of D_{min} produce in general many more but less reliable regions (i.e. fine but unstable views). Alternatively, D_{min} can be set based on domain knowledge to only include nodes that are considered central for a given context. For example, in an OSN graph, nodes with degree larger than 500 or even 1000 may be viewed as core nodes. In this chapter, we primarily focus on the application of WalkAbout to OSNs and set D_{min} to 500.

We have developed WalkAbout as an interactive tool with GUI that allows users to arbitrarily slice the histogram and generate the resulting regional view in an interactive manner. This publicly available tool can be downloaded from the project web site [199].

WalkAbout in Action

In this section, we use our proposed technique to characterize coarse views of large popular OSNs such as Flickr, Twitter, and Google+. In the process, we not only demonstrate the key features and capabilities of our technique, but also show what sort of coarse views WalkAbout produces for the well-known OSNs.

Datasets and Methodology

In the following, we rely on anonymized snapshots of the largest connected component (LCC) of the social graphs of Flickr (FL) that was captured by Mislove et al. [191], a snapshot of the Twitter (TW) social graph that was collected by Kwak et al. [163], and a snapshot of Google+ (G+) from a recent study by Gonzalez et al. [119]. Table 1 summarizes the main characteristics of these snapshots.

When applying the WalkAbout technique to each OSN, we consider these snapshots as undirected graphs, i.e. converting any directed edge between two nodes (for TW and G+) into an undirected edge, and collapsing a pair of edges if they are reciprocal. For each OSN, we apply WalkAbout and show the following results: *(i)* the evolution of the conditioned *dvr* histogram (see Section 3.4) as a function of walk length to illustrate the selection of target walk length. *(ii)* the shape of the modified histogram at the target walk length that shows the peaks used for identifying individual regions, *(iii)* a table that summarizes the main features of the identified cores (number of nodes and the average degree in each core) and the corresponding regions (the percentage of total nodes and edges, average degree and modularity), and *(iv)* a sketch of the regional view of the OSN.

We refer to the collection of specified values for the WalkAbout parameters, namely D_{min} and wl, as the *target setting*. In particular, we used $D_{min} = 500$ throughout this analysis. To examine the robustness of our results to different choices of D_{min} values, we repeated our analysis with D_{min} values that are 10% larger or smaller and observed no significant differences.

TABLE 2. FL – Basic features of identified regions

	core		region			
Region	Size	Mean Degree	%Nodes	%Edges	Mean Degree	Mod.
$R0$	4.04×10^3	1.10×10^3	92.8	58.2	11.9	0.4
$R1$	5.69×10^2	1.01×10^3	1.2	3.2	50.1	0.5
$R2$	3.01×10^3	1.12×10^3	4.0	17.6	83.7	0.7
$R3$	2.12×10^3	1.35×10^3	1.8	16.6	174.2	0.6
$R4$	1.14×10^3	1.10×10^3	0.2	4.4	431.0	0.3

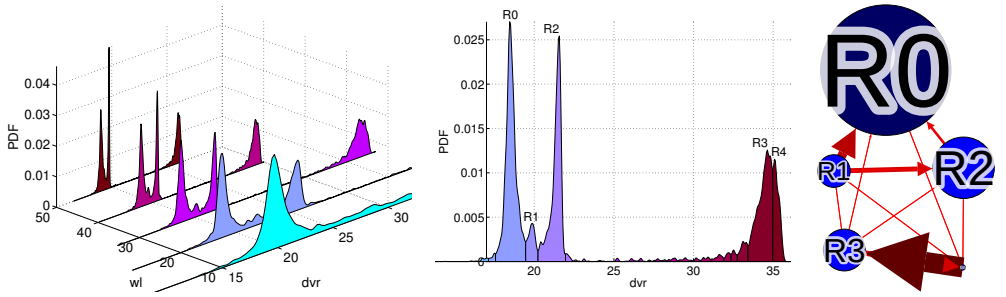

(a) Effect of wl (b) *dvr* histogram at the target setting, $wl = 30$, $D_{min} = 500$ (c) Regional View

FIGURE 3.7. Applying WalkAbout to Flickr snapshot

OSNs & Their Regional Views

The regional characteristics of our target OSN evaluated by WalkAbout are as follows:

Regional View of Flicker (FL)

Figure 3.7(a) shows the evolution of *dvr* histogram for a FL snapshot as a function of walk length around the selected target setting ($wl = 30$, $D_{min} = 500$). We observe that $wl = 30$ reveals the largest number of pronounced peaks; i.e. a total of five peaks. Figure 3.7(b) shows the shape of *dvr* histogram at our selected target setting for FL where the five major peaks are marked and their associated ranges of *dvr*-values are colored. Note that regions R_3 and R_4 could have been considered as a single region. However,

because of the observed dip around $dvr = 35$, we split that peak into two regions. We later discuss the effect of this decision. Due to their small sizes and to keep the number of regions within limits, we did not consider several very small peaks in the middle of the histogram whose *dvr* was $21.96 < dvr < 33.4$ and contained between 1 to 100 nodes (with the median of 8 nodes). This is indeed one way to explore the tradeoff between the accuracy or resolution (by keeping many core components) and complexity of the resulting view. Note that WalkAbout reveals these peaks and allows us to explore them if a higher resolution is desired.

Table 2 summarizes the key features of the five identified cores and their corresponding regions. We observe that the cores include between 500-4000 nodes and collectively contain less than 1% of nodes of the graph. Except for R_1, they are all of similar sizes. The resulting regions are very imbalanced, with R_0 containing more than 92% of all nodes and 58% of all edges and having average degree of 11.9 and modularity of 0.4. The other regions are very small and contain only some 0.2%-4% of all nodes. However, regions R_2 and R_3 have a high average degree and thus include a much larger fraction of edges. At the same time, regions R_2 and R_3 have a much higher modularity than R_0. All the identified cores and regions form connected components. Figure 3.7(c) sketches the regional view of the FL structure. This figure shows that for all practical purposes, regions R_3 and R_4 are weakly connected to the other three regions. We recall that these two regions are created as a result of splitting the right most peak of the *dvr* histogram into two parts. Given their strong inter-connectivity, an option would be to merge these two regions together and consider them as a single region, thus producing a yet coarser view of the FL connectivity structure.

TABLE 3. TW – Basic features of identified regions

	core		region			
Region	Size	Mean Degree	%Nodes	%Edges	Mean Degree	Mod.
$R0$	8.05×10^4	1.02×10^3	2.6	4.5	124.2	0.4
$R1$	2.75×10^5	1.47×10^3	54.1	31.0	40.4	0.3
$R2$	2.72×10^5	2.16×10^3	40.8	42.6	73.5	0.2
$R3$	1.20×10^5	4.70×10^3	2.5	20.7	596.2	0.4
$R4$	4.57×10^3	5.21×10^3	0.01	0.8	3 167.7	0.4
$R5$	1.90×10^3	5.83×10^3	0.002	0.4	4 066.3	0.4

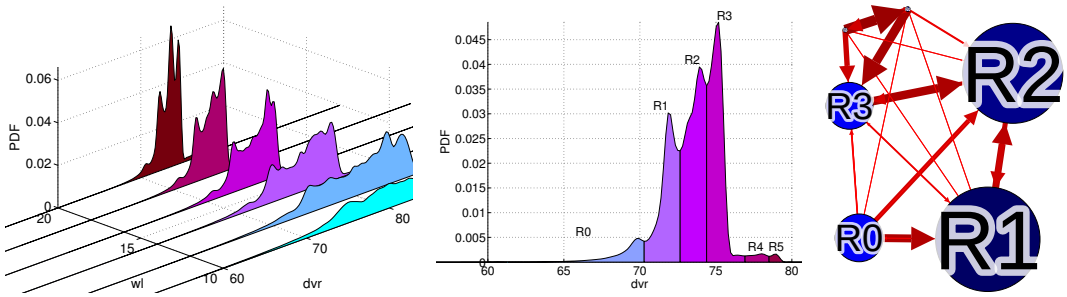

(a) *dvr* histogram vs wl (b) *dvr* histogram at the target setting, $wl = 18$, $D_{min} = 500$ (c) Regional View

FIGURE 3.8. Applying WalkAbout to Twitter snapshot

Regional View of Twitter (TW)

Figure 3.9(a) depicts the evolution of the *dvr* histogram for the TW social graph as a function of wl where $D_{min} = 500$. We observe that the transition phase for the formation of peaks for different regions is rather short, between wl values of 14 and 22. We select $wl = 18$ for our target setting as it reveals the most clear set of peaks in the histogram. Figure 3.8(b) depicts six peaks in the *dvr* histogram at our target setting.

Table 3 summarizes the main characteristics of the identified cores and their corresponding regions. We observe that the cores have between 1.9K and 275K nodes. There are two large (R_1 and R_2), two rather small (R_0 and R_3), and two tiny (R_4 and R_5) regions. The regions generally exhibit low modularity (≤ 0.4). The low level

of modularity for regions in TW indicates that regions do not exhibit tight internal connectivity. An interesting fact about the two tiny regions is that they have an order of magnitude larger average degree than the other regions but still exhibit the same modularity. Figure 3.8(c) depicts the resulting regional view for the TW structure and reveals that regions R_1 and R_2 have strong mutual connectivity and play a central role in the graph. R_0 is connected to R_1 and R_2 from one side while R_5, R_4 and R_3 form a triangle structure that connect to the rest of the regions primarily through R_2.

Regional View of Google+ (G+)

Figure 3.9(a) depicts the evolution of the *dvr* histogram for the G+ graph as we change wl. The histogram which most clearly reveals different regions is formed around $wl = 20$. Therefore, we select this wl as our target setting. The corresponding histogram is shown in Figure 3.9(b) and reveals the existence of six distinguishable peaks. While the regions R_4 and R_5 result from rather small peaks, we still use them as cores because they are clearly separated from other peaks and also have large average degrees.

TABLE 4. G+ – Basic features of identified regions

	core		**region**			
Region	Size	Mean Degree	%Nodes	%Edges	Mean Degree	Mod.
$R0$	2.18×10^5	1.73×10^3	82.0	62.8	25.8	0.3
$R1$	4.00×10^4	7.13×10^3	16.3	33.5	69.2	0.6
$R2$	6.51×10^3	1.70×10^3	0.6	1.0	54.2	0.7
$R3$	9.94×10^3	2.28×10^3	0.9	1.9	73.8	0.8
$R4$	7.40×10^1	3.71×10^4	0.2	0.5	74.5	0.7
$R5$	1.45×10^2	1.78×10^4	0.1	0.3	175.4	0.6

Table 4 summarizes the main features of the identified cores and regions. We observe that the core sizes vary between 74 and 218k which is much more skewed

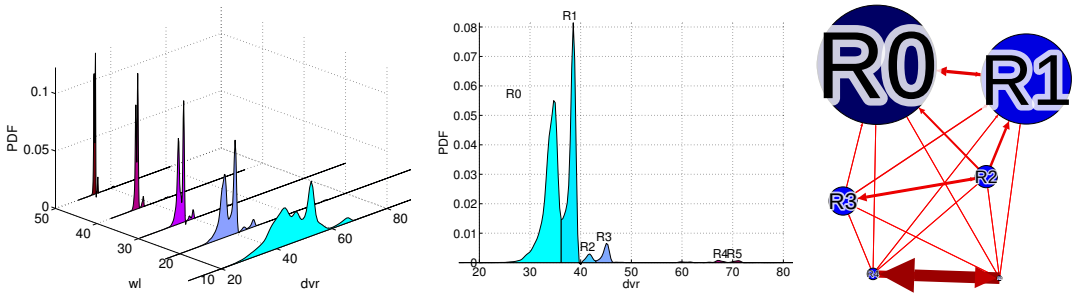

(a) *dvr* histogram vs wl (b) *dvr* histogram at the target setting, $wl = 20$, $D_{min} = 500$ (c) Regional View

FIGURE 3.9. Applying WalkAbout to Google+ snapshot

compared to the other OSNs. These cores lead to a dominant region R_0, a moderate-sized region R_1, and four tiny regions. All regions except for R_0 exhibit a rather high modularity (0.6-0.8). Figure 3.9(c) plots the regional view of the connectivity structure for G+. We observe that R_4 and R_5 are tightly inter-connected but have a weak connectivity to the other regions. The other four regions have a moderate chain-like inter-connectivity structure of the form R_2-R_3-R_1-R_0.

Lessons Learned

The obtained regional views of the connectivity structures of some of the most popular OSNs provide a novel and useful abstraction of the large-scale real-world systems. They offer a manageable high-order view of how nodes are mapped into various regions of different sizes, along with a quantitative assessment of the corresponding inter- and intra-region connectivity.

A common observation from applying WalkAbout to the three OSNs is that separate regions (peaks) with close-by *dvr* values tend to have stronger inter-region connectivity than regions that result from clearly separated peaks in the *dvr* histogram. Such behavior is to be expected for real-world graphs. For one, our approach for mapping high degree

nodes to cores based on slicing peaks in the histogram is ambiguous for high degree nodes whose *dvr* values are close to the border value of a region. Moreover, the size of a region and its mixing time can vary widely across different regions of a large graph. This in turn makes the selection of a proper walk length challenging. For example, a particular walk length that is close to a region's mixing time and thus clearly reveals the associated peak in the *dvr* histogram could be too long for other regions. This behavior can cause some of the RWs of other regions to leave their starting points and move to other close-by regions. The fraction of such "misbehaving" RWs depends on the walk length and the relative connectivity between starting and neighboring regions. Both of the above factors tend to decrease the gap between the *dvr* ranges of close-by regions proportional to their pairwise connectivity. However, given the coarse resolution of the considered regional views of a graph, the resulting ambiguities do not significantly impact the value that can be derived from examining such coarse views of large-scale graphs.

Also note that the number of peaks that appear in a *dvr* histogram changes with the walk length which, in turn, can change the perspective of what peak size should be considered to be significant. Our focus here has been on considering only a handful of regions so that the resulting regional views are manageable. WalkAbout is clearly an interactive framework and can be used to identify a different number of regions and examine how such selections affect the characteristics of the resulting regional views.

As our results show, the identified regions by WalkAbout could be very imbalanced in size. In particular, a large region may consist of two or more smaller regions that are not properly recognizable during the first round. One way to explore the structure of these larger regions is to apply WalkAbout to each identified regions. This hierarchical application might be able to identify the internal structure (sub-regions) of a large region

if they have sufficiently distinct average degrees and shorter mixing time than the entire region. This issue remains as a future work for us to explore in more detail.

The other proposal that is left as future work is to utilize the *dvr* values computed at various walk lengths for clustering the vertices in the core. In this schema, each node will be associated with a vector of *dvr* values for a range of walk lengths during which the *dvr* histograms exhibit separation between peaks. Classic clustering techniques such as Gaussian Mixture Models or K-means can be used to identify cluster of nodes that have similar *dvr* values at different walk lengths, are indeed in areas in the graph with similar average degree. This approach can be used to *(a)* identify regions that have different mixing times, and *(b)* automate the process of region identification in graph.

WalkAbout as an Interactive Tool

We have implemented WalkAbout as an interactive tool for browsing coarse-view of connectivity for large graphs. Our tool accepts the edge view of a large graph and produces *dvr* histogram. A user can browse through the evolution of the histogram as a function of the walk length and D_{min} to select its desired parameters, and then focus on the desired histogram to interactively determine the number and location of individual peaks (regions). Our tool then generates the input for viewing the resulting regional view on an existing visualization program (such as Gephi [36]). The key feature of our tool is the ability for a user to interact with the process to determine the proper parameters based on those interactions. Our tool is publicly available at the project webpage [199].

Regions vs. Communities

Community detection in graphs is a commonly used technique that can also be viewed as providing a coarse view of a graph (i.e. community-level instead of regional-

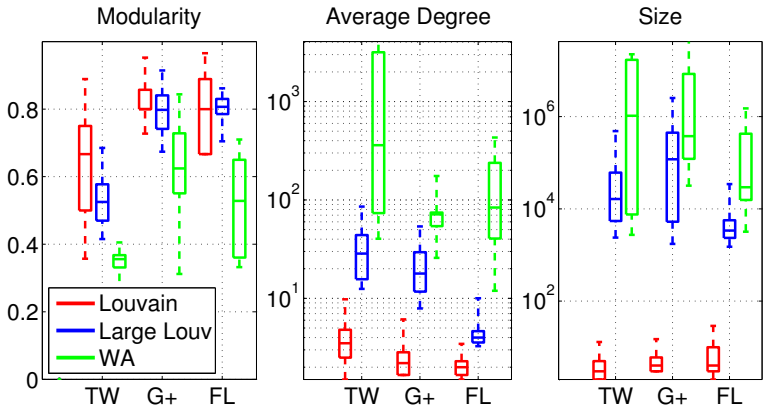

FIGURE 3.10. Comparison of Louvain communities and WalkAbout regions.

level view). Community detection techniques typically group nodes into tightly connected groups, called a community, based on an objective function (e.g. modularity) and present characteristics of the detected communities without emphasis on the inter-community connectivity. In this section, we compare and contrast the regional view that WalkAbout produces with the community view of a large graph. Given the similarity between the notion of a "community" and a "region", and the popularity of applying community detection techniques for graph analysis, this comparison helps us relate the regional view of the graph with a related concept (i.e. community) that is widely used. To this end, we have to run a community detection technique on our large target graphs. Unfortunately, most of the commonly-used community detection techniques do not scale to graphs with more than tens of millions of nodes [84], or require the number of communities as an input (e.g. Metis [150, 151]), or recursively partition the graph into balanced communities that may not lead to the most tightly connected communities [150]. Due to these limitations, we use the *Louvain community detection technique* [40] that implements a greedy method to optimize the "modularity" of identified communities. Louvain is often considered to be the gold standard for scalable community detection and has a publicly available and robust implementation.

We applied Louvain to our targeted OSN structures and identified 28K, 39K, and 24K communities of various sizes in FL, G+, and TW, respectively. Importantly, these results show that *the number of communities in these graphs are several orders of magnitude larger than the number of regions. This large number of communities implies that the graph connectivity at the community level is still too complex for high-level analysis (e.g. determining the full picture of inter-community connectivity.)*

Figure 3.10 presents the summary distribution of the main features (modularity, size and average degree) across all regions and all communities associated with each each OSN. It has been shown that community detection techniques such as Louvain tend to identify a large number of small communities to achieve a high modularity score [169]. To examine the effect of community size, we have also included the results where we only consider the large communities that consist of 1000 or more nodes. We observe that communities are typically more than four orders of magnitude smaller than regions. However, size-wise, the largest communities clearly have an overlap with the obtained regions. While the modularity of communities is typically higher than the modularity of regions, this gap is more pronounced in less clustered graphs (e.g. TW) than in more clustered graphs like FL and G+. Also, the large communities exhibit higher modularity than the WalkAbout-derived regions, and the average degree of the communities is smaller than its counterpart for regions (irrespective of community size).

To gain more insight into connectivity-related features, we examine the placement of the 1000 nodes with the highest degree in each region across the different communities. Interestingly, we find that in all three OSNs, the top 1000 nodes are located in 5 or 6 communities, with some of those communities attracting significantly more nodes than others. Moreover, both the size (15K-359K for FL, 72K-22M for TW, and 336K-16M for G+) and the modularity of these few communities (0.48-0.75 for FL, 0.28-0.78 for

TABLE 5. Number of mapped communities to each region

FL

Region	Communities
$R0$	26 987
$R1$	173
$R2$	639
$R3$	251
$R4$	7

TW

Region	Communities
$R0$	142
$R1$	13 171
$R2$	10 003
$R3$	724
$R4$	9
$R5$	5

G+

Region	Communities
$R0$	29 577
$R1$	9 545
$R2$	93
$R3$	32
$R4$	18
$R5$	2

TW, and 0.35-0.89 for G+) are comparable with typical values for the WalkAbout-derived regions. *These results suggest that the large communities that are needed for accommodating high-degree nodes exhibit characteristics very similar to the WalkAbout-identified regions.*

Mapping Communities to Regions

To further explore the relationship between the community- and regional-level views of these graphs, we map individual Louvain communities to the identified regions for the same graph. In particular, for each community c, we determine the region where each node of this community is located and identify the region R that contains a majority of nodes in that community. Then community c is mapped to that region R that hosts a majority of its nodes, and the confidence for this mapping is equal to the fraction of c's nodes that are located in R. Table 5 summarizes the number of communities that are mapped to the individual regions of each OSN. In the extreme case, if the nodes in each community are randomly located in different regions, then all communities are mapped to the largest region(s) with a confidence equal to the region's relative size. We observe that the mapping confidence for 75% of the communities in every single region is 100%, and for 90% of communities, all but one small region in FL (R_4) has a mapping confidence

higher than 80%. Even for the large communities with more than 1K nodes, the mapping confidence for 90% of them is larger than 80% for all regions of all OSNs except for TW, where it is 60%. *These results clearly demonstrate that the vast majority of nodes in most communities are mapped into a single region. This in turn suggests that a region can be viewed as a collection of connected communities and thus offer a coarser view of the graph.*

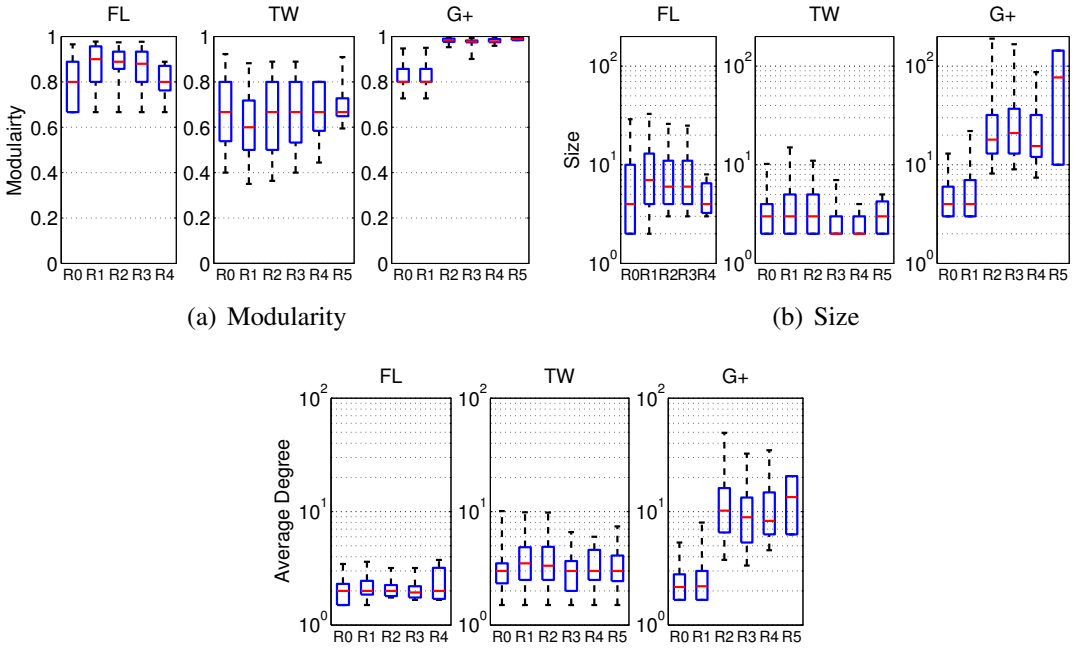

(a) Modularity (b) Size

(c) Average Degree

FIGURE 3.11. Characteristics of Louvain communities mapped to different WalkAbout regions

Per-region Analysis of Communities

We now examine the group of communities that are mapped to each region to determine whether they exhibit any distinguishing features. Figure 3.11 uses box-plots to summarize the distribution of modularity, size and average node degree across

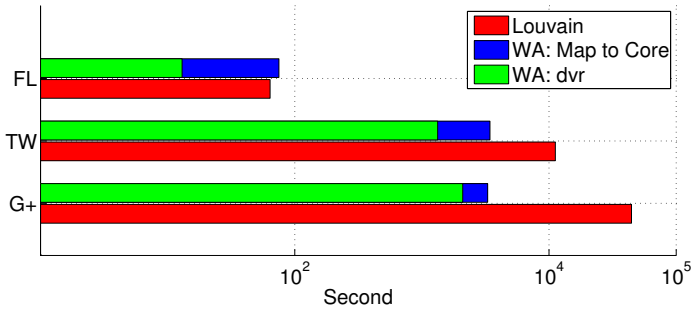

FIGURE 3.12. The comparison of the execution time for different techniques.

all communities that are mapped to each region of individual OSNs. These figures illustrate that there does not appear to be a strong correlation between the modularity of communities in a region and the modularity of the entire region. This observation is explained by the fact that the modularity of a region depends, among other factors, on the inter-community connectivity. We also observe that in general, there is no significant difference in the modularity, size and average degree of the communities that are mapped to each region, i.e. regions are not generally distinguishable based on the characteristics of their communities despite the difference in their average degree and size. The only exceptions to this observation are regions R_3, R_4 and R_5 in G+ that contain communities with a significantly higher and more homogeneous modularity, larger size and higher average degree. This is intriguing since larger size or higher node degree could lead to lower modularity in a single community. *These findings suggest that identifying individual regions by merging communities in a bottom-up fashion (using modularity) is in general challenging. Alternatively, a top-down approach to region detection such as WalkAbout shows more promise.*

Comparing Run-time

Finally, we compare the run times of WalkAbout and the Louvain community detection technique on an Intel X5650 2.66GHz computer with 72GB RAM which is sufficient to hold the entire social graph of any target OSN in memory. Figure 3.12 shows the comparison of the run time per individual technique over each OSN using log scale for the x-axis. We further split the run time of WalkAbout into two components: *(i)* the calculation of the *dvr* values for high degree nodes to detect cores and *(ii)* mapping of low-degree nodes to those cores. These results show that the run times of both techniques are similar over small graphs (e.g. 10 second difference for FL). However, as the graph size increases, Louvain requires a significantly longer run time and the gap between WalkAbout and Louvain seems to be widening. We also recall that for graphs of the size of these OSNs, many popular community detection or graph clustering techniques (including spectral clustering [72]) quickly run into scalability issues and cannot be used at all [107].

A New Kind of Validation

So far we have primarily focused on the connectivity features of regions and how they are aligned with smaller entities in a large graph such as communities. Since regions are not derived based on an objective function, there is no obvious way to validate/examine their accuracy. To tackle the challenging problem of "validation" of WalkAbout-derived regions, we conduct a case study to investigate *whether users in each identified region exhibit similar social attributes that act as the underlying factors for the formation of the region*.

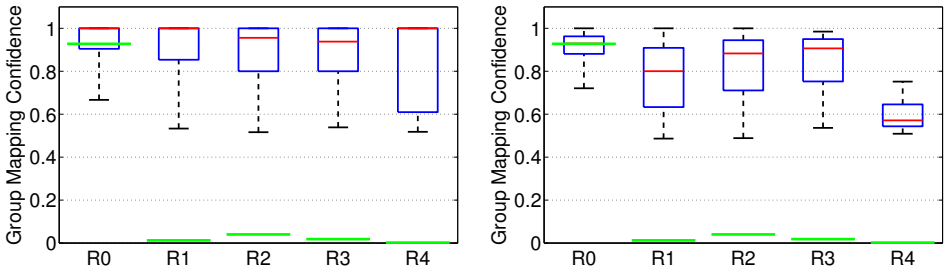

(a) FL – 99K groups (b) FL – 44K large groups

FIGURE 3.13. Distribution of confidence in mapping groups to identified regions. Large groups have more than 10 members.

Are Regions Meaningful?

Our ability to answer the posed question depends on the availability of semantically-rich metadata that contains social context. However, given adequate metadata, answering the above question will shed light on whether an identified region represents a meaningful portion of an OSN. In our case study, we focus on FL because of the availability of rich metadata with social context for this OSN.

More precisely, for our FL snapshot, we have a list of 99K social groups (with their names) where each group consists of a collection of users with common interest. A user can be a member of multiple groups. The names of most groups provide great deal of information about the groups' interests or context (e.g. big_and_hot, bigblkmuscles, bigbulls, boys, everydaymen, fatboys). Similarly to the mapping of communities to regions (Section 3.6), we map each group to a region where most of their users are located. Figure 3.13(a) and 3.13(b) shows the summary distribution of mapping confidence for all groups and for the 44K groups with more than 10 users to the five regions in FL, respectively. We observe that groups that are mapped to regions R_1-R_4 exhibit a very high confidence despite the small size of these regions. The mapping confidence drops for larger groups but it is still a couple of orders of magnitude larger

than the relative size of the group. More specifically, regions R_1, R_2, R_3 and R_4 make up 1.2%, 4%, 1.8%, and 0.2% of nodes in the graph but the typical confidence for their mapped groups is 0.8, 0.9, 0.92, and 0.58, respectively. These results suggest that the social context of each group is likely a driving force for its mapping to these four regions. In contrast, the typical confidence for mapped groups to region R_0 is comparable to its relative size. This indicates that social forces discernible from our data may not be primarily responsible for the mapping of groups to region R_0. To learn the context of individual regions, we manually examined the names of groups that are mapped to that region. Our examination reveals a very pronounced pattern among group names associated with the following regions[2]: Group names in R_1 are mostly related to male nudity and adult content, group names in R_2 are hinting at female nudity and adult content, and group names in both R_3 and R_4 have a common ethnic attribute, i.e. either have Arabic names or posts in Arabic, which is aligned the finding is Section 3.5 that positions the two regions in close proximity of each other. As expected, group names in R_0 do not show a coherent theme.

Are Communities Meaningful?

We use the same methodology to examine the "validity" of communities; i.e. checking whether the names of mapped groups to individual communities indicate a common social theme in the community. In the case of regions without any pronounced social theme (e.g. R_0), one of their large communities may indeed have a social context whereas for regions with an existing social context (e.g. R_1), a community may offer an even more specific context. The large number and diverse size of communities in the FL

[2]The spreadsheet of FL group names that are mapped to each FL regions (or community) are available online at `http://onrg.cs.uoregon.edu/WalkAbout/group_per_region/`

social graph make it difficult to examine all communities. Since small communities do not provide sufficient information to identify their social theme, we only focus on the three largest communities that are mapped to each region of FL. Careful examination of names of groups that are mapped to each one of these large communities reveals that large communities in R_0 do not seem to have any social theme and large communities in all other regions often exhibit a theme that is very similar to the identified theme for the whole region. The only exception is a community in R_2 that contains groups with clearly more specific group names. In summary, our preliminary investigations suggest that some large communities that are embedded within a region are not "meaningful" in the sense that they exhibit rather diverse social themes that makes them not much more focused than the WalkAbout-identified region in which that they reside.

Summary

In this chapter, we present a new scalable framework called WalkAbout for examining and inferring regional views of connectivity for very large graph and demonstrate its application to three well-known OSNs. Moreover, we conduct a comparison between regional- and community-level views of large OSN and present a case study where we "validate" the individual regions and communities; i.e. examining in detail the available meta-data for social themes that are associated with the obtained groupings of nodes in an OSN and are prime candidates for the root cause(s) behind the formation of these groupings.

The presented design of WalkAbout and the experience we gained from applying it to real-world OSNs suggest a number of extensions and improvements. We are currently exploring the usage of different walk lengths for computing a *dvr* vector, as opposed to a single *dvr* value, that could result in identification of region cores at different

random walk lengths. We also plan to explore the recursive application of WalkAbout to identify potential sub-regions within each identified region. In the same vein, we intend to examine how the regional- and community-level views of a large graph can inform each other to yield a hybrid approach for a "multi-scale" exploration of the graph's connectivity (e.g. examining the connectivity between large communities within a given region to obtain a higher-resolution view of graph connectivity). Extending WalkAbout to allow for overlapping regions by dealing region core as landmarks in the graph is another line of future research. Finally, collecting semantically rich meta-data that enables the illustrated validations of groupings such as regions, clusters, or communities is another item on our research agenda in this area.

CHAPTER IV

CHARACTERIZING AND COMPARING GROUP-LEVEL USER BEHAVIOR IN MAJOR ONLINE SOCIAL NETWORKS

The research conducted on the characterization of Online Social Networks in the last years has created a solid basis to address fundamental, yet challenging issues such as identifying the most suitable OSN for different purposes (e.g. broadcasting information or obtaining feedback) and defining initial guidelines for an informed utilization of OSNs. What is necessary to address many of these issues is a quantitative comparison between the behavior of users in different OSNs. The challenge is, however, the large size of these networks, which renders such a comparison not trivial. On the other hand the user properties and behavioral attributes are reported to be skewed which further complicates this comparison. In this chapter, we propose a new methodology for a detailed measurement study to characterize and compare the behavior OSNs at the "group-level". Based on this methodology, we conduct a comparative analysis on the behavior of users in Facebook (FB), Twitter (TW) and Google+ (G+). We focus on Popular, Cross (with account in three OSNs) and Random groups of users in each OSN since they offer complementary views. We capture user behavior with the following metrics: user connectivity, user activity and user reactions. Our group-level methodology enables us to capture major trends in the behavior of small but important groups of users, and to conduct inter- and intra-OSN comparison of user behavior. Furthermore, we conduct temporal analysis on different aspects of user behavior for all groups over a two-year period. Our analysis leads to a set of useful insights including: *(i)* Popular Facebook users have 4 and 47 times more followers than Popular Twitter and Google+ users, respectively. *(ii)* The more likely reaction by Facebook and Google+ users is to

express their opinion whereas Twitter users tend to relay a received post to other users and thus facilitate its propagation. Despite the culture of reshare among Twitter users, a post by a Popular Facebook user receives more Reshares than a post by a Popular Twitter user. *(iii)* Added features in an OSN can significantly boost the rate of action and reaction among its users.

Introduction

Major Online Social Networks (OSNs) such as Facebook or Twitter are among the most popular services on the Internet with billions of subscribers and hundreds of millions of daily visitors. OSNs enable individual users to connect to other users, disseminate their information throughout the network while collecting the reactions from other users without any geographic or time constraint. These unique capabilities have motivated different entities, ranging from individuals and celebrities to companies and sport teams to join OSNs often with different goals. For isntance, OSNs enable individual companies to closely interact with their customers and receive feedback on their products [42]. The growing popularity of major OSNs has effectively turned them into "online societies" with a profound impact on the social, political and economical aspects of our daily lives.

The growing importance of large OSNs raises a basic question: *How do users behave with respect to publishing posts and reacting to other users' posts in a specific OSN?* Shedding any light on these seemingly simple questions not only informs current users of an OSN that to what extent an OSN might serve their goals but also enables non-member entities to assess whether the OSN might be a fit for their needs. To underscore the importance of these issues, it is worth noting that many companies pay large premiums in order to adopt various techniques that may help them attract a larger

number of active followers in a major OSN. However, tackling the above questions is challenging for several reasons including the following: First, users in an OSN often exhibit a diverse characteristics with skewed distributions [97]. Identifying interesting groups could be difficult specially if there is not a reliable way of identifying their users. Second, existing theories and techniques in "behavioral sciences" are not easily applicable to OSNs in large scale because they often require the collection of specific data through customized questionnaires which is not feasible for large scale data collection over OSNs. Third, even characterizing the behavior of individual users based on their basic attributes (e.g. connectivity, posted content and their reactions) could be complex due to the difficulties in determining user intentions (for establishing a connection, or generating a post, or reacting to other users' posts). Fourth, in the absence of a uniform methodology to characterize user behavior across multiple OSNs, it is not feasible to meaningfully compare and contrast them. In the face of these challenges, a large body of prior empirical research on OSNs has often focused on specific characteristics of a single OSN such as user connectivity [119, 163, 117], evolution of OSN size [217] or user behavior [127, 275].

In this chapter, we characterize and compare the behavior of users in three major OSNs, namely Facebook (FB), Twitter (TW) and Google+ (G+). The first contribution of this study is our methodology which relies on "group-level" data collection, characterization and comparison. We focus on the following three interesting groups of users in each OSN as follows: *Popular* users with a very large number of followers, *Cross* users with verified accounts in all three OSNs, and *Random* users. Popular users represent the most well-connected entities in each OSN while Cross users are entities with common interest in all three OSNs and Random users show the behavior of the crowd (i.e. many low-degree, moderately active users). Our approach to characterize user behavior

at the group-level has several advantages: *(i)* It allows us to cope with the diversity of user behavior which is expected to be much more homogeneous within each group, *(ii)* it naturally lends itself to sampling as we need to focus on sample users in selected groups, *(iii)* we can meaningfully compare the behavior of similar groups in different OSNs, and *(iv)* comparing the behavior of different groups in a single OSN often offers a valuable insight. We rely on three set of metrics to characterize the behavior of a user in each group: the *connectivity* of the user in the social graph, the *activity* of the user with respect to publishing posts, and the *reaction* of other users (e.g. likes and comments) to the user's posts.

The second contribution of this study is a detailed measurement that presents a head-to-head comparison between FB, TW and G+. We carefully populate the three target groups in each OSN, collect their information using custom crawlers and characterize the group-level behavior using our three sets of metrics as we present in Section 4.2. In particular, users in the Cross group allow us to view and compare the ecosystem of these three OSNs from the perspective of the same set of users. Using the collected information for users in target groups, we conduct group-level characteristics of users by examining different aspects of their connectivity (in Section 4.4), activity (in Section 4.5) and received reactions to their posts (in Section 4.6). We also conduct temporal analysis on the daily rates of actions and reactions for each groups in different OSNs in Section 4.8. Our analysis leads to a series of inter- and intra-OSN comparison between groups that reveal to the following important insights:

(i) TW is the OSN that observes a higher volume of information (i.e. posts). However, despite the lower volume of posts, FB presents a higher volume of reactions. G+ is currently far behind both FB and TW in both the volume of activities and reactions,

except in the case of Popular G+ users that exhibit a similar level of activity to Popular FB users.

(ii) Our results indicate that TW users prefer to broadcast (i.e. Retweet) information posted by their friends whereas in G+ users prefer to provide feedback (in the form of Comments or Likes). FB users also show a preference toward feedback reactions, however the number of Reshares per post is equal in FB and TW.

(iii) The level of popularity among Popular users in major OSNs seems to be dictated by external factors and is not influenced by the level of activity of users in the OSN. However, popularity is correlated with both level of activity and reactions among unpopular users.

(iv) Posts including photos and videos are more attractive compared to posts including a link or text only posts. However, videos are still one of the least common types of posts representing less than 11% of all posts.

The previous observations help to shed a light on some of the initial questions. In particular, we conclude that:

(i) TW seems to be the most suitable OSN for users interested in consuming information (i.e. readers) due to the higher volume of information in that OSN. Furthermore, TW or FB would be the more appropriate OSN for those users interested on propagating their information (e.g. advertisement campaigns), and FB and G+ are also a great fits for users interested in obtaining feedback (e.g. from voters or fans).

(ii) Popular users do not need to be very active in major OSNs to increase their popularity. Instead, users interested in attracting more reactions should focus on publishing photos and videos.

Methodology & Datasets

Characterizing user behavior is challenging because user attributes often exhibit a very skewed distribution in major OSNs. Therefore, any characterization of the overall user population in an OSN would primarily represent a significant number of users with a low level of connectivity to the rest of social graph andmoderately active users. Clearly such characterization does not reveal much about other important group of users (e.g. users with a large number of followers) if they only compose a very small fraction of total user population. Furthermore, the characteristics of individual users in a specific group may also significantly vary. To cope with these issues, we conduct our analysis at the group-level rather than user-level since the collective characteristics of users in a group offer a more reliable measure of their behavior. We consider the following three groups of users that intuitively represent complementary subsets of user population in each OSN:

- *Random users* provide a global view of user population that primarily represents a large fraction of typical users with moderate to low connectivity and activity (i.e. the crowd).

- *Popular users* attract the largest number of followers in an OSN and thus represent the most visible (i.e. well connected) accounts in an OSN.

- *Cross users* represent samples of users that have an account in all three target OSNs. Having a concurrent footprint in all three OSNs suggests the particular interest among these users and a special role that they might play in the overall ecosystem of major OSNs.

Considering these three groups in each OSN enables us to conduct meaningful comparisons between different groups within each OSN or similar groups across different

OSNs without the need for capturing a complete snapshot of individual OSN which is not often feasible. While we generally refer to an account in each OSN as a "user", each account can clearly represent many other entities ranging from celebrities and politicians to companies and sport teams. Next we briefly describe our techniques for populating the dataset of each group.

Random Users

Given various constraints for data collection from each OSN, we need to use a different approach to select random users in each OSN: For G+, we have collected a snapshot of the largest connected component (LCC) of the network and selected a random subset of LCC users. FB offers two types of accounts: *(i) regular accounts* and *fan pages*. Regular accounts are created by individual users and their number of friends is limited to only 5K[1]. Fan pages, however, are created by individuals, groups and companies in order to broadcast information to their fans as they do not have any limitation on the number of followers. In order to properly compare inter- and intra-OSN comparison between groups, we only focus on random fan pages (or pages) in FB. FB provides an indexed list of all the fan pages[2], that allows us to easily identify a random subset of these users. Finally, we select random TW users by examining random IDs that are associated with valid users [217]. Toward this end, we monitor TW's public timeline to detect some of the newly generated accounts and use a conservative estimate for the valid range of ID space.

[1]We recall that connections between FB users are bidirectional. Thus, the number of followers and friends for each users is the same.

[2]`https://www.facebook.com/directory/pages`

Popular Users

This group includes accounts with a very large number of followers (i.e. popular users). In G+, we have selected accounts from the LCC with the largest number of followers. Since capturing complete snapshots of TW and FB are not feasible due to their large size and the limitations imposed by their APIs, we have relied on external sources[3] to obtain sorted lists of 20K most popular users. We have crawled the reported 20K most popular users in each OSN to collect their up-to-date number of followers and determine their proper ranking within the list of most followed accounts. Our approach to identify popular users is reasonable since *(i)* very popular users in major OSNs are often well-known in the marketing and social-media communities, and *(ii)* potentially missing few popular users from this group should not qualitatively affect our analysis.

Cross Users

Identifying users that have an account in all three OSNs is a non-trivial task. To achieve this goal, we leverage the explicit links that G+ users provide to their FB and TW accounts in their profiles. We examined all G+ users inside its LCC and identified all G+ users with explicit links to their TW and FB accounts. We filtered users who provided more than one links to another OSN[4] and identified 7.3K G+ accounts with exactly one link to FB and TW. We have manually inspected some of these "triplet accounts" and confirmed that they are associated with the same individual user or company in all cases.

[3] `www.socialbakers.com`, `www.alianzo.com`, `www.twitaholic.com`

[4] Our closer inspection revealed that some of these users improperly set these links, e.g. listing links to their favorite accounts in another OSN.

While we have a large number of random and popular accounts from all three OSNs, we limited the number of users in all groups to 7.3K (i.e. the size of the Cross group) in order to ensure a proper comparison.

Collected Information

We have developed a separate crawler for each OSN that uses its API features to collect the following information for the selected users in each group:

- *User Profile*: The profile provides the number of followers and friends and (in some OSNs) the creation otime of user account. If account creation time is not explicitly specified in the profile, we use the time of first user post as a good estimate for its creation time.

- *Account's Activity*: In this study, all the public posts (or tweets) generated by the user along with their timestamps make up its activity. This information enables us to classify collected posts based on their content into five categories: "text", "video", "photo", "link" and "other"[5]. Examples of "other" post types are check-in in FB and Hangout in G+. One limitation in collecting account activity is that the TW API only provides the last $3\,200$ tweets for each user. This implies that the captured tweet history for very active TW users could represent a limited recent window of time in case the user published more than 3.2K tweets. We discuss the implications of this limitation on our analysis in Section 4.8. Throughout this chapter we use the terms post and tweet interchangeably.

- *Reactions to Posts*: For any captured public post, we also collect all the following types of public reaction to the post: *(i)* Likes (in FB), +1s (in G+) and Favorites (in

[5]Twitter only supported "text" and "link" type of posts at the time of this study.

TW) are reactions by other users who indicate their interest to a post; *(ii)* Shares (in FB), Reshares (in G+) and Retweets (in TW) are reactions by which a user relays a received post to her followers; *(iii)* Comments on a post are (positive or negative) reactions by other users. Note that the support for retrieving comment reactions did not exist in the TW API at the time of our data collection. For clarity of discussion in the rest of this chapter, we will refer to these types of reactions as Likes, Reshares and Comments, respectively.

Crawlers

Further details about our crawlers and their performance is as follows.

Facebook crawler: This crawler receives a user ID (or username) as input and uses the FB API to collect the number of fans, the posts as well as all the reactions to each individual post of that user. Furthermore, the crawler allows the gathering of more detailed information such as the type of post. To gain access to posts (and other information) the FB API requires the use of a valid access token that is provided to registered FB applications. In addition, FB imposes a maximum number of 600 queries in the period of 10 minutes. In order to speed up our crawling process we use multiple instances of the crawler working in parallel.

Twitter crawler: Our TW crawler receives as input a user identifier that can be either a TW id or screen-name and queries the TW API to obtain the user's profile attributes, the total number of published tweets, and the most recent $3\,200$ tweets published by the user along with the number of reactions associated with each one of the user's tweets. Consequentially if a user has published more than $3\,200$ tweets, we can only retrieve the last $3\,200$. At the time of this study, TW imposed a limit of 150 requests per hour per IP address. To overcome this limitation, we used PlanetLab [71] infrastructure to parallelize

our data collection process. Specifically, our crawler sends requests to TW API using approximately 450 PlanetLab machines as proxies[6], so that we can multiply the speed of our data collection in proportion to the number of used proxies.

G+ crawler: This crawler is composed by two modules. The first one collects the public profile information as well as the connectivity information of all the users in the largest connected component (LCC) of G+. This module is a web-crawler that parses the web page of G+ users to collect the previous information. The second module uses the G+ API to collect all the public posts as well as their associated reactions. Google limits the number of queries to the G+ API to 10K per hour per access token. In order to overcome the rate limit we have created several hundred accounts with their correspondent access tokens and leverage the proxies infrastructure in PlanetLab explained above to speed up our crawling data collection. Further details on this crawler can be found in [119].

We re-emphasize that our crawlers only collect publicly available information. Prior studies have reported that 92-94% of Twitter accounts are public [217, 59] whereas roughly 33% of posts in G+ are public [148]. Furthermore, all the posts published by FB pages are public by definition.

TABLE 6. The duration of data collection for different target OSNs

OSN	Start date	Duration
FB	3/12/2013	9 days
TW	4/28/2013	5 days
G+	5/27/2013	1 days

Table 6 lists the start time and duration of crawl for each dataset. Table 7 summarizes the basic information for the datasets associated with our three target groups in each OSN as follows: *(i)* the aggregate number of posts (and some other attributes)

[6]Note that the proxy functionality is not native in PlanetLab nodes, so we have installed these proxies in PlanetLab nodes.

TABLE 7. Basic characteristics of the collected datasets for Random, Cross and Popular accounts in all three OSNs.

		Aggregate Information for Users Per Group					
OSN	Dataset	#Posts	#Followers	#Friends	#Likes	#Comments	#Reshares
FB	Popular	14.4M	19.4B	-	21.3B	1.8B	2.9B
	Cross	3.85M	620M	-	447M	37.8M	33M
	Random	902K	8.1M	-	6.3M	1.1M	1.6M
TW	Popular	20.1M	6.9 B	136M	4.5B	-	13B
	Cross	7.9M	220 M	6.4M	78.4M	-	188M
	Random	997K	264 K	414K	175K	-	320K
G+	Popular	7.1M	1.5B	5.4M	358M	116M	40M
	Cross	435K	83.5M	874K	4.9M	1.3M	669K
	Random	22K	77K	120K	18K	7K	2.6K

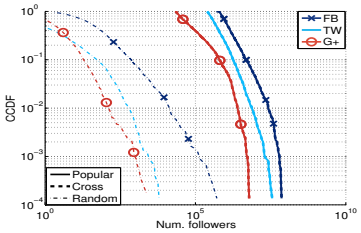

(a) CCDF of the #followers for Popular, Cross and Random groups in all OSNs.

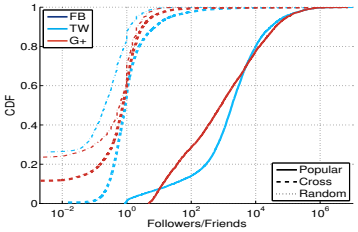

(b) CDF of the ratio of #followers over #friends for Popular, Cross and Random groups in TW and G+.

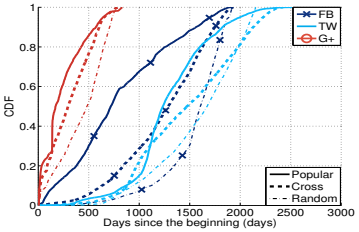

(c) CDF of the account age for Popular, Cross and Random groups in all OSNs.

FIGURE 4.14. Basic user characteristics in different groups of each OSN.

among users in each group, and *(ii)* per-user average of number of followers and posts. The provided user types collected by the FB crawler reveals that Cross group is composed of more than 150 FB account types (with a skewed distribution among them) and the top three types are *music band* (12%), *local business* (9%), and *artist* (4%). While we have selected each dataset independently, there is a negligible number of overlapping users (less than 50) between the popular and cross groups in each OSN.

Connectivity & Account Age

In this section, we briefly examine the connectivity of individual users and their account age. These basic characteristics of target groups not only provide useful context for the rest of our analysis but can also be viewed as a part of group-level behavior. Figure 4.14(a) depicts the CCDF of the number of followers for users in each target group using a log-log scale. Groups associated with each OSN are shown with a different colors using a different line type for each group. Figure 4.14(a) demonstrates that the distribution of number of followers (i.e. out-degree) among users in each group is much less skewed than the entire user population as it was reported in prior studies (e.g. [257, 29, 163, 119]). Furthermore, Popular users in all OSNs exhibit a larger variations in their number of followers (out-degree of the nodes in the social graph). We observe a clear separation in the popularity of groups in different OSNs where FB is the most and G+ is the least popular among similar groups. For instance, the median number of followers among Popular FB, TW, and G+ users are 1.92M, 490K and 41K, respectively. Figure 4.14(b) presents a complementary aspect of user connectivity by depicting the CDF of the ratio of #followers to #friends for individual users in TW and G+ groups. This figure clearly illustrates that the connectivity of Popular users is very imbalanced as they have thousand times more followers. The connectivity of Cross users is relatively more balanced as this group contains users with more followers and also users with more friends. The Random group also has a relatively balanced connectivity but its fraction of users with more friends is larger than Cross group.

Figure 4.14(c) shows the CDF of account age (i.e. the time between the account creation and our data collection time[7]) for users in each group. We observe that accounts

[7]Since FB and G+ do not explicitly provide the account creation time, we estimate it using the time of the first post.

in TW groups are rather older than FB and much older than groups in G+. Interestingly, the relative age of accounts among three groups in each OSN is similar, with Random accounts are generally older and Popular accounts are generally younger than other groups.

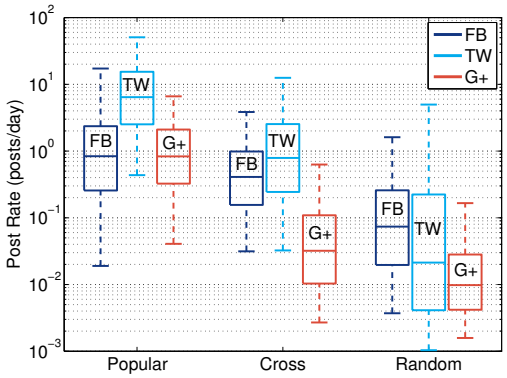

FIGURE 4.15. CDF of average number of daily posts per user

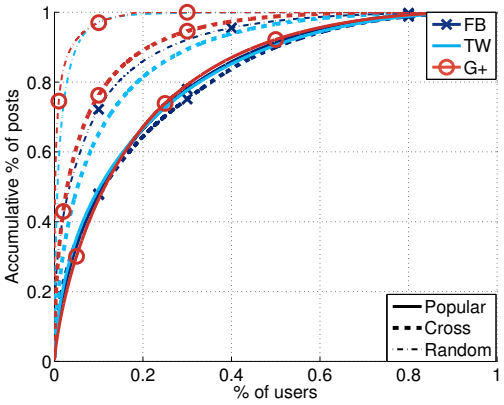

FIGURE 4.16. Skewness of posts/tweets contributions

User Activity

This section focuses on the group-level analysis of user activity in the three OSNs from a few different angles. By "activity", we refer to an action of a user that leads to the created of a post (or tweet). The published post can be original or a reshare of another user's post.

Average Activity Rate

We use the average post rate of a user in terms of the number of posts per day as the primary indicator of her level of activity which is independent of her account age. Figure 4.15 shows the summary distribution of activity rate among users in each target group for all three OSNs using the boxplot format (representing 5th, 25th, 50th, 75th and

95th percentiles) with log scale y axis. This figure reveals the following interesting points: First, within each OSN, the relative order for user activity from high to low is Popular, Cross and Random group. This relative ordering is more pronounced in TW and G+. The activity rate within each group often varies around two orders of magnitude. The skewness in the distribution of activity rate in all groups varies among different groups (as shown in Figure 4.16). In Popular groups as well as Cross groups in FB, the top 20% of users generate roughly 66% of daily posts. However, the top 20% of users in the cross groups in TW and G+ and random group in FB are responsible for 80%-90% of all posts in their group. The contribution of users in random G+ and TW is the most skewed with 5% of users being responsible for 90% of the posts. Second, comparing the activity rate of popular users across three OSNs indicates that popular FB and G+ users exhibit a rather similar rate (with respect to the median and the range of values) which is roughly an order of magnitude lower than popular TW users. Third, the activity rate of cross users on TW is the highest (with the median value of 1 post/day) which is followed by their posting rate on FB (with the median value of 1 post every 2.5 days). These users post on their G+ accounts at a much lower rate of once a month. Fourth, among the Random groups, FB is the most active one and is followed by TW and then G+. Specifically, a typical FB, TW and G+ user publishes 0.07 posts/day, 0.02 posts/day, and 0.01 posts/day, respectively. Random TW users show a significantly larger variation in their activity rate compared to user in other Random groups.

Abandoned Accounts

The average activity rate of a user only offers a coarse measure of the overall rate at which a user publishes posts over the age of her account. More specifically, the activity rate does not directly indicate whether a user regularly visits her account to publish post

or not. For example, a user might be very active for a period of time and then never login to her account. In practice, a seemingly active user might have abandoned her account and does not generate any more post. While it is difficult to reliably determine whether a user has really abandoned her account, the ratio of the time since a user's last post to her average inter-post time offers a good estimate for the likelihood that the user has abandoned her account. For instance, account of a user who publishes once a week on average but has not published for the last 20 weeks, can be view as abandoned. If we assume that the ratio of 20 or more indicates an abandoned user, then roughly 35% of all TW and G+ users and 20% of all FB users have abandoned their OSNs. A more conservative ratio of 40 reduces the percentage of abandoned users to 10% for all OSN.

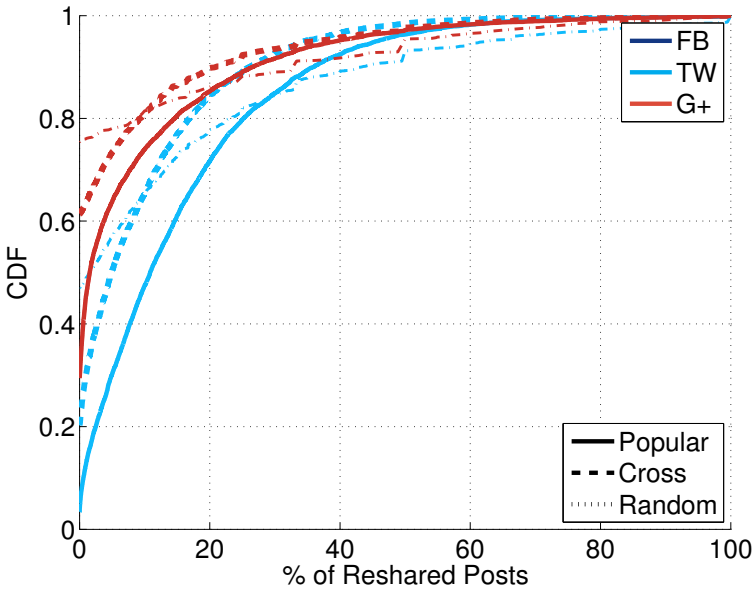

FIGURE 4.17. CDF of average percentage of reshared posts per user

Posting vs. Resharing

To gain a deeper insight on the activity of different group of users, we examine the fraction of their reshared posts, i.e. posts that they relayed from other users. This

demonstrates to what extent users in each group publish original posts instead of propagating other users' posts. Since FB API does not provide this information, we only consider TW and G+ for the following analysis. Figure 4.17 plots the fraction of original posts by individual users in different groups in G+ and TW. The fraction of Random, Cross and Popular user that only send original posts are 83%, 65% and 40% in G+ and 60%, 30% and 18% in TW, respectively. Therefore, in each OSN, Random users proportionally send more original posts than other groups while Popular users send the less. In short, users in each G+ group relatively publish more (often double) the fraction of original posts than the corresponding group in TW.

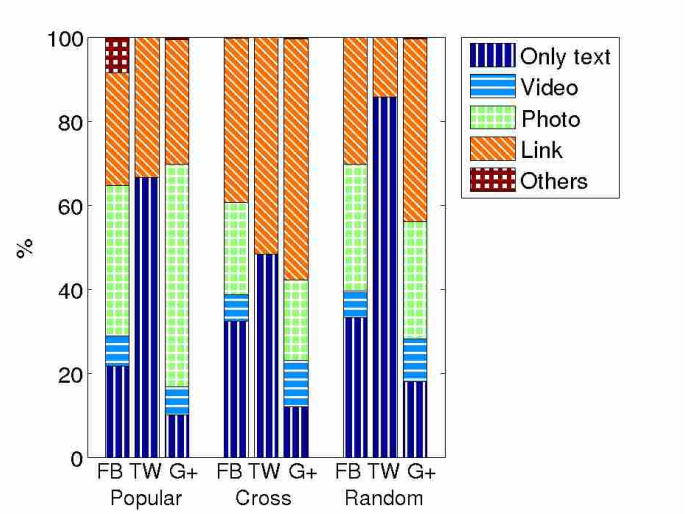

FIGURE 4.18. Percentage of post of each type for FB, TW and G+

Types of Posts

We now examine the activity of users in different groups with respect to the type of posts that they publish. Each vertical bar in Figure 4.18 depicts the fraction of all posts in each group across different post types, namely "text", "video", "photo", "link" and "others". We recall that TW users only generate two types of posts, "text" or "link". This

figure demonstrates the following points about the type of generated posts by all users in each group: *(i)* The combination of "text", "photo" and "link" posts represent more than 85% of posts in all FB and G+ groups. Despite its increasing contribution in the Internet traffic [35], the "video" posts only comprises 6-11% of posts in these OSNs. *(ii)* Popular G+ users show a clear preference for "photos" which makes up more than half of their total posts. *(iii)* "link" is the dominant post type among Random G+ and all Cross users. *(iv)* We observe a larger fraction of "text" posts among users in all FB groups (21-33%) than the corresponding G+ groups (10%-18%). This suggests that users in all FB groups are more likely to express themselves using text posts than G+ users. *(vi)* Popular and Random TW users show a clear preference for "text" posts that makes up roughly half of posts among Cross TW users.

We also examined the fraction of post types across all posts by individual users in each group and observed that this fraction generally follows the distribution of all published posts by the Popular groups (Figure 4.18). Furthermore, we did not observe any measurable correlation between the activity rate of a user and its tendency to publish a certain type of posts.

The summary of our main findings on group-level analysis of user activity is as follows: User activity is skewed in all groups and the relative order of activity among groups in each OSN is Popular, Cross and Random. Popular FB and G+ users exhibit a similar rate of activity which is roughly an order of magnitude less than Popular TW users. Similarly, Cross users publish more posts on TW followed by FB at a much higher rate than G+. FB and G+ Random groups are the most and least active among the Random groups, respectively. Up to one-third of TW and G+ users and one-fifth of FB users might have abandoned their OSN or at least they do not actively publish. TW users generally reshare other users' post much more often than G+ users. However, in

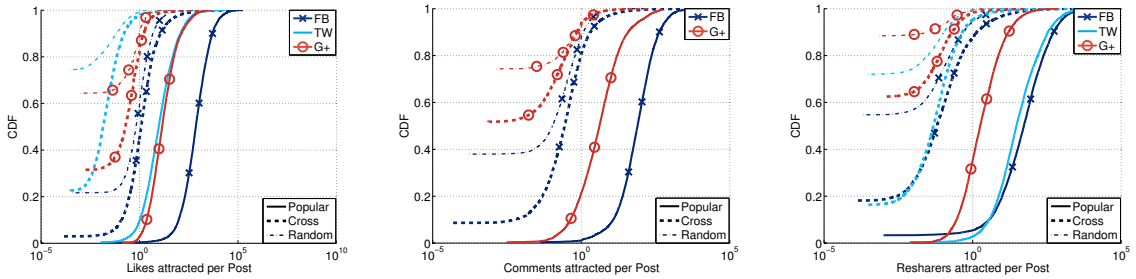

(a) Like (b) Comment (c) Reshare

FIGURE 4.19. CDF of average number of reactions received per user per post

each OSN, Random users publish more original posts whereas Cross and Popular users primarily relay the post from other users. Cross users have a tendency to publish "link" posts while Popular (FB and G+) groups publish "photo" posts more often than other groups.

User Reactions

One of the main motivation for different entities (specially companies, brands, celebrities, politicians) to join an OSN is to obtain other users' reactions to their post. The level and type of reaction by users in an OSN depends on many factors including the popularity of certain type of reactions (i.e. its culture), its offered features for user reaction and possibly the content of a post. Therefore, characterizing user reactions in an OSN provides a valuable insight on how and why different group of users publish their information at that OSN. Toward this end, we consider user reactions at the group-level as a key aspect of behavior for individual groups in this section. In particular, we examine three types of reactions to each post, namely Likes, Comments, and Reshares, as we described in Section 4.2. We do not consider Comments for posts in TW since its API does not provide this information.

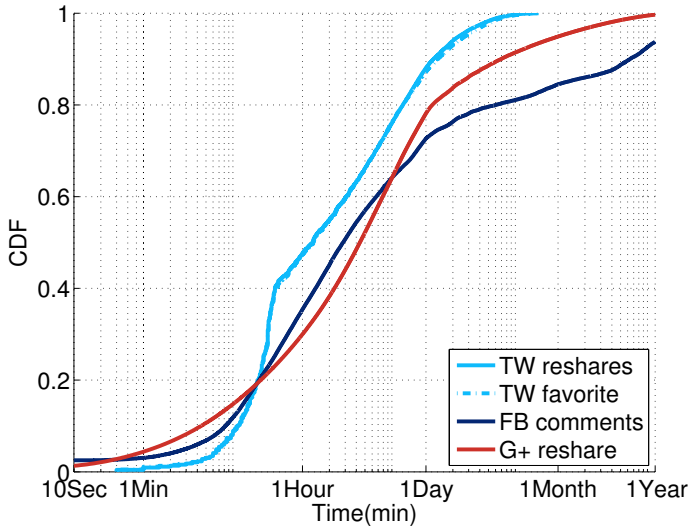

FIGURE 4.20. The distribution of the time between post creation and reaction across different target OSNs

Prior studies have reported that a significant majority of reactions to a post, regardless of its popularity, occurs within a short window (e.g. a day) after it is published [261, 119]. To validate this observation in our datasets, Figure 4.20 presents the distribution of time between creation of a post and individual reactions (of a certain type) across all posts of all users in our target groups[8]. The figure focuses on the Reshare and Comment for G+ and FB, and Reshare and Like for TW. While the timestamp of the mentioned reactions are available for FB and G+, these information is not explicitly available in TW. In order cope with this limitation, we monitored all TW users in all three groups and collected their posts repeatedly every one hour for a week. This allows us to capture the number of new reactions that appear every hour. As the figure shows, 75% of all reactions to posts in TW, G+ and FB arrive within 0.5, 1 and 2 days, respectively. The short duration of the reaction window to individual posts implies that the level of reaction

[8]We focus on a specific type of reaction for which timestamp information is available or can be obtained in some other ways.

to a post can be properly measured by the absolute number of reactions rather than its rate.

Post-Level Reaction

We start by examining the distribution of the number of reactions (of each type) to individual posts across all generated posts by users in each group that are shown in three plots of Figure 4.19. This figure reveals the following important points: First, for any type of reaction, only posts of Popular users typically receive a significant number of reactions. In fact, except for the number of Likes for roughly half of the post from Cross and Random FB users, published posts by all other non-Popular users only receive a negligible number of reactions of any types. Specifically, the distribution of reaction per posts across all groups are very skewed with roughly 10-15% of posts attracting 80% of all reactions. Second, we observe that posts by Popular FB users typically attracts one to two orders of magnitude more reactions than posts by Popular G+ users for any type of reactions. Popular TW users attract the lowest number of Likes. Surprisingly, despite the fact that Reshare is a common reaction type in TW, posts by Popular FB users receives more Reshares than posts by Popular TW users. Third, for posts by Popular FB users, the median number of Likes, Comments and Reshares is 625K, 60K and 44K, respectively. We observe a very similar trend between different types of reactions to posts by Popular G+ users. In contrast, the typical number of received Reshares for published posts by TW users is more than three times larger than the number of received Likes. We note that Like and Reshare reactions require a similar effort (i.e. one or two clicks depending on the OSN) while Comments demand more effort (i.e. writing some text) from reacting users. Furthermore, given the large number of followers for Popular users, the observed reaction to their post offers a reliable view of user reactions in an OSN. Therefore, these

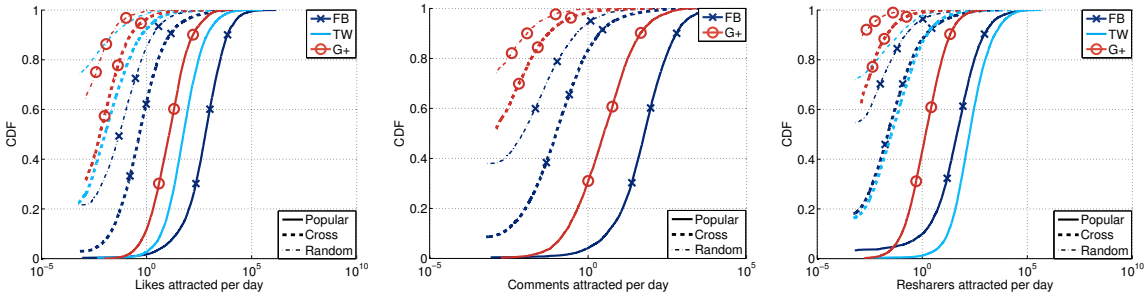

(a) Like (b) Comment (c) Resharer

FIGURE 4.21. CDF of average number of daily reactions to posts of individual users

results collectively suggests that FB and G+ users are more interested to express their own opinion through Like and Comment reactions rather than relaying a post to other users. In contrast, TW users are three times more likely to relay a post and facilitate its propagation throughout the TW network. Despite this difference in the culture of reaction, a post by a Popular FB user receives 75% more Reshares than a post by Popular TW user.

Daily User-Level Reaction

Reactions can also be viewed at the daily-rate for each user which shows the aggregate number of reactions that a user receive to all her published posts in one day. We refer to this view as the daily user-level reaction which is clearly a byproduct of the user's average daily publishing rate and the average number of reactions (of each type) to each post. Figure 4.21 shows the distribution of daily user-level reactions across users in each group. These distributions exhibit trends that are qualitatively similar to the distribution of post-level reaction (shown in Figure 4.19). The only exception is the distribution of daily user-level Reshares that is shown in Figure 4.21(c). Comparing the distribution of daily user-level and post-level Reshare for Popular FB and TW users reveal the following interesting point. Posts by Popular FB users typically attracts more Reshares than posts by Popular TW users. However, because of a significantly larger activity rate among

Popular TW users (demonstrated in Figure 4.15), the daily user-level reaction for Popular TW users is larger than that for Popular FB users as shown in Figure 4.21(c).

Another interesting aspect of user-level reaction is the level of balance in the number of reactions (of any type) to different posts of individual users. To elaborate on this issue, consider two user u_1 and u_2 that have a different number of posts but the same average reaction of 50 per post. u_1 receives no reaction to half of her posts and 100 reactions to each one of the other half whereas u_2 receive 40 reactions per post to half of her posts and 60 reactions to each one of the other half. In this example, the number of reactions for u_2 are more balanced than u_1. We use Jain's fairness index [144] to quantify the level of (im)balance (or fairness) in the number of reactions across posts of a single user. The value of 1 for Jain's index indicate perfect balance whereas smaller values signals a more imbalanced reactions among posts of a user. Figure 4.22 depicts the summary distribution of Jain's index only among users (with more than 10 posts)[9] in each candidate group. This figure reveals that: *(i)* The level of reaction to posts is generally imbalanced, i.e. the index is smaller than 0.5 for a majority of users; *(ii)* TW users, especially in Cross and Random groups, exhibit a very imbalanced level of reactions. In the case of G+ users, however, half of the Popular group receive a rather balance reaction to their posts; *(iii)* The level of balance in reactions is particularly diverse among Popular FB users.

Effect of Content Type on Reactions

We investigate whether certain type of post by a particular group of users might trigger a larger number of reactions. To do so, we split all generated posts by each group of users across different types and examine the distribution of the number of reaction

[9]For a user with a smaller number of post, the index could be very noisy.

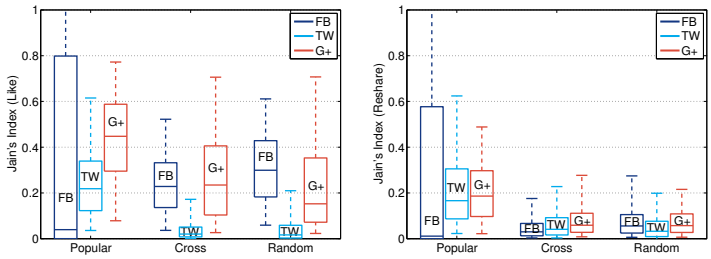

(a) Like (b) Reshare

FIGURE 4.22. The balance in the distribution of reaction across the posts of a single user measured using Jain's fairness index

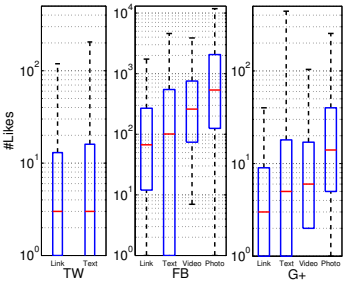

FIGURE 4.23. Summary distribution of Likes to each type of posts for the Popular group in FB, TW and G+

(of each type). Figure 4.23 depicts the summary distribution of Likes across posts of each type published by all users in Popular groups in our target OSNs. This figure clearly illustrates that the number of Likes is similarly decreasing among different types of post in the following order Photo, Video, Text and Link for all OSNs (only text and Link for TW). This trend is much more pronounced in FB.

Our main findings from group-level analysis of different types of user reactions can be summarized as follows: Only published posts by Popular groups in all three OSNs attract a non-negligible number of reactions where roughly 10% *of posts receive* 80% *of all reactions of any type. The number of reactions (of any type) to posts by Popular FB users is a couple of orders of magnitude larger than Popular G+ users. The culture of reaction varies among users in diffrent OSNs. FB and G+ users are more likely to react by expressing their own opinion through Likes and Comments, whereas TW users tend to relay a post to other users and thus facilitate its propagation. Despite this difference in the culture of reaction, a post by a Popular FB user receives* 75% *more Reshares than a post by Popular TW user. However, a significantly larger activity rate for Popular TW users leads to a higher rate of daily user-level reaction to Popular TW users. The number of reaction to posts of individual users are generally imbalanced in particular for TW*

TABLE 8. Rank (Spearman) correlation between popularity, activity and reactions of users in each dataset; #RS/P:#ResharePerPost; #C/P: #CommentPerPost; #L/P: #LikePerPost

		FB			TW			G+		
		Popular	Cross	Random	Popular	Cross	Random	Popular	Cross	Random
#Followers	PostRate	*0.00*	0.49	0.61	-0.04	0.60	0.54	-0.05	0.31	0.03
#Followers	#RS/P	0.26	0.62	0.59	0.41	0.69	0.58	0.18	0.44	0.23
#Followers	#C/P	0.30	0.62	0.68	-	-	-	0.14	0.52	0.32
#Followers	#L/P	0.32	0.70	0.74	0.44	0.66	0.47	0.18	0.52	0.31
PostRate	#RS/P	0.27	0.31	0.52	-0.16	0.48	0.41	*0.03*	0.43	0.30
PostRate	#C/P	0.08	0.18	0.47	-	-	-	-0.02	0.30	0.08
PostRate	#L/P	0.14	0.19	0.44	-0.22	0.49	0.31	*0.00*	0.26	0.13
#RS/P	#C/P	0.74	0.59	0.52	-	-	-	0.80	0.53	0.32
#RS/P	#L/P	0.86	0.71	0.59	0.90	0.75	0.63	0.85	0.58	0.42
#C/P	#L/P	0.90	0.87	0.78	-	-	-	0.90	0.61	0.51

users. The number of reactions seem to be correlated with post type which is decreasing in the following order: photo, video, text and link

Exploring Relation Among Different Group Behavior

In previous sections, we separately analyzed group-level connectivity, activity and reactions of users in three major OSNs. In this section, we explore the correlation between each pair of these user attributes. This analysis reveal any strong relationship among these attributes and could explain the underlying causes for some of our findings. Table 8 shows Spearman Rank Correlation (RC) [123] between #followers, post rates, and the rate of different types of reactions for users in individual target groups within each OSN [10]. Note that RC measures the correlation between the rank of user within a group based on two different characteristics. The RC value changes between -1 (ranks are reversed) and 1 (ranks are the same) where 0 indicates that ranks are independent. The rest of the section discusses the correlation between different pairs of attributes among users of each group of different OSNs.

[10]The P-values for all correlation values are smaller than 0.02, except for the values in *italic*, for which the correlation is also very small.

– **Connectivity vs. Activity**: We observe that these two user characteristics are not correlated for Popular groups in all OSNs (RC $\leq |0.05|$). However, they exhibit a moderate correlation among users in Cross and Random groups especially for TW and FB ($0.49 \leq$ RC ≤ 0.61).

– **Connectivity vs. Reactions**: These two characteristics exhibit a high correlation in FB and TW Cross and FB Random groups ($0.59 \leq$ RC ≤ 0.75) and moderate correlation in TW Random and Popular as well as G+ Cross groups. This suggests that only in these groups having more followers leads to a larger rate of reactions of any types. For other groups, the correlation between connectivity and reaction rate is generally positive but low (RC ≤ 0.32).

– **Activity vs. Reactions**: Interestingly, only FB Random and TW Cross groups show a moderate correlation between these two characteristics ($0.44 \leq$ RC ≤ 0.52). In contrast, there is no correlation between activity and any type of reaction for Popular G+ group and even low inverse correlation for Popular TW group. All other groups show low positive correlation.

– **Different Types of Reactions**: The RC between different types of reactions indicate a significant positive correlation between all pairs in all Popular groups ($0.74 \leq$ RC ≤ 0.90)). In fact, the correlation between all pairs of reactions is at least moderate or high in all Cross group and only slightly lower in all Random groups.

In summary, increasing the rate of activity has a moderate effect on the number of connection (number of followers) and received reaction only in a few groups. In general, higher level activity by a user does not lead to more reactions from others. Different types

of reactions are generally correlated and this correlation is more pronounced in Popular and then Cross groups.

Temporal Analysis

So far we have examined the average user activity and received reaction during the time that a user has participated in an OSN. These average metrics provide an overall measure of user behavior but do not reveal any information on the short term evolution of users activities and reactions. In this section, we examine the temporal evolution of group-level user activities and reactions in different OSNs to compare these characteristics of different groups over time and identify any event that affected user behavior. We focus on daily activity or reaction over a 26-months measurement window between January 1st 2011 and March 1st 2013. We recall that TW API only provides the last $3\,200$ tweets published by users. We refer to a user who has published more than $3\,200$ tweets during our 26-months measurement window as a *saturated user*. Saturated users make up 65%, 17% and 2% of users in Popular, Cross and Random TW groups, respectively. The collected tweets for 90% of saturated users in Popular (and Cross) groups represent a recent window of user activity whose length is uniformly distributed over our measurement window.

To demonstrate this effect Figure 4.24 compares the *observable* with the *complete* history of activity for OSNs. In these analysis we assume that users have uniform daily activity rates over their entire age. For each date, *observable* history includes the non-saturate users, whereas the *complete* includes the users that exist in the system (i.e. the accounts that are created before that date). Figure 4.24(a) shows *observable* history as the sum of daily post rate of users that our dataset captures in comparison to the *complete* history in Figure 4.24(b) for the three systems. Figure 4.24(b) shows that the

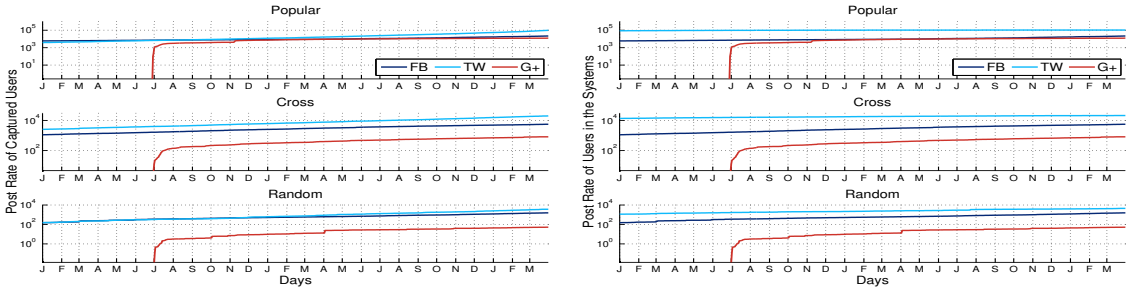

(a) Sum of post-rates for captured users (b) Sum of post-rates for users in the three OSNs

FIGURE 4.24. The sum of the average post rate of users in the three systems in comparison to the sum of the post rate of users that we can collect their post in each day. (The picture shows the effect of 3 200 accessible tweets.)

total daily post rate of users in TW is higher than the other systems. Therefore, when drawing conclusions from the captured history (Figure 4.24(a)), which only shows the daily observable post rate, extra care is needed to conclude meaningful findings.

In summary, the incomplete history of activity for saturated users indicates that the activity (and their associated reactions) for Popular and Cross TW users are generally underestimated in our analysis and the error is larger for earlier months. In particular, we have the complete datasets for approximately 30 days, and from that date backwards our dataset progressively loses TW posts due the saturated users. We carefully consider this limitation of TW datasets in our analysis.

Evolution of Daily Activity

We start by exploring the temporal evolution of the aggregate number of daily published posts by all users in individual groups that are shown in Figure 4.25 with a log-scale y-axis. This figure unveils a few interesting points: First, the saw-tooth pattern in all plots is due to the roughly 30% lower level of activity during weekends compared to weekdays for all groups. Second, the activity rate for all groups exhibits a generally growing trend over time but the slope of increase is much higher among Popular

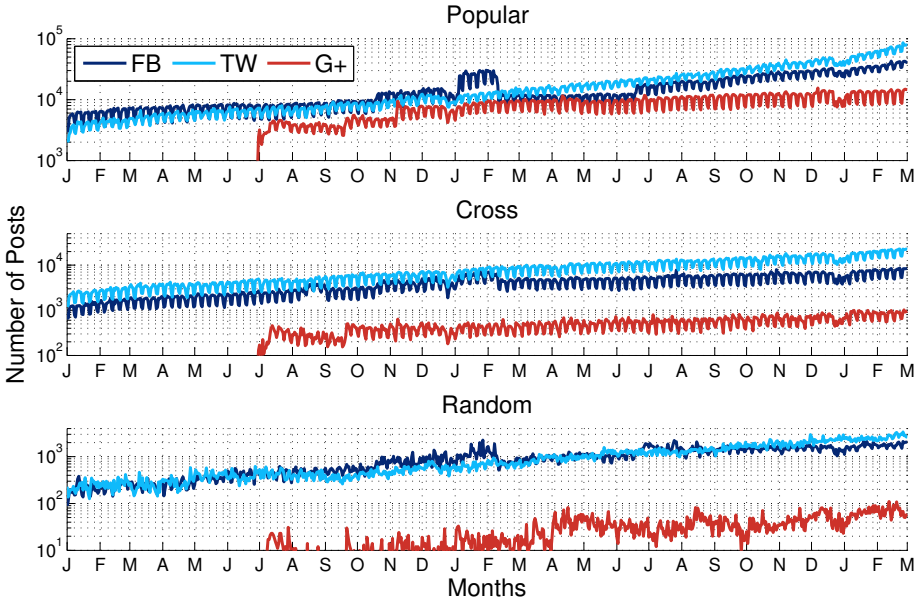

FIGURE 4.25. Aggregate number of posts per day (Jan. 1st 2011 - March 1st 2013) and Cross groups. The activity rate for any TW group is consistently higher than the corresponding FB group despite the fact that the presented rate for TW is merely a lower bound (because of the saturated users). In fact, the gap in the activity of Popular TW and FB groups in the last few months of our measurement appears to be widening. Third, we observe a significant jump in the activity of all G+ groups shortly after Jun. 21, 2011 when the system was released. After this initial surge, all G+ groups exhibit a slower growth in their activity rate compared to other groups and even appear to become flat during some periods of time. For the activity rate of both Cross and Random groups, we can observe a significant gap between G+ and other two OSNs that has persisted during the entire life-time of the G+ system. This indicates that Cross users clearly prefer to publish their posts in TW and FB rather than G+. The activity rate of the Popular G+ group has initially increased in multiple steps till it reaches close to the rate of Popular FB and TW groups (around Feb-Jun of 2012) and has become seemingly flat during the last nine months. This has led to an increasing gap between the activity of Popular G+

users and other Popular groups. With the current growth patterns, it seems unlikely that G+ groups can close the gaps in activity with the corresponding group in FB or TW. Our closer inspection of activity in all groups showed that both the increase in the number of active users and the growth in the average activity of participating users has contributed to the growing trend in their activity over time. Fourth, the time of some of the noticeable changes in the activity rate of different groups appear to be aligned with and thus must be caused by the following events:

- *(i) Introduction of "Timeline" feature by FB (Jan. 2012)*: The short-term increase in the activity of all FB groups around Jan-Feb. 2012 appears to be caused by to the newly-introduced Timeline feature that allows users to publish their historical posts.
- *(ii) Introduction of interface with 3rd-Party website by FB (Jun. 2012)*: The step-like increase in the activity of Popular FB users is apparently triggered by a new feature that allows users to share a post through a 3rd party website and collects associated reactions on users' FB accounts.
- *(iii) Introduction of new G+ features:* The step-like increases in the activity rate of Popular and Cross G+ group are aligned with release of certain G+ features during the first few months after its release [118].
- *(iv) Holiday season*: The small drop in the activity of users in all groups during the last two weeks of Dec. is due to the holiday season.

It is intriguing that the introduction of new features in FB leads to a significant and long-term increase in user activity whereas new features in G+ appear to create a short-term excitement among users that quickly fades away.

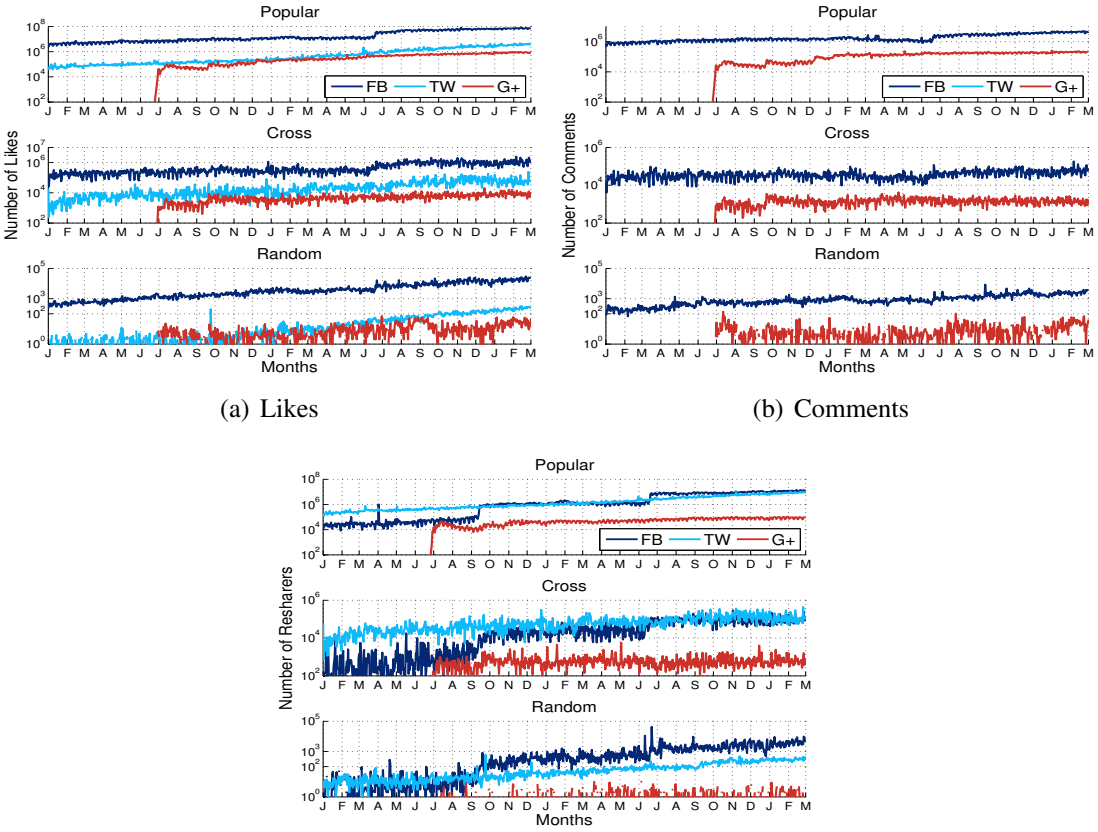

(a) Likes

(b) Comments

(c) Resharers

FIGURE 4.26. Aggregate number of reactions per day (Jan. 1st 2011 - March 1st 2013)

Evolution of Daily Reaction

We now turn our attention to the temporal evolution of aggregate daily reactions of each type to posts by all users in each group that is shown in Figure 4.26. We can observe that all types of reactions to most groups (except for some G+ groups) exhibit a steady growth with time. Apart from the initial major jump in reactions for all G+ groups, their growth is slower than the corresponding groups in other OSNs. The main findings for each type of reactions can be summarized as follows:

Like: Like is known to be a very popular type of reaction among FB users. Figure 4.26(a) confirms this observation and shows that the daily rate of Likes by users in all FB groups is a couple of orders of magnitude larger than other OSNs. The sudden increase in the rate

of Likes for posts in all FB groups in Jun. 2012 is aligned with the addition of 3rd party feature by FB. Interestingly, the introduction of timeline feature by FB does not seem to have a measurable effect on its rate of Likes despite its impact on the activity rate.

Reshares: Among all three OSNs, resharing is the most common type of reaction in TW (retweeting). This observation coupled with the higher activity rate for all TW groups (reported in Figure 4.25) suggest that TW groups should attract the highest rate of Reshares. However, the daily rate of Reshare for all groups in Figure 4.26(c) depicts a different picture. Between Jan.-Sep. 2011, the rate of attracted Reshare by Popular and Cross TW groups is significantly higher than the corresponding groups in FB and G+[11]. However, the introduction of the timeline and 3rd-party features by FB has dramatically boosted the rate of Reshares for published posts by all FB groups since Sep. 2011. These step-like increases are particularly visible in the number of Reshares for posts of Popular groups. Interestingly, as a result of these two features, the rate of Reshare reactions for all FB groups has clearly surpassed (or reached the same level as) the corresponding TW groups despite the strong culture of Resharing (i.e., Retweeting) among TW users. We note that while the activity and reaction rates for TW groups in the last few weeks of our measurement window are very accurate, they are still lower than (or equal to) the rate of corresponding FB groups. Therefore, any potential error in the activity or reaction rate of TW groups does not affect the above conclusions.

Comments: The number of daily Comments for FB groups is much larger than G+ groups. The boosting effect of new FB features is not as visible in the daily Comments of FB groups except for the 3rd-party feature among Popular FB users. While the number of Comments for all FB groups has increased during our measurement period, the slope of this increase is significantly lower than other reactions types for FB groups. The daily

[11] Since the TW rates could be greatly underestimated during this period, the actual gap in received Reshares between TW and other OSNs must be even larger than what Figure 4.26(c) suggests.

rate of comments for G+ groups remains significantly lower than FB groups and does not exhibit much growth for Cross and Random groups. The rate of Comments for Popular G+ groups only show sudden increases that are clearly triggered by added features and promotional events during the first six months after G+ was launched.

Note that any increase in the daily rate of reaction for each group is a byproduct of the increase in the daily number of posts by its users and the growth in the average number of reactions to their posts. Our careful examination of these two factors indicated that the daily activity of users in each group is the primarily contributing factor that determines the rate of received reactions (of any type) by the users. The perfect temporal alignment between the sudden increase in the activity in FB and G+ groups with the sudden growth in the rate of some reaction types, is another evidence that user activity is the main determining factor for the rate of reaction.

The main findings of our temporal analysis can be summarized as follows: The activity in all groups exhibits a persistent growth with a higher pace for Popular and Cross groups during the past two years. This growth in the activity is driven by the increasing number of users and the higher rate of activity among them. The activity of all TW groups is consistently higher than the corresponding FB group and a couple of order of magnitude larger than the corresponding G+ groups. The introduction of new features by different OSNs (in particular FB) has led to a significant and long-term increase in the activity of their users. The rate of Likes is much higher for FB groups and seems to have been affected only by a the introduction of 3rd-party feature. As a result of two newly added features by FB, the rate of observed Reshare reaction by FB users has dramatically increased and clearly surpassed the observed rate by TW users despite the fact that resharing is a native feature in TW. Cross users publish posts on TW at a higher

rate than FB, but receive a larger rate of Likes, Comments and even Reshares from FB users.

Summary

This chapter presents a measurement-based characterization of group-level user behavior in three major OSNs, Facebook, Twitter and Google+. We consider Popular, Cross and Random groups of user in our analysis as they reveal a complemenary view of user population. Our group-level approach to characterize user-behavior enables us to compare the behavior of uses in similar groups across different OSNs or the behavior of users in different groups of a particular OSN. We consider several aspects of user connectivity, user activity and user reactions as three key dimensions of user behavior in our analysis. We also conduct termporal analysis to examine short-term changes in group-level user behavior and their potential causes. Our analysis provide a set of interesting and insightful findings such as the following examples: *(i)* Only published posts by Popular groups in all three OSNs attract a non-negligible number of reactions with a very skewed distribution among Popular users. *(ii)* The number of reactions (of any type) to posts by Popular FB users is a couple of orders of magnitude larger than Popular G+ users. *(iii)* The more likely reaction by FB and G+ users is to express their own opinion whereas TW users tend to relay a received post to other users and thus facilitate its propagation. Despite the culture of reshare among TW users, a post by a Popular FB user receives more Reshares than a post by Popular TW user. *(iv)* Added features in an OSN can significantly boost the rate of action and reaction among its users.

We plan to extend this work in the following directions: First, we plan to examine post content to gain a deeper insight on the published content and associated context by individual users in each group. Second, we are conducting a more detailed study on Cross

group to better determine their publishing strategy in different OSNs and identify whether they use multiple OSNs for a similar or complementary purposes.

CHAPTER V

"WHO'S WHO" IN TWITTER: A FIRST LOOK AT THE TWITTER ELITE NETWORK

Accounts with the largest numbers of followers in Online Social Networks (OSNs) such as Twitter can be viewed as "social elites". The power-law distribution of degree in social graphs posits that these elites are followed by many users [18, 200]. All these elites along with their pairwise relations form a structure that we refer to as the *elite network*. Despite their importance, the characterization of elite networks has received little attention among researchers [230, 111]. As a result of the high visibility of elites within the OSN, the elite network can be viewed as the core of the OSN social graph, thus its characteristics offer valuable insights about the backbone of the network.

This chapter presents a detailed analysis of the micro- and macro-level structures of the Twitter elite network. We start by explaining our methodology used to capture a complete snapshot of the Twitter elite network that contains the 10K most followed accounts on Twitter. We show through component analysis that a significant majority of users in the elite networks with sizes equal to or smaller than 10K nodes form a large strongly connected component (LSCC) and users that are not inside this component are followed by the users in the LSCC. We identify communities of tightly interconnected elites and show that these communities exhibit similar social and/or geographical attributes. We further use these communities to characterize the topological structure of elite network at the micro-level. Finally, we identify the most influential elites by characterizing pairwise influence between them using three different measures.

Introduction

Recent research on OSNs is inundated with studies on their social graphs as a whole. However, due to the large number of nodes and edges in the social graph of any major OSN, coupled with the commonly-reported skewed distribution of user properties (e.g. degree – number of friends and followers – and user activity), most characteristics are dominated by users that often play insignificant social roles. This motivates our study to shift the focus from the entirety of an OSN to a very small number of outliers that matter the most. A small percentage of nodes with the highest degree (accounts with the largest number of followers) in any OSN social graph can be viewed as "social elites" since they directly influence the millions of users they are connected to or followed by. In fact, the induced sub-graph [86] of these high degree nodes and their inter-connection that we call *elite network*, can be viewed as the "core" or "backbone" of the OSN social graph. Capturing and characterizing the connectivity structure of the elite network reveals the key attributes of this core component. Characterizing this core component also offers valuable insights about the impact/influence of elites on each other, which is interesting on its own. In fact, while social scientists have extensively examined the characteristics of elite power networks and elite influence in offline social networks [265, 89, 192, 216], this topic has received limited attention in the context of OSNs from computer scientists. Few prior studies focused on the elite network in major OSNs [26], and those that explore connectivity among high degree nodes (e.g. [191]) only explored their basic connectivity features (e.g. reciprocity, density) or focused on rich-club properties [206] by measuring the tendency of high degree nodes to interconnect to each other. In the absence of insights about the elite network in various OSNs, existing graph generation models for OSNs (e.g. [18, 166, 55]) do not incorporate any requirement for the connectivity features among

high degree nodes (i.e. elites). Therefore, the backbone of their resulting graphs do not properly represent the structure of a typical OSN [25].

Additionally, since many regular users directly follow at least a few elites, elite users can serve as *landmarks* for clustering regular users in the OSN as well. Therefore, the characterization of the elite network potentially leads to impactful findings, not only about about elites, but also about the OSN as whole.

In this chapter, we tackle the following three fundamental questions about the elite network in a major OSN, namely Twitter: *(i)* What are the macro- and micro-level structural characteristics of the Twitter elite network? *(ii)* What insights can be gained by studying the elite networks about the entire graph? *(iii)* How can we assess the influence among Twitter elites?

In Section 5.2, we describe our technique for identifying the top 10K Twitter accounts with the largest number of followers and the pairwise directed friend-follower connections among them. The resulting social sub-graph among the top 10K Twitter accounts enables us to examine the Twitter elite network at different sizes (smaller than 10K). Furthermore, we obtained the social category and country information for these accounts along with their profile information and all the available tweets for all 10K elite accounts. The "view" n-ELITE is defined as the Twitter elite network which is the graph of friend-follower relationships between the top-n most followed accounts. We use these views to study the elite network and examine how various characteristics of the elite network evolves as less popular elites are included in the elite network.

In Section 5.3, we explore the macro structure of the Twitter elite network. In particular, we show that the elite network, regardless of its size, is a single weakly connected competent, but has multiple strongly connected components where 90%+ of the nodes are located in the largest strongly connected component (LSCC). Furthermore,

the elite network exhibits an "onion-like" layered structure where users with more followers have the highest PageRank centrality values as well (calculated on the elite network). Hence, the most followed elites are at the core and less popular elites form layers around the core.

We then focus on the structure of the elite network in Section 5.4 at the community level. Toward this end, we first motivate and define the notion of *resilient community* [57, 229] and then identify such communities (and their associated nodes) among elites as well as a group of *unstable* nodes that includes accounts that do not belong to a single community in each of the views of the elite network. Leveraging the social and country attributes of individual elites, we demonstrate that the identified communities exhibit a strong social cohesion (i.e. clear social theme among accounts in resilient communities). This in turn confirms that these communities represent meaningful units of the elite network. We further explore how these communities evolve as one extends the size of the elite network to include less popular accounts. We characterize relative connectivity and coupling between communities which in turn reveals an *inter-community structure* (or inter-community interest) in the elite network. Furthermore, we demonstrate that *unstable* nodes act as "hubs" as they sit between two or more elite communities and also identify community members who serve as *bridges* to other communities.

Finally, we investigate the influence of individual elites on the rest of the elite network in Section 5.5. Similar to prior studies [59] we use different measures, namely PageRank, retweet and reply to capture influence over other elites. We argue that the number of retweets and replies are not necessarily enough to capture the influence and that the number of elites who have been influenced is also an important factor. We determine the aggregate influence of an individual elite on the rest of the elite network and show the factors that affect the measured influence. We then identify the list of top-

N most influential users based on each measure and examine the overlap among them as a function of N. We show that the top-10 most influential accounts based on PageRank, Retweet, and Reply are mostly political/corporate elites, news media and magazines, and gossip/entertainment celebrities, respectively. Section 5.6 summarizes and concludes this chapter.

Capturing the Elite Network

Our goal is to capture the Twitter elite network - that is a subgraph of Twitter that includes the top-N most-followed accounts (i.e. node with the highest (out)degree) and the relationships among them (i.e. edges)[1]. Furthermore, we need to annotate each node with its social and geographical (location) attributes in order to explore the impact of these attributes in relationships among elites. There are a few issues that we need to address before we achieve this goal as follows. First, we need to specify the minimum number of followers that qualifies a user as an elite. Second, we need to efficiently identify all of the qualified Twitter accounts, their attributes, and the connections (e.g. friend-follower relationship) among them. In particular, since these users have millions of followers, it is prohibitively expensive to find all their pairwise connections by collecting and examining all their followers.

To cope with these challenges, our data collection strategy for capturing Twitter elite network consists of the following four steps:

1. Capturing a list of most-followed Twitter accounts through public resources and random walks used as seeds.
2. Inferring their pairwise connections.

[1]We use the terms *nodes with highest degree* and *most followed accounts* interchangeably.

3. Identifying missing accounts, validating the information, and collecting pairwise connections.
4. Collecting all profile information and available tweets of discovered accounts.

The details of individual steps are as follows:

Step 1: To bootstrap the data collection process, we crawl lists of the most followed accounts from online resources. In particular, marketing websites such as `socialbakers.com` offer professionally maintained lists of most followed accounts in variety of OSNs in different social categories (e.g. celebrities, actors, sport, community, ...). Each list on `socialbakers.com` provides up to 1000 top accounts in the selected category along with the number of followers and username for each account. We collect the list associated with all offered categories and subcategories and create a unified list that includes all the uniquely-discovered user accounts with their number of followers (and associated rank), their category and location. This resulting unified list consists of $59\,832$ unique users whose number of followers varies from 263 to 81M, and they are associated with 123 categories and 191 unique countries.

We also conduct approximately 2K random walks on the list of friends from randomly selected Twitter accounts to identify high-degree nodes. The theory of random walk [173] indicates the likelihood of a visit by a walker to a node is proportional to the degree of that node in the graph. Therefore, random walks offer an efficient technique to identify highest degree nodes [248, 215].

Equipped with these two techniques to identify potential highest degree nodes, we then create a master list that includes more than 60K accounts. We mainly focus on the top 10K accounts with the most followers from this master list. In this list, 89% are exclusively reported on `socialbakers.com`, 3.2% are exclusively identified through random walks, and 7.8% are found through both techniques. It is worth noting that the

overall popularity rank of the accounts exclusively found by random walk is at least 133 out of 10K.

Step 2: To collect all the connections among the identified accounts in the previous step, our key observation is that the number of friends for elites are almost always several orders of magnitude smaller than the number of followers. Therefore, instead of followers, we collect the complete list of friends for each selected account from Twitter (using its API). This implies that the connection between account u_{fri} and its follower account u_{fol} (denoted as $u_{\text{fri}} \rightarrow u_{\text{fol}}$) is discovered when we collect the friend list of account u_{fol}, i.e. each edge is discovered from the follower side. This simple observation ensures that all pairwise connections among the selected accounts are identified efficiently (without collecting all followers of all accounts). The total number of crawled friend-follower relationships for all elite accounts is 504.8M which consists of 95M unique friends for the top 10K most-followed elites.

Step 3: At this point, we have a snapshot of the most-followed Twitter accounts and their pairwise directed connections. It is indeed possible that the identified top 10K accounts from online sources supplemented with the the list collected from random walks do not accurately capture the top 10K accounts on Twitter, i.e. some elite accounts might be missing. We take a few steps to verify whether the collected information is correct and complete. Our final step is similar to the approach proposed by Avrachenkov et al. [27]. The observation is that any such missing elite account should be followed by many elites already identified as top 10K accounts. Note that we already obtained the entire list of friends for top 10K accounts. We calculate the number of elite-followers for all these collected friends that are not among the elites, and sort the resulting list by the number of elite-followers. We start by scanning this list from the top and collect account information including the number of followers for users in this list. If the number of followers for

any of these accounts is larger than the number of followers for the account at rank 10K, we add it to the master list (at the proper rank) and update the ranks for all elites. We continue this process until 100 consecutive accounts from this sorted list do not make it to the master list. We finally identify the edges between these accounts and other top 10K accounts by collecting their friend list. Using this technique, we detected 264 accounts that are between the rank of 500 and 10K among the top 10K accounts. The small percentage of missing accounts along with their relatively low ranking indicate that our master list is accurate. All in all, among the top 10K most followed accounts, 8 704 were exclusively reported in `socialbakers.com`, 301 were found exclusively using random walks, and 731 are from both the mentioned resources. Finally, checking the most followed friends of elites placed 264 new elites on the list of top 10K most followed elites.

Step 4: We collect all the available tweets for the top 10K Twitter accounts. The available tweets[2] for each account are used to investigate the influence between elites and gain some insight on how they use Twitter.

Who is Elite?

It is certainly compelling to consider Twitter users with the highest number of followers as Twitter elites. One remaining question is *how many most-followed accounts should be considered for forming the elite network?* We argue that the 10K-ELITE offers a significantly large view of the elite network in Twitter for several reasons as follows: First, the skewed distribution of the number of followers implies that the number of followers rapidly drops with rank. For example, the top 10 most followed accounts have between 51.9M to 81.7M followers while the last 10 accounts in the top 10K have

[2]Twitter only provides the last 3 200 generated tweets by each user.

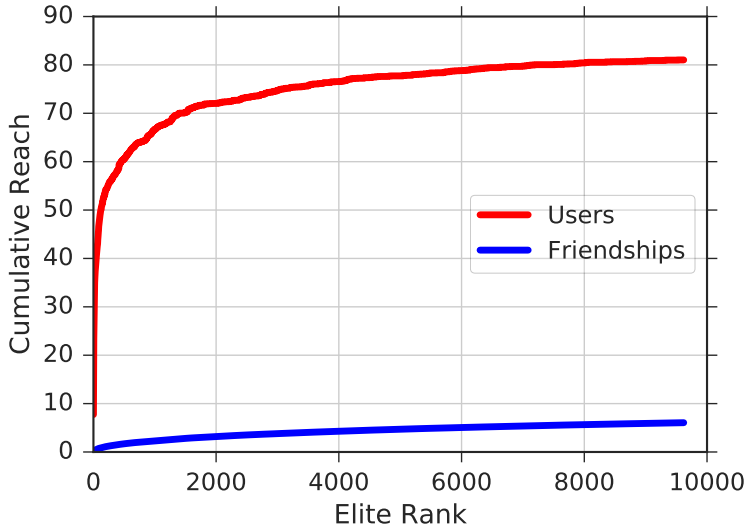

FIGURE 5.27. The total number of nodes and edges that are reached by top-n elites.

around 0.4M followers and the median number of followers among the top 10K is 0.8M. Therefore, the popularity (and thus importance) of any account beyond top 10K would be much less. Second, we demonstrate that the followers of the top 10K elites make up a substantial portion of the entire Twitter network. To this end, we collect an unbiased set of random twitter users using random walk based techniques described in [248]. Figure 5.27 presents the fraction of random users that are direct followers of the top-n elite users as the elite network is extended. As the figure shows, 80% of the random users are immediate followers of the top 10K elites. The figure also shows that the gain from extending the elite network dramatically diminishes as we pass the 2K-ELITE mark. Third, while it is feasible to expand the size of the elite network beyond 10K, reliably collecting the desired attributes (social and location) for these users is very expensive and has diminishing return. Therefore, we limit our elite network to 10K.

To examine whether and how the criteria for selecting elites and thus the size of the resulting elite network affects its structural properties, we consider the Twitter elite network at different sizes (or views). Each view, which we refer to as nK-ELITE, contains

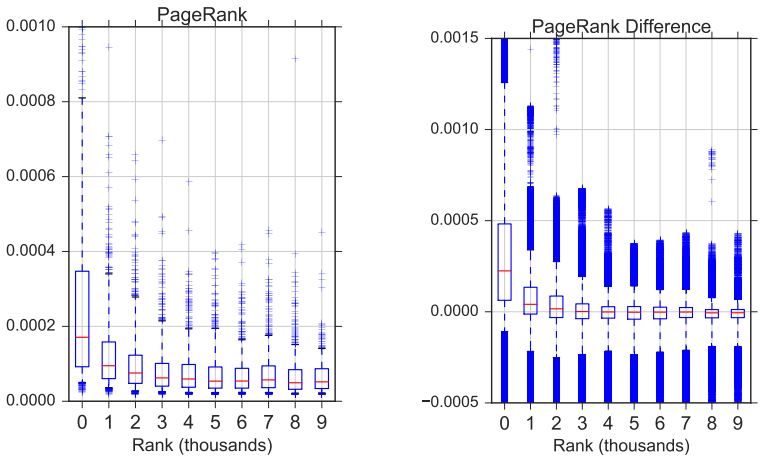

(a) Nodes PageRanks grouped by rank

(b) Difference in PageRank for edges

FIGURE 5.28. PageRank of elites in 10K-ELITE grouped by their rank; Difference in PageRank of follower-friend at both ends of each edge in 10K-ELITE, grouped by the rank of the friends

the top n-*thousand* most-followed accounts and friend-follower relationships between them.

Our final argument with respect to the size of the elite network lies in its structure as a graph as it extends to cover less popular elites. The question that helps characterize this extension is *"whether the centrality of individual elites in the elite network is a function of their overall popularity (i.e. total number of followers)?"* Given the directed nature of the elite network, we compute the PageRank [207] of each node as a measure of its centrality[3]. Figure 5.28(a) shows the summary distribution of nodes' PageRanks computed over the 10K-ELITE presented as boxplots. In this plot, nodes are grouped according to their rank based on the number of followers in buckets each one with 1K nodes. In essence, each group represents the new set of nodes that are added to each view to create the next extended view. This figure reveals a pattern where the PageRank centrality of elites in the elite network generally decreases with their overall popularity.

[3]We computed PageRank on a network with inverted edges, to ensure that PageRank values correspond with importance and reasonable definition of centrality.

We also included a similar plot for the difference in the PageRank of users at the ends of each edge in 10K-ELITE in Figure 5.28(b). Similar to the previous analysis, all edges are grouped into 10 buckets according to the rank of the friend and the summary distribution presents $\text{PageRank}_{\text{fri}} - \text{PageRank}_{\text{fol}}$. We observe that as we go to buckets that contain less popular elites, the the difference between the centrality of friend and follower decreases. These two figures suggest that elites form an "onion-shape" structure where the highest ranked elites are in the center, and other groups with lower ranks form layers around the core. Most friend-follower relationships (directed edges) have their friend side in the inner layers and the follower side in the outer layers. This result supports our choice of the size of the elite network, since the plot demonstrates the PageRank of elites at lower rank buckets are effectively similar. Therefore, including more elites only adds more layers around this onion-like topology structure.

In summary, our data collection pipeline is capable of identifying the top 10K most followed Twitter accounts and all their friend-follower relationships, i.e. 10K-ELITE. More than 80% of the users in Twitter follow at least one account in 10K-ELITE, and including less popular accounts seems to have a minimal effect on the reach of 10K-ELITE. Additionally, this network exhibits an "onion-shape" structure, with more popular elites in the center of the network and less popular elites forming outer layers. Most elites in the outer layers are following elites in the inner layers, but are being followed by elites in close by layers.

Macro-Level Structure

Before we conduct any analysis on the Twitter elite network, we present a number of basic characteristics for each view of the elite network in Table 9, including the number of nodes and directed edges ($|E|$), reciprocity (Rcp), transitivity or clustering coefficient

TABLE 9. Basic characteristics of the elite networks and their weakly and strongly connected components

					CC			SCC		
View	$\|E\|$	Rcp	Tran	Diam	#CC	$\%\|V\|$	$\%\|E\|$	#SCC	$\%\|V\|$	$\%\|E\|$
1K-ELITE	49K	0.35	0.3	7	1	100.0	100.0	64	93.5	94.6
2K-ELITE	126K	0.34	0.24	7	2	100.0	100.0	110	94.2	95.6
3K-ELITE	231K	0.32	0.2	7	3	99.9	100.0	171	94.1	95.8
4K-ELITE	344K	0.31	0.18	7	3	100.0	100.0	231	94.0	95.9
5K-ELITE	491K	0.32	0.17	7	3	100.0	100.0	279	94.2	96.1
6K-ELITE	648K	0.33	0.16	7	2	100.0	100.0	337	94.1	96.2
7K-ELITE	816K	0.34	0.16	7	2	100.0	100.0	370	94.5	96.4
8K-ELITE	1.0M	0.37	0.17	7	2	100.0	100.0	401	94.8	96.7
9K-ELITE	1.2M	0.4	0.18	8	2	100.0	100.0	439	94.9	96.9
10K-ELITE	1.4M	0.42	0.19	9	2	100.0	100.0	454	91.5	97.0

(Tran), and diameter (Diam). We also include the number of connected components and strongly connected components. This table clearly shows that as the size of the elite network is extended (from 1K to 10K), it becomes denser (average degree increases from 49 to 152), the fraction of reciprocated edges initially drops and then increases, and its diameter slightly increases. In all views, 32-40% of the friend-follower relationships are reciprocal, which is higher compared to the reported 22% for the entire Twitter social graph [163]. Interestingly, we observe that all views of the elite network have a single weakly connected component that includes an absolute majority of all nodes except for one or two nodes. However, the number of strongly connected components (SCC) grows roughly proportional with the size of the elite network. The rank correlation between the number of public vs. elite followers for top-10K elite is around 0.55 while the rank correlation between their public vs. elite friends is 0.1, i.e. the popularity of elites among all users and elites are moderately correlated.

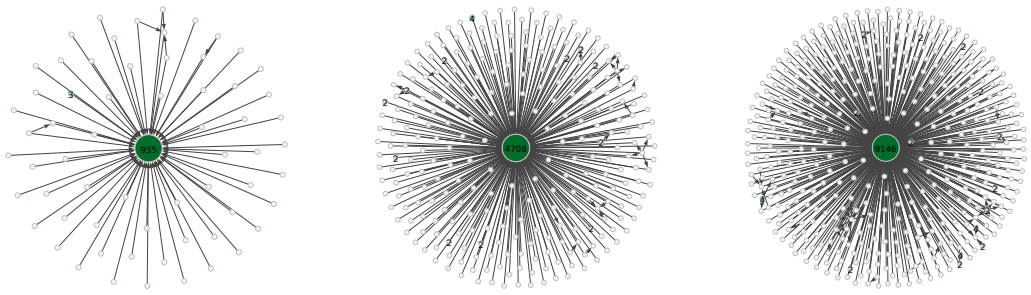

(a) 1K-ELITE (b) 5K-ELITE (c) 10K-ELITE

FIGURE 5.29. The connectivity of strongly connected components of the elite networks

Overall Structure of the Social Graph

In this section, we conduct (strongly) connected component analysis [97] on different views of the elite networks in order to reveal their overall topological structure. As we reported in Table 9, each view of the elite network has many strongly connected components (SCC). However, the largest strongly connected component (LSCC) in each view contains an absolute majority of all elites while all other SCCs have a single node (and in a few cases a handful of nodes). The right section of Table 9 summarizes the fraction of nodes and edges that are within the LSCC in each view. This table shows that the LSCC in each view contains 91-94% of all nodes and 94-97% of all edges of the corresponding elite network.

To gain more insight into the structure of the elite network, Figure 5.29 visualizes the strongly connected component structure of 1K-ELITE, 5K-ELITE, and 10K-ELITE as directed graphs where each circle represents a SCC with the number indicating the number of nodes in that SCC. LSCC is shown with a green circle in the center. Arrows represent friend→follower relationships between users in different SCCs. These figures clearly illustrate that in all views the SCCs form a "star-like" structure where the LSCC is in the center and there are a number of directed edges from every other SCC (that we

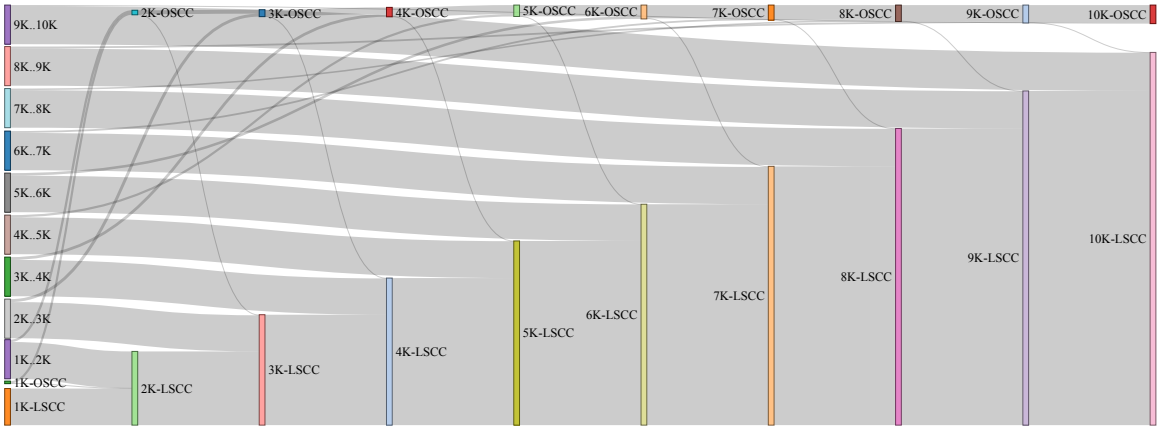

FIGURE 5.30. The dynamics of LSCC as the network expands

call "outsider") to nodes in LSCC. We recall the direction of edges are from a friend to a follower (or the direction of tweet propagation.) Therefore, Figure 5.29 indicates that nodes in the LSCC have an interest in and receive tweets from nodes in other SCCs (through the elite network) but the opposite is not true. In fact, more than 99% of outsiders are followed by users in the LSCC. Most outsider nodes are in a single node SCC and few of them consist of two or more nodes. For example, the Pope has four accounts that only follow each other but they are followed by many accounts inside the LSCC.

As more nodes are included in the view of the elite network, other SCCs in one view may be pulled into the LSCC in the next view since the extended view may include more shortcuts. Figure 5.30 illustrates via Sankey diagram [5] how the LSCC and the outsider in each view are mapped/split to the LSCC and the outsider in the next view[4]. In this figure individual views of the elite network are shown along the x axis. For each view, the two vertical boxes represent LSCC and the outsider. The vertical box at the bottom of each column represents the LSCC and the box on the top represents the

[4]An interactive visualization of this diagram is available on our project page `ix.cs.uoregon.edu/~motamedi/research/elite/evol/sankey_in_out_lscc.html`

outsider. Groups of elites ranked by their number of followers are all presented in the first column alongside 1K-ELITE. Extending the elite network adds one of the groups to a view to create the next view, for instance accounts with rank [1K..2K] join 1K-ELITE to create 2K-ELITE. As the plot shows, more than 95% of these newly added elites join the LSCC and the rest join the other SCCs. An examination of these views also reveals that roughly 13-20% of nodes in other SCCs are pulled into the LSCC in the next view. Note however that a group of other SCCs have no friends (i.e. no incoming edges) and thus remain outside the LSCC regardless of the size of the elite network.

Micro-Level Structure

In this section, we characterize the connectivity structure of the elite network at the community level.

Detecting Communities Among Elites

We start by exploring whether there are groups of tightly connected nodes (or communities) inside the network and then use these communities as the basic elements to explore the coarser representation of each view of the elite network.

There are two basic issues in identifying communities in the elite networks. First, most commonly-used community detection techniques take undirected graphs as input while the elite network is a directed graph [107]. To address this issue, we first convert each view of the elite network into an undirected graph by turning *each* directed edge into a single undirected edge, therefore connecting nodes with two undirected edges (or an edge with the weight of 2) when reciprocal edges exist. This representation allows us to encode tighter binds between users with reciprocal edges. Our approach is therefore different from prior studies (e.g. [169]) where they simply consider a directed graph

as undirected. Second, the outcome of the most commonly used community detection techniques (e.g. Louvain [40], BigCalmm [276], InfoMap [222]) is non-deterministic. More specifically, multiple runs of a single algorithm on the same graph produce different numbers of communities and/or different grouping of nodes into communities. Our empirical stability comparison of a few well-known community detection algorithms showed that COMBO results in communities with more stable mapping of nodes to those communities while maximizing the community modularity, i.e. the identified communities in various runs are more similar compared the detected communities by other techniques. To address the stability issue, we use COMBO [240] that relies on multi-objective optimization to find tight communities. We only consider a group of nodes as a community if they consistently mapped to the same community across different runs. Toward this end, we adopt the following strategy: We run the community detection technique on each view of the elite network k times and determine the communities that individual nodes are mapped to in each run in a vector with k values, called the "community vector". Then, we group all the nodes that are consistently (i.e. all k times) mapped to the same community (i.e. have the same community vector) and refer to the group as a *Resilient Community*. The process of detecting communities also results in groups of nodes for which no other node has the same community vector. We group this set of nodes and nodes in resilient communities with a size smaller than 10 and refer to them as *Unstables*. Therefore, unstable nodes are those that have none to only a few other nodes in their resilient community. These unstable nodes have the tendency to be grouped with other resilient communities of nodes as a single traditional community across different runs, and therefore can not be considered as a part of any resilient community.

Clearly increasing k is more restrictive and may lead to smaller resilient communities since more runs can simply split a community to two (or more) smaller

ones. Figure 5.31 shows the effect of k on the number of resilient communities identified in 1K-ELITE, 5K-ELITE and 10K-ELITE. As the figure shows, increasing k can split resilient communities and increase the number of resilient communities. This number may shrink, however, when the newly created resilient communities include less than the minimum threshold size of resilient communities, which we set to 10. Note that in all runs of COMBO, a community smaller than 20 nodes was never identified, i.e. our threshold does not dissolve a community in the *unstable* group. It is also interesting to note that the effect of increasing k is more considerable in 5K-ELITE. This indeed suggests that this view has a less pronounced community-level structure since each run leads to the identification of a very different grouping of nodes as communities [57]. Figure 5.31 also shows that in all cases the number of resilient communities stabilizes after the initial increase. We conservatively consider $k = 100$ in our analysis, as having more runs does not lead to the identification of more resilient communities in the elite networks. Since the term "community" is the well accepted term to refer to a group of nodes that are tightly connected, we simply use the term "community" to refer to a resilient community, and when necessary use term "traditional community" to specifically refer to a community identified in a single run of the community detection algorithm.

Table 10 presents the general statistics of the communities identified in each view. As the table shows, COMBO detects different numbers of communities in each run. The minimum and maximum number of detected traditional communities are reported in the table. Note that detecting the same number of communities does not mean that the run of COMBO lead to the same splitting of nodes across communities. Using the previously described approach, we identified between 10 to 29 resilient communities with 10+ nodes that collectively cover 92-99%+ of all the nodes in each view of the elite network. Thus,

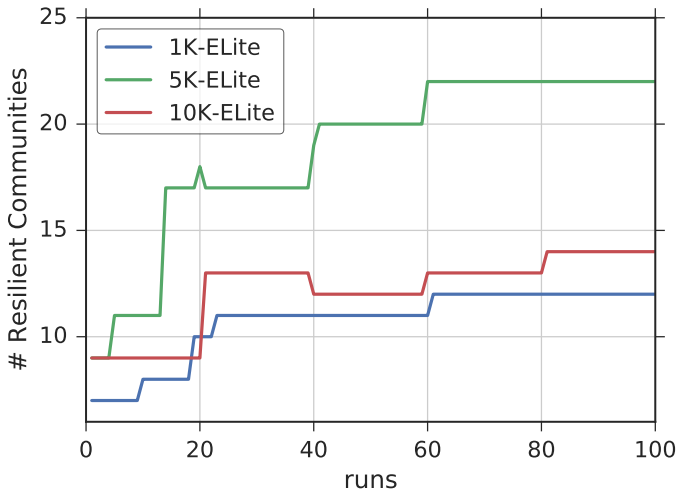

FIGURE 5.31. The number of identified resilient communities as a function of k in three views of the elite network.

less than 8% of the elites are categorized as the *unstables* and this percentage in 10K-ELITE is only 1.6%.

We should reemphasize that the identified communities in (different views of) the elite network could hypothetically be very different from communities on the entire Twitter social graph that contain many regular (i.e. non-elite) users. Later in this chapter we discuss and demonstrate that these identified communities provide a great potential for identifying communities among regular users as well.

Resilient vs. Traditional Communities

It is not clear if the resilient communities contain groups of well-knit nodes inside the community with a low level of interconnection to other resilient communities. To examine whether resilient communities exhibit different connectivity/size characteristics compared to regular communities, which in turn could affect the result of our community-based analysis, we compare the identified communities and traditional communities. We use conductance [41] and modularity [201] as two measure of a graph structure with respect to the identified communities in the graph. Conductance measures how well a

TABLE 10. General statistics of communities identified in each view.

	Min Trad. Com.	Max Trad. Com.	Res. Com.	% Unstable
1K-ELITE	6	7	12	7.9
2K-ELITE	7	9	20	8.0
3K-ELITE	8	9	11	2.5
4K-ELITE	9	10	16	4.0
5K-ELITE	8	10	22	6.5
6K-ELITE	8	9	29	5.5
7K-ELITE	9	11	13	2.4
8K-ELITE	8	8	11	1.7
9K-ELITE	8	9	10	1.2
10K-ELITE	8	9	14	1.6

certain bipartition of nodes splits in the graph. Therefore, for each community – a cut through the edges in the graph – we can compute a single conductance value. Small conductance values mean that a small number of edges are cut to split the graph into two halves (i.e. the community and the rest of the graph). On the other hand, modularity measures how well a graph divides into modules. In other words, a graph with high modularity computed for a certain grouping of nodes into modules (communities) has dense connections between the nodes within modules, but sparse connections between nodes in different modules. For each graph partitioning into communities a single modularity is computed.

We separately identified communities in each view of the elite network. Figure 5.32 shows the scatter plot of conductance and size of traditional communities identified in all 100 runs of COMBO, the resilient communities, and also the *unstables* in the 10K-ELITE view. We recall that smaller conductance suggests a better separation of the community from the rest of the graph. A close comparison of the communities with the identified traditional communities shows that for similar sizes, their conductance values are indeed smaller or similar. There are only two rather small resilient communities that higher

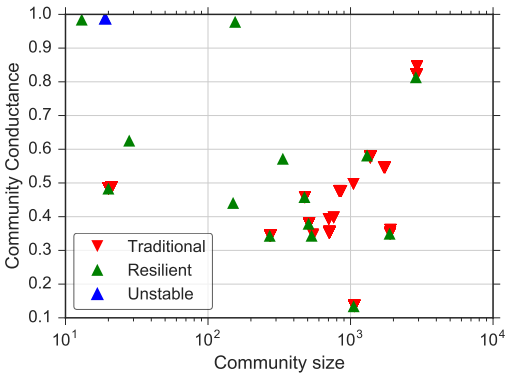

FIGURE 5.32. Conductance vs. size of traditional and resilient communities and *unstables* identified in 10K-ELITE.

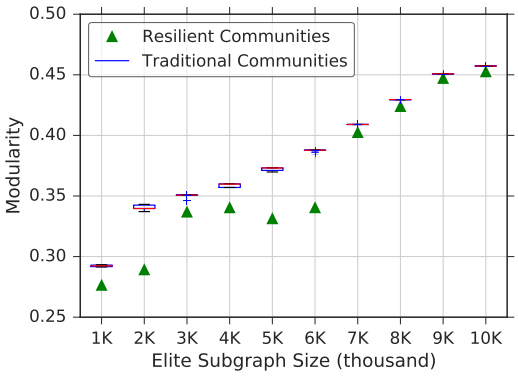

FIGURE 5.33. Modulairty of resilient communities and the summary distribution of modularity for traditional communities in the 100 runs of COMBO

conductance compared to traditional communities. Also, a very small group of *unstables* have a very high conductance, which suggest they are very well meshed to the rest of the elite network.

We also compute modularity to evaluate the strength of the division of each view of the elite network into traditional and resilient communities. Figure 5.33 shows the modularity of resilient communities and the distribution of modularity values for each run of COMBO in different views. With regards to modularity, a higher modularity shows a better grouping of the graph into tight modules. The figure shows that as the network is extended to cover more elites, COMBO is able to find tighter communities. The figure also shows that resilient communities are slightly less modular than the traditional communities in certain views. For instance in 2K-ELITE, 5K-ELITE, and 6K-ELITE the modularity of resilient communities is approximately 0.04 lower compared to traditional communities. This result, in addition to the findings in Figure 5.31, shows that the connectivity in this view exhibits less pronounced modular structure and has higher similarity to the connectivity in a random graph [57]. For the other view, however, the modularity of resilient and traditional communities are very similar. We conclude that

resilient communities each contain a group of nodes with a large number of social ties within the resilient community and a small number of friendships with users in other resilient communities.

Social/Geo Footprint of Communities

In this section, we address the root cause of community formation in the elite network. Our focal question is "*do nodes in a community exhibit any social cohesion?*" Answering this question reveals whether the identified communities represent meaningful elements of the elite network or not. It is worth reminding that approximately 90% of elites are collected from `socialbakers.com`. This resource tags each account with 8 categories, 137 subcategories and 196 countries. To tackle the problem at hand, we leverage this category and location information that we collected for elites. We present two histograms that show the number of nodes across 10 most common categories (i.e. social footprint) and countries (i.e. geo footprint) in each community. Figure 5.34 depicts the social and geo footprints for the 9 largest communities in 10K-ELITE. The footprints of these communities exhibit varying levels of social and/or geo (or language) cohesion. Since many of these accounts belong to easily recognizable individuals/entities, we can also examine the identity of accounts in each community and use their social context to learn more about the "theme" associated with each community[5].

Here we describe the dominant themes in the 10 largest communities in 10K-ELITE. The number in the parenthesis following each community name is the number of accounts in that community.

C_1 **- US Popstar (**2799**):** This community is associated with celebrities, popstars and entertainment media. The vast majority of these elites are from the US with the remainder

[5]The identity of accounts mapped to individual community in each view are available online at `ix.cs.uoregon.edu/~motamedi/research/elite/tables/elite10000_20160112` for readers.

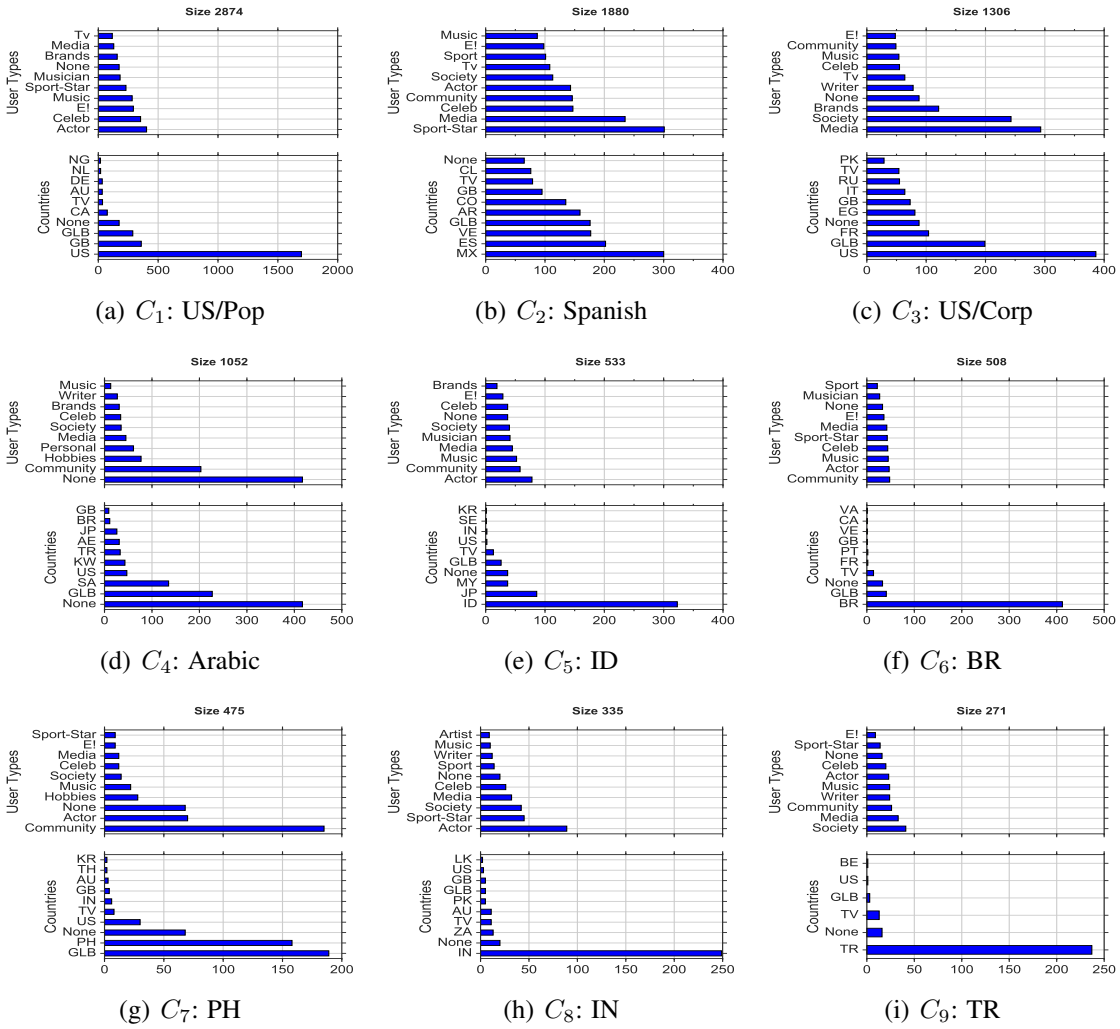

(a) C_1: US/Pop (b) C_2: Spanish (c) C_3: US/Corp

(d) C_4: Arabic (e) C_5: ID (f) C_6: BR

(g) C_7: PH (h) C_8: IN (i) C_9: TR

FIGURE 5.34. The distribution of category and country across accounts in the identified communities of the 10K-ELITE.

almost exclusively from English-speaking countries. US popstars, such as Katy Perry and Justin Bieber, and pop media programs, such as the Ellen Show and the X Factor, play a prominent role in this community. A noticeable teen or "tween" icon thread weaves through this community with Selena Gomez and Ariana Grande and with former Disney stars, such as Justin Timberlake, Christina Aguilera, Britney Spears, and Demi Lovato.

C_2 **- Spanish Speaking** (1827)**:** A common theme across accounts in this community is its common language of Spanish. Geographically, 40% of these elites are from Mexico

and 30% are from Spain. Yet, the geographic distribution draws from a wide swath of both Spanish-speaking elites with a small, but important group of non-Spanish speaking elites. Another theme which is less pronounced in this community is the focus on sports. This community consists of numerous globally popular soccer icons, such as Cristiano Ronaldo and Wayne Rooney, and sports organizations, such as FIFA and the Olympics, but also Spanish-speaking actors and popstars, such as the Columbian singer Shakira and Puerto Rican singer Ricky Martin.

C_3 **- US Corporate Celebrities & Media (**1234**):** This community is associated with the US and Global media stars and corporate elites in the US and UK. This community consists of accounts associated with media groups, corporations and global entities. For example, this community consists of global news and media organizations, such as the BBC, the Guardian (the entire news family), Reuters, CNN, The Economist, all major TV channels in the US, and personalities such as Anderson Cooper and Piers Morgan. Global business leaders, corporations, and institutions are also central to this community, such as Bill Gates, Samsung Mobile, Unicef, Facebook, Google, and NASA. We refer to this community as "US/Corp".

C_4 **- Arabic Speaking (**956**):** This community mainly consists of Arab elites. Interestingly, these accounts mostly belong to media agencies and communities.
We should note that the many of the elites in this community are not indexed in `socialbakers.com`, hence the most common country and user type in Figure 5.34(d) is *None*. However, we extract its social and language context by manually inspecting elites in this community. Mentionable famous Arab accounts in this community are Al-Arabiya and the Al-Jazeera news group.

C_5 **- Brazilian (**496**):** Referred to as "BR", this community is almost entirely populated by Brazilian cultural elite individuals and organizations, such as the soccer stars Kaka and Neymar, and the television network, Rede Globo.

C_6 **- Filipino (**461**):** Referred to as "PH", Most accounts in this community are celebrities from the Philippines. Although many accounts in this community are categorized as GLOBAL (see Figure 5.34(g)), close examination revealed that they are in fact Filipino.

C_7 **- Indonesian and Malaysian (**231**):** Users in this community are mostly from Indonesia and Malaysia. Interestingly, the elites within this community represents a diverse selection of celebrities and communities. An example of a user in this community is Agnes Monica, the Indonesian popstar. We refer to this community as "ID".

C_8 **- Indian (**317**):** Referred to as "IN", this community represents a range of Twitter accounts for cultural and political Indian elites. For example, the actor Amitabh Bachan, the cricket star Suresh Raina, and Narendra Modi, the Prime Minister of India, are in this community.

C_9 **- Turkish (**242**):** This community consists of various categories of Turkish elites. Popular Turkish organizations, such as the soccer club Galatasaray, NTV television networks and online media celebrity Cem Ylmaz are in this community.

C_{10} **- K-Pop (**142**):** This community mainly consists of Korean popstars. Among well known elites we can name the Korean actor Siwon Choi. Even non-Korean accounts within this community are focused around K-Pop (e.g. @allkpop).

Other communities, which each include less than 50 users, include *Thai* (28), *Adult* (20), *US TV stars* (19), and *Global fun* (13).

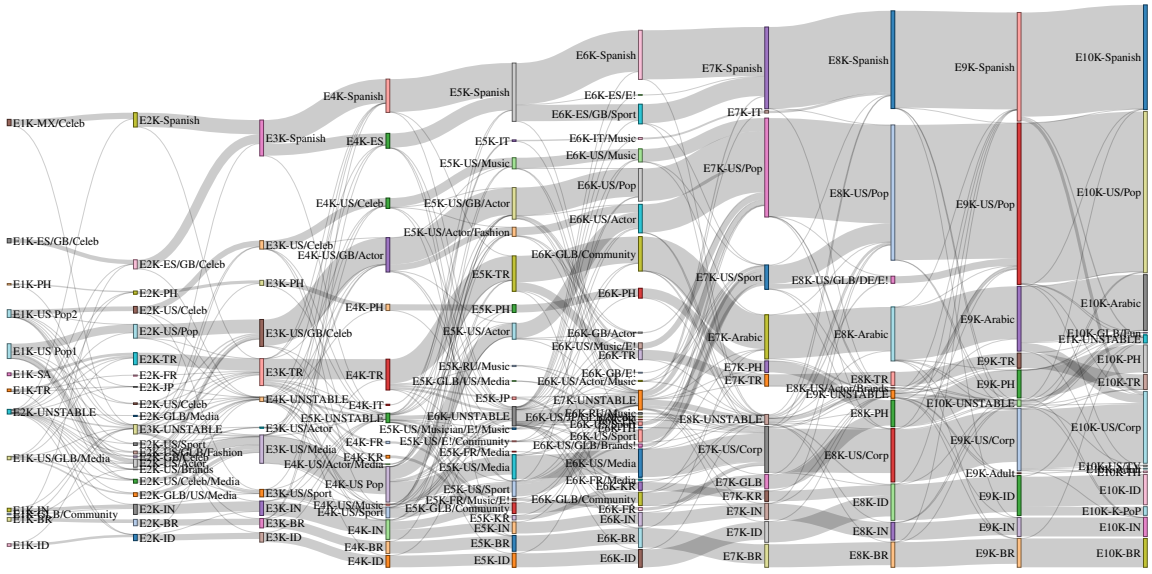

FIGURE 5.35. The dynamics of communities as the elite network expands; 1K-ELITE through 10K-ELITE

Communities in Different Views

Since different views of the elite network are related and are formed simply by adding less popular elites, this raises the following questions: *"Are communities in different views of the elite network are related, and if so how?"* To answer this question, we keep track of the communities by following their individual nodes across different views. This in turn reveals the overlapping users between two communities in consecutive views and shows the similarity of the communities. Figure 5.35[6] shows the relationships among communities in consecutive views as we extend the size of the elite network using a Sankey flow diagram [5]. Each group of vertically aligned boxes represents communities in a single view that are ordered from the smallest (in the left) to the largest (in the right) view of the elite network. Each community is labeled with the view where it is identified (e.g. E10K) and the theme of the community (e.g. US Pop). Each edge/flow

[6]The interactive version of this figure is available on our project page: `ix . cs . uoregon . edu / ~motamedi/research/elite/evol/elite-extension_rcom-sankey`

(from left to right) between two communities indicates the number of overlapping nodes between them. Note that at each view, 1K of the nodes are new compared to the previous view. Hence, the cumulative height of all boxes in each column increases from left to right. The abundance of thick edges on this plot suggests that many users in any community across various views remain together and form a community in the next view. Specifically, 60-98% of node pairs in one community fall within the boundaries of a single community in the next consecutive view. Not surprisingly, careful examination of the social and geo footprint of related communities in different views also shows that the theme of most communities remains the same across different views (e.g. "E8K-BR" to "E9K-BR"). On the other hand, the theme for a small number of communities slightly evolves as more nodes join the community (e.g. "E6K-US/Media" evolves to "E7K-US/Corp" in which more "corporations" joined the community and slightly generalized its social footprint). We can also observe some splits and mergers in the graph (e.g. "E9K-ID" splits into a larger "E10K-ID" and a smaller "E10K-K Pop", and "E6K-Spanish" and "E6K-ES/GB/Sport" merge to form "E7K-Spanish" – a large mostly, Spanish speaking community.) For the rest of our analysis in this section, we primarily focus on the communities in the largest elite network, 10K-ELITE, as it contains the most modular communities.

Inter-Community Connectivity

As we showed earlier in this chapter, communities represent meaningful elements of the elite network. In this section, we characterize its structure at a coarse view with regards to the communities and their inter-connectivity. To this end, we explore their pairwise connectivity in terms of *(i)* direct friend-follower relationships, and *(ii)* indirect pairwise coupling.

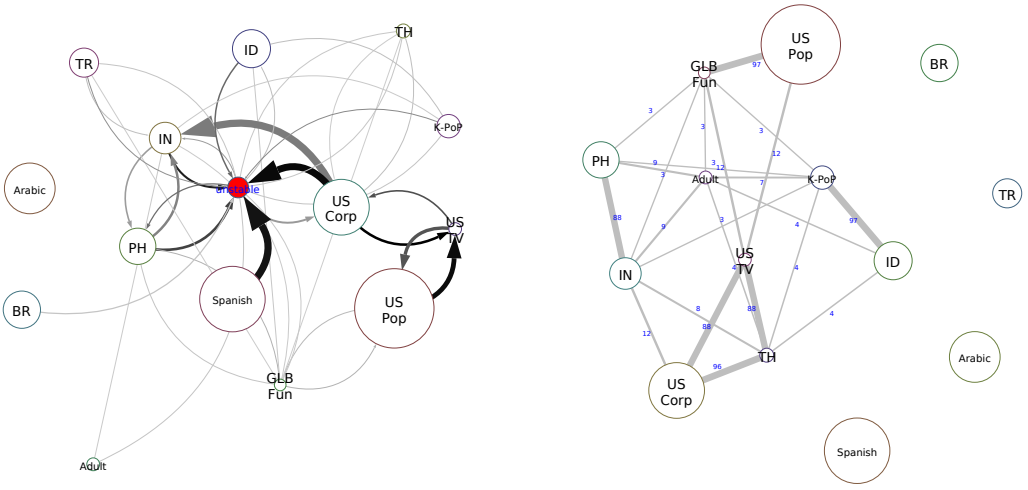

(a) The number of direct friend-follower relations between communities identified in 10K-ELITE

(b) The frequency of co-appearance of communities identified in 10K-ELITE

FIGURE 5.36. Graph structure at the community level

Direct Friend-Follower Relationships

Figure 5.36(a) sketches the inter-community connectivity in the 10K-ELITE. In this figure, each circle represents a community (or the group of unstable nodes) where the size of the circle indicates the population of nodes in the community[7]. The direct link from C_i to C_j represents a relationship between accounts in C_i and their followers in C_j. The width of each link encodes the absolute number of friend-follower relationships, while its color (level of darkness) encodes the level of bias in connections between two communities. Bias is measured as the difference between the number of follow relations between two communities and the same number in the randomized version of the elite network. It is worth noting that in order to avoid messiness, Figure 5.36(a) only shows a link when the inter-community bias is positive (i.e. the number of edges between two communities is larger than the randomized version of the network) and also does not present the self loops. As the figure shows, the communities in 10K-ELITE mainly sit

[7]A minimum size is used for the circles to fit the labels.

around the *unstable* group. The following observations can be drawn from this diagram: First, we clearly observe a structure among these US-based communities which indicates the relatively high level of interest/attention among them. The connectivity bias between them is very large compared to rest of the graph (dark gray and black edges), although the number of links between these communities are not very large (thickness of the edges). The largest number of inter-community edges are from "US/Crop" to "unstables" and "IN", and from "Spanish" to "unstables". Second, there is a substantial number of links between PH and IN that suggest interest between these two communities. Third, a number of nation-centric communities (e.g. BR, ID, PH, TR) do not have any significant connectivity to any other community, but are following the "unstables". Fourth, the only community with negative connectivity bias to all other communities including the "unstables" is the Arabic speaking community. Similarly, the "Adult" community has a very small connectivity bias to other communities.

Indirect Pairwise Coupling

Direct connections between communities are only one aspect of inter-community relationships. In this section we introduce *pairwise coupling* between two communities, which is a more subtle measure of relationships among communities. While the last analysis reveals the interest between different communities captured by friend-follower relationships, this one shows which communities have tighter interconnections or perhaps contain overlapping sections. To assess the notion of coupling between each pair of communities in the 10K-ELITE, we examine different runs of the community detection to determine whether two communities "co-appeared in one traditional community". We use the frequency of co-appearance for each pair of communities across all runs as a relative measure of coupling between resilient communities. We recall that as we

increase the number of runs of the community detection algorithm (or k in Section) to identify resilient communities, it is more likely for a traditional community to split into two or more resilient communities. This analysis illustrates whether some groups of communities are tightly coupled and could address any side effect of using a large k.

Figure 5.36(b) summarizes the pairwise coupling between communities in 10K-ELITE where each circle represents a community and the thickness of the undirected edge between them shows their co-appearance (i.e. indirect coupling) in traditional communities. We also included the number of the pairwise co-appearances on the edge labels. This graph demonstrates coupling between communities that are mainly aligned with the discovered relationships in Figure 5.36(a). The figure shows high level coupling among *a)* US/Corp, US/TV and Thai, *b)* Indonesian and K-PoP, *c)* Indian and Filipino, and *d)* US/Pop and Global/Fun communities. We also see that Turkish, Spanish, Arab, and Brazilian communities never co-appear with another community, which is mostly aligned with the results in the previous section. Note that some of these high levels of coupling are not so obvious by looking at the direct follow relation. For instance, while ID and K-Pop have high coupling in this view, only a small number of edges exist between the two communities. Later in this chapter we investigate the possible root cause of this high coupling. The notion of pairwise-coupling can also be used to further coarsen the community-level structure in the network. We can achieve this by simply considering communities with a high level of coupling (a threshold on coappearance) as one community. As a result, if we consider the threshold of 50 coapperances for merging communities, the summary view would include 9 communities instead in 15.

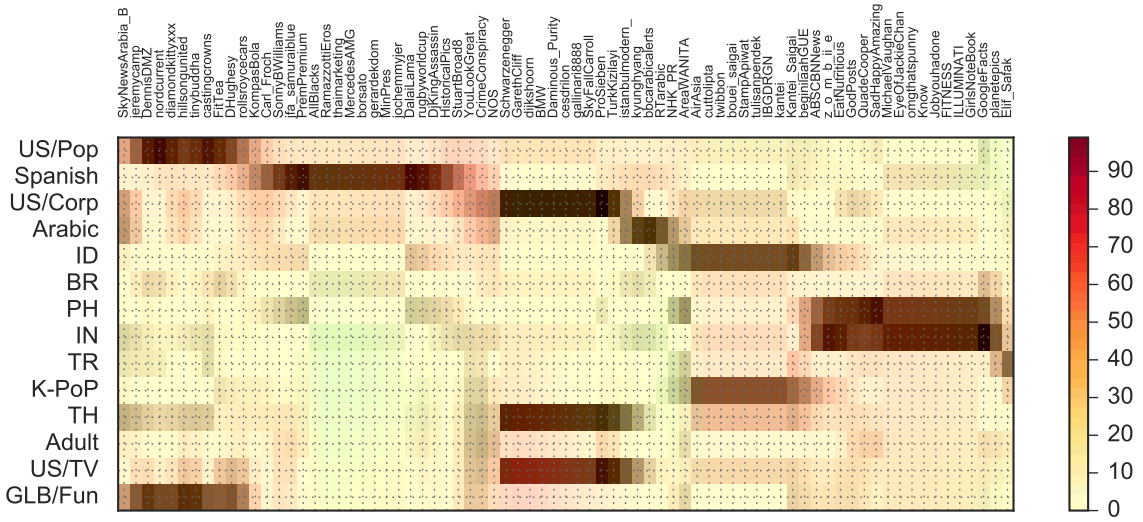

FIGURE 5.37. Coappearance of 75 unstable accounts with the highest number of elite followers with communities

Node Level Analysis of Communities

We examine the most visible elites to determine the role that they play in the elite network by focusing on the 10K-ELITE. Toward this end, we consider the *unstable* group in this view (the 1% of all elites in 10K-ELITE that were not a part of any community) separate from the nodes in communities.

Unstable Nodes

As we showed earlier, unstable nodes have a large number of relations to the elites in different communities. Per definition these nodes do not belong to a particular community. We examine their frequency of coappearance with individual communities across different runs of the community detection algorithm. Figure 5.37 presents the result as a heatmap for 75 out of 155 unstable nodes with the largest number of elite followers. The color of the cell (i, j) indicates the frequency of coappearance for account j with community i. Using a simple reordering algorithm, we arranged unstable nodes along the x-axis in such a way that those with similar coappearance patterns are

closer. We emphasize that the sum of the values in each row is not necessarily 100%, because a node may coappear with more than one resilient community in each run of the community detection. We recall that the higher the frequency of coappearance of a node and a community suggests a tighter coupling between them. In fact, a node that frequently coappears with two (or more) communities could be viewed as a (overlapping) member of those communities which was disconnected from the communities due to our strict coappearance requirement in forming resilient communities. Therefore, this analysis illustrates how the set of unstable nodes can be further divided in accordance with the coupling with the resilient communities. As the figure shows, there are a few distinct coappearance patterns among nodes in Figure 5.37. These patterns are in fact aligned with inter-community couplings in Figure 5.36(b), i.e. groups of communities that have many unstable nodes coappearing with them have high coupling as well. A few examples of these patterns are as follows: *(i)* A group of unstable nodes mostly coappears with US/Pop and Global/Fun communities. The manual inspection of these accounts shows that they are associated with less popular US-based accounts with various foci. *(ii)* Another group of unstable nodes mostly coappears with the Spanish speaking community and has a lower level of coupling with any other community. The users in this set are mostly sport-related but not necessarily Spanish speaking, such as @rugbyworldcup, @StuartBroad8, and @AllBlacks. *(iii)* The figure also shows that a group of unstable users coappears with the ID and the K-Pop communities. Although the direct interconnection between the two communities is low (as shown in Figure 5.36(a)) and the communities do not seem to be contextually similar when compared to other communities, unstable nodes in this group are tightly coupled with both communities and seem to be a part of both communities. Users in this group include a few Asian online celebrities.

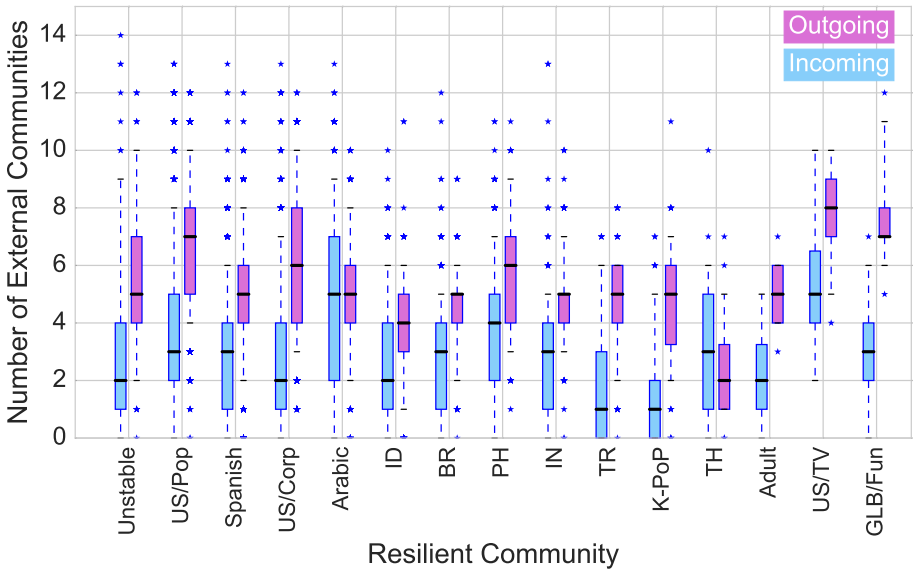

FIGURE 5.38. Distribution of the number of related communities for nodes in communities in the 10K-ELITE

Accounts that Connect Communities

Since individual communities contain related accounts, one natural question is *"Do specific nodes act as bridges to/from other communities?"* In general, our analysis shows that almost all users in the 10K-ELITE have at least one external incoming or outgoing connection to a community other than their own. To answer this question, we make a distinction between *incoming* ($inBr(C)$) and *outgoing* ($outBr(C)$) bridge node(s) for community C that have incoming/outgoing connections from/to users in the largest number of other unique communities. In other words, we measure the importance of a bridge node based on the number of unique communities that it connects to rather than the actual number of connections to other communities. For example, if node n_1 has $1\,000$ external followers (i.e. followers in other communities) that are all located in two communities and node n_2 has 100 external followers that spread across 10 communities, we consider n_2 to be an $outBr(C)$ as it is visible among a larger number of communities.

TABLE 11. The accounts that act as in/out bridges in each community.

Community	$inBr(s)$	$outBr(s)$
US/Pop	6BillionPeople, JonahLupton, p0tcom	katyperry, justinbieber, rihanna, ladygaga, ArianaGrande, aliciakeys, NICKIMINAJ, kanyewest, ParisHilton, rickygervais
Spanish	HalfordisMe	instagram, verified
US/Corp	EnergyDrinkRen	twitter, HuffingtonPost, Support
Arabic	KavalonThatsMe	benlandis, paulatooths, TheGodLight, AxelKoster, neoseol, sodan4
ID	fadjroeL	UberSoc, echofon
BR	drangelocarbone	KAKA, neymarjr, giseleofficial
PH	itsmovies, Drrake	Earth_Pics
IN	LeBronJames, LordLouis3	GreatestQuotes, LordLouis3, Brilliant_Ads
TR	Doarutkay, hidoturkoglu15, ertemsener, omerrcelik	RT_Erdogan, cbabdullahgul, Ahmet_Davutoglu, memetsimsek, TurkishAirlines
K-PoP	siwon407, jucklee	TwitBird
TH	Woodytalk	Woodytalk
Adult	Hot_Girls_247, nlpantyhose, SexyCreeps	gspot1177
US/TV	yokoono, shwood	yokoono, MarthaStewart
GLB/Fun	History_Pics	History_Pics

Figure 5.38 presents the summary distribution of the number of unique external communities for elites in each community. In essence, the boxplots of Figure 5.38 illustrate how many other elite communities the users in each community of elites generally *pay attention to* (i.e. have in-edge or follow) and *receive attention from* (i.e. have out-edge or being followed by), respectively. As the figure shows, users in most communities are following a less diverse set of elites, compared to the variation of the elites that are following them. On average, elites pay attention to 1-5 other communities, but receive attention from 2-8 communities. The Arabic speaking and the Thai communities are exceptions, because their set of friends are more diverse than the followers. On one hand, users in Arabic speaking and US/TV communities follow the most diverse set of other elites. On the other hand, elites in US/TV and Global/Fun have the most diverse set of followers. There are a few outliers in most communities (shown as stars) that have friends and followers in almost all communities. Per our definition, these outliers act as an incoming/outgoing bridge for each community from/to external communities in the elite network.

We individually examine these bridging accounts and their social contexts. Table 11 presents the usernames of the accounts in each community that have followers and friends in the largest number of other communities as $inBr$ and $outBr$ for their community. We observe that most of the $outBr$ are well-recognized and popular individuals/entities with appeal across diverse groups. However, the $inBr$ are either not recognizable or are genuinely interested in many different groups. We examine whether $inBr$/$outBr$ are different from the users in each community who have the largest in/out degrees. Indeed, the users with the largest number of in/out degrees are among the $inBr$ and $outBr$ in most of communities, respectively. Inversely, in all communities, $inBr$/$outBr$ are among the top 5% accounts with the highest in/out degree in that community. We have also examined the PageRank of the incoming and outgoing bridge nodes in Table 11 to see whether these bridges are among the most central nodes in the elite network. In general, there exists a positive correlation between the number of external communities that a node connects with and the PageRanks centrality of the node, and the PageRank of $outBr$ are higher than the rest of the nodes.

In summary, the analysis of social and community footprints along with the identification of accounts in each community reveals cohesion among users in each community around themes that are obvious in some cases (e.g. language, region, country, business) and more subtle in other cases. The observed cohesion in these communities indicates that they represent meaningful elements of the elite network. As we extend the elite network, the number of communities could change. However, there is a clear relationship among communities in different views as these related communities represent the evolving view of a group of nodes with a specific and slowly changing social theme. The inter-community connectivity and coupling can be used to create coarse views of the topology of the elite network. These coarse summary views capture the interest among

communities and community hierarchies, respectively. Finally, the analysis at the node level either among nodes inside a community or unstable nodes reveals the nodes that are bridging a community to other communities or reside at the boundary of two or more communities.

Tracing Elite Communities in the Entire Social Graph

As we mentioned earlier, the identified communities in the elite network only reveal the modular structure of friendships among elites, and therefore the communities of regular users could hypothetically be very different from communities of the elite network. Our goal in this section is to check *"whether the communities detected in the elite network provide any insight about the topological structure of the entire graph."* Our analysis is in part motivated by the observation that many communities remain effectively the same as the elite network is extended in its size, as provided earlier in this section. Since it is impossible for us to capture the full social graph of Twitter, our methodology uses a random sample of Twitter users and traces the existence of modular structures using the communities identified among elites. To this end, we use communities of elites in particular as landmarks for an interest-based clustering of regular users.

Landmark Clustering Using the Elite Communities

As we showed earlier in Figure 5.27, 80% of the regular users follow at least one elite in the 10K-ELITE. Given the high reach of the elites in this view, it seems natural to use them as landmarks to classify regular users based on the elites that they follow. Figure 5.39 presents a detailed view of the elite friends of the 10K+ regular randomly sampled Twitter users. In each plot we group the regular users on the x-axis based on the number of elite friends (elites that the sample user follows). Figure 5.39(a) presents the

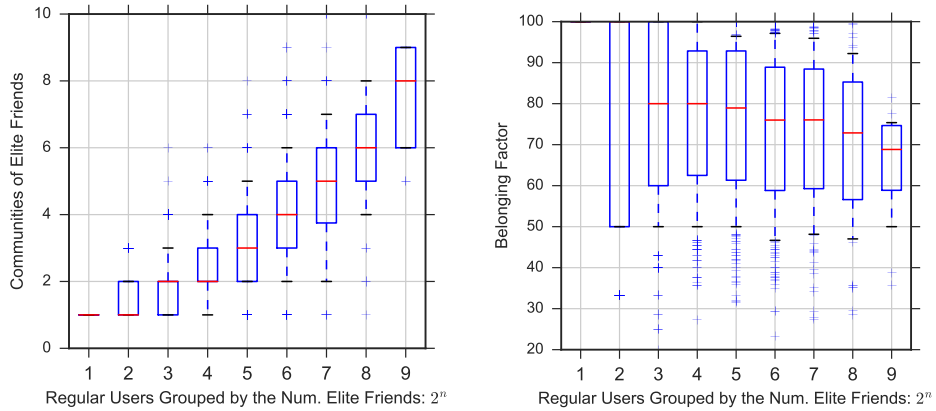

(a) Distribution of number of elite communities that a regular user follows

(b) Distribution of the belonging factor

FIGURE 5.39. Using elite communities as landmarks to cluster regular users.

summary distribution of the number of communities amongst the corresponding elite friends. As the figure shows, each regular user follows elites that are in 1-8 different communities. We use these elite communities as landmarks to cluster regular users. For each regular user, we first compute a *belonging vector* that counts the fraction of its elite friends that are in any community. A regular user is then mapped to the elite community that makes up for the majority of its elite friends. Figure 5.39(b) shows the maximum element in the belonging vector that we refer to as the *belonging factor*. As our results demonstrate, the median belonging factor is at least 70%. Therefore, most regular users can be confidently mapped to a single elite community.

We also examined the friend-follower relationships between regular users (edges) with respect to the elite communities for approximately 100K edges. For each edge, we map the friend and the follower to a community as previously explained and check if they map to the same community. Our examination shows that 64.8% of the friend-follower relationships are between users who map to the same community. Note that 69.1% of relationships among elites are within the same community.

We conclude that the identified communities in the elite subgraph provide a great set of landmarks for clustering regular users that follow the elites. Therefore, via community detection on a very small portion of the social graph, namely the elite network, we can effectively identify groups of tightly connected nodes in almost the entire graph.

Influence Among Elites

In this section, we turn our attention to how the elites may influence other elites on Twitter. Influence is a rather subtle effect of user u on other users that may not be properly measured by a single metric. In the context of graph theory and complex network analysis, various indicators of centrality have been proposed to measure the importance of each node, e.g. the number of followers (out degree), betweenness, closeness, or eigenvector centrality. Alternatively, historical measurements of a user's user in engaging an audience, such as the number of retweets, mentions, or comments have also been used to quantify users' influence. These measures of importance are in fact correlated with the degree to which a user can influence others in the same network [97]. Prior studies on Twitter mention the subtleties in quantifying the influence and used various metrics to capture different aspects of influence. Kwak et al. [163] used three metrics – the number of followers, PageRank, and the number of retweets – and found that the ranking of the most influential users differed depending on the metric. Cha et al. [59] also compared three different measurements of influence – the number of followers, retweets, and mentions – and reported that the most followed users did not necessarily score high on the other metrics.

We consider the following two sources of information to measure the influence of elite user u on other elites in the 10K-ELITE: *(i) Social graph*: The social

interconnections captured in the elite network help us measure the centrality of a user's topological position within that network. *(ii) User engagement*: The success of an elite in engaging others also serves as a resource to measure influence. Specifically, we use interactions in the form of *retweet* and *reply* in our analysis.

Our objective in this work is slightly different than those of the prior studies, since our focus is to capture the influence of elites on each other and not the regular users in the OSN. Hence, we extend or modify the formerly introduced measurements of influence as needed. For instance, we do not use metrics such as the total number of retweets or favorites of a user's tweet, since they cannot be broken down by the regular or the elite users who contributed to those numbers. We also do not intend to reconstruct the actual diffusion tree which may contain regular users. Therefore we specifically focus on the engagement-based influence regardless of its diffusion. With respect to indices that are based on user engagement, we extend the commonly used metrics (e.g. number of retweets) and consider the number of unique users that engage with the influencer as well.

Next, we describe how we identify the most influential elites using each one of these data sources, and then examine the overlap among influential users based on each metric.

Social Graph

The most primitive measure of influence captured through the elite subgraph is the user popularity, i.e. the number of elite followers. In the context of the social graph, popularity translates to the node out-degree. It is important to remember that since tweets cascade through the system, the number of followers alone does not reflect the influence comprehensively. More sophisticated measures such as PageRank [46] are used to better capture propagation of influence along the network.

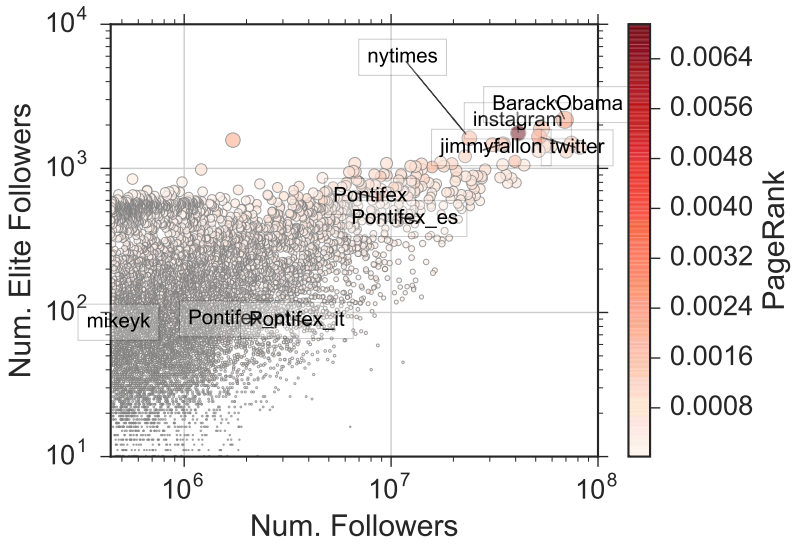

FIGURE 5.40. Visualizing centrality captured through the social graph.

The PageRank of a node measures its centrality in the network by showing its relative reachability to other nodes. PageRank is essentially a generalization of degree centrality and is correlated with the number of nodes that can be reached from the node by different paths. However, the contributions of faraway nodes are penalized as the length of the paths increase. In the elite network, PageRank translates to how easily a tweet by an elite reaches (and influences) other elites. We compute the PageRanks of nodes in the 10K-ELITE to measure their centrality. A key question is *"whether (and to what extent) the PageRank of a node is correlated with its number of followers and elite followers (i.e. the out-degree in the entire network and the out-degree in the elite network)?"* To explore this issue, Figure 5.40 presents the number of followers (on the x axis), number of elite followers (on the y axis), and the PageRank (as the size and the color of circles) for all elites in the 10K-ELITE using a log scale for both axes. We also labeled 10 accounts with the highest PageRank values in this figure. We observe a few interesting points in this figure. First, the figure shows a high correlation between the number of followers and the number of elite followers. Second, we observe that many

accounts with the highest PageRanks have indeed a large number of followers and elite followers (notice the top right corner of the figure). However, it is interesting that some users (e.g. all Pope Francis's accounts) whose number of (elite) followers are an order of magnitude smaller than the maximum number of (elite) followers, still achieve some of the highest PageRanks. An example of such a case in the figure is @mikeyk, the co-founder and CTO of Instagram, that has the second highest PageRank despite having a small number of regular and elite followers. Our hypothesis is that his high PageRank is due to his close tie to @instagram (Instagram's official account on Twitter), which has the highest PageRank. To test this hypothesis, we remove instagram from the elite network, which leads to the drop of mikeyk's PageRank to rank $3\,288$, hence our hypothesis is correct.

Social Engagement: Reply & Retweet

The number of reactions to a certain tweet is a measure of the tweet's popularity and in turn the popularity of the user who posted it. Prior studies have used retweets to measure influence among Twitter users [59, 163, 30, 60]. They mostly use the total number of retweets for all tweets posted by a user to measure her influence [59]. Calculating PageRank over the retweet graph has also been proposed a metric to measure influence [267]. The main difficulty in using this method is the way Twitter organizes the retweets; for each retweet by user u_x, Twitter indicates the identifier of the corresponding original tweet and the user u_{orig} that posted the original tweet. Therefore, the intermediate users involved in the diffusion of a tweet are obscured. To tackle this limitation, some studies proposed techniques to reconstruct the *diffusion tree* and compute the PageRank on the diffusion construct. All these measures, however, count the users under influence as equal and cannot distinguish influence on elite and regular users.

Our proposal is to measure pairwise influence of elites on each other and then aggregate those measurements. In addition to using retweets, we also use replies as they provide a measure of an elite's capability to trigger a reaction in other elites. Our dataset contains more than 31M tweets from the accounts in 10K-ELITE. 6.5M of these tweets are retweets and 5M are replies.

We capture the overall influence of user u (in terms of retweet or reply) on all other elites with the following three metrics: *(i) Number of reactions* is the total number of retweets (or replies) of original tweets posted by u that is captured in our dataset. Note that this metric is a simple extension of the *number of retweets* used in prior studies to identify key influential users that counts all the reactions, not just those by the elites. *(ii) Number of influenced elites* is the number of unique elites that have retweeted (or replied to) at least one of u's original tweets. *(iii) Aggregate influence* of user u is the summation of the fractions of any other elites' captured tweets that is a retweet of (or is a reply to) tweets originally generated by u. More specifically:

$$\textit{Aggregate Influence}(u) = \sum_{v \in Elite} \frac{RT_{u \to v}}{N_v} \tag{5.1}$$

where $RT_{u \to v}$ and N_v denote the number of times that user v retweeted (or replied to) user u and N_v is the total number of v's tweets.

Figure 5.41 shows a three-dimensional measure of retweet and reply influence for users in the 10K-ELITE as scattered plots. Each circle in Figure 5.41(a) (Figure 5.41(b)) represents a single elite u where its x coordinate indicates the total number of retweet (reply) by other elites, and its y coordinate shows u's aggregate retweet (reply) influence. We also encode the number of influenced elites by each user in both the size and the color of each circle. Additionally, we labeled some of the key circles with the name of their corresponding user. Figure 5.41(a) illustrates a few interesting points: First we observe

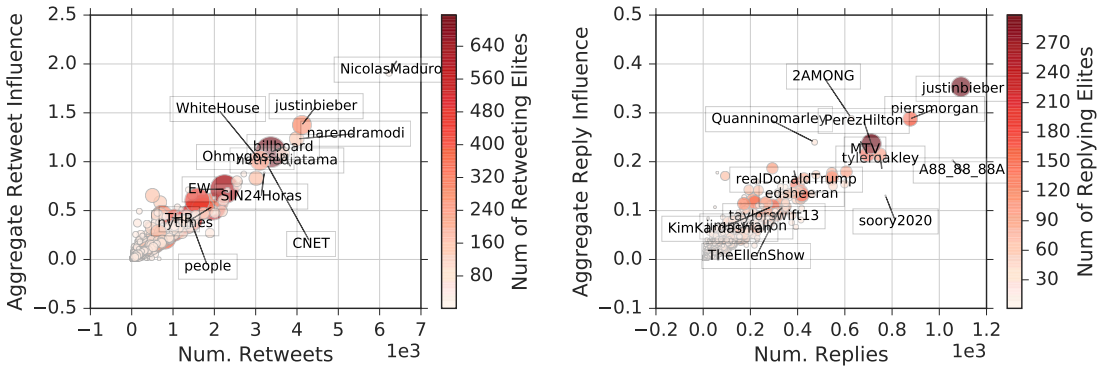

(a) Retweet (b) Reply

FIGURE 5.41. Visualizing reaction-based influence metrics of elites.

a generally linear correlation between the number of retweets and the aggregate retweet influence. Second, we observe a few users whose aggregate influence and number of retweets are rather large (larger than 1.0 and 4K, respectively) but they are retweeted by a small number of elites. For example, @nicolasmaduro (President of Venezuela), @justinbieber and @narendramodi (Prime Minister of India) have more than 4K retweets but are being retweeted by only 90, 272 and 160 elites, respectively. In comparison, @EW is retweeted by approximately 500 elites, but has only 2K retweets. In essence, users such as @nicolasmaduro and @narendramodi have a high influence but only on a small number of elites. Third, we can easily recognize the username of the accounts who are being retweeted by more than 500 elites. Many of these accounts belong to news and media agencies (e.g. @billbord, @nytimes, @people). The aggregate influence and the number of retweets of these elites widely varies.

Figure 5.41(b) presents the three dimensions of reply influence among elites with an encoding similar to Figure 5.41(a). We observe the same general linear correlation between the aggregate reply influence and the number of replies. However, the figure shows some clear differences between reply and retweet influence. First, the number of replies and replying elites and the aggregate reply influence are much smaller than the

TABLE 12. Top 10 most influential elites in the 10K-ELITE based on different metrics: PageRank, the number of retweeting or replying elites

Rank	PageRank	Reply	Retweet
1	instagram	PerezHilton	billboard
2	mikeyk	justinbieber	EW
3	twitter	TheEllenShow	nytimes
4	BarackObama	taylorswift13	people
5	Pontifex	MTV	Variety
6	Pontifex_es	edsheeran	THR
7	Pontifex_pt	realDonaldTrump	TIME
8	Pontifex_it	piersmorgan	AppleMusic
9	nytimes	jimmyfallon	mashable
10	jimmyfallon	KimKardashian	RollingStone

corresponding measures for retweets. This suggests that retweeting is a more common reaction in Twitter compared to replying. Considering the effort needed for replying to a post vs. retweeting it, this result is indeed reasonable. Second, we observe a few users with a large number of replies that only receive reactions from a small number of elites. @sorry2020 (an Arabic fan account of Liverpool FC) and @a88_88_88a (an Arab online celebrity) are two accounts that stand out in this figure. Finally, examining the usersnames, almost all of the key accounts that receive replies from many elites belong to individual celebrities in the entertainment industry and gossip media, for instance @PerezHilton (the gossip blogger and columnist) and @justinbieber (the popstar singer) receive replies from as many as 300 elites.

Table 12 summarizes the top-10 most influential elites based on their PageRank and one measure of retweet or reply influence, namely the number of influenced elites. We observe that except for @jimmyfallon, who appears in two top-10 rankings, there is no other overlap between them.

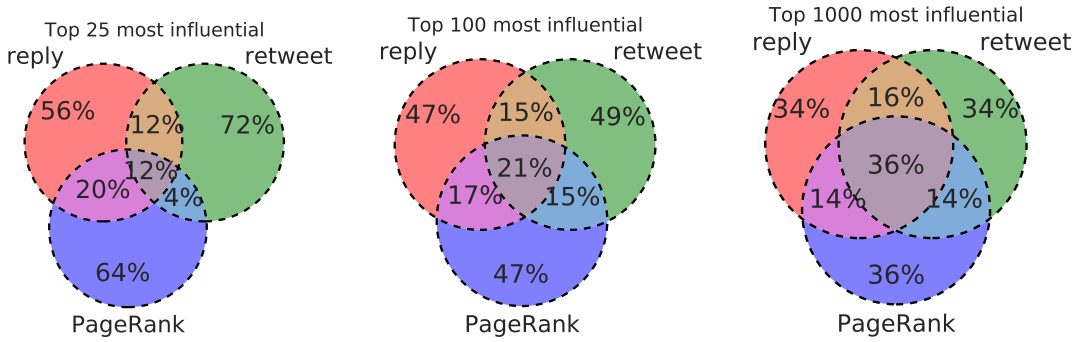

(a) Ranked as top 25 (b) Ranked as top 100 (c) Ranked as top 1K

FIGURE 5.42. Overlap among different influence measures

The observed minimal overlap among the top-10 most influential users based on different measure raises the following question: *"How does the overlap among the top-N most influential users based on different metrics change with N?"* Exploring this question reveals the level of separation between the influential users according to each measure. The three Venn diagrams in Figure 5.42 present pairwise and three-way overlap among top-N influential users according to the three metrics for N equal to 25, 100 and 1K. We observe that the 3-way overlap among different groups of influential users grows with N from 12% to 21% and 36%. Interestingly, even for the top-1K, between 34-36% of users are considered influential based on just a single metric, and the plots do not reveal any similarity between ranking observed by any two metrics. Hence, each of these metrics captures a different aspect of importance/influence, and the topological centrality of a user's position in the social graph does not lead to his success in attracting large reactions from other elites. This finding is generally aligned with the lack of correlation in various measurements of influence in prior studies [59, 163].

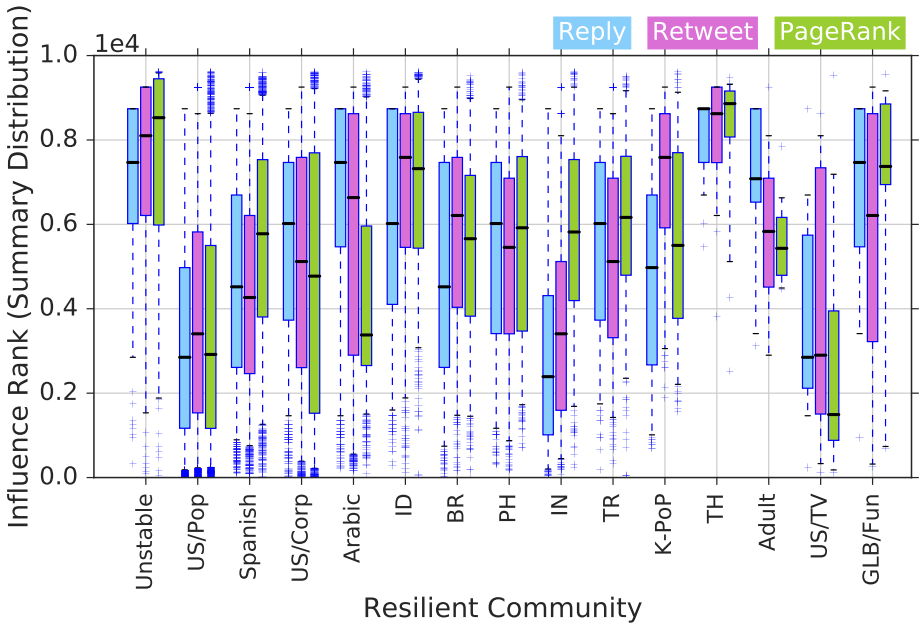

FIGURE 5.43. Distribution of the rank of influential nodes in communities in the 10K-ELITE

Influential Communities

Our analysis of the influence among elites untill this point was the at the user level, however it is also important to examine the relation between influence and communities identified in the elite network. To this end, in Figure 5.43 we present the distribution of rank of users based on various measures of influence across different communities. While communities such as "Thai" and "Adult" contain users with low ranks based on all influence measures, no community is clearly ahead of all others, and the US-based communities seem to be only slightly more influential than others. "US/Pop" and "US/TV" score the highest PageRank influence, and the "Indian" community has the highest reply influence. Finally, the most retweet-based influential users seem to be more uniformly distributed in different communities.

In Summary, our analysis to identify key users in the elite network shows that holding prime positions in the social graph (high PageRank) does not guarantee a high

influence measured through retweet and reply. Users with the highest level of influence captured via retweet are mostly related to news media and music industry, while those who exhibit the highest level of reply influence are present with the entertainment gossip media industries. Analyzing the distribution of influential users among communities, we observe a couple of communities have disproportionately few influential users, and US-based communities include the most influential ones.

Summary

In this chapter, we captured and analyzed the elite network of Twitter. We define n-ELITE as the view of the elite network that contains all the friend-follower relationships between the n most followed accounts in Twitter. We showed that the most popular elites (accounts with the largest number of followers) are more central in the elite network, and as the less popular elites are added to the network, they sit in outer layers of an "onion-like" structure. We demonstrated that the followers of the 10K-ELITE comprise 80% of the users in the entire OSN, and argued for limiting the size of this elite network to the top 10K most followed accounts. We showed that the network is composed of tightly connected communities with strong social cohesion. We unveiled the coarse level structure of the elite network using these communities and identified at the user level the accounts that sit at the overlapping boundaries of some communities. We also demonstrated the potential usage of these communities as landmarks to cluster the OSN by mapping a regular user to the community that contains the majority of the elites that it follows. While 35% of the friend-follower relationships between elites fall across the boundaries of different communities, the percentage of friend-follower relationships between regular users that are mapped to different elite communities is 39%. Finally, we assessed the aggregate influence of each elite on the rest of the elite network using three

different methods and explored the (dis)similarities among top-N influential users based on various metrics. We plan to extend this work by investigating the temporal evolution of the elite network along with its underlying causes and implications.

Part II

The Internet

CHAPTER VI

INTERNET TOPOLOGY MAPPING; TAXONOMY & TECHNIQUES

Capturing an accurate view of the Internet topology is of great interest to the networking research community as it has many uses ranging from the design and evaluation of new protocols and services to the vulnerability analysis of the network's infrastructure. However, the scale of today's Internet coupled with its distributed and heterogeneous nature makes it very challenging to acquire a complete and accurate snapshot of the topology. The purpose of this survey is to examine the main research studies that have been conducted on topics related to Internet topology discovery in the last 15-20 years and present some of the main lessons learned from these past efforts. To this end, we classify these prior studies according to the "resolution" or "level" of the topology; that is, interface-level, router- level, PoP-level and AS-level. For each resolution, we describe the main techniques and tools used for data collection, identify their major limitations and issues, and discuss the key implications that these limitations have on the quality of the collected data. In the process, we present the latest efforts in modeling the Internet's topology at the different levels and report on the role that geographic characteristics play in this context. We present the lessons learned as a checklist that every researcher working on Internet topology discovery-related problems should consult to minimize the risk of repeating some of the same or similar mistakes that have been made in the past and as a result have hampered progress in this important area of Internet research.

Introduction

Composed of approximately $50\,000$ networks or *Autonomous Systems (AS)*, the Internet reigns as the ultimate network of networks. Most of these networks are separately owned and managed (however companies that own and manage multiple ASes do exist [50]), cover different geographic areas, build their own physical infrastructures, and serve different purposes. For example, an AS can be a Network Service Provider (NSP), an Internet Service Provider (ISP), an education network, a Content Provider (CP), a Content Distribution Network (CDN) or can provide any combination of these or other services. The diversity in network type and business along with their autonomous management makes it clear why individual ASes use network equipment from different vendors to build and operate different infrastructures, possibly with greatly varying physical topologies and why, in turn, not all ASes deploy the same intra-domain routing protocol but instead use the one(s) that best support(s) their operational needs. It also explains why one of the critical features of the Border Gateway Protocol (`BGP`) is its expressiveness – the ability to let ASes with potentially competing business interests express different policies for interconnecting with one another, presumably for the purpose of enabling the smooth and economically viable exchange of traffic.

As a result of this diversity, its scale, and its distributed and heterogeneous nature, mapping the Internet's global topology is inherently difficult and enormously challenging. For one, since the decommissioning of the NSFNET [189], there exists no entity or organization that has a complete picture (i.e., "ground truth") of the entire Internet or its individual constituents or ASes. Moreover, there exists no protocol or service whose sole purpose is the discovery of the network topology[223, 202]. In fact, the measurement tools that are most often used for topology discovery are merely "engineering hacks" that researchers have proposed to collect information about the

Internet topology. In particular, the two most commonly used techniques for topology discovery, namely traceroute and BGP, have originally been designed for entirely different purposes – traceroute as originally introduced by V. Jacobson is a network debugging tool [253, 282, 23] and BGP is the de-facto standard inter-domain routing protocols in today's global Internet that indicates reachability rather than connectivity of individual ASes [49].

These difficulties and challenges notwithstanding, the study of the Internet's topology has fascinated both networking and non-networking researchers for the last 15-20 years. While non-networking researchers view the Internet or its topology as a prime example of a complex and large-scale technological network and are mainly interested in studying its structural properties and predicting its behavior, the network research community's interest is in general motivated by more practical concerns. For example, various topological properties of the Internet affect the performance of network protocols, network applications and services. Thus, a better understanding of the Internet topology and its main characteristics would enable network researchers to design better network protocols or services and evaluate them under more realistic conditions. Moreover, an accurate map of the Internet would be very helpful for network engineers and operators who are constantly trying to improve or optimize the allocation of network resources such as proxies, replica servers, and data centers. Similarly, having a detailed and complete map of the Internet's topology, preferably annotated with attributes such as the exact geographic location of certain network equipment, could inform the study of a wide range of security-related problems and protocols such as backtracking malicious traffic or assessing the vulnerability of the Internet to blackouts or attacks on parts of its physical infrastructure.

The purpose of this survey is twofold. First, by viewing the Internet's topology at different well-defined resolutions or levels of detail (i.e., interface-level, router-level,

Point-of-Presence or PoP-level, and AS-level), we present a systematic assessment of the main studies that have dealt with measuring and/or modeling the Internet's topology and have been published in the last 15-20 years. Second, by describing in detail the data collection techniques and tools, types of collected datasets, and inference methods used in these different studies, we provide a checklist that every researcher interested in working on Internet topology-related problems should consult before using these tools, datasets, or methods in their own work. Importantly, this checklist collects in one place our current understanding of the main limitations that these tools, datasets or methods have when used in the context of Internet topology research. In a nutshell, by being aware of these limitations and understanding their root causes, researchers will be able to answer for themselves whether or not the used tools, datasets, or methods are of sufficient quality to successfully tackle the particular research problem they are interested in. In this sense, this survey reports on lessons learned from 15-20 years of Internet topology research that will hopefully prevent researchers from repeating some of the same or similar mistakes that have been made in the past and that have negatively impacted progress in this important area of networking research.

The rest of this survey is organized as follows: Section 6.2 presents the notion of different Internet topology resolutions which defines our taxonomy. Sections 6.3, 6.4, 6.5, and 6.6 cover Internet topology at interface-level, router-level, PoP-level, and AS-level, respectively. In each section, we discuss the main data collection techniques and tools, types of collected datasets, and inference methods that have been used to study the topology at the corresponding resolution. We conclude our survey in Section 6.8 with a discussion of the main lessons learned and mention some of the exciting open research problems that will require new and creative solution methods.

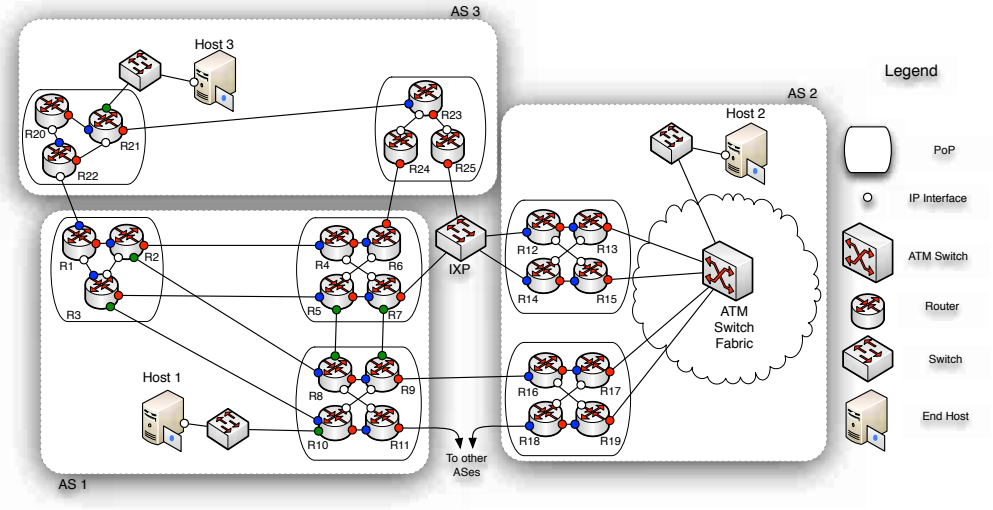

FIGURE 6.44. A detailed toy topology representing the Internet topology at different granularities

Taxonomy

The Internet's topology is often presented as a graph. However, different communities use the term "Internet graph" to refer to different structures. The latter range from the graph structure of the World Wide Web (WWW) and other overlay networks such as P2P systems or Online Social networks to the Internet's physical infrastructure and the more logical or virtual constructs that are enabled by the layered architecture of the network. The focus of this survey is the Internet's physical topology, where nodes represent meaningful network entities and links represent relations between those entities. However, even with this definition in place, a physical topology of the Internet can still mean different things to different interested parties.

Internet Graphs at Different Resolutions: To further disambiguate the meaning behind the notion of a physical Internet topology, we rely on the following taxonomy that considers the *resolutions* of the Internet topologies that have been studied in

the past [223, 45, 283, 91]. In particular, we view Internet topology at four different granularity or resolution levels, organized from finest to coarsest as follows:

I) Interface level: At this level, a node represents a network interface with a designated IP address. An interface belongs to a host or a router and there is a one-to-one mapping between nodes and IPs [231, 177]. At the same time, a link between two nodes shows a direct network layer connectivity between them. This implies that the topology at this level ignores devices functioning at OSI layers lower than the network or IP layer (e.g. hubs and switches).

II) Router level: The topology at this level is often the result of grouping interfaces that belong to the same router [244]. At this level, a node represents an IP-compliant network device (e.g. a host or a router with multiple interfaces). Two nodes are connected by an edge if the corresponding devices have interfaces that are on the same IP broadcast domain.

III) PoP level: A PoP (Point of Presence) is a concentration of routers that belong to the same AS [104, 279]. ASes commonly build their physical networks in a more or less pronounced hierarchical manner; that is, an AS's PoPs are interconnected to form the AS's "backbone" and are also the locations where the AS connects to the PoPs of other ASes [271] and where it provides access to its customers or end users. In this sense, a node in the topology at this level represents a PoP that belongs to an AS. A link between two PoPs indicates that there is physical connectivity between the routers of the two PoPs.

IV) AS level: As opposed to the previous constructs, the AS-level topology represents a more logical view of the Internet [181, 87]. A node at this level represents an AS identified by a 16-bit (recently also a 32-bit) AS number. A link in the AS-level topology represents a business relationship between two ASes. Theses relationships reflect who pays whom when traffic is exchanged between the ASes in question and

are key to a properly functioning and financially viable Internet ecosystem [223, 188]. Traditionally, these relationships are categorized into a) customer-provider (C2P), b) peer-peer (P2P), and c) sibling relationships, but other forms of relationships are known to exist as well. Since ASes typically cover entire geographic regions, with different PoPs in those regions' major cities, the physical connectivity between two ASes that have an established business relationship often occurs at multiple locations. Thus, an AS link is virtual rather than physical in nature in the sense that it is an abstraction and typically represents multiple physical connections between the two ASes [264].

In this survey, we make use of this taxonomy to categorize prior Internet topology studies. Moreover, for the different studies concerned with one and the same resolution, we (i) provide a detailed assessment of the limitations of the techniques employed to collect data, as well as an assessment of the quality of the collected data that is used to study the topology at the given resolution, and (ii) carefully examine the geographic characteristics of the inferred topology and the extent to which the topology at the given resolution is annotated with geographic attributes.

Figure 6.44 shows three resolutions of the topology. At the finest level, the router-topology is presented. The PoP-level topology is generated when PoPs and the connections between them are considered. Finally, the AS-level topology is obtained when we look only at the ASes and the links between them.

Data Types and Data Collection: The nature of the data and the type of data collection techniques are two other elements that we use to classify prior Internet topology studies. Regarding the nature of the collected data, measurements can be performed in the *control plane* or the *data plane*. In terms of measurements performed in the control plane, the collected data reveals information about routing in the Internet. For instance, `BGP` tables store the AS paths to reach different prefixes and they are classic examples of control

plane data. In contrast, data plane measurements aim to discover the actual paths that packets travel along. The simplest measurement of this form is `Ping`. It measures the reachability of a target IP address and also reports the Round Trip Time (RTT) between the target IP and a source, based on the route that the probe packets take in the Internet. Regarding the collection technique, a measurement can be either *active* or *passive*. In active measurements, actual packets (i.e. probe messages) are sent into the network and the replies are collected. On the other hand, passive measurements only tap into a wire and collect the information that is already flowing over that wire. traceroute and `BGP` monitors are examples of active and passive measurement techniques, respectively. A list of commonly-employed data sources and measurement techniques used for studying the Internet topology at each resolution is provided in Table 13.

Geographic Attributes of The Topology: Although a main element of a topology is connectivity, *geography* is another element that, when appropriate, can be added to the topology to increase its usability. However, the definition of a geographically annotated topology depends on the different resolutions of the Internet topology. Interfaces, routers and PoPs are entities that can in theory be geographically mapped to an exact location on a map. A geographical Internet map at these three levels of resolution involves assigning a pair of longitude and latitude coordinates to each entity. Therefore, the topology graph consists of points on the map and the links that connect those points together.

However, in the case of the AS-level topology, geography is a more subtle notion and typically refers to the geographic region covered by an AS. In such a view, an AS is shown as a colored area on a map that represents its coverage, and different ASes covering parts of that same region are stacked vertically and are shown in different colors. In such a representation, AS relationships can be represented by connections between the differently-colored regions and can be further refined by incorporating the ASes'

TABLE 13. Different resolutions of Internet topology and the commonly used data sources to capture the topology in addition to the corresponding limitations and challenges

Resolution	Tools & techniques	Limitations & challenges
Interface-level	traceroute	Router response inconsistency
		Opaque Layer 2 clouds
		Load balance routers
		Probe message filtering
Router-level	Subnet discovery	Router response inconsistency
		Probe message filtering
	Alias Resolution	Scalability
		Inaccurate (false positive and false negative)
	SNMP	Only applicable to one AS
		Requires administrative authorities over the AS
	MRINFO	Only applicable to ASes with DVMRP multicast-ready routers
	Aggregation techniques	Mapping IP to Geo is inaccurate
		DNS name to Geo is not always applicable
		DNS misnaming can add more error
	Delay based techniques	Sensitive to knowledge of geography and placement of candidate PoPs
	Online data sources	Public online data is not always up-to-date
AS level	BGP	Reachability announcement protocol with built in information hiding
	traceroute	Mapping IP to AS number is not trivial
		Using private IPs and other interface level inconsistencies add more complexities
	Internet Routing Registries	Obsolete data

PoPs and showing the inter-AS connections at the PoP-level. This picture is further complicated by the existence of Internet eXchange Points (IXP), where multiple networks connect at one (or a few close-by) physical locations through a multipoint connection. As a result, the complete geo-annotated AS-level topology should be viewed as a hyper-graph [223] where nodes cover areas and links are annotated by the locations of the their corresponding PoPs.

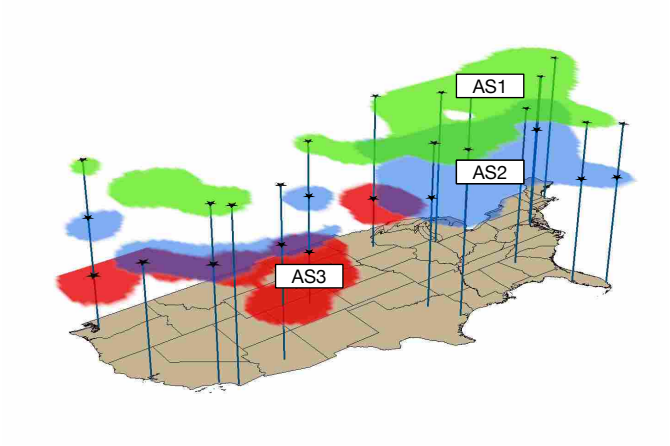

FIGURE 6.45. Sample view of geo-footprint for multiple ASes. The vertical lines indicate the city where PoP for and is located.

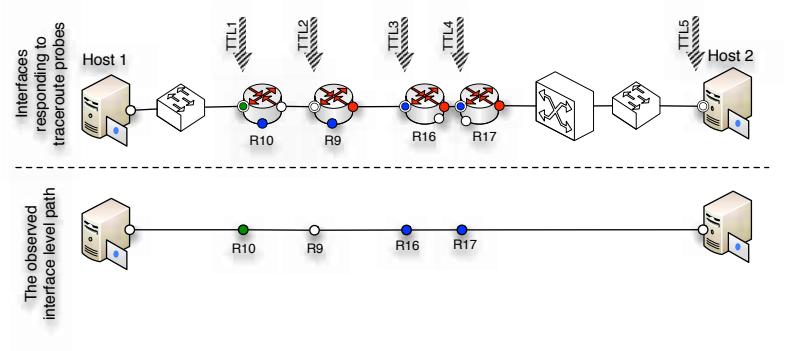

FIGURE 6.46. traceroute from *Host1* towards *Host2* and the corresponding interface-level path.

Figure 6.45 depicts a sample AS-level topology graph, where each AS covers a certain area. Inter AS connections through vertical lines suggest AS level connectivity. As the figure shows, two ASes might be connected at different locations.

Interface-Level

The interface-level abstraction of the Internet topology portrays the network layer connectivity of its IP interfaces. IP interfaces of routers and end-hosts are represented as nodes. Having in general multiple interfaces, each router appears as multiple nodes,

while normal end-hosts with one interface are depicted as a single node. The topology is typically simplified by ignoring end-hosts, therefore nodes only represent router interfaces. Links represent direct network layer connectivity between nodes. However, not all these links are point-to-point. For instance, layer 1 and layer 2 clouds can be traversed, although the connectivity is represented as a single link.

traceroute is the most widely used tool to map the topology of the Internet at this resolution. Based on the nature of the technique and the type of data it produces, it is an active measurement method performed in the data plane [49, 39]. It uses limited Time-To-Live (TTL) probes. The traceroute probes launched from a source to a target successively discover the IP addresses of IP-compliant router interfaces along the forward path, and at each hop measured RRT values are also reported. Multiple probe messages with the same TTL can be used to discover the IP at the same hop. In the perfect scenario, probes for the same hop would initiate a response from the same IP, but each would produce a slightly different RTT due to the inherently dynamic nature of network traffic. In the rest of this survey we assume that a single probe message is used for each hop discovery. Figure 6.46 shows the conducted traceroute from *Host1* to *Host2* and the observed interface-level path. Only one IP address per hop is identified, and the result does not indicate any layer 2 infrastructures.

Each individual traceroute measurement reveals one IP path composed of multiple IP segments. To discover the topology at the interface-level, the outcome of many traceroute measurements should be merged. traceroute-based techniques require a number of traceroute capable hosts (vantage points), and a list of target IPs. During a measurement campaign, a set of vantage points launch traceroute probes towards a given set of targets. The overall observed interface-level topology is generated from the union of all the IP paths, each measured by a traceroute.

In the following, we first describe traceroute in more detail, mainly because it is the most commonly-used active measurement tool, and then discuss its limitations. We also provide an overview of some of the main measurement-based studies that use active measurements to infer the interface-level for Internet topology and discuss a number of more recent proposals for collecting interface-level data.

traceroute

Basic Technique & Variants

traceroute involves actively sending probes into the network, rather than merely monitoring it. It is the most widely used active measurement tool to obtain a map of the physical Internet. V. Jacobson's traceroute– the first implementation of this tool – uses ICMP packets as probes [143]. However, other versions of traceroute exist that use other types of probe messages, for instance UDP and TCP packets [253].

UDP traceroute reveals the IP hops from a source to a destination by sending packets with limited TTLs and large (destination) port numbers. When an intermediate router receives such a probe with TTL equal to zero, it responds back to the source with an "ICMP time exceeded" message. The source progressively increases the TTL until the probe packet reaches the target. In this fashion, this technique identifies with each TTL one segment of the IP route in addition to its corresponding RTT. An "ICMP port unreachable message" indicates that the message was successfully received by the target, and using large destination port numbers minimizes the chance of randomly probing an open port on the target. In addition, the port number is used to match the probes and responses. Unix-like operating systems use this UDP traceroute by default, with port numbers between 33435 and 33534. The port number is incremented after each probe, thus enabling the source to identify the hop distance of the received responses.

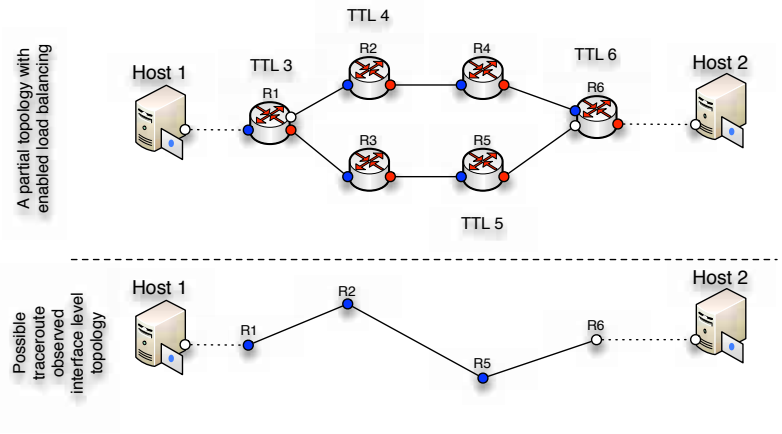

FIGURE 6.47. False links inferred by traceroute in the presence of load balanced routers

ICMP traceroute also uses limited TTL but sends "ICMP echo requests". Since ICMP messages do not have port numbers, the matching of the probes and responses is done using an ICMP id/sequence that is part of the ICMP packet header. ICMP traceroute is the default setting for Microsoft Windows.

The main limitation of UDP and ICMP traceroute is that both UDP messages to high ports and ICMP messages are prone to be filtered by firewalls [226]. To bypass firewalls, TCP traceroute has been designed and uses TCP-SYN probes' well-known ports (e.g. port 80). However, some firewalls are configured to filter TCP packets when no host behind the firewall accepts the TCP connection at the well-known port. This is especially the case at the edge of the network.

A comparison of using the UDP, ICMP and TCP traceroute techniques for topology discovery shows that ICMP traceroute reaches targets more successfully. Moreover, while UDP traceroute identifies more IP links, it is the least successful technique in terms of reaching the targeted IP [176].

The Internet is designed to route packets based on the destination IP. However, network administrators often employ load balancing techniques at certain routers to increase the utilization of their resources. They achieve this goal using "equal cost path"

in their implementation of the inter-domain routing protocols OSPF [195] or IS-IS [56]. Per packet and per flow load balancing are the two types of load balancing techniques that network administrators typically use. In per packet load balancing, each packet is individually load balanced, while in the per flow case, packets from the same flow are routed along the same path. Routers use IP headers to identify flows, and these headers include fields such as Source IP Address, Destination IP Address, Protocol, Source Port Number, Destination Port Number, the IP Type of Service (TOS), the ICMP Code and the Checksum. Note that in the case of the traditional traceroute technique, the values in some of these fields vary for different probes so as to be able to match the probes and the responses.

As a result, per flow load balancing may result in the routing of probes of the same traceroute measurement through different paths. Put differently, when measuring a load balanced route, some traceroute techniques will infer the existence of an IP segment that does not exist in the actual topology. Figure 6.47 shows a possible traceroute when it travels through a load balanced path. *R1* is a load balanced router. Probe messages can either visit *R2* or *R3* based on the load balancing decision made at *R1*. In our example, for TTL 3, 4, and 5, the visited routers are *R1*, *R2*, and *R5*, respectively. As a result, a false link between *R2* and *R5* is inferred. Paris traceroute [23] has been designed to address this issue by using probes that are routed similarly when per flow load balancing is in use. By manipulating the ICMP headers in the probes, Paris traceroute ensures that all the packets of a traceroute measurement take the same path. Paris traceroute resolves the flow based load balancing anomalies in the observed route, but anomalies due to per packet load balancing are not resolved.

traceroute is used predominantly in network troubleshooting. In fact, it has been designed as a generic reachability diagnosis tool, and using it for discovering the interface-level topology of the Internet is both an after-thought and a less-than-perfect heuristic [183]. In general, the limitations and issues concerning the use of traceroute for interface measurements have to do with the nature of the measurement method itself and with the inherent difficulties of using large-scale distributed measurement platforms for performing Internet-wide traceroute campaigns. In the following, we summarize the most important limitations and issues when using traceroute for the purpose of discovering the interface-level topology of the Internet.

Measurement Limitations: First and foremost, there exists no unique setting for a router's response to a TTL zero probe. The router configuration determines the response, and network operators are in charge of, among other tasks, configuring routers. With respect to responding to TTL zero probes, network operators typically choose one of the following five policies: (i) *Null interface routers* means to remain reticent to the probes. For these routers, traceroute detects their existence, but not their interface address ("anonymous routers") [277]. In this case, the RTT is also not reported. (ii) *Probed interface routers* means to respond with the IP address of the probed interface. This configuration is most common when the router is directly probed. (iii) *Incoming interface routers* says to respond with the IP address of the interface from which the probe message was received. This configuration is reported to be the most common setting when the router is probed with indirect TTL-limited messages [122]. (iv) *Shortest-path interface routers* says to respond with the IP address of the interface that is closest to the source. Note that because of asymmetric routing in today's Internet, the incoming interface and shortest-path interface are not necessarily the same. (v) *Default interface routers* says to

respond always with a designated fixed interface IP address (i.e. irrespective of the probed interface). (vi) *Default IP routers* says to respond with a randomly-selected IP address. This IP can be configured indifferent to the IPs assigned to any of the router's interfaces. In addition to these router configuration settings, firewalls can also be configured to prevent probed routers from responding. In short, a traceroute probe packet suggests the existence of one interface per router in the foreword path, at best.

A second limitation of traceroute is that the IP address it records at each hop is not necessarily a valid IP address. This can occur due to (mal)practices in assigning IP addresses to router interfaces. (Mis)configured IP addresses sometimes suggest the appearance of private non-routable addresses and carrier-grade NAT (large scale NAT) addresses. Such addresses can lead to routing loops or other anomalies because they can be used by multiple ASes. In addition, these IPs cannot be mapped to a single router or an AS and cannot be used to map the location of the interface because of the one-to-many relationship between the IP and the assigned interfaces.

Third, the RTT value reported at each hop cannot be used to accurately measure the delay to and from the target. traceroute is a foreword route diagnostic tool, and a rule of thumb in Internet routing is that routes between two IPs are not always symmetric. Hence, the path taken by a traceroute probe may differ from the path taken by its response. In fact, variations in the delay between two consecutive hops could be due to congestion on the link, variable delays in the router's queues, or asymmetric routing.

A fourth limitation that has become increasingly more relevant in today's Internet is that layer 2 clouds are generally opaque to a traceroute. These clouds have the explicit purpose of hiding the network infrastructure from the IP layer. For example, ATM (Asynchronous Transfer Mode) clouds are completely hidden from traceroute. From the perspective of traceroute, an AS using ATM switches provides direct connectivity

between its IP routers, although in reality the IP interfaces are interconnected via a collection of ATM switches. For instance, in the observed topology of AS2 in Figure 6.44, routers directly connected to the ATM cloud have a mesh-like interconnectivity. A more popular layer 2 technology is MultiProtocol Label Switching (MPLS), and it is commonly used to configure tunnels passing through multiple routers. It has been reported that at least 30% of the paths tested in a recent study traverse an MPLS tunnel [242, 92]. Routers using MPLS can be configured to either decrement the TTL (MPLS opaque option), as traceroute requires, or ignore the TTL field completely. If MPLS routers are configured to respond back to ICMP traceroute messages, extra tags (e.g. `MPLS Label=1048 Exp=7 TTL=1 S=0`) appear in the resulting traceroute measurement and reveal the existence of an MPLS tunnel. Although it is be possible to detect MPLS tunnels from traceroute measurements [242, 92], the inference methods are known to be imperfect and are very specific to MPLS tunnels.

Large-Scale Measurements Issues: Clearly, the choice of vantage points and targets impacts the observable interface-level topology. For example, the probability of sampling an IP segment is directly related to the placement of the vantage points and the type of IP segment. In particular, back-up inter-AS routes are hard to discover, and IP segments representing inter-AS peer-to-peer relationships are among the least discoverable ones [49]. To deal with these and similar issues, two approaches have been proposed. First, Eriksson et al. [101, 28] suggested a statistical approach to infer the unseen components of the Internet. By proposing to map the problem to a statistical "unseen species problem", they first estimate the number of unseen components using incomplete observations. Next, matrix completion techniques are used to infer the components and the connectivity between the inferred components and the rest of the topology. The inferred topology is then validated by adaptive targeted probing. The

second approach relies on targeted probing to discover less visible IP segments. In this case, domain experts use their knowledge of the topology and routing policies to devise targeted mapping experiments. The rationale behind this approach is that doing more measurements does not compensate for the measurement bias [49]. Instead, this bias can be addressed by making informed decisions about the locations of the vantage points and targets in relation to the IP segments in question. For instance, Augustin et al. [24] use targeted probing with traceroute to discover peering links at Internet Exchange Points (IXPs) that are otherwise hard to detect.

Given a platform with a set of vantage points and targets, orchestrating a large measurement campaign often imposes a high load on the network as a whole and the measurement infrastructure in particular. The measurement load is higher closer to the vantage points and the set of targets as these segments are redundantly sampled. The high probe traffic may be even be viewed and identified as a Denial of Service (DoS) attack by Intrusion Detection Systems (IDS) [236]. The redundant measurements are classified in [93] into two different types. “Intra-monitor redundancy” occurs close to a vantage point. An individual vantage point redundantly measures the IP segments in its vicinity due to the tree-like structure of routers rooted at the vantage point. “Inter-monitor redundancy” occurs close to targets. Similar to the former type of redundancy, the tree-like structure of routers close to a target causes these routers to be redundantly probed by multiple vantage points.

Different methods to reduce the overhead resulting from such redundancies have been proposed in the literature. On the one hand,“far probes” [93] are proposed to address the intra-monitor redundancy. In this case, when the topology close to the vantage point is fully discovered, instead of using traceroute with probes starting with TTL 1, a higher TTL value is chosen. On the other hand, “top set” (collaborative probing) [93, 252] aims

to address the inter-monitor redundancy. Consider two vantage points running traceroute to the target t. The idea is that if the corresponding routes merge at an intermediate router, they will follow the same path toward t due to destination based routing. Therefore, a per target stop list is required to halt the measurement from one vantage point when the rest of the route is already discovered from former measurements conducted by the other vantage point. Beverly et al. [39] used high frequency measurement with adaptive probing techniques to limit the imposed measurement load, while keeping the discovery rate high. In each cycle, their "interface set cover" algorithm minimizes the traceroute load while maintaining a high discovery rate. To maximize the gain from each traceroute, "subnet centric probing" selects targets to reveal the maximum information from the inside of a network.

Large-Scale traceroute Campaigns

Obtaining the Internet-wide interface-level topology hinges on the idea of performing traceroute measurements between many different vantage points and targets, i.e. collecting data from a large-scale traceroute campaign. In the following, we discuss in more detail the pre-requisites for performing such campaigns and using the resulting data for inferring the interface-level Internet topology; that is, the availability of appropriate measurement platforms and a solid understanding of the coverage and completeness of the obtained data.

Measurements Platforms: Starting with the original paper published in 1998 by Pansiot and Grad [208], there have been many traceroute-based Internet topology studies that have gradually improved our understanding of the Internet's topology. These studies have either used a single vantage point (e.g. Pansiot and Grad [208]), a moderate number of dedicated instrumentation boxes located across the network (e.g. Skitter

[54] or its successor Archipelago [51]), or relied on a publicly available general-purpose experimentation platform like PlanetLab (e.g. iPlane [177], RocketFuel [244] and [252]).

The use of public traceroute servers, also known as *looking glasses*, to conduct active measurements has also gained much attention, mainly due to the large coverage in term of the placement of vantage points. However, as publicly available resources that have been deployed with the network operator community in mind, these traceroute servers impose limits on the rate at which active measurements can be performed. As a result, they are mainly used for small-scale measurement experiments and validation (e.g. RETRO [133] and [24]). Note that in addition to traceroute, many looking glasses also have the capability to issue other network-related debugging commands, especially in support of `BGP`, and their use for collecting `BGP` data will be described in Section 6 below.

Although using dedicated boxes or relying on PlanetLab are still very common approaches to conducting Internet-wide active measurement campaigns, more recent studies have started to deploy platforms that support "crowd-sourcing measurement campaigns"; that is, use of software agents to collect measurements from a large number of vantage points (e.g. Scriptroute [245], Dimes [231], Bitprobe [142]). By asking end users to download a simple measurement plug-in, the idea is to turn massive numbers of unpredictable end-users (in terms of their availability and capabilities) at the edge of the Internet into vantage points and not rely on a small number of dedicated machines in well provisioned networks (e.g. PlanetLab).

These newer platforms use either an altruistic model (e.g. Dimes [231]) whereby individual users are encouraged to participate in the platform and serve as a measurement node for the good of science, or deploy incentive-based models (e.g. Ono [68] and Dasu [224]). Based on recent experience with such incentive-based platforms that aim to ensure

that the measurements conducted by the software agents are beneficial for both the users and the experimenter, they are able to attract and retain end users in larger numbers than their altruistic counterparts. As such, they have the potential of growing into Internet measurement platforms that will consist of an unprecedented number of powerful vantage points. However, as already alluded to in Section , performing, for example, crowd-sourcing traceroute campaigns on such platforms requires extra care in their design and instrumentation due to concerns over excessive network loads and security issues (for more details, see for example [224]).

Coverage & Completeness: Early studies such as [54] or [51] have suggested the utilization of a few vantage points and a large set of targets that are well distributed across the network. The claim was that the gain from adding vantage points increases only marginally by adding more vantage points [33]. However, later studies reported that despite the diminishing return of extra vantage points, the observed topology is more complete [232]. This discussion of the quantity (i.e. number) vs. the quality (i.e. location) of the vantage points of a measurement platform is in need of yet another revision with the recent discovery of massive amounts of peering links at IXPs, the vast majority of which being completely invisible to past traceroute campaigns [13]. This finding confirms earlier observations that only purposefully-placed new vantage points have a chance to detect certain types of IP segments when relying on data plane measurements only [49] and serves as an important reminder that networking researchers have a long way to go before being able to claim to have a complete map of the interface-level Internet topology.

In their quest to produce a more complete picture of the interface-level topology, researchers have not only increased the number of vantage points and targets [68, 224] but also the duration of the period over which the measurements are performed [39]. While the former can increase the scope of the captured topology but depends critically

on the placement of the vantage points, the latter can also reveal a more complete view by exploiting the dynamic nature of the topology (e.g. measurement probes launched at certain times may take rarely used back-up routes due to, for example, router failure-induced route changes). However, the drawback of this solution is that it cannot easily distinguish between routes that have been seen in the past but no longer exist. In general, it is not easy to account for such an inherent churn when allowing longer measurement periods, and there are currently only error-prone heuristics in place to deal with the problems caused by this "solution."

Other Approaches

Although traceroute is the most commonly used method for obtaining the interface-level topology, its limitations have expedited the proposal of other approaches to collect additional connectivity information. While traceroute with different types of probe messages mainly attempts to penetrate through firewall filters, other active measurement techniques are used to address its other limitations.

IP Options

IP options are fields in the IP packet header that provide additional information for the packet's routing. Packets with enabled IP options are processed according to the type of enabled IP option by intermediate routers. As a result, these packets may be routed differently than other packets, or additional information can be registered in the packets. To obtain a more accurate and complete topology, IP options have been widely employed to enrich the collected data with more information when possible.

The completeness of a captured topology is correlated with the number of vantage points performing the traceroute measurements. The cost and the complexity of the

deployment of these vantage points may limit the observed view of the interface-level topology. “Source Routing” (SR) offers more flexibility to discover network topology because it allows the sender to specify at most 9 routers that a given packet should go through before reaching the destination. The intermediate routers should also have this option enabled. When used in conjunction with traceroute, source routing increases the scope of the discovered topology. This can be used to direct the probes to a route that is not usually taken by packets. In essence, source routed probes allow the vantage point to observe an additional view of the network. Although the number of SR-capable routers is a small fraction of all routers in the Internet (around 8%), Govindan et al. [122] show that this number is enough to capture 90% of the topology in a sparse random graph using simulation. However, this number seems very optimistic for traceroute measurements, due to the sensitivity of the observation to the placement of source route enabled routers and the fact that the Internet topology is not random. Augustin et al. [24] have also exploited the IPv4 “Loose Source Record Route” (LSRR) option to increase the coverage of their vantage points without increasing their number. Although they found LSRR-capable routers in many different ASes, they report that routers ignore traceroute probe messages with LSSR option much more frequently than regular traceroute probes. In effect, source routing is used only very infrequently in the context of topology measurement.

The asymmetric nature of Internet routing implies that the discovered routes are only forward routes from the vantage points to the targets. Reverse traceroute [153] uses the “Record Route” (RR) option and “IP Timestamp” to detect the interfaces on the reverse routes as well. An RR enabled probe stores the router interfaces it encounters. The IP standard limits the number of stored interfaces to 9. If the distance from the vantage point to the target is shorter than 9 hops, then the probe will return interfaces observed on the reverse path. A probe with IP timestamp option stores up to four ordered

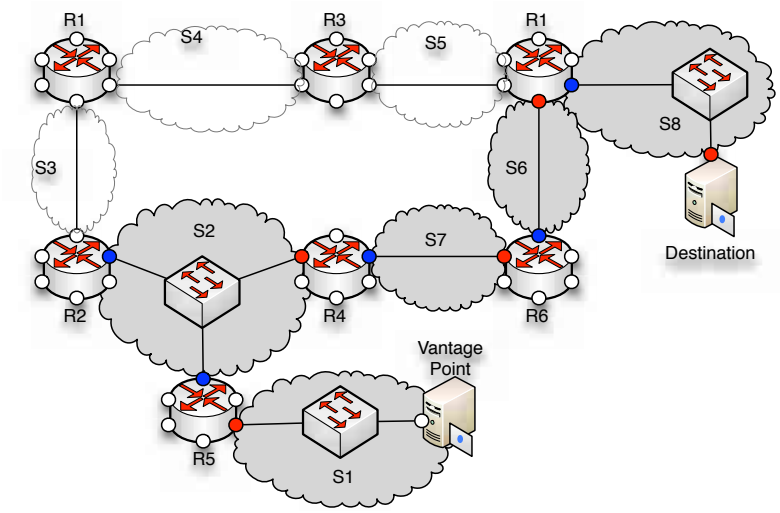

FIGURE 6.48. An example topology and corresponding subnets represented by clouds. Subnets identified by tracenet are marked grey.

IP addresses. The probe queries the router by specifying its IP to record the timestamp if the previously specified IP addresses on the list are already stamped. This method can be used to validate the existence of a sequence of routers with specified IPs on the same route.

While using IP options can provide information that is not available using simple traceroute, it increases the chances for processing delay, being discarded, or triggering an alarm at IDSs [80].

Subnet Discovery

In the subnet discovery, the idea is to map the subnet view of Internet topology. A subnet is a link layer (layer 2) concept. It is a logical grouping of connected network interfaces that are all in the same broadcast domain. All IPs in a subnet are addressed with a common most-significant bit-group (IP prefix). Studying this topological structure of the Internet map has two advantages. First, it improves our understanding of the interface-level topology. Second, applications that require disjoint route segments can benefit from

this view of the Internet. In the subnet graph, each subnet is a node and subnets adjacent to one router are connected via an edge. Figure 6.48 shows the topological structure of a sample network. Corresponding subnets are depicted as clouds.

Subnet level discovery tools such as xnet [256] aim to reveal all ping-able IP addresses on a subnet. xnet identifies boundaries associated with the IP prefix of a subnet with a series of tests on IPs that can potentially be in one subnet. The methodology is developed based on the fact that all IP addresses in one subnet share a prefix and have at most one-hop distance difference from a vantage point. The problem is that the size of the subnet is in general unknown. Given IP address t that is n hops away from a vantage point, xnet probes IPs in the prefix that includes t starting from the smallest /31 prefix (mate-31). If the probes to all IPs in this prefix travel through the same route and their hop distances to the vantage point are within the boundaries that support their existence in the same subnet as t, then the target prefix is expanded and IPs in this expanded prefix are subjected to the same tests. xnet incrementally expands the prefix until at least one IP fails the tests. At this point the last successfully tested prefix identifies the subnet that includes t.

tracenet [255] uses the same principles as xnet to find subnets along a path. It runs xnet on IP addresses discovered by traceroute from a vantage point to a destination. Figure 6.48 shows the application of tracenet on a sample topology and identified subnets are depicted in grey. In this figure, Interfaces discovered by traceroute are marked as red circles, and blue circles represent interfaces discovered by the xnet component of the tool. If traceroute returns the incoming interface of each visited router, tracenet is able to identify the corresponding subnets along the route from the vantage point to the destination. The principal assumption in tracenet is that routers are configured with an incoming interface response setting. However, if a router is configured with another

setting, xnet discovers an invalid subnet on the path. For instance, in Figure 6.48, if *R1* responds with its green interface, *S5* is discovered instead of *S6* as the fourth subnet on the route.

Router-Level

The router-level topology shows the routers and the interconnectivity among their interfaces in the Internet. At this resolution of the Internet topology, nodes represent end-hosts (with one interface) or routers (typically with multiple interfaces) and links show layer 3 connectivity between these devices. The topology at this level can be viewed as the outcome of the aggregation of IP interfaces that belong to a single router. The following two main techniques are considered for collecting the router-level topology:

- **Alias Resolution:** Alias resolution [122, 243] or router disambiguation [33] is a set of techniques used to identify the IP interfaces that belong to the same router. Such disambiguation is necessitated by the aggregation of traceroute data that underlies the inference of the router-level topology from the interface-level topology. The main challenge consists of relating different interfaces of a router that were discovered in different traceroute measurements.

- **Recursive Router Discovery:** Another class of techniques employed for obtaining the router-level topology relies on a router's capability to be queried for its neighbor on each interface. The Simple Network Measurement Protocol (`SNMP`) and the Internet Group Management Protocol (`IGMP`) are two methods that can be used to discover the neighboring routers of a queried router in an intranet and the Internet, respectively.

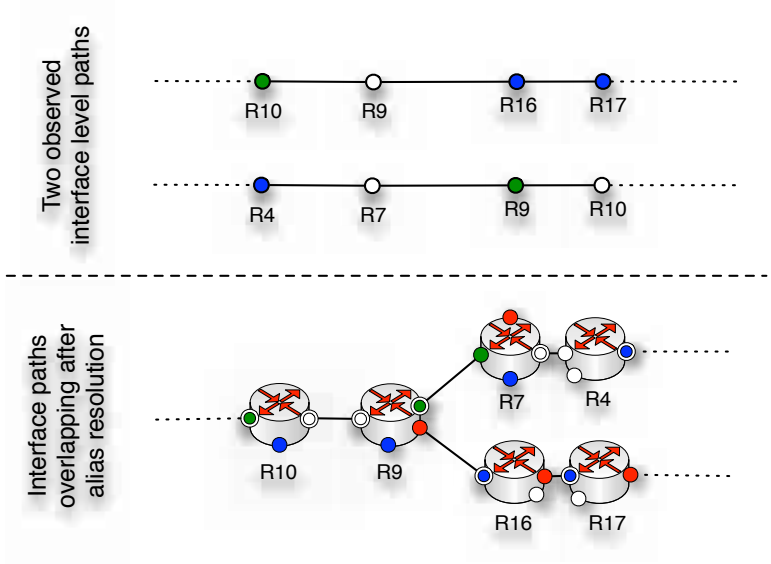

FIGURE 6.49. Two partial traceroute with no common hops. Resolving IP aliases shows that the paths overlap.

Alias Resolution

Typically, routers have multiple interfaces, each with a different IP address. Two IPs are referred to as aliases if they are assigned to the interfaces of a single router. Alias resolution is the process of grouping IP addresses that belong to the same router. In theory, the true router-level topology can be obtained or derived from the interface level topology, as the result of this process. Figure 6.49 shows two partial interface paths observed from traceroute measurements in the topology of Figure 6.44, the first from *Host1* to *Host2* and another from *Host3* to *Host1*. The measurements do not have any IP hop in common. However, resolving alias IPs shows that the two measurements visit two different interfaces of *R9* and *R10*. In the context of alias resolution, a false positive detects interfaces belonging to multiple routers as aliases. On the other hand, in the case of a false negative, alias resolution falls short in relating two alias interfaces. We next list and discuss the most widely-used alias resolution methods.

Common Source Address: This technique was proposed and used by Pansiot et al. [208] in their original traceroute-based topology study and was also implemented in Meractor [156]. When resolving the alias of the IP address *A*, Meractor sends a TCP or a UDP alias probe towards an unused port number of *A* that replies with an ICMP "port unreachable" message. This message typically has the IP address of the router's shortest-path interface as its source address. If the source IP address of the reply message is different from *A*, these two IPs are aliases of the same router. This method is prone to the router response configuration problems discussed in Section .

Common IP-identification Counter: The packet ID in the IP header is used for packet reassembly after fragmentation. This technique assumes that a router has a single IP ID counter. For such a router, consecutive packets generated from the router have consecutive IP IDs, regardless of the interface from which the packet left the router. The Ally tool described in [244] and used in the Rocketfuel project implements this mechanism to detect aliases. It sends a UDP probe packet with a high port number to two potential alias IPs. The ICMP "Port Unreachable" responses are encapsulated within separate IP packets and each includes an ID (x and y) in the IP header. Then, it sends the third packet to the address that responded first. Assuming that z is the ID of the third response, if $x < y < z$ and $z - x$ is small (e.g. smaller than 200 in case of Ally [244, 157]), the addresses are assumed to be aliases [244].

Alias resolution based on the ID fingerprint is prone to false negatives due to ID increment settings on routers that are larger than one [69], the absence of a global IPID counter for some router [69], or unexpected jitter in the delivery of probe messages. False positives can also occur as a result of randomly synchronized ID counters of two routers, but this problem can be mitigated by running more tests after a wait period. The other major drawback of this ID-based technique is the overhead of running it on a large set of

discovered interfaces; its complexity is $O(n^2)$ for a set of n interfaces. In the case of Ally, some heuristics have been proposed to improve the efficiency of the tool by restricting the possible alias candidates using delays and TTLs [244]. The idea is that alias candidates should have similar TTLs from different vantage points. Thus, the list of candidate aliases can be pruned based on the difference in the hop count distance from common vantage points.

RadarGun [37] mitigates the limitations of Ally by modeling the changes in the packet ID counter. Instead of directly testing each pair of IP addresses separately, it iteratively probes the list of IP addresses at least 30 times. Two IPs are inferred to be aliases if the "velocity" of their corresponding ID counters are consistent in all their responses. The probe complexity of RadarGun is $O(n)$. The main drawback of this technique is the potential of error when used on a large list of IPs. Since routers use a 16-bit counter for the packet ID, counter wrap-arounds can occur during the measurement period. If the probes to the same IP are separated by a period of 40 seconds or longer due the large number of IPs on the list, multiple wrap-arounds are likely to occur. Although the designers of RadarGun have accounted for the possibility of a single wrap-around, the accuracy of the technique diminishes in the presence of multiple wrap-arounds.

DNS-Name: The similarities in DNS names associated with router interfaces can also be used to infer aliases [244, 243], but this approach also has a number of limitations. For one, this technique only works when an AS uses a clear naming convention for assigning DNS names to router interfaces. Second, the complexity of the naming conventions may require human intervention to resolve aliases which limits the scalability of this method. Lastly, the technique is known to be highly inaccurate at the AS borders. The interfaces of border routers usually belong to different ASes which are likely to use

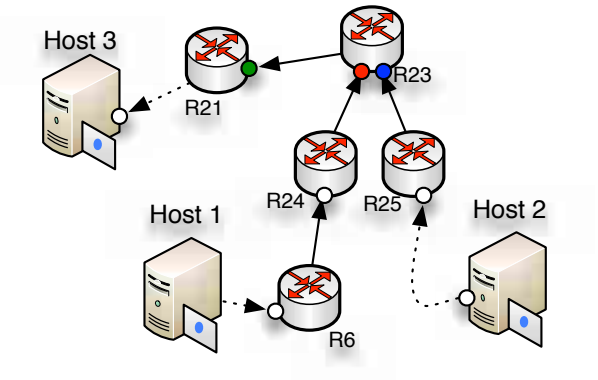

FIGURE 6.50. Graph based alias resolution; The green interface succeeds the blue and the red interface in two traceroute so red & blue would be aliases.

different naming conventions. This observation complicates the use of this technique for performing alias resolution at the AS borders [122].

Graph-Based Resolution Heuristics: traceroute measurement can offer heuristics on alias inference [243]. Graph-based alias resolution constructs a directed graph by overlaying an individual traceroute measurement as illustrated in Figure 6.44. The "common successor" heuristic suggests which two IP addresses may be aliases. This heuristic relies on the prevalence of routers that respond to traceroute probes with the incoming interface. When two traceroute paths merge, the common IP belongs to the second router on the shared path. IP addresses prior to the common IP should belong to different interfaces of a single router and hence would be aliases. Figure 6.50 shows a partial view of a traceroute measurement from $Host1$ and *Host2* toward *Host3* in our toy example. In this example, the black interface succeeds the red interface in one traceroute and succeeds the blue interface in another traceroute. The heuristic suggests that the blue and the red interfaces are aliases.

This heuristic falsely infers aliases in the presence of layer 2 switches or multiple-access clouds. Figure 6.51 depicts an alternate topology to Figure 6.50. The traceroute

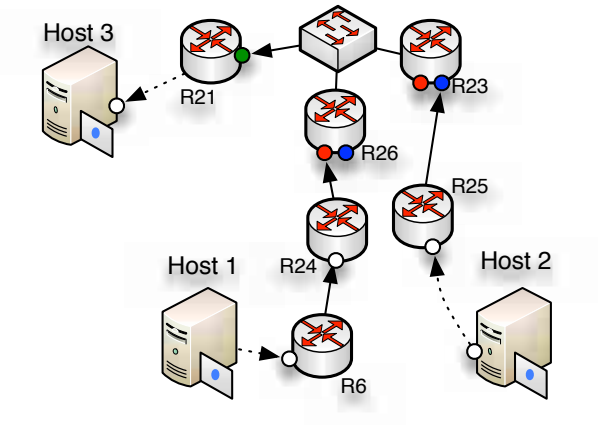

FIGURE 6.51. False positive in graph based alias resolution due to the presence of a layer 2 switch; The green interface succeeds the blue and the red interface in two traceroute so red & blue are inferred to be aliases.

view in both figures are similar, hence the heuristic infers *R26*'s red interface and *R23*'s blue interface are aliases.

The "same traceroute" heuristic identifies IP addresses that can not be aliases. Since each packet visits a router only once, this heuristic states that two IPs occurring on the same traceroute can not be aliases.

Analytical Alias Resolution: Given a set of traceroute-derived paths, Analytical Alias Resolver (AAR) [126] utilizes the common IP address assignment scheme to infer IP aliases within two opposite paths, one from *A* to *B* and the other from *B* to *A*. It first identifies the subnets that are linking the routers (as discussed in). Then it aligns the two traceroute paths using the discovered subnets. Alias IPs are easily resolved when point-to-point links are used and the route is symmetric. To illustrate this technique, consider the traceroute measurements between *Host1* and *Host2* shown in Figure 6.52. The top view shows the two traceroute paths and the identified subnets. The bottom view depicts how the detected subnets can be used to align the two traceroute paths and resolve aliases.

The Analytic and Probe-based Alias Resolver (APAR) [125] consists of an analytical and probe-based component. The analytical component uses the same

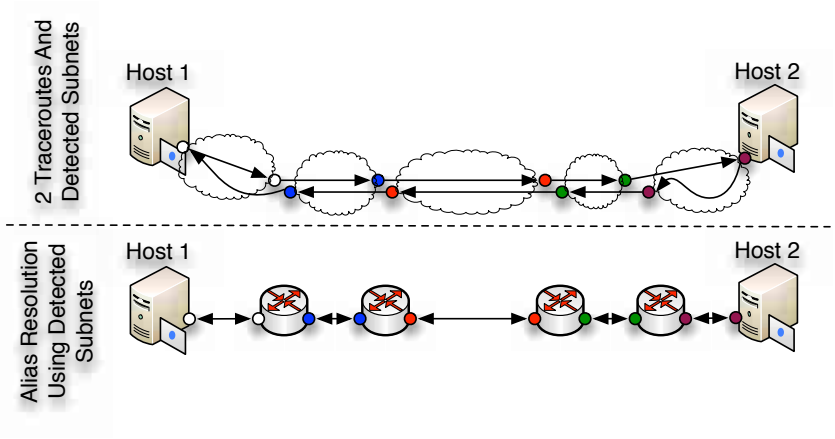

FIGURE 6.52. Analytical Alias Resolution for detecting IP aliases on a symmetric path segment.

scheme as ARR, while the probe-based component increases the accuracy of mapping with limited probing overhead. The probe-based component uses `ping`-like probes to determine the distance to each observed IP and mitigates false positives. Any two interfaces can be aliases only if their hop distance differs by at most one hop from a single vantage point. This `ping`-like probe also helps to identify aliases when the source address of the reply is different from the probed IP (i.e. the Common Source Address approach).

Record Route Option: The DisCarte tool [235] uses the standard traceroute with enabled Record Route (RR) IP option to detect IP aliases. For the first nine hops, two interfaces are captured, one in the forward path and one in the reverse path. Although the technique sounds intuitive, it is difficult to use effectively in practice because of inconsistent RR implementations by routers and the complexity of aligning RR data with traceroute data. DisCarte uses Disjunctive Logic Programming (DLP) to intelligently merge RR and traceroute data. However, its implementation does not scale to large datasets. For instance, the application of DisCarte on traces between 379 sources and 376,408 destinations is reported to be so complex that is in fact intractable.

Progressive Router Discovery

In some networks, routers store information about their neighboring routers. Using this information, the topology can be discovered progressively. In a local area network with SNMP-enabled routers, a list of neighboring interfaces can be identified from the "ipRoute Table MIB" entry of the router [237]. This technique can be used recursively to discover new routers and the connectivity between them. Although accurate, the use of this technique is limited to the interior of an AS and can only be used by the network administrators with adequate privileges.

More recently, MRINFO has been used to discover the topology at the router-level using IGMP messages with a similar incremental method [209, 187]. Upon receipt of an IGMP "ASK NEIGHBORS" message, an IPv4 multicast-capable router replies with an IGMP "NEIGHBORS REPLY" message that lists all its interfaces and the directly connected interface of the neighboring router. The applicability of this technique is however limited to DVMRP multicast-enabled routers, and their number in today's Internet is small.

Modeling

The most-cited work on Internet topology modeling is by Faloutsos et al. [102]. In their paper, they relied on the traceroute data collected by Pansiot et al. [208] in mid-1995 which consisted of the inferred router-level paths taken by packets in the Internet and produced an observed router topology. One of their main observations was the scale-free structure of the inferred router topology; that is, the power-law degree distribution of routers. Intuitively, this finding implies the existence of a small number of high-degree core routers and a large number of lower degree edge routers. This paper fueled many of

the subsequent studies on modeling the Internet's router-level topology (e.g. [19]) that aimed at reproducing the observed scale-free structure of the inferred topology.

Although the observations reported in [102] seem plausible, many domain experts argued that they are indeed erroneous [269]. For one, no publicly available router topologies exhibit the claimed scale-free structure. For example, in the publicly available maps of Internet2, there is no evidence of a few highly-connected core routers. Second, technology constraints and engineering intuition rule out the existence of high-degree core routers in real-world networks. When configuring a router, network operators are limited by the tradeoff between traffic volume vs. degree. In particular, a core router that processes a large volume of traffic on each interface cannot have a large number of interfaces. On the other hand, routers at the edge of the network carry less traffic per interface and are capable of having more interfaces. These constraints suggest that while router topologies can in theory exhibit degree distributions that are consistent with the reported power-law behavior, the high-degree routers must necessarily be at the edge of the network and not in its core. Ironically, because of the measurement platforms used, none of the traceroute campaigns performed in the past would be able to detect those high-degree nodes at the network edge. Third, there is a clear mismatch between the observed scale-free topology and the design philosophy of the Internet. An important requirement of the original DARPA network design was that "Internet communication must continue despite loss of networks or gateways" [271]. However, in a scale-free topology, a failed high-degree central router can lead to a partitioning of the network as shown by Albert et al. [19], an alleged property that became well-known as the Internet's "Achilles' heel". Lastly, it has been shown that the errors in the router-level topology considered in [102] are a result of the afore-mentioned limitations of the alias resolution methods and the fact that the inferred high-degree nodes are an artifact

of traceroute's inability to penetrate opaque layer-2 clouds—the observed topology of a group of routers at the edge of a layer-2 cloud appears as a mesh-like (e.g. complete graph) interconnection among all routers and automatically results in the appearance of high-degree nodes.

Alternatively, Heuristically Optimal Topology (HOT) models have been proposed to model the Internet topology. These models are based on the method of reverse-engineering and rely on domain knowledge as an alternative resource as compared to using data in the form of traceroute measurements to drive the modeling effort. HOT models are comprised of the following three main components: *(i)* An objective function that captures the ISP's business goals, *(ii)* technology constraints that dictate that the basic design of the ISP's router topology reflect a tradeoff that has to be made between cost and efficiency, and *(iii)* the uncertainty in the environment in the form of the traffic demands imposed on the network. When combining all these ingredients, *constraint optimization* can be used to construct an optimal router topology for an ISP with the stated objective and demands. The construction of such an optimal solution may be NP-hard, but HOT models are not concerned with optimality. Instead, they are concerned with the construction of heuristically optimal solutions that result in "good" performance [271]. A hallmark of the resulting ISP router topologies is the presence of a pronounced backbone consisting of low-degree but high-capacity routers. Moreover, such a backbone is fed by tree-like access networks that are built from high-degree but low-capacity routers, with additional links added for redundancy and resilience.

PoP Level

The PoP-level is the ideal resolution to study the connectivity of an AS when the objective is identifying all the locations where, at least in theory (i.e. ignoring routing

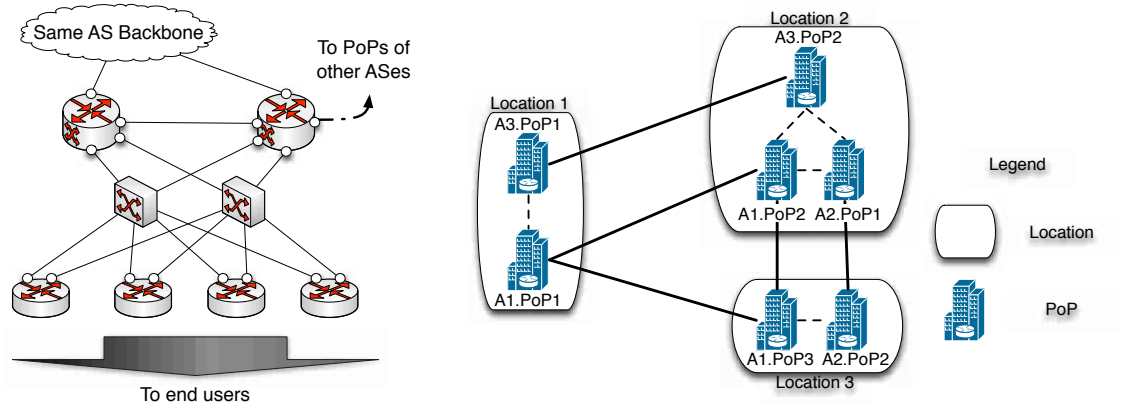

(a) Cookie cutter design used in the PoP of an AS [34, 131]

(b) The PoP-level topology our example

FIGURE 6.53. PoP level topology.

policies), the AS can exchange traffic with its neighbors. As a result, the topology at this level is also very useful for potential customers of an AS who may be interested in the geographic coverage of the AS or in knowing the locations where they can connect.

Terminology & Approaches

The term PoP (Point of Presence) is a loosely defined term within the Internet community. Internet service providers use PoP to refer to either a physical building with a specific address where they keep their routers, or a metropolitan area where customers can reach their services. In the research community, however, a PoP usually means a collection of tightly connected routers owned by an AS that by design work as a group to provide connectivity to users or to other PoPs of that same AS or other ASes. Therefore, PoPs are the reflection of a hierarchical design principle that many ASes apply when designing their physical infrastructure. Adhering to such a design achieves scalability and facilitates maintainability of a network.

Network operators often apply “cookie cutter” patterns when designing PoPs [34, 131]. This modular design strategy simplifies network debugging and management.

Figure 6.53(a) depicts an example of such a cookie cutter pattern applied to the design of a PoP. Certain patterns are explicitly recommended by some network equipment vendors and show how their products are best used for the buildup of PoPs of certain sizes and with desirable properties (e.g. redundancy, scalability). The design typically ensures redundant within-PoP connectivity, access for customers of the AS that owns the PoP, and connectivity to the rest of the Internet. As a result of this practice, the PoPs of many different ASes have similar internal (e.g. router-level) structure and are found as repeated patterns across the global Internet.

A node in the PoP-level topology of the Internet is the PoP of a given AS and is ideally tagged with the PoP's owner (i.e. AS) and geographical information (i.e. location). Inter-PoP links can be categorized into two types. While *core* or *backbone links* connect two PoPs of the same AS, *peering* links connect PoPs of different ASes. Figure 6.53(b) shows the PoP-level topology corresponding to the network in Figure 6.44. Each PoP is identified by its AS and its location. Although *AS1.PoP1* and *AS3.PoP1* are in the same location (building), each one is represented by a PoP or node. Backbone links are represented by lines, and dotted lines show peering links.

Prior studies in this area have considered three different basic approaches for obtaining the PoP-level topology of the Internet. The first and the most common approach has been to identify PoPs by aggregating data collected from `traceroute` measurements. This method receives either an interface-level or a router- level topology as input and groups nodes that belong to one PoP. Relevant studies are discussed in Section .

The second approach is delay-based, but instead of using the per-hop RTT information from `traceroute`, it relies on delay estimates obtained from `ping` measurements. Yoshida et al. [279] used this technique to detect the PoPs of four major

ISPs in Japan. They argue that the information about an ISP's core network (e.g. routers, DNS names) that is obtained through `traceroute` is unreliable. Instead, they used their own Japan-wide measurement platform to perform large-scale `ping` campaigns. Based on a model that relates the measured end-to-end delays to the sum of the delays between consecutively traversed PoPs, they inferred the presence of PoPs.

FIGURE 6.54. The PoP-level topology of Cogent retrieved from http://www.cogentco.com/files/images/network/network_map/networkmap_global_large.png in September 2013

The third approach relies on information that is published by different ISPs on their websites. Figure 6.54 shows one example of an AS's PoP-level topology (i.e. Cogent Communications) that is available online. The map depicts cities that have a PoP of this AS and also shows the interconnection among PoPs of the AS. Topology Zoo [160] is a collection of about 200 topology maps taken from online pages published by a range of different ASes. Since this data is published by the provider itself, it should be more accurate than maps generated by measurement-based techniques. However, obtained maps from online resources are prone to errors due to the out-dated data. Moreover, these maps typically only show the connectivity within an AS and do not reveal AS peerings. The Internet Atlas is another research project that aims at providing a map of physical connectivity of the Internet [94]. Nodes in this Atlas (map) represent buildings (e.g. hosting facilities, data centers or colocation buildings), and links show interconnectivity

between them. Atlas is built using resources such as online maps and other publicly available information from different repositories or databases.

Aggregation Methods

In the following, we discuss prior studies that focused on interface and router aggregation to unravel PoP-level topology. Due to the importance of geography at this resolution, we also discuss the studies that examined geographical characterization of PoPs.

The first study that focused on the discovery of PoPs was Rocketfuel [244]. It tried to infer the structure of an AS using `traceroute` measurement and used the PoP-level topology to visualize an AS infrastructure. Rocketfuel first identified alias IPs using Ally's packet ID counter method. It then leveraged the inferred DNS naming conventions used by an AS to geolocate the discovered IPs using a tool called `UNDNS`. `UNDNS` uses a large set of regular expressions to extract city and airport codes embedded in DNS names and infer the geographical location of an interface. In the end, Rocketfuel groups interfaces that are mapped to one and the same geographical location into a PoP.

iPlane [177] extends the approach advanced by Rocketfuel. First, a Meractor-like [156] alias resolution is used to identify routers. Additionally, iPlane uses a mate-30 heuristic similar to AAR [126] and identifies subnets to find candidate alias pairs. A Packet ID fingerprinting technique is used on the candidate alias pairs to infer aliases [244]. Next, DNS names are used to geo-locate routers and group them into PoPs. However, this step is riddled with issues. For one, for some routers, there is no DNS name assigned to any of their interfaces. Also, there is no guarantee that assigned DNS names contain any relevant geography-related information. Furthermore, DNS misnaming can introduce error to this mapping process. DNS names are voluntarily assigned by network

administrators and interface misnaming is fairly common especially due to relocating routers and using old assigned DNS names [281]. In a final step, iPlane considers all routers that it has not been able to map to a location and assigns them a location using a clustering approach that is based on a notion of similarity between interfaces with respect to routing and performance. To this end, iPlane probes all interfaces with `ICMP echo` probes from different Planet Lab nodes. Each interface is assigned a vector in which the i^{th} element is the length of the path from the i^{th} vantage point. Hence the PoP detection problem is translated into a clustering problem involving these measurements, and interfaces in one cluster are assumed to belong to the same PoP.

Note that both projects rely heavily on the capability to extract information about the location of a router from the DNS name assigned to it. The structure of DNS names was recently revisited by Chabarek et al. [62]. Their study shows that aside from geographical information, DNS names may include information about interface types, bandwidth, and router manufacturers. However, meaningful encodings are more common in the core of the Internet [62], and the naming structure tends to be strongly tied to the AS that owns the router [105].

Another popular approach is to use geo-IP databases to assign a location to an IP address. Tian et al. [252] use these databases in conjunction with a heuristic approach to locate router interfaces. They initially rely on existing geo-IP databases to annotate the given interface level topology graph with geographic information. The resulting annotated graph contains some clusters corresponding to each city. Their heuristic technique re-annotates an interface to a new location if the new annotation results in more coherent groupings, where more links are inside a group. Each group is detected as a PoP. One basic problem with this approach is the well-known inaccuracy of the freely or commercially available geo-IP databases [212, 239, 124].

A PoP consists of a set of routers with high interconnectivity among them. Links inside a PoP are usually very short, implying small delays in general. These properties were used by Feldman et al. [104, 233] to propose a more automatic approach for detecting PoPs. In their graph-based approach, network "motifs" are used to detect repeated patterns in `traceroute`-derived interface-level topologies collected by DIMES [231]. These repeated patterns are used to identify tightly connected interfaces. To this end, they ignore all links with a delay above a certain threshold (5 ms); these links are likely to be long-haul connections between distant PoPs. This step generates a graph with disconnected components, each of which is a candidate to represent either a single PoP or multiple PoPs. Different refinement techniques are applied to either split one component or merge different components to detect the PoPs based on graph motifs. To geolocate the inferred PoPs, they use several geolocation services including the MaxMind GeoIP [185]. Finally, they validate their PoP-level topology using a DNS name-based geo-localization data base and two geo-IP data bases. Their claim is that by not using the DNS names as part of their methodology, this information can be used as "ground truth" to validate the accuracy of their technique. Unfortunately, the accuracy of using DNS names to infer geographical location of an interface is questionable [281].

AS-Level

The Internet's topology at the AS-level is typically modeled using a simple graph where a node is an AS identified by an AS number. As previously described, an Autonomous System or AS is commonly defined as a collection of IP prefixes under the control of a single network operator that presents a common, clearly defined routing policy to the Internet [132]. In such an AS graph, links represent logical connectivity between two ASes and are labeled according to the type of connection; customer-

provider, peer-peer, and sibling relationship. The logical connectivity between two ASes usually represents multiple physical connections that are established between PoPs of the two ASes, presumably to enable the efficient exchange of traffic between them.

This graph representation of the AS topology has a number of limitations. First, each AS has a geographical footprint that may overlap with the footprint of another AS. This feature cannot be illustrated using a simple node to represent an AS, unless the node is replaced by a region that covers the area in question. Second, ASes are widely considered to be coherent entities with a clearly defined routing policy. However, for historical reasons or due to their often global reach, some ASes use different policies in different parts of their network. In this context, Muhlbauer et al. [196] demonstrated that treating ASes as atomic structures is a severe over-simplification and negatively impacts our understanding of inter-domain routing. Third, the fact that many inter-AS links represent multiple geographically dispersed physical AS connections cannot be captured by a simple graph. Fourth, IXPs also complicate the AS-level topology by providing connectivity between many ASes, most commonly through layer 2 multiple access clouds. As a result, in a realistic AS topology graph, IXPs should be modeled as links that connect more than two ASes. Together, these issues suggest that a hyper-graph [223] provides a more detailed and informative structure of the Internet's AS topology. However, these numerous limitations notwithstanding, simple graph representations of the AS-level topology are considered to be useful and have been studied for the past two decades to a great extent.

AS Topology Data Sources

Techniques for discovering the AS-level topology rely mainly on the following three data sources: `BGP` information, traceroute measurements, and Internet Routing

Registries (IRR) [139]. Below we discuss each type of data source and its limitations in more detail.

BGP Information: BGP is the de-facto standard inter-domain routing protocol of the Internet. BGP is a path vector protocol in which routing decisions are made based on reachability via the advertised AS paths and expressed network policies. The term "reachability protocol" has been used to emphasize this characteristic of BGP. BGP uses the AS number to specify the origin AS of a prefix and ASes along the path to reach the origin AS.

BGP data has been collected by various projects and has subsequently been used in different forms. BGP information can be obtained from various resources, including (i) BGP *archive*: Oregon RouteViews [12] and Reseaux IP Europeens (RIPE) Routing Information Service (RIS) [9] collect BGP route information through a set of route collectors also known as BGP monitors or vantage points. The original purpose of these projects was to help network operators with troubleshooting and debugging tasks, and for these purposes, the data has proved to be invaluable. Both services collect routing table dumps and route update traces on an ongoing basis. While BGP dumps show the best path to reach other ASes, the back-up links and the dynamic nature of BGP routes are more likely captured by "route updates". (ii) *Route Servers*: A route server is a BGP-speaking router that offers interactive login access via `telnet` or `ssh` and permits third parties to run many non-privileged router commands [280]. For example, BGP summary information can be obtained by executing the "`show BGP summary`" command. (iii) *Looking Glasses*: A looking glass is a web interface to a BGP router which often allows basic BGP data querying and supports limited use of debugging tools such as `ping` and traceroute [280].

BGP information was the first data source used to map the AS-level topology [121]. Two representative studies that use both BGP dumps and updates to capture the AS-level topology are [280, 179]. Although passive collections of BGP tables and updates have fueled many studies concerned with the AS-level topology, there also have been efforts that used active measurements of BGP. In this context, a BGP beacon [180, 49] is a router that actively advertises and withdraws prefixes. Observing the resulting announcements from the perspective of different route collectors within the larger Internet enables researchers to infer some of BGP's overall behavior (e.g. protocol convergence time and the average AS distance an advertisement travels in the control plane). In a similar manner, BGP route poisoning prevents BGP announcements from reaching an AS. Bush et al. [49] used this technique to measure the prevalence of default routes in the Internet and explain the differences in the AS-level topologies obtained from control vs. data plane measurements.

Using BGP for inferring the AS-level topology has several advantages. First, compared to Internet registries, the data collected from BGP shows the actual reachability as seen from the perspective of the Internet control plane. Hence, the data is typically not prone to being stale, obsolete or incorrect. Second, BGP updates can be used to study the dynamic behavior of Internet routing which, in turn, can reveal otherwise hard-to-detect backup links. Third, engineering solutions such as the use of BGP beacons and route poisoning can be applied on top of BGP to improve our view of the topology.

Despite all its advantages, using BGP information to infer the AS-level topology is not without limitations. The main reason is that BGP is merely an information hiding protocol and only indicates reachability, not connectivity. More specifically, AS path announcements are primarily used for loop detection. For traffic engineering reasons, adding an AS in the announcements is not uncommon. Also, ASes may announce AS

paths that do not correspond to real paths [196]. Moreover, as a path vector protocol, BGP does not announce information about every available path. As a result, back-up paths might never appear in the BGP dumps. In fact, since BGP only announces the best paths, many alternative AS paths remain hidden from any route collector. Since route collectors are normally deployed in larger ISPs and mostly in the US and Europe, their observed AS-level topology is biased to be more complete for these regions. Additionally, even if the route collectors were randomly placed in different ASes, the likelihood of discovery of an AS relationship is proportional to the number of ASes using that link [133, 49]. This finding proves a measurement bias in BGP-based AS topologies because P2P links are only used for traffic originating from the customers of any of the peering ASes. Hence P2P AS relations are in general much harder to discover than C2P AS relationships [133]. In fact, the majority of the missing AS links in AS-level topologies inferred from BGP data are known to be P2P links [202]. The severeness of this bias and the resulting degree of incompleteness of even the most-carefully inferred currently available AS-level topologies have recently come to light with the discovery of massive amounts of public peering links (i.e. P2P AS connections) at a large European IXP [13], most of which have remained invisible in presently available BGP data.

traceroute Measurement: Another approach to discover the Internet's AS-level topology is to use the interface-level topology obtained from traceroute measurements. In this approach, each IP in a traceroute is mapped to its corresponding AS. BGP routing tables and IRR can be used to map an IP to an AS based on the IP prefixes that are announced by the AS [182]. Consecutive IPs that belong to two different ASes reveal the connectivity between ASes.

This technique has the advantage of revealing a potentially more detailed view of the AS-level topology. Recall that ASes can be connected at multiple locations.

traceroute-based measurements allow us to distinguish between multiple inter-AS connections between two ASes. In addition, traceroute measurements often use more vantage points, mainly because deploying a traceroute vantage point is much easier than deploying a BGP route collector. As a result, the AS-level topologies inferred from data collected by large-scale traceroute measurement campaigns are generally considered to be more complete than those collected from BGP information [231, 68, 224].

Apart from the limitations of traceroute that we discussed in Section , active measurements in the data plane have other limitations when used for mapping the AS-level topology. First, IP-to-AS mapping is a non-trivial task. Prefix registries are often incomplete and using BGP for mapping IPs to AS numbers is not accurate due to BGP's information hiding characteristics. Second, discovering a false inter-AS connection is likely due to inconsistencies in router responses [68, 282]. Third, private IPs and IPs in the carrier-grade NAT (large-scale NAT) IP range may also appear in a traceroute which renders the IP-to-AS mapping impossible for these IPs[282].

Finally, it is worth mentioning that when measuring the AS-level topology using BGP and traceroute measurements respectively, what is really measured are the Internet control and data planes. While the control plane focuses on "reachability", the data plane is all about "connectivity". The inconsistencies in the data plane and the control plane measurement may result in different and inconsistent views of the Internet AS-level topology. In general, these issues stem from the limitations of the data that is used to infer the topology and the lack of knowledge about the effects of these limitations on the observed topology [49]. For instance, "default routing" limits the view of passive BGP measurements while it has the potential of enhancing the view of active measurements (e.g. observe the route). The general consensus is that the AS-level topology inferred from measurements in the data plane results in a more accurate and complete view as

compared to relying on measurements in the control plane [49, 271, 223]. However, [13] is a reminder of the caveat associated with this consensus.

Internet Routing Registries: The Routing Arbiter Database (RADb) provided by IRR is a group of look-up databases maintained by several organizations. These databases are designed to provide fundamental information about routing in the Internet, including documented routing policies, regulations, and peering information

The main advantage of using IRR is its simplicity. All the information is accessible via the `WHOIS` command and can be obtained through `FTP` servers. Being based on data provided by the different ASes themselves, this resource does not exhibit the sort of limitations that data obtained through measurements have. However, when using this resource, extra care is needed for different reasons. For one, since these registries are populated and maintained on a completely voluntary basis, the available data may be stale or incomplete due to confidentiality reasons, personnel changes in the different ASes, or because of the overhead of updating an external data store. For instance, reports that checked the accuracy of RIPE-provided data show inconsistencies in different IRR-provided databases [219].

AS Relationship & AS Tiers

Although the logical AS-level topology is interesting in itself, to be more useful in practice, the inter-AS routing policies should also be inferred. We recall that the business relations between connected ASes are broadly classified into [137] (1) Customer-Provider (C2P), (2) Peer-Peer (P2P), and (3) Sibling relations. From a financial perspective, in a

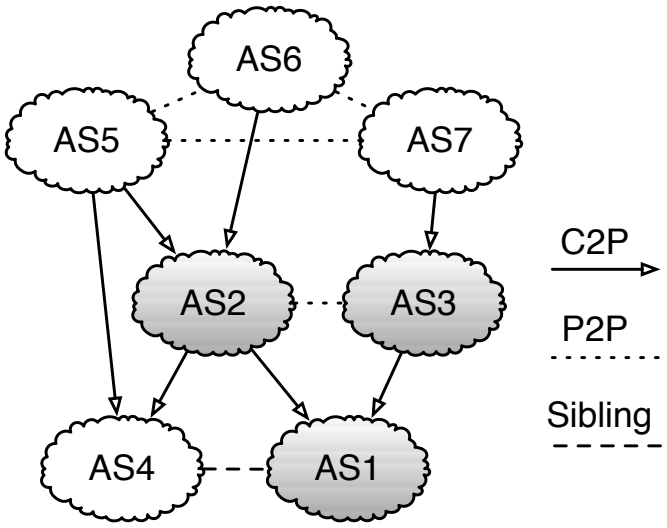

FIGURE 6.55. AS graph annotation with AS relations

C2P relation, the customer is billed for using the provider to reach the rest of the Internet. The other two types of relationship are in general settlement-free; that is, no money is exchanged between the two parties involved in a P2P relationship. A P2P relation helps, for example, two small ASes with high inter-AS traffic profiles to reduce their cost by directly exchanging traffic, hence reducing the traffic sent towards their providers. Sibling relations typically occur when business mergers happen or when multiple ASes are owned and operated by one and the same company or organization.

Early approaches to inferring AS relations used AS size and AS degree. Gao et al. proposed an algorithm based on the intuition that a provider typically has a larger size than its customers and that the size of an AS is typically proportional to its degree in the AS graph [112].

The commonly-used approach to infer inter-AS relationships is to use the observed routing paths and assume that the "valley-free property" holds without exceptions in the Internet [85, 112, 273]. For an AS path, if we number links as +1, 0, -1 for provider-to-customer, peer-to-peer and customer-to-provider, the valley-free property states that

any valid path should only see a sequence of +1's, followed by at most one 0, followed by a sequence of -1's. The type of relationship assignment can be formulated as an optimization problem. Given an undirected graph representation of the AS topology and a set of AS-level paths, the aim is to assign policy labels to the links in such a way as to minimize the number of invalid routes. Although this problem is proven to be NP-hard, some approximation techniques have been presented in the literature [85].

An alternative approach is to check the consistency of inferred relations (using any of the above methods) with other measurements [181]. For instance, Muhlbauer et al. [196] used traceroute measurements to estimate the accuracy of the inference by comparing the inferred routes and the real routes. In their approach, they use multiple quasi-routers to capture route diversity within the ASes.

Traditionally, the AS-level topology is widely regarded to be hierarchical in nature, where ASes are categorized into different tiers [85, 273]. Tier-1 ASes are defined as those that don't buy transit from any other AS. These tier-1 ASes form a complete graph (i.e. full mesh connectivity) at the highest tier. Tier-2 providers are customers of the tier-1 ASes using them for Internet transit. Additionally, tier-2 ASes use peer-peer relations with other tier-2 ASes to decrease the transit cost. This hierarchical structure can be extended to more levels. However, this perception is changing. First, many new ASes (e.g. content providers and Content Distribution Networks (CDN)) are inherently different from the traditional ISPs and also tend to have many connections at various locations. These new types of ASes do not fit within the traditional tiered AS hierarchy. In addition, new studies explain this changing perception using the abundance of missing links and the limited observability of P2P connections in currently studied AS topologies [271]. Although the existence of large transit ASes at the highest tier remains valid, the tier-based hierarchical view is replaced by a flatter but more modular view. Figure 6.55 shows

an example of an annotated AS graph. *AS1*, *AS2*, and *AS3* are the ASes in our previous examples. *AS5*, *AS6*, and *AS7* are tier-1 ASes forming a full mesh at the highest tier. However, there is no longer a pronounced hierarchical structure below these tier-1s.

Coverage & Completeness

As of 2011, diligently-inferred AS-level topologies consists of approximately 40,000 ASes and 115,000 to 135,000 edges, with 80,000-90,000 C2P links and the rest P2P links [271]. While such topologies seem to be complete with respect to their node sets (i.e. ASes), their edge sets are typically inaccurate and miss a large number of AS-links, especially with respect to P2P links.

A great deal of research has been dedicated to studying the question of completeness of inferred AS-level topologies. The "Lord of the Links" study [133] compares `BGP` routing tables, Internet Routing Registries, and traceroute measurements, cross validates the topology captured from these various sources and captures a more complete view of the AS topology. The authors of this study also extract a significant amount of new information from the operational IXPs worldwide and use this information in their cross validation process.

The incompleteness of the Internet AS map has also been studied (e.g. [202, 203]). Oliveira et al. [204] use ground truth data provided by a large tier-1 ISP to validate the accuracy of their derived AS maps for a few target ASes. The ground truth is built upon router configuration files, syslogs, `BGP` command outputs, and personal communications with the network operators. Oliveira et al. [202] categorize the missing links into *hidden* and *invisible* links. Invisible links are missing due to the limitations imposed by the placement of vantage points. Hidden links, on the other hand, can be found with further measurements. On the active measurement side, the importance of the distribution of

traceroute vantage points is studied by Shavitt et al. [232]. Given a large set of vantage points, they use sensitivity analysis and measure the changes in the discovered topology using a different number of vantage points. They show that although increasing the number of vantage points can help reducing sampling bias, it can not overcome the bias due to their placement. They conclude that measuring from within a network is important for discovering more of its links, mainly for low-tier ASes.

More recently, the AS-level map underwent a major revamping due to the availability of ground truth data from one of the largest IXPs in Europe with some 400 AS members [13]. The main finding was that in this single IXP, there are more than 50,000 P2P links visible, which is more than the total number of P2P inferred Internet-wide. This finding suggests the total number of P2P links in the Internet is likely to be larger than 200,000. More importantly, this recent observation shows that the presently-used AS-level Internet topologies are far from complete, with much room for improvement.

Geolocation

Apart from prior studies on the geographic locations of PoPs of an AS, little has been done on mapping the geography of ASes (i.e. the geographical area that is served by an AS). The notion of the geography of an AS has become even more delicate with the emergence of newer types of ASes such as larger content providers, CDNs and and cloud providers. While the geography of a traditional AS like 7018 (AT&T North America) is well defined in the sense that it covers the US, defining the geography for ASes like 15169 (Google) or 20940 (Akamai) is more complicated as they cover roughly the whole globe.

Internet registries and directories such as PeeringBD [211] provide a plethora of information about the geography of ASes. PeeringDB for instance provides a list of

public and private facilities where an AS has PoPs. Similar to other online resources, these directories are easy to use but can be out of date and incomplete.

The geographical footprint of eyeball ASes (ISP that serve residential costumers) was studied in [214]. Using large-scale measurements from Peer-to-Peer applications, the authors of this study identify a large set of end-host IPs. These IPs are then mapped to ASes. Next, the geographical coverage an of AS is estimated using the geo-density of a large number of its customers. Different IP-to-geolocation databases are used to find the location of an IP address, taking into account the errors inherent in those databases. Since a large volume of customers are used to map the geo-footprint of an AS, the potential error in IP-to-geo mapping does not influence the final discovered coverage of the AS.

Modeling

Several studies have examined the presumed AS topology of the Internet from a graph-theoretic perspective and have proposed different graph-based network models. However, there is no consensus on which of the studied models is more relevant or realistic due to the incompleteness of the inferred topologies. Zhou et al. [285] propose a growth model with Positive-Feedback-Preference which reproduces many topological properties of inferred AS-level topologies. Their model, however, uses the Skitter [54] traceroute dataset to infer the target AS-level topology. As discussed earlier, this dataset suffers from well-known limitations of traceroute-based mapping efforts. For instance, the observed power-law degree distribution of this AS topology is known to be due to the bias in the measurement techniques [223, 271]. Mahadevan et al. [179] used the AS topologies inferred from multiple data sources that included BGP, traceroute and `WHOIS` measurements. They compared the resulting graphs from a graph-analysis perspective and reported that the "joint degree distribution" can be used to characterize the Internet AS

graph. They also showed how the data collection peculiarities can explain differences in their graph comparison study.

The evolution of the Internet AS map has also been investigated. The main challenge with respect to the long-term evolution of the topology is to distinguish between topology changes and changes due to routing dynamics. Oliveira et al. [205] compose a model that distinguishes between the two different events. Their findings suggest that the impact of transient routing dynamics on topology decreases exponentially over time. Dhamdhere et al. [82, 10] take a different approach in characterizing the AS map evolution. They compare the AS maps collected during the past 12 years using `BGP` dumps. They report that the AS-level topology was growing exponentially until 2001, but this growth has settled into a slower exponential growth in terms of both ASes and inter-AS links. However, the average path length has remained the same. These measured graph properties can be used in topology generators to build AS-level models of the Internet.

In view of the latest understanding of the quality of the different inferred AS-level topologies that have been studied in the past, a recent common theme in AS topology modeling has been that a proposed model is only as good as the underlying data. Moreover, there has been increasing awareness that any strict graph-theoretic treatment of the AS-level Internet topology necessarily misses out on the key fact that this topology is a construct that is mainly driven by economic factors and decisions. [64, 65, 82] are early attempts at addressing these points. For example, Chang et al. [65] use a policy-based graph model, where policies are implemented in a simulated environment and effect how ASes decide to create new AS relations. Similar to the HOT modeling approach for the router-level topology, their model follows the reverse-engineering approach. As part of an AS's decision making process, they consider the gain from P2P links and C2P links, using

simulated traffic demands. Using different profiles for ASes with different objectives, they model the behavior of these ASes and model the Internet using an evolutionary framework. To validate the model, they use publicly available measurements and perform their own measurement experiments to check for consistency of the model with the real-world Internet. Lodhi et al. [172] build on this initial attempt described in [64] and consider an agent-based network formation model for the AS-level Internet. The proposed model, called GENESIS, is based on realistic provider and peering strategies, with ASes acting in a myopic and decentralized manner to optimize a cost-related fitness function.

Discussion

Examples of "Big (Internet) Data"

The Internet is arguably the largest man-made complex system. As such, it has attracted the attention of the larger scientific community, and the number of studies on topics related to measuring, analyzing, modeling, predicting and providing a basic understanding of the structure and behavior of this highly-engineered network has increased dramatically over the last two decades. Importantly, this increase in Internet-related publications started with the initial availability of large new datasets of Internet-specific measurements (e.g. traffic traces [167, 210], routing data [12, 121]), and the subsequent explosive growth has been largely driven by "big Internet data"; that is, publicly available or proprietary datasets resulting from large-scale measurement experiments that tend to produce voluminous amounts of observations.[1] Typically, these observations have rich semantic content and often provide useful information about the

[1] As part of the Ark project [51] alone, some 10 billion `traceroute` measurements have been collected during September 2007 and January 2011.

Internet as a whole or about its individual components (e.g. ASes, routers, protocols, services).

In general, the producers and owners of the various types of "big Internet data" are network researchers or operators, and while their reasoning for collecting data may vary, practical reasons (e.g. for trouble shooting) almost always trump altruistic arguments (e.g. for the good of science). For example, in the case of Internet topology-related big data which is the focus of this survey, the realization that the influence of the Internet's structure or topology on the network's functionality (and vice versa) is in general not well-understood but is the root cause of many encountered networking problems has been the main motivation for data collection projects such as Route Views [12] and RIPE RIS [9]. The measurements from these and similar efforts have proven to be invaluable for purposes such as network management, trouble-shooting, and debugging. In addition, they have also informed the design of new protocols, applications, and services and have contributed to an increased awareness of the vulnerability of the Internet to a growing number of ever more potent cyber threats.

Economics of the Internet and Interconnection

Economics is the driving force for two networks or autonomous systems (ASes) to interconnect or peer with one another for the purpose of exchanging traffic between them directly rather than indirectly (e.g. by relying on a third party such as a transit provider). In case the two parties determine that interconnecting makes sense financially, they then must decide on the geographic locations where their networks will physically interconnect as well as on the type of interconnection. For example, the two parties are likely to first examine opportunities where both networks already have a presence in the same city or even in the same colocation facility in a city and then consider the available

interconnection options. Among the available peering options, the most common ones are private peering and public peerings. Two networks peer privately by buying a dedicated fiber or point-to-point circuit (also called cross-connect, or x-connect, for short) from the colocation facility provider where they are both customers (e.g., rent cabinet space for accommodating their routers and servers). That same facility may also house (parts of) the switching fabric of an Internet eXchange Point (IXP), in which case the two networks have the opportunity to establish a public peering by simply purchasing and utilizing a port at the IXP[2].

For the past 15+ years, researchers have studied in great detail the non-physical construct known as the Internet's AS-level topology, where nodes are (routed) ASes and links are logical entities indicating that the involved ASes interconnect with one another in one or more locations around the world (e.g. see [10, 223, 271] and references therein). However, these past efforts have largely ignored the physical realizations of these logical AS-links; that is, the different geographic locations (e.g. city, colocation facility) where two networks interconnect physically to directly exchange traffic with one another.

To appreciate the need for a better understanding of physical interconnections in the Internet, consider the case of the U.S. where there is a range of small to large colocation companies that are in the business of selling interconnections. As for-profit companies that are often also publicly traded, they are mandated to provide business-specific details in their SEC filings, and a cursory reading of the financial statements released by these for-profit companies shows that Equinix dominates the x-connect market in the US with some 97K connections (as of 1Q 2016) [3], followed by companies such as Telx[3] with some 50K and CoreSite with about 20K [106, 152, 7, 77, 76]. In terms of the underlying

[2]Recent technological advances, especially the introduction of VLAN services over an IXP switching fabric, have started to blur the notions of public and private peering.

[3]Telx was acquired by Digital Realty Trust in late 2015.

economics, with an approximate monthly cost of $\$300$ for a x-connect in some of the major cities in the US [251], in the case of Equinix, the revenues from selling x-connects in the US alone amount to about $\$270M$ per year [99, 100]; sale of x-connects is the second largest revenue generator for these companies after selling cabinet or colocation space in their buildings. However, little to nothing is known publicly about where all these x-connects in the US or elsewhere are located (i.e. in which colocation facility in which city) and which ASes are parties to which x-connect. As a result, developing a principled approach to accurately answering questions such as "In which cities and with which networks a major content provider (e.g. Google or Netflix) establish private peering? , and with whom?" or "Where are all the x-connects that Netflix uses to deliver its content to an eyeball provider like Comcast and which networks are parties of these interconnections?" has loomed as an important open problem that has vexed network researchers and operators alike. Such an approach would not only allow for a systematic assessment of reported peering disputes (e.g. see [175] and references therein), but would also complement recent work on mapping the US long-haul fiber-optic infrastructure [96] by adding the missing x-connects between service providers in colocation facilities across the US. In turn, such an augmented map of the US long-haul fiber-optic cables could be used to aid recent efforts for a speed-of-light Internet [238] by examining the nature of the delay that is due to packets traversing x-connects (i.e. being handed over from one network to another) in different colocations along their end-to-end paths.

The current lack of transparency about the geography of (and parties to) x-connects is akin to an earlier problem that concerned public peerings at IXPs and arose from a need to understand which member ASes of an IXP peer publicly with one another; that is, exchange traffic over the IXP's public switching fabric. However, the task of mapping the x-connects inside a commercial colocation facility is inherently more difficult than

mapping the public peerings between the different members of an IXP. At IXPs, member ASes use their IXP-assigned addresses to establish peerings with other member ASes. The existence of an IXP-assigned address within general-purpose traceroute probes is a commonly used heuristic for inferring the presence of a public peering link between two member ASes of an IXP [274, 24, 224, 116, 13]. In the absence of any such comparable solid "hints" or indicators, the problem of inferring the presence of x-connects between ASes that are customers of one and the same colocation facility is extremely challenging and requires creative new solutions.

Lessons Learned & a Check List

A key lesson learned from surveying the existing literature on Internet topology discovery has been the realization that "more is not always better." That is, using more measurements from the same `traceroute` campaign or from the same set of `BGP` monitors is now viewed as a non-starter for solving the severe degree of incompleteness of all past and current inferred Internet topology maps at all four levels. In this sense, "big Internet data" is a reminder that the extraction of key information from big data cannot rely on big data analytics alone but is often intimately tied to applying detailed domain knowledge and hard-to-quantify engineering intuition.

A closely-related lesson is that in the context of data sources for Internet topology discovery, "less can actually be more" in the sense that a strategically-placed vantage point can have much better visibility in certain substrates of the Internet topology than a large number of vantage points that have been selected in an ad-hoc fashion or are tied to a fixed measurement platform. The recent IXP studies [13, 67, 66] are prime examples that highlight this point.

At a more technical level, the main lesson from getting to know the lay of the land with respect to Internet topology discovery is that "details matter." For example, using `traceroute` measurements "blindly" without knowing the technique's main idiosyncrasies detailed in Sections 6.3 and 6.4 is bound to lead to incorrect result, flawed claims or wrong findings about the Internet in general and its topologies at the different levels in particular. Similar comments apply to the "blind" use of `BGP` measurements or other data sources that have been tapped for Internet topology discovery.

Even though many of the datasets that have been used in the context of Internet topology discovery have been created by network researchers, as owners of these datasets, they have largely failed to communicate to the users or consumers of their data the main limitations and issues. A notable exception is the original work by Pansiot and Grad [208], but unfortunately, their diligent efforts listing critical issues with `traceroute` and highlighting important artifacts in the obtained data has been all but ignored and forgotten by the networking community [161]. As illustrated in this survey, this failure to properly educate the networking community and scientific community at large about the pitfalls and drawbacks of using the available data "as is" has led to numerous dead-end research efforts. Importantly, it has in general hampered progress in this important area of Internet research as evidenced by a lack of high-quality maps of the Internet topology at any of the described levels, even to this date.

To improve upon this unfortunate situation, we provide in the following a checklist that is a compilation of the main lessons learned from past work in this area. We encourage every researcher interested in working on Internet topology-related problems to consult this checklist before embarking on their own work of any measurement, analysis or modeling efforts that make use of tools, datasets, or methods that have been precisely

addressed in past work in this area. Our checklist consists of a number of increasingly more detailed questions for that any interested researcher should ask upfront:

- What datasets are used or generated for the planned work?
- What techniques have been used to obtain the data?
- What are the (known) limitations of the used techniques and what is known about how these limitations impact the quality of the data?
- How can the known data quality issues impact the results of the planned work?
- If the known data quality issues are claimed to be minor, do the obtained results and findings withstand further scrutiny based on alternative data or available domain knowledge?

In a nutshell, by raising researchers awareness of the limitations of the used measurement techniques and how they may affect the resulting data, researchers will be able to answer for themselves whether or not the used tools, datasets, or methods are of sufficient quality to successfully tackle the particular research problem they are interested in. We view consulting this straightforward checklist as a first step that will hopefully prevent researchers from repeating some of the same or similar mistakes that have been made in the past and that have negatively impacted the progress in this important area of networking research.

Outlook

If past experience is any indication, progress in terms of discovering more accurate, complete, and internally consistent Internet topologies at different levels will come from renewed effort that gives quality priority over quantity when it comes to Internet

measurements. Here, quality refers first and foremost to the choice of the locations of the vantage points used in large-scale measurement campaigns but also includes the diligence necessary to eliminate as many of the known idiosyncrasies inherent in most of the presently-used measurement techniques. Recent examples that demonstrate the promising results that measurement platforms with purposefully-chosen vantage points can produce over conventional measurement infrastructures in the context of Internet topology discovery are seen in [24, 13, 224, 116]. However, these are early efforts, and the potential for carefully and purposefully-designed next-generation measurement platforms with programmable vantage points in strategic locations indicates an exciting future for research in Internet topology discovery.

Regarding many of the measurement techniques underlying Internet topology discovery, we have shown in this survey that despite gradual and significant progress and achievements in increasing our understanding of the many idiosyncrasies of `traceroute` or `BGP` and how they affect the integrity and quality of the resulting data, the Internet topologies that one can infer are at best inadequate. A main reason for this unfortunate situation is that neither `traceroute` nor `BGP` have been designed for Internet topology discovery but have been "re-purposed" by researchers for that very task. Instead of accepting this situation as a "fait accompli", the time seems ripe to try and do away with the utilization of such "engineering hacks" for the purpose of Internet topology mapping. To this end, we advocate for the pursuit of a "clean slate" design of techniques and/or protocols for the explicit and exclusive purpose of Internet topology discovery at a given level. The objective of such an effort is plain and simple: the design of new measurement techniques that enable researchers to measure what they *want* to measure, and not just what they *can* measure.

Lastly, main Internet topology-related modeling studies covered in this survey indicate a clear preference for treating Internet topologies at any level strictly as graph-theoretic constructs and relying mainly graph theory to study their properties and behavior. However, from a networking perspective, such an approach is largely counter-intuitive because the existing Internet topologies at the different layers are highly-engineered systems with pronounced structures and well-defined functionalities. As such, structure trumps randomness when it comes to Internet topology design, and even the latest random graph models (e.g. scale-free networks of the preferential attachment type or the many variants thereof [19]) fail to account for the networks' real-world structures, let alone their functionalities. The HOT models discussed in Section 6.6 are proof that real-world technological networks such as the Internet's interface-level, router-level, or PoP-level topologies are amenable to mathematical formulations of network design problems that can account for the main underlying engineering-based design criteria and principles and have solutions that are fully consistent with networking reality. Extending this approach to non-technological networks such as the Internet AS-level topology, an inherently economics-driven construct, looms as an exciting open research area, and studies such as [64, 65, 171] are initial attempts in this direction.

Summary

This chapter is concerned with the use of "big Internet data" in the form of massive amounts of traceroute measurements and `BGP`-derived observations for the main purpose of Internet topology discovery. To this end, we consider the Internet's topology at different resolutions or levels and organize the body of research that has been produced in the past 15-20 years on Internet topology discovery and related topics into studies

concerned with the interface-level, router-level, PoP-level, and AS-level topologies of the Internet, respectively.

For each level, we introduce the data used to capture the corresponding topology and classify the data sources based on their type (i.e. data plane vs. control plane measurements) and the techniques used to collect them (i.e. active vs. passive measurement methods). We explain in detail the problems of the different most commonly-used techniques and discuss the limitations and issues that these problems create when using the resulting data for Internet topology discovery at each level. In the process, we show how the main studies in this area have dealt with these known issues of the different data sources and also review the existing literature in this area with an eye on efforts that address geographical properties of the Internet topology and present innovative approaches to Internet topology modeling at different levels.

We conclude with a discussion of some of the main lessons gained from surveying the existing literature on Internet topology discovery. By transforming these lessons into a simple and straightforward checklist, it is our hope that future researchers interested in working on Internet topology-related problems will first consult and reflect upon this checklist, and by doing so will avoid making the same or similar mistakes that have hampered progress in this important area of Internet research. At the same time, we also list a number of challenging new problems as part of an exciting research agenda, and the timely solution of these and similar problems promises the advancement of Internet topology discovery by leaps.

CHAPTER VII

POP-LEVEL TOPOLOGY OF THE INTERNET; ON THE GEOGRAPHY OF X-CONNECTS

Companies like Equinix, CoreSite, and Digital Reality Trust manage and operate carrier-neutral colocation facilities (*colos*) where they provide, among other offerings, interconnection services. Given such a colo facility, our goal is to rely exclusively on publicly available data to identify all interconnections of the *cross-connect (x-connect)* type in that facility, where a x-connect is a dedicated point-to-point private network interconnect that network operators can buy from the colo provider so that their networks can exchange traffic within the confines of the colo. Determining the geographic locations of the x-connects between two networks is a prerequisite for studying a number of inter-domain related networking problems including peering disputes, congestion, or routing problems. This chapter presents a multi-pronged approach for inferring the x-connects in a given colocation facility. We illustrate our approach with case studies of colos in Los Angeles, Chicago, and Miami, and compare our results to those obtained from related ground truth and prior efforts. Our findings attest to the potential of our approach, and highlight the remaining open challenges in accurately mapping x-connects to the colo facilities where they are established.

Introduction

In this chapter, we provide more transparency in the ways networks interconnect with one another by presenting a methodology that is specifically designed to map interconnections of the x-connect type to the geographic location where they are established and utilized. In particular, given any colocation facility in the U.S., we

describe a new approach for determining which ASes use x-connects to interconnect with which other ASes in the same facility. Our starting point is publicly available information about the tenants of the target colocation facility that can vary greatly in quality with respect to completeness, accuracy, and recency and that exists in various forms (e.g. data sheets, marketing materials, company websites, PeeringDB [211]). Note however, that these or similar public resources provide no interconnection-related information, for the listed tenants, a business aspect that most networks treat as proprietary information and are under no obligation to share with third parties. Intended to shed more light on these largely propriety interconnection-related business practices, our methodology for mapping the target facility's x-connects consists of the following four main components:

- *Input data: Localized measurements:* To increase the likelihood that a traceroute probe "hits" the target colocation facility, we utilize different Internet measurement platforms for performing purposefully-designed and geographically-constrained traceroute measurements in the data plane as we describe in Section 7.3.
- *Inferring candidate x-connects:* To accurately detect the x-connects between two ASes from traceroute data, we adopt a new approach of identifying the boarder router for each AS and we present a number of heuristics for tackling this problem in Section 7.4.
- *Pinning x-connects to target facility:* In Section 7.5, we construct a Markov Random Field – a probabilistic graphical model – that captures the inferred underlying router-level connectivity structure surrounding the target facility in a way that is as consistent as possible with the comprehensive view derived from our traceroute measurements. The resulting model serves as input to a probabilistic inference technique, namely Belief Propagation algorithm, for pinning discovered x-connects to a target facility.

– *Output data: A list of mapped AS-interconnections:* Our final product is a number of different sets of mapped interconnects, including the set of x-connects inside the target facility. In particular, we document how inaccurate accounting of x-connects can easily lead to inflated numbers.

Our validation efforts are described in Section 7.6. In particular, we rely on control plane information obtained from a few strategically-situated routers and compare their (naturally very limited) visibility into the x-connects inside our target facilities with our results. Moreover, from one tenant AS in the largest colocation facility we targeted in our study, we obtained the ground truth with respect to the x-connects that this tenant (i.e. a large CDN) utilized in that facility at the time of our measurements. This allows us to compare our results against hard-to-come-by ground truth for one tenant AS in one of our target facilities.

Finally, we make use of some original findings reported in a recent study by Giotsas et al. [115] who developed a specialized inference method for mapping the peering interconnections of some 10 networks to physical facilities. As a by-product of their work, the authors obtained a set of x-connects that their approach mapped to one of our target facilities. We report on a careful comparison study between this dataset and our findings and illustrate why mapping x-connects to their geographic location (i.e. colocation facility) is an extremely delicate affair that requires great care at each and every step of any specialized inference method that is designed to geographically map interconnections.

Our Approach in a Nutshell

When two ASes decide to establish a peering interconnection at a colo facility, they have basically two options. They can peer privately by buying a dedicated transport

service or fiber from the colo provider. We refer to this form of peering as cross-connect ("x-connenct", for short), also known as private network interconnection (PNI). Alternatively, they can peer publicly at an IXP. While detecting public peerings at IXPs has been an active area of research, the problem of detecting x-connects and geo-mapping them at the colo facility level has been under-studied and is the sole focus of this study.

Note that colo providers such as Equinix or CoreSite often operate and manage multiple colo facilities in a single city and typically use different layer-2 technologies to interconnect them, as a part of the "hub-and-spoke" expansion strategy. Using this scheme the colo providers have extended their data center footprint by connecting their newer facilities, the *spokes*, to the established data centers, the *hubs*, which allows their customers leasing space at the spokes to leverage the significant interconnection capabilities of the hubs [78]. As a result, individual tenant ASes that are present (i.e. have a PoP) in one of the provider's facilities can establish x-connects with other tenants ASes at any of the provider's other facilities in the same city. Therefor each colo provider (viz. Equinix, CoreSite, or Telx) creates *colocation market places*, often time extended over a metro area such as Los Angeles, New York, San Francisco Bay and Northern Virginia, in which any customer can interconnect with other customers. Since such a constellation makes it very difficult to detect individual x-connects from basic traceroute data and geo-map them at the level of the provider's different facilities (i.e. individual building), we consider all the colos manged and operated by one and the same colo provider in the same city or metro area as one "virtual colo facility". In the rest of this chapter, we use the term "colo facility" to refer to either such a virtual colo or to a single colo in case the provider operates only one colo facility in the city or metro area of interest.

The key to our approach is to leverage domain knowledge to establish a number of rules/constraints for the "co-presence" of a group of interfaces in the same building.

TABLE 14. Target CoreSite colos: their addresses, and the number of unique primary ASNs for tenants from CoreSite (CS), from PeeringDB (PDB), and their union (ASN).

Colo	Address(es)	CS	PDB	ASN
LA1/2	One Wilshire / 900 N Alameda St	290	217	444
CH1	427 S La Salle St	38	13	44
MI1	2115 NW 22nd St	27	10	27

For instance, the very definition of an IP alias set implies that the group of interfaces that comprises an alias set must be co-present in a colo facility. Then, we would like to consider a collection of independent pieces of evidence to infer whether individual interfaces are located at a specific facility. The key challenge in adopting this intuitive strategy is that any individual instance of a co-presence rule/constraint is prone to error (e.g. DNS misnaming of an interface results in it being geo-mapped to a different city). This in turn could lead to the conflicting inference from different rules. More importantly, conducting inference by iteratively applying these rules could easily magnify a seemingly small error and render this approach useless.

To cope with these issues, we adopt a novel element for this problem in the form of a probabilistic inference approach from a collection of independent and potentially inconsistent pieces of evidence. In particular, we apply Belief Propagation algorithm to perform inference on a Markov Random Field graphical model that is tailored to the problem at hand. This probabilistic framework has the additional advantage that it can be used as a starting point by anyone who may have more informative measurements and/or access to better or improved heuristics that can be used to refine the underlying graphical model (e.g. modify inter-dependencies by imposing tighter constraints). Over time, incorporating such improvements can be expected to improve the completeness and accuracy of this mapping effort to the point where the desired transparency in the ways networks interconnect with one another becomes reality.

Localized Measurements

This section describes how we conduct purposefully designed data-plane measurements in the form of traceroute probes such that they are more likely to pass through (and thus reveal the presence of) a potential interconnect between a pair of tenant ASes in our target facility. To maximize the likelihood of detecting possible interconnects between tenants in a target facility with a limited number of measurements, our probing strategy consists of the following three steps: *(i)* collecting publicly available data about our target colo facility in full measure; *(ii)* selecting the source and destination of traceroute probes to be as close to the facility as possible with respect to both network and geographic distance; and *(iii)* launching probes in a criss-cross fashion to examine all possible pair-wise interconnects between tenants of our target facility. We next describe the first two steps steps in more detail.

Colocation Data Acquisition

Collecting publicly available information about a target colo facility includes obtaining *(i)* the physical address of the facility, *(ii)* a list of customers (i.e. colo tenants), and *(iii)* a list of partner IXPs that are reachable in the facility. For a given facility, to capture a comprehensive list of tenants and partner IXPs, we use publicly available information on different web sites (including those of the facility provider's company, the different tenants that publicize their presence in the facility, and third-parties that collect some of this information) and supplement (and compare) it with similar information provided by databases such as PeeringDB [211] that are maintained for the main purpose of facilitating the exchange of information related to Internet interconnections (i.e. peerings).

TABLE 15. Characteristics of vantage points and destination IPs selected for campaigns around each colo

	MI1		CH1		LA1/2	
	IP	AS	IP	AS	IP	AS
LG	24	21	23	22	95	77
RIPE	10	6	24	16	47	21
Local IP	24	19	23	29	95	179
Local Web	86	15	272	17	1,049	64
Unseen AS	78	1	20	8	2,493	68

One complicating factor in acquiring colocation data is that many of the available lists of tenants include the names of the different tenant networks/organization but don't provide the ASNs that these networks use to announce their routed prefixes. However, to be able to identify possible interconnections in a target facility from traceroute measurements, we need to be able to obtain the relevant ASNs for each of the facility's tenant. To this end, we combine various ASN-related information obtained from pulic sources (such as Hurricane Electric BGP Toolkit [98], whois services, and AS-related repositories maintained by CAIDA [52]) and infer for each tenant AS its primary ASN. To identify the primary ASNs for each tenant network, we use AS relationship data from CAIDA [53] and count the number of relationships between individual ASN and all other ASNs associated with the customer list in a target facility. Then, for each tenant, we pick the ASN(s) with the maximum number of relationships as the primary ASN(s) for the rest of our analysis.

Table 14 summarizes the collected information about our target facilities, including their street address and the number of primary ASNs for the list of tenants that we obtained from CoreSite, PeeringDB and their union, respectively.

Source Selection

Our ability to effectively localize our probes depends primarily on having access to vantage points (VP) at close-by locations. To address this issue, we leverage both *Looking Glasses* and *RIPE Atlas nodes*.

Looking Glasses (LG)

Major ISPs usually offer a LG as a web-based front-end to one or more back-end routers that allows a user to interactively run network debugging commands on the back-end routers. The associated web page also provides the ASN and the city where individual routers are located. Providers often enforce a tight rate-limit on their LGs' usage which renders them unsuitable for large-scale measurement campaigns. Using a list of $200+$ LGs from traceroute repositories (e.g. [155]) and PeeringDB, we select the sources for our traceroute probes as follows. First, we select those LGs that are within a tenant AS; next, if no LG exists inside a given tenant AS, we look for LGs in its customer cone and select the LGs with the shortest AS-hop distance. For these selected LGs, we subsequently obtain their list of back-end routers and their locations. Given the list of back-end routers associated with these selected close-by LGs, we select all that are inside the city of our target colo. If no such VP is found, we pick one that is geographically closest to the target facility. In our case studies, the median geo-distance of the selected VPs/routers used for our measurement is less than 10 miles, and 95% of the routers are within $1\,000$ miles of the target facilities.

RIPE Atlas

RIPE Atlas is a global network of remotely programmable probes that can launch basic network measurements such as `ping` and traceroute. RIPE's API allows one to

select probes in specific ASes (if there are any) that are within a certain geographic area. This feature is ideally suited for our localized measurement, and we select all RIPE probes that are within a 100-mile radius of the target colo regardless of their ASes and use them to run Paris traceroute [23].

These two measurement infrastructures offer complementary views of the data-plane. While LGs are usually located in major transit ASes and only very rarely in small eyeball ASes, RIPE probes are typically found in eyeball ASes and less frequently in transit ASes. The top part of Table 15 shows the number of tenant ASes in which we have identified VPs from each platform, along with the total number of VPs for our target facilities. LGs provide a desired vantage point in more tenant ASes than RIPE Atlas does.

Destination Selection

To increase the likelihood that our localized data-plane measurements traverse an interconnection inside our target facility, we select destination IP addresses in the tenant ASes and ensure the IPs are geolocated to the vicinity of the target colo. Specifically, we rely on the following three sets of destination IPs for our localized traceroute measurements.

Local IPs

Using a large pool of geo-located IP addresses collected from a few major P2P applications [214], we look for an IP address within each of the tenant ASes that has the shortest geo-distance from the target colo facility. If we do not find such an IP for a tenant AS or if the obtained distance is found to be more than 100 miles from the target colo, we examine the advertised /24 prefixes by that tenant AS, geolocate the prefixes, and select the one with the shortest geo-distance from the colo facility. Similar to [234], to infer the

geographic location of individual IPs, we use the majority vote among different IP-geo databases that include EdgeScape [17], MaxMind [185], and IP2Location [141][1]. The average distance of IPs in this pool from their corresponding target facility is between 40 to 75 miles for different campaigns, i.e. these destinations IPs are usually within the same metropolitan area of the target facility.

Local Web Servers

Some colo customers provide web hosting services and use the colo facility to house (parts of) their server farms. However, hosting providers also tend to distribute their deployments in a few colo market places for fault tolerance and avoiding single point of failure, therefore selecting a single IP in these ASes may not be sufficient. By targeting the web services that they host, and are potentially deployed in our target colo, we should be able to hit their interconnects with other tenant ASes in our target colo. Assuming that local institutions (e.g. schools, local government agencies, and small businesses) are likely to use these hosting providers, the web address of these institutions offer promising local targets for our traceroute probes. To identify these local institutions, we crawl online directories (e.g. Yelp, Google maps and Yellow Pages) and compile a list of their web pages. We then look up the corresponding IP addresses and infer their geolocations and their ASes (using Team Cymru IP-ASN service [250][2]). We only select IP addresses as destination IPs that belong to a tenant AS of the target colo and are geolocated within a 50-mile radius of the facility. Our *primary* localized targeted measurements include traceroutes from RIPE VPs to both local IPs and local web servers, and from LGs to local

[1]Unless stated otherwise, we always use the majority voting scheme throughout our work when geo-locating IPs using IP-geo databases.

[2]We primarily rely on Team Cymru IP-ASN service [250] to identify the ASN that advertises each IP

IPs. We then supplement these measurements with additional measurement as discussed in the next section.

Unseen ASes

Irrespective of how we select VPs and/or destination IPs, our traceroute measurements may fail to reveal some of the tenant ASes in the target facility. To detect these "unseen ASes", we use simple BGP-based IP-ASN mapping and rely on IP-geo mapping. If for a tenant, no IP is found in the target city, it is marked as an unseen AS. To discover the local footprint of these ASes, we conduct more comprehensive localized data-plane measurements. Specifically, we identify all the $/24$ prefixes advertised by each unseen AS, geo-locate the first IP in each prefix, and select all those IPs that are within a 50-mile radius of our target colo as destinations for our probes. We supplement the primary measurements with additional localized measurements obtained by running traceroutes from the local RIPE VPs to the IPs associated with the "unseen ASes."

The bottom part of Table 15 summarizes the number of tenant ASes for each target colo in which we found at least one close-by destination IP using each of the three discussed methods. Local IPs provide a desirable target in a majority of tenant ASes in each of the target colos.

Inferring AS Interconnects

As a result of performing only localized measurements, we are able to significantly limit the number of traceroute measurements that we exploit for mapping the x-connects in a target facility. In total, we only ran 170K, 8K, and 2.5K traceroutes for our measurement campaigns in LA, Chicago, and Miami, respectively. Moreover, we were able to run all of these measurements in a single day, and repeated the data collection five

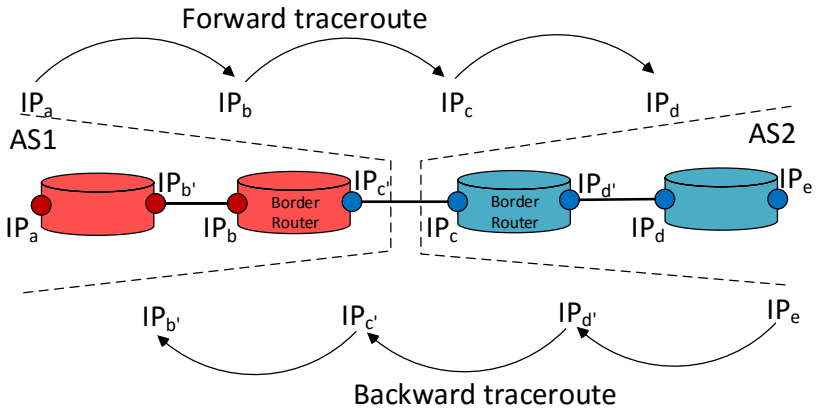

FIGURE 7.56. An example router-level topology depicting an inter-AS x-connect.

times during both, December, 2015 and January, 2016. In this section, we describe how we identify x-connects (or any interconnects) between ASes from the collected traceroute data.

An Illustrative Example

Figure 7.56 illustrates the case of a simple linear topology comprising a x-connect between two ASes. The figure shows four routers, with the left two (in red) belonging to AS_1 and the right two (in blue) owned by AS_2. The 2nd and 3rd routers are *border routers* of AS_1 and AS_2, respectively, with a private x-connect between them. Figure 7.56 also depicts the traceroutes, one in each direction, from which the topology was inferred. Being able to accurately identify the *inter-AS IP segment*, defined as the traceroute *hop* (or *segment*) where the IPs on either side belong to different ASes, e.g. IP_b-IP_c along the forward traceroute, is key to locating the AS interconnects.

A common approach (e.g. [95, 224, 231]) to identify AS interconnects from traceroutes involves two steps. The first step consists of mapping the IP addresses at each hop to their corresponding ASNs (e.g. using Team Cymru's "whois" service [250]) to produce an AS-level view of the IP-level traceroute. The second step requires searching

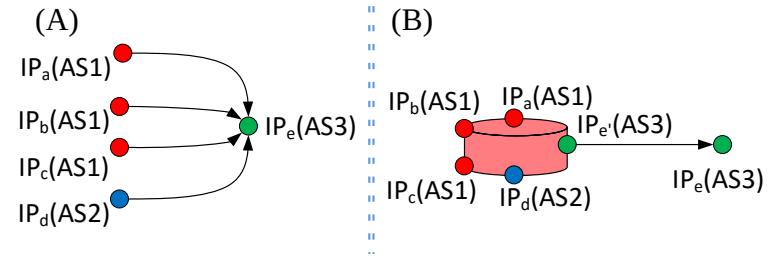

(a) Fan-in

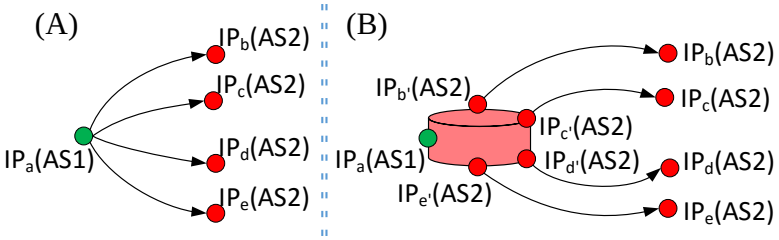

(b) Fan-out

FIGURE 7.57. Fan-in, and Fan-out structures, each illustrated with the *(A)* observed traceroute segments and *(B)* the inferred physical router-level topology.

the obtained AS-level view to find adjacent hops with different ASes which is then viewed as an indication of an interconnect between those ASes at that hop. Since the IP-to-ASN mapping in step one is known to be error-prone ([63, 180, 138]), we take a different approach and focus on the more challenging problem of inferring the inter-AS IP segment in measured traceroutes.

What makes the task of accurately inferring the inter-AS IP segment corresponding to a x-connect from traceroutes difficult is the required sharing of IP addresses between two connected ASes [175, 32]. Specifically, the IP addresses on both ends of a x-connect should be part of the same subnet, often a $/30$ or $/31$ subnet. This implies that of the two parties (i.e. ASes) to a x-connect, one is supposed to allocate the IP addresses for both interfaces of the x-connect at hand. What complicates the problem even further is the fact that the nature or direction of shared IP addresses between two connected ASes is generally unknown and could even vary across different x-connects on a single router. Since the commonly-used approach described above is in general not capable of dealing with these complications, alternative solutions or heuristics are needed.

To highlight this issue, consider Figure 7.56 where the interfaces on both ends of the x-connect (IP_c and IP'_c) are allocated by AS_2. A traceroute from AS_1 to AS_2 traverses through $IP_a \rightarrow IP_b \rightarrow IP_c$ which identifies IP_b–IP_c as the inter-AS IP segment. However, a traceroute in the reverse direction—$IP_{d'} \rightarrow IP_{c'} \rightarrow IP_{b'}$—identifies an incorrect inter-AS IP segment, namely $IP_{c'}$–$IP_{b'}$. Similarly, the case where the VP from where traceroutes are launched resides on a border router of, say, AS1, but the IP visited at the first hop of the resulting traceroutes is in a different AS also causes problems and needs special attention. To deal with such cases, we also consider the segment from the VP to the first

hop's IP (i.e. the segment between hop_0 and hop_1)), representing the *hop-zero* segment to be part of the traceroute.[3]

Inferring AS Owner of Border Routers

To tackle the problem of accurately inferring from traceroutes the inter-AS IP segments corresponding to x-connects, we build on prior studies, especially [32] that have proposed various heuristics to identify these inter-AS IP segments. However, instead of tackling the problem directly, we change our focus and are explicitly interested in systematically identifying the owner ASes of border routers. Once this ownership is established, we can associate all interfaces of a border router with its owner AS, regardless of their BGP-based mapping, and the sharing of IP addresses between (the border routers of) any two ASes does therefore no longer complicate the task of inferring the location of the x-connects between (the border routers of) these ASes. To solve this new and previously largely ignored problem of inferring the AS ownership of border routers, we describe below a number of old and new heuristics and illustrate how they help us achieve our goal.

A Majority AS in an Alias Set

While "majority voting" is not a new heuristic, we include it here for completeness and to illustrate its particular implementation for the problem at hand. To start, each alias set that is identified by an alias resolution technique represents a subset of interfaces associated with a router. Utilizing some conventional IP-to-AS mapping technique (based on BGP information) for individual IPs in an alias set, we use a (*conservative*) majority voting among the interfaces to determine the owner AS of the router. More specifically,

[3]We identified a substantial number of AS-links at hop-zero. For instance, in our LA campaign we find 76 x-connects exclusively at hop zero.

given an alias set, we consider the corresponding router to belong to AS_1 if the number of interfaces in the set that are owned by AS_1 is more than *two-times plus one* the number of interfaces mapped to any other AS, i.e. a clear majority of interfaces are mapped to AS_1. This conservative majority criteria ensures that no owner is determined when the alias set is small or does not have a dominant owner AS. In such cases, we call the corresponding router "ambiguous" (i.e. its owner AS is not determined) and rely on other heuristics to resolve the ambiguity.

Fan-in & Fan-out

To explain this new heuristic, consider a collection of inter-AS IP segments (with two IPs, one on either side) from different traceroutes that either share the first or the second IP (of the segment). We refer to these scenarios as *fan-in*, shown in Figure 7.57(a), and *fan-out*, shown in Figure 7.57(b)). In these figures, the color of each IP address denotes the AS that advertises the IP and the color used for routers indicates the owner AS of the router.

In the absence of layer-2 switches along the path, a plausible router-level topology that is consistent with all these inter-AS IP segments is shown on the right-hand side of Figure 7.57(a) for *fan-in* and on the right-hand side of Figure 7.57(b) for *fan-out*. In the case of *fan-in*, a router-level is plausible if it satisfies the condition that the first hops of all inter-AS segments in a fan-in scenario (e.g. IP_a through IP_d in Figure 7.57(a)) form an alias set. In the case of *fan-out*, the condition is that for each second hop in a fan-out scenario, there is an IP address from the same subnet (thus owned by the same AS) that is a member of an alias set with the first hop IP address. Once such alias sets are inferred, we apply our conservative majority voting heuristic to determine the owner AS of the set or label the router as "ambiguous."

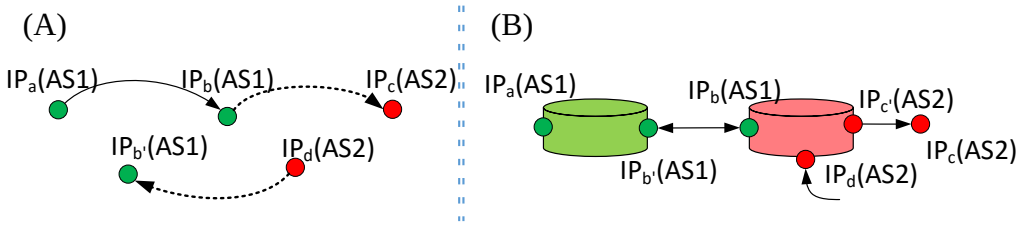

FIGURE 7.58. (A) "traceroute views" of an inter-AS IP connection observed from opposite directions, and (B) the corresponding physical router-level topology.

Note that a consistent alignment of AS-level IP-segments with the router-level topology in each scenario implies that there is a router that may have been missed by the alias resolution technique. Such "misses" are well-documented for the commonly-used alias resolution techniques; for example, MIDAR is known to exhibit *false negatives* when routers do not respond, or do not use monotonic counters, or do not share a counter across interfaces. In fact, any IP ID-based alias resolution technique is unable to detect such routers [157].

Subnet Matching

This useful but rarely-considered heuristic is based on the observation that a x-connect between two ASes can be reliably identified whenever our traceroute probes traverse the interconnection in both directions. To illustrate this scenario, consider the following two traceroute segments that are obtained over the router-level topology shown in Figure 7.58: $\text{IP}_a(\text{AS1}) \rightarrow \text{IP}_b(\text{AS1}) \rightarrow \text{IP}_c(\text{AS2})$ and $\text{IP}_d(\text{AS2}) \rightarrow \text{IP}_{b'}(\text{AS1})$ where $\text{IP}_x(\text{ASN})$ denotes that IP_x is mapped to ASN. If IP_b and $\text{IP}_{b'}$ share a subnet, and assuming that the border routers respond to traceroute probes using the IP of their ingress interface [255], these traceroute segments indeed pass through the same subnet (i.e. $\text{IP}_b(\text{AS1})$–$\text{IP}_{b'}(\text{AS1})$) in both directions (i.e. the subnet matching condition holds). Since the IPs of the next hop in both directions belong to different ASes, the right-side

router must be owned by AS2 and therefore the link $\text{IP}_b(\text{AS1})$–$\text{IP}_{b'}(\text{AS1})$ is the x-connect between these two ASes. Indeed this implies that $\text{IP}_d(\text{AS2})$ and $\text{IP}_b(\text{AS1})$ are part of an alias set, but failed to be identified as such by the alias resolution technique.

To apply this heuristic, we use XNET [255] to identify all IP address pairs that are on the same subnet. Among the IP-segments from AS1 to AS2 and the reverse direction, we examine whether the far-side of one inter-AS IP segment ($\text{IP}_{b'}(\text{AS1})$) is in the same subnet as the near-side of another IP-segment ($\text{IP}_b(\text{AS1})$) in the reverse direction. If this condition is satisfied, we then set the owner AS of the near-side (IP_b) to be AS2 instead of AS1.

Sink IPs

Another original heuristic is based on the empirical observation that traceroutes that are destined toward small regional tenant ASes reveal two common patterns. For one, many such traceroutes terminate at a specific set of IP addresses, referred to as *sink IPs*, before they reach the destination AS. In addition, these *sink IP* addresses are never encountered in traceroutes toward other ASes. The observed strong association between small regional ASes and *sink IPs* suggests that these *sink IPs* indeed reside on a router that is owned by the regional AS.

To validate this heuristic, we manually examined more than 500 *sink IPs* and observed that while the PTR record (DNS name) of a *sink IP* has a domain that matches the AS that advertises the IP address through `BGP`, the name also tends to contain hints that point to the regional AS. For instance, the *sink IP* for *Televergence Solutions Inc. (AS30188)* is advertised by *GTT (AS3257)* and its DNS name is **`televergence`**`-gw.ip4.gtt.net`. Thus, instead of relying on inaccurate `BGP`-based AS

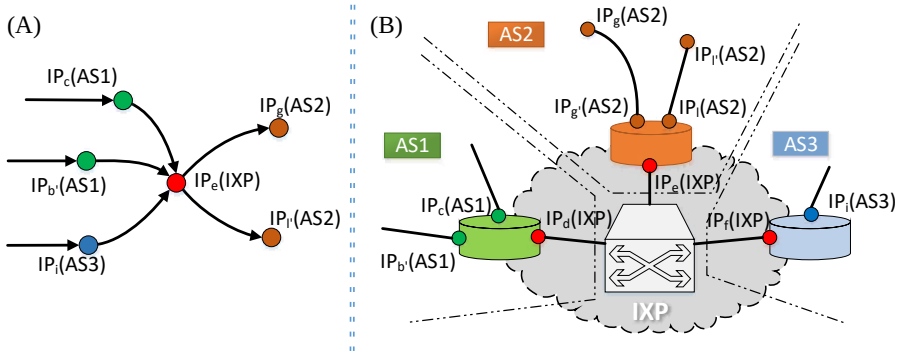

FIGURE 7.59. (A) "traceroute view" of traces hitting the IXP. (B) Physical inferred router-level connectivity at the IXP.

mappings, we apply this particular heuristic to map these *sink IPs* to their destination ASes (regional networks).

IPs Assigned by an IXP

To complete our set of heuristics, we also consider the well-known special case of IXP-assigned IPs. In short, IXPs enable their members to establish public peerings to directly exchange traffic with one another over a shared switching fabric [24]. In this setting, each IXP owns a block of IP addresses, and allocates IP addresses from this block to individual customers called member ASes. The customers use IP addresses from the IXP's IP block on their router interfaces attached to the IXP switch. To identify the customer AS to which an observed IP_{ixp} was assigned, we consider all the next hops of that IP across different traceroutes. We conclude that IP_{ixp} is assigned to (and the corresponding router is owned by) an AS if that AS appears as the next hop after IP_{ixp} in all traceroutes. For instance, in Figure 7.59, $\text{IP}_e(\text{IXP})$ is always followed by IPs in AS2, and, hence, we infer that the IP is assigned to a router that belongs to AS2.

TABLE 16. Details on heuristics used in each campaign

	Miami	**Chicago**	**Los Angeles**
Alias sets	576	738	3644
IPs in alias sets	3279	3996	22573
Alias sets with majority	512	645	3074
Fan-in	336	370	4023
IPs in fan-in	658	696	6441
IPs fan-in with majority	404	401	3823
Fan-out	285	366	3125
IPs in fan-out	362	473	4122
IPs fan-out with majority	215	226	2278
Sink IP	284	475	3063
Resolved IXP IP	26	43	420
Subnets matched IP	10	16	180

Evaluation of our Heuristics

To evaluate the effectiveness of the different heuristics, we consider all of our collected traceroute measurements and give in Table 16 a detailed account of how the heuristics performed for each of our measurement campaigns.

We use MIDAR [157] to identify all alias sets that belong to the same router in order to apply the majority voting heuristic among all the IPs that traceroutes visited. As the input to alias resolution, we consider the union of two sets S_1 and S_2 of IP addresses in a measurement campaign; S_1 is the set of IP addresses observed in the traceroutes and S_2 denotes the set of IP addresses in $/30$ subnets of the IPs in S_1. Including the set S_2 allows us to identify more IPs from each alias set due to IP sharing. The top portion of Table 16 shows, for each campaign, the number of identified alias sets, the counts of IPs in these sets, and the number of alias sets where our conservative majority voting scheme identifies an owner. Such an owner is identified for 83-88% of alias sets. 2-4% of the IP addresses in the discovered alias sets (when the scheme identifies an owner AS) are

inferred to be on routers that do not belong to the AS that advertises them via BGP. The second and third portions of Table 16 reports the same quantities for our *fan-in* and *fan-out* heuristics. The bottom portion of the table gives the number of IPs that result from applying the *subnet matching*, *sink IP*, and *IXP-assigned IP* heuristics, respectively, for each of our campaigns.

Where our heuristics have insufficient evidence to reliably infer the owner AS of a router and therefore label that router as "ambiguous", we apply an additional heuristic (here called the "valley-free heuristic") that leverages commonly used control plane information in the form of inferred AS relationships (e.g. [53]). Specifically, we consider all traceroutes that pass through an interface, say IP_x, of an ambiguous router (i.e. IP_x represents an IP from the relevant alias set) and focus on the AS-level view of the three hop segment containing the hop before and after IP_x. We then iterate through the list of potential owner ASes of IP_x and check each time whether the resulting AS-level path segment is indeed *valley-free*. A valley-free route is one in which the transit AS is not the customer of either ASes connected by the transit provider. Any candidate AS that results in a valley-free AS-level segment in *all* traceroutes is considered as a viable owner for this particular ambiguous router. In our data where we encounter more than 400 ambiguous routers, we identify a single AS owner in 90% of the cases using this valley-free heuristic.

Note that once we identify the owner AS of a router, we assign all IPs in the alias set to the owner AS (of the router). Some of these IPs may have been originally mapped to a different AS (e.g. based on BGP advertisements), and these IPs are now *reassigned* to the owner AS. We observe such IP-to-AS reassignments for 10-15% of all observed IPs in each measurement campaign and different heuristics contribute between 5-35% to the

TABLE 17. Percentage of IPs reassigned to owner ASes of routers by different heuristics in each campaign.

	Miami	**Chicago**	**Los Angeles**
Alias	23.00	14.60	16.91
IXP	8.67	13.35	13.33
Sink	24.33	35.40	32.55
Fan-in	20.67	17.08	18.78
Fan-out	36.33	28.57	36.48
Subnet Match	3.33	4.04	2.66
Valley Free	16.00	18.32	15.04

reassignments. Table 17 shows the percentages[4] of IPs that get reassigned to a different AS by the different heuristics in each measurement campaign.

We validate this router-aware IP-to-AS mapping heuristic using two different data sources. For one, we use information published by IXPs and PeeringDB to validate the owner AS of IXP-assigned IP addresses inferred through our heuristics. We observe that more than 92% of the inferred owner ASes for IXP-assigned IPs are consistent with this public information. Second, we use hints embedded in DNS names that suggest IP address sharing between two ASes. A DNS naming convention used by some ASes (e.g. Level3, GTT, NTT and PCCW) is to embed the name of the peer AS in the DNS name for the IP address used to establish the peering link. For this type of validation, we focus on the IP addresses that our heuristics mapped to an AS other than the `BGP`-based owner AS. For example, in the case of `ae-0.`**`teliasonera`**`.chcgil09.us.bb.gin.`**`ntt.net`** we check to see if the IP address is inferred to be assigned to AS1299 (i.e. TeliaSonera). Out of nearly 4K such IP addresses that we examined, some 25% have a valid DNS name, and about 40% of these names explicitly indicated IP address sharing. More than 90%

[4]The sum of percentages along a column can be more than 100% as multiple heuristics may suggest the same remapping.

TABLE 18. Aggregation guidelines

(I) *Fan-in aggregation*

Near-side		Far-side
141.136.106.153	→	63.218.42.5
89.149.130.129	→	63.218.42.5
141.136.106.157	→	63.218.42.5
141.136.106.161	→	63.218.42.5
141.136.106.5	→	63.218.42.5
141.136.111.205	→	63.218.42.5
89.149.129.121	→	63.218.42.5

(II) *Subnet matching aggregation*

Near-side		Far-side
141.136.106.153	→	63.218.42.5
63.218.42.129	→	63.218.42.6

of the hints extracted from the DNS names match the router owner AS inferred by our heuristics[5].

Accurate AS Interconnect Counting

An important implication of accurately inferring the owner AS of border routers is that the resulting router-level view allows for a more accurate accounting of the actual number of x-connects encountered in traceroutes. For example, the fan-in scenario in Figure 7.57(a) clearly shows that there is a single x-connect between the two ASes; simply counting inter-AS IP segments in different traceroutes [95, 224, 115] would result in over-counting x-connects.

The following two guidelines are concerned with properly aggregating different views of a single x-connect between a pair of ASes.

[5]We provide the list of all the remapped IP addresses with the associated PTR record through the following online tables: onrg . cs . uoregon . edu / impact / resources / router - asn/validate/

Fan-in Aggregation: Motivated by the *fan-in* scenario illustrated in Figure 7.57(a), this guideline advises to aggregate all the observed AS-level IP segments or interconnects that have the same far-side IP address and consider them as different views of the same x-connect in the same direction. For instance, Figure 7.57(a) shows 7 inter-AS IP segments, but we count them as only one x-connect.

Subnet Matching Aggregation: This guideline is motivated by our subnet matching heuristics. It suggests aggregating all the discovered AS-level IP segments whose far-side IP addresses are used for the two ends of an interconnection and consider these segments as different views of one and the same x-connect in opposite directions (See Figure 7.58). Table 18(II) shows an example case with 2 inter-AS IP segments that are counted under this guideline as a single x-connect since the far-side IP addresses belong to a $/31$ subnet and therefore are two ends of one interconnection.

Note that these guidelines can be used in combination as well. As our examples in Tables 18(I) and 18(II) demonstrate, all the AS-level IP segments in the two examples can be aggregated to a single x-connect between AS3257 and AS3491. To illustrate the practical relevance of these aggregation guidelines for properly accounting for the actual number of x-connects in a target facility, the median number of aggregated views across our measurement campaigns is 2, but we encountered cases were as many as 40 different views were aggregated to yield a single x-connect.

Pinning X-Connects to Facilities

Equipped with the ability to infer x-connects between the owner AS of border routers from our localized traceroute measurements, in this section we describe our strategy for determining whether those x-connects can be mapped to the inside or outside of our target facility. This "pinning" process consists of considering the interface IPs

on both sides of the inferred AS interconnections, identifying a set of "anchors" (i.e. interfaces that can be reliably mapped to the inside or outside of the target facility), and then performing belief-propagation-based inference on a purposefully constructed graphical model. This model reflects our best efforts described in Sections 7.3 and 7.4 at inferring an underlying router-level connectivity structure surrounding the target facility that is as consistent as possible with the comprehensive view derived from all our traceroute measurements. In this section, we describe this pinning process in more detail.

Pinning Process: Anchors

We start by selecting all the observed IP addresses in a measurement campaign for which we have any clues that they may be located in the target colo. To identify this "relevant" pool of IP addresses for pinning, we first remove all IP addresses that are associated with routers owned by ASes that are not tenants in the target facility. Next, we eliminate all the observed IP addresses in a measurement campaign for which we cannot find any evidence that they are geo-located to the target city. To this end, we remove all interfaces associated with any alias set if geo-location hints in *all* their PTR records (when available) indicate a location other than the target city. We also remove any interface that is not mapped to the target city by any of the IP-geo mapping databases (see Section 7.3). Any remaining IP address is included in the relevant pool and considered for pinning.

To bootstrap the pinning process, we rely on a set of anchors that can be reliably mapped to the inside or outside of our target colo. For determining which subset of the "relevant" pool of IP addresses can serve as reliable inside/outside anchors, we examine

the relevant pool of IP addresses for the following three types of solid location-specific evidence:

Facility Information in DNS Names: Some networks encode specific information about the colo that hosts their deployment site in PTR records (DNS names). This in turn provides reliable information about the interface location at the facility level. Examples for such encodings include `rt0as-`**`equinix`**`.vx.shawcable.net` which clearly suggests deployment in an Equinix colo or `as22822-9.`**`111eighthave.ny`**`.ibone.comcast.net` which reveals the address of the facility to be 111, 8^{th} ave, NYC, which is a well-known major Internet hub in NYC. We rely on our in-house DNS parser (i.e. ALFReD [194]) to detect and extract any such hints from the PTR records of relevant interfaces.

IPs co-located with IXPs: Publicly-available partnerships between IXPs and colos (e.g. Any2 IXPs and CoreSite) offer additional specific evidence for identifying IP addresses that are located inside a colo. For one, individual IXPs have their own dedicated and well known IP prefixes from which they assign an address (IP_{ixp}) to the interface of a member's router that connects to the IXP switching fabric [24]. Unless the IXP partners with other colo facility providers, all these IPs are clearly located in the colo of interest.[6] Second, any IP address that is observed on a traceroute prior to the IP from the partner IXP's prefix should also be located in the same colo [115]. To explain, consider a traceroute segment with the consecutive 3 hops $\text{IP}_a(\text{AS1}) \rightarrow \text{IP}_{IXP} \rightarrow \text{IP}_b(\text{AS2})$ that belong to AS1, IXP and AS2, respectively. If AS1 is a member of the IXP and is only present in the target colo facility, we conclude that IP_a must be located inside the same facility. Note that we cannot reliably draw the same conclusion for IP_b that is attached to the next-hop router [115]. Furthermore, an IXP partnering with other colo

[6]Some of the larger IXPs typically partner with multiple colo facilities e.g. `www.laiix.net`.

facility providers in the same city helps identify anchors that are located outside our target facility.

Using Small Regional ASes: The presence of small regional ASes at a colo provides a good opportunity for identifying anchors at that facility or validating already discovered anchors. For economic reasons, a small regional tenant AS is most likely to have its PoP only in a single colo in that city where it establishes all its interconnects. In fact, presence in colos of different providers in the same city is proportionally more costly and unnecessary for a small regional AS that typically deals with limited traffic volume. We consider all observed IPs (including any LG) associated with such small regional ASes to be located in the same colo facility. More formally, we use CAIDA's AS rank data [52] and consider a tenant AS to be a small regional AS if it has less than 5 ASes in its customer cone and advertises less than 50 $/24$-prefixes. We also cross check any selected regional ASes with PeeringDB to ensure that they do not have deployment sites at multiple colos in the metro area of our target facility. Note that this evidence only provides anchors inside the target facilities.

Table 19 presents the number of in/out anchors that we identified using each of these three techniques in each one of the target cities. The number and relative fraction of in/out anchors in each campaign depends on various factors including the number of colo facilities in the target city and the number of tenant ASes in the target colo.

Pinning Process: Graphical Model Construction

We first present a set of domain knowledge-based co-presence rules/constraints that indicate whether a group of interfaces is (or is not) co-located in the same colo facility. We then construct a Markov Random Field (MRF) graphical model to encode all these association rules/constraints along with their level of strength/certainty. The resulting

TABLE 19. The number of in- and out-anchors identified by the individual techniques for each target colo facility

	Miami		**Chicago**		**Los Angeles**	
	IN	OUT	IN	OUT	IN	OUT
DNS hints	0	21	0	40	3	43
Small regional AS	11	0	126	0	336	0
IXP	0	5	2	18	153	37
IXP near-side	0	2	1	9	85	27

model serves as input to a probabilistic algorithm to determine whether individual IP addresses are mapped inside or outside of the target facilities in a city.

Defining Co-presence Rules: We consider the following rules (or associations) that will later on aid in the (probabilistic) inference of the co-presence of a group of interfaces in a colo. These rules are ordered based on the level of confidence in their outcome (from low to high).

1. *Intra-domain links*: The presence of two adjacent IPs from the same AS (i.e. intra-domain IP-segment) on a traceroute with a very short RTT difference hints at co-location of the IPs. The likelihood of co-location is inversely proportional to the RTT difference.

2. *Inter-domain Links*: Similar to the previous case, the existence of two adjacent IPs from different ASes (i.e. inter-domain IP segment) on a traceroute suggest that the IPs are co-located. The likelihood of co-location is higher for interconnects compared to intra-domain IP segments, since remote AS peering is often times avoided for economical reasons. Note that in our case studies we require the difference in RTT delays to be no more than 30ms to imply even the weakest likelihood of co-presence.

3. *PoP-Tag Rules*: Among a number of operators, it is common practice to use DNS naming conventions that embed a city name (or code) concatenated with numerical values as a "PoP-tag" to distinguish interfaces associated with individual PoPs in a metro area. For example, the DNS name for all interfaces associated with a specific PoP of Level3 in Seattle has the format `*.seattle1.Level3.net`. We extract these PoP-tags (in the form of `Level3.net:seattle1`) from DNS names and leverage them to define the following two rules: *(i)* All interfaces of a tenant AS of a colo facility that are associated with the same PoP-tag must be located in that same colo facility. *(ii)* Two IPs of one and the same tenant AS of a colo facility that are associated with different PoP-tags must be located in different colo facilities.

4. *Alias Association*: All interfaces in an alias set belong to a single router and must therefore be co-located in the same colo facility.

Graphical Model Construction: We examine the "relevant" pool of interfaces derived from a measurement campaign against our co-presence constraints and identify any group of interfaces that satisfy any of these constraints. Then, we use a graphical model of the *Markov Random Field* (MRF) type [158, 174] to encode all the observed instances of individual co-presence constraints as an undirected graph. MRF is a mathematical framework that is particularly well suited for solving inference problems with uncertainty in observed data. We represent each interface as a node in the graph and its association with other interfaces are encoded as edges with the proper weight (i.e. level of confidence) between them. For instance, each instance of an alias or PoP tag association rule is represented as a star-shaped graphlet where all relevant interface nodes connect to the "association type" node in the center. Each node can be in a finite number of states that statistically depend only upon the state of its neighbors. The probabilistic independence of non-neighboring nodes is a key requirement for the applicability of

TABLE 20. Sample propagation matrices for association and disassociation, $\varepsilon < \varphi$

(a) Association

V1	*V2*	ϕ	*P*
0	0	$\varepsilon + \varphi$	$\frac{\varepsilon+\varphi}{4\varepsilon+2\varphi}$
0	1	ε	$\frac{\varepsilon}{4\varepsilon+2\varphi}$
1	0	ε	$\frac{\varepsilon}{4\varepsilon+2\varphi}$
1	1	$\varepsilon + \varphi$	$\frac{\varepsilon+\varphi}{4\varepsilon+2\varphi}$

(b) Disassociation

V1	*V2*	ϕ	*P*
0	0	$\varepsilon + \varphi$	$\frac{\varepsilon+\varphi}{4\varepsilon+3\varphi}$
0	1	$\varepsilon + \varphi$	$\frac{\varepsilon+\varphi}{4\varepsilon+3\varphi}$
1	0	$\varepsilon + \varphi$	$\frac{\varepsilon+\varphi}{4\varepsilon+3\varphi}$
1	1	ε	$\frac{\varepsilon}{4\varepsilon+3\varphi}$

the MRF model; That is unrelated nodes in an MRF (i.e. interfaces for which there is no joint probability distribution on their location) have independent random variable (conditioned over the location rest of the nodes). This essentially means that if two IPs are *a)* not aliases, *b)* have not been seen in an IP-segment, or *c)* do not have similar PTR, knowing the location of one does not affect our belief about the location of the other.

In our MRF model, we assign a binary random variable to each node. The two states of IN and OUT indicate whether the node is inside or outside the colo (i.e. $P(n =$ IN) = 1 - $P(n =$ OUT)), respectively. The state of each inside (outside) anchor node is set to 1 (0). The joint probability distribution between all connected pairs of nodes is represented by a *Propagation Matrix*, where entry (i, j) equals the probability (i.e. based on the relative confidence of the constraint) of a node being in state j given that its neighbor is in state i. A desired feature of MRF is its ability to effectively encode both association and disassociation between nodes, i.e. whether two nodes must have similar or opposite states. More specifically, for a pair of connected nodes, v_1 and v_2, we can define the joint probability for each one of the four possible states. As shown in Table 20, a co-presence association (e.g. being in an alias set) is encoded by assigning high probability to similar states (e.g. $(v_1 = 0) \wedge (v_2 = 0)$) and low probability to opposite states (e.g. $(v_1 = 1) \wedge (v_2 = 0)$). Conversely, disassociation (e.g. different PoP tags) requires the

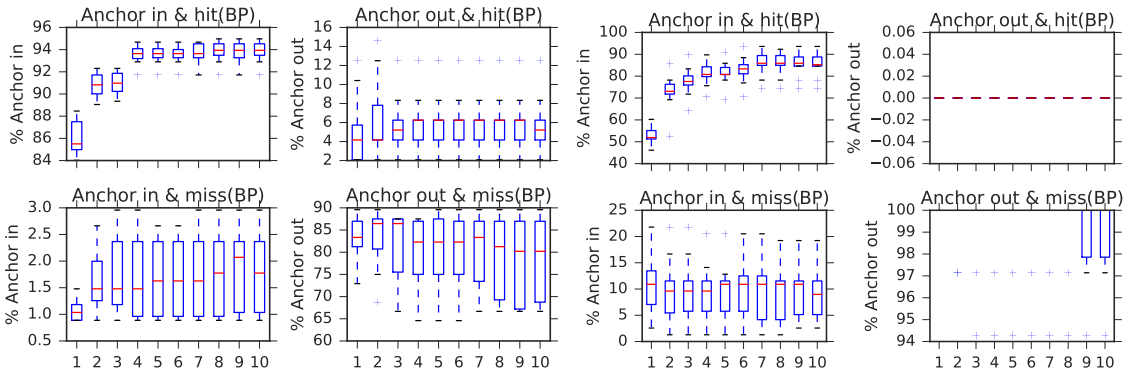

(a) Los Angeles; Test and validate to find the proper $\boldsymbol{c}$ (b) Chicago; Test and validate to find the proper $\boldsymbol{c}$

FIGURE 7.60. The effect of $\boldsymbol{c}$ on *i)* the inferred believes about the anchors not used in BP; 40% anchors used in BP, and *ii)* the distribution of believes for all nodes.

opposite assignment of probabilities (Table 20). Note that the model allows two PoP-tags of a network to be both OUT.

The joint probabilities are defined based on two parameters: φ is the main parameter as ϵ is often set to a small value (0.05). In theory, a large training set should be used to "learn" the value of φ. However, for our problem, this approach is not feasible. Instead, we take a more pragmatic approach and argue that *as long as the joint probability for each co-presence constraint captures the relative ranking of our level of confidence associated with these constraints, a probabilistic inference technique properly pins individual interfaces without being too sensitive to the value of* φ. In fact, the insensitivity to the value of φ implies that the inferred solutions represent a basic pattern that is not an artifact or side-effect of a specific parameter setting. We enforce the relative ranking of the above-defined co-presence constraints by setting $\varphi = k \times c$, where k is the order of a co-presence constraint based on our level of confidence, i.e. the higher the confidence, the larger the value of k. Therefore, c is a parameter that defines the relative gap/difference between the value of φ for two adjacent constraints.

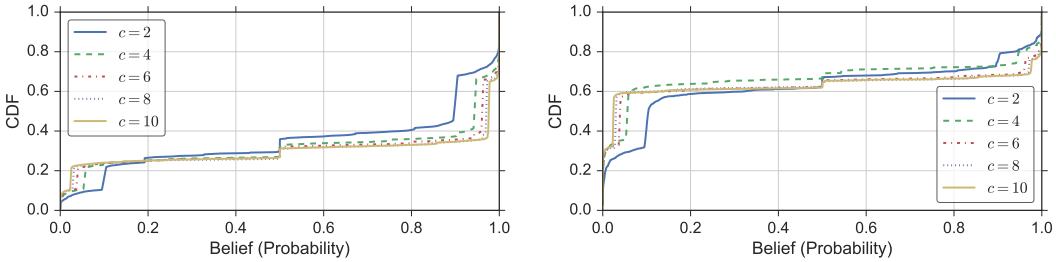

(a) Los Angeles; Distribution of believes

(b) Chicago; Distribution of believes

FIGURE 7.61. The effect of c on the distribution of believes for all nodes.

Pinning Process: Belief Propagation

Belief Propagation (BP) [278] is an algorithm for performing probabilistic inference on data with probabilistic inter-dependencies. It has been successfully applied in various domains to conduct probabilistic inference on data with probabilistic inter-dependencies. In all these applications, BP usually takes as input some form of a network where the nodes can have a finite number of states and the edges or connections represent the pairwise inter-dependencies between nodes (e.g. MRF). The algorithm then infers the posterior state probabilities of all nodes in the network given the observed states for some of them. The algorithm proceeds by iteratively passing messages between nodes based on the previous beliefs and pairwise joint probabilities. The algorithm updates the state of each node (i.e. belief) in each iteration until it reaches an equilibrium where the states assigned to individual nodes are as compatible with their neighbors as possible. While BP's convergence is not guaranteed theoretically, in practice it has been known to quickly converge quickly to a reasonably accurate solution. The rate of convergence is not similar for all nodes, and the time to reach equilibrium is also affected by the underlying MRF (the choice of ε and φ).

To apply BP to our pinning problem, we first create an MRF for each colo mapping campaign which encodes the inter-dependencies (i.e. constraints). A suitable prior

belief/state for anchor nodes is initially set to be inside or outside the target facility. We then run the BP algorithm until 90% of the nodes reach a steady state. The outcome of the algorithm shows the probabilistic beliefs about the location of each node. We divide the location of nodes into three sets based on their resulting probability: *(i) hit*: stable nodes whose probability to be in the target facility is more than 90%. *(ii) miss*: stable nodes whose probability to be in the target facility is less than 10%. *(iii) close call*: the rest of the nodes including those that did not reach an equilibrium.

We use a common test/validation technique to assess the sensitivity of BP's outcome to the value of c. We remove $10\% - 60\%$ of randomly selected anchors for testing, and run the BP algorithm with the remaining anchors. We repeat each test 10 times using different random sets of anchors. As an example, consider the case where the goal is to maximize the number of correctly inferred inside/outside anchors for our measurement in LA using 40% of anchors for testing. The left-side plots in Figure 7.60 (from top to bottom) show the summary distribution of the fraction of test anchors inside the target facility in LA that are mapped as *hit*,*close-call* or *miss*, as a function of c. The right-side plots show the same information for test anchors outside the target facility in LA. These results demonstrate that once the value of c exceeds 3 or 4, more than 94% of inside anchors are correctly mapped and the variations across different runs is very small. The mapping accuracy for outside anchors is around 82% and exhibits a somewhat larger variability. Given the significantly smaller fraction of outside anchors in LA, the relatively lower accuracy in mapping outside interfaces is not surprising. This examination suggest that for c-values between 4 and 9, the BP algorithm results in the highest level of accuracy.

This examination suggest that for c-values between 4 and 9, the BP algorithm results in the highest level of accuracy. To offer more insight into the choice of c on

the outcome of BP algorithm, Figure 7.61 presents the inferred distribution of belief probabilities for all nodes when running the BP algorithm with different values of c. This results illustrate that the probability distribution quickly become bimodal as we increase c. This implies that the inferred probabilities represent a basic pattern in the data that is not an artifact of the choice of c or of the selected thresholds for defining hits and misses.

Pining Results

To demonstrate the applicability and feasibility of our pinning process for mapping AS interconnections or peerings inside a target colo, we present the results of pining for three CoreSite colos in Los Angeles, Chicago, and Miami, respectively. Table 21 summarizes the total number of nodes of each kind in our MRF framework and gives the breakdown of their pinning to inside and outside of the colos. Table 22 shows the number of IP-level interconnects where both ends are mapped to the target colos with their breakdown between private and public in each target facility. Finally, we apply the two aggregation guidelines alluded to in Section to avoid over-counting the number of physical x-connects between two AS. The bottom row of Table 22 presents the number of consolidated x-connects in each facility and shows that the number of physical x-connects is two to four times smaller than the number of IP-level interconnects before aggregation.

Validation & Comparison

Colocation facility providers in general are not willing to disclose information regarding interconnectivity of their tenant ASes, and our attempts at obtaining such information from some colo providers were futile as well. In addition, tenant ASes themselves are reluctant to share the details of their interconnectivity with other ASes, unless they are sufficiently coarse so as to not reveal the type, precise location, and name

TABLE 21. The number of pinned nodes of various types

	Miami			**Chicago**			**Los Angeles**		
	IN	OUT	Total	IN	OUT	Total	IN	OUT	Total
Facility	0	1	1	0	3	3	1	3	4
IXP	0	2	2	1	3	4	3	0	3
PoP-tag	6	22	30	10	30	45	66	57	165
Router	16	80	108	59	140	223	479	129	773
Interface	50	480	601	303	512	943	2502	974	4416
Alias	27	287	347	109	467	668	2262	720	3632
LG	1	5	10	1	2	8	15	5	33

TABLE 22. The number of mapped IP-level inter-AS peerings and aggregate number of x-connects that they represent

		Miami	**Chicago**	**Los Angeles**
IP Segments	Public	0	1	1857
	Private	51	168	4811
Physical Links	X-Connect	25	46	1306

of the peer of an interconnection [103]. With the scarcity of any reliable ground truth, it is inherently challenging to directly validate our approach for detecting and pinning x-connects at a target colo. In light of these difficulties, we assess the completeness and correctness of our pinned x-connects through comparison with independent sources of information.

At a high level, note that as of June 2016, CoreSite [77] claims that some 2.4K x-connects are used in LA while our approach maps a total of $1,306$ to the LA CoreSite location. Although we appear to map only about 55% of CoreSite's x-connects in LA, it is important to recall that our approach is not designed to reveal colo-specific internal connectivity support such as CoreSite's Open Cloud Exchange [79] which alone serves some 100 tenant ASes.

Using Control-Plane Information

The presence of BGP routers that are accessible via LGs at specific colos in the target city provides a valuable validation opportunity. In particular, we obtain the output of `SHOW BGP SUMMARY` on a router that is owned by a tenant AS of a target colo to identify which tenant ASes "established BGP session" with other tenant ASes. The output also includes the *next hop* IP associated with each session which enables us to extract the corresponding PoP-tag from its DNS name (if any). We obtained this information from three BGP routers in Los Angeles: two routers owned by Hurricane Electric (HE) that are located at Equinix and CoreSite, and a router owned by Akamai located at CoreSite. Our approach has identified and pinned all 5 AS links between Akamai and other tenant ASes, and 124 out of 160 AS links between HE and other tenants, captured through their router at CoreSite. A manual inspection of the missing AS links for HE revealed that the

AS links at CoreSite serve as backup routes while routes through Equinix are a preferred option. This path preference, in turn, prevents our probes from discovering these links.

We also validate the PoP-tags that are pinned to the inside and outside of our CoreSite facility by BP against PoP-tags extracted from these three BGP routers in Los Angeles. More specifically, we consider a PoP-tag that is pinned to the inside (outside) of our CoreSite facility as valid if it is associated with an obtained next hop IP from a BGP router at the CoreSite (Equinix) facility. We observe that out of the 14 PoP-tags inferred by BP that can be evaluated with information obtained from the HE routers, 12 are valid. Moreover, out of the 9 PoP-tags inferred by BP that can be checked with information obtained from the Akamai router, all 9 are valid.

Comparison with CFS

A recent study by Giotsas et al. [115] focused on pinning interconnects associated with 10 target networks to colo facilities using a technique called Constrained Facility Search (CFS). As a by-product of their approach, they opportunistically inferred and pinned a number of interconnections between other networks at various locations using traceroute data collected between Feb. and Sep. of 2015. We obtained from the authors of [115] all the AS interconnect records including 620 records of x-connects type that they mapped to the CoreSite facility in Los Angeles, and we used this set to cross-validate our mapped x-connects in the same facility since it is one of our target facilities. Each interconnect "record" in this set that was obtained via the CFS method includes the two connected ASes (AS-level), the IP address of the near-side of the interconnect, and the peering type (public-local, x-connect, private-tethering, public-remote).

Since we consider x-connects as a physical interconnection between routers, we first consolidate all the CFS interconnect records of the same type whose near-side IPs are

aliases. This consolidation reduces the number of CFS-based records of x-connect type from 620 to 342 that are associated with 265 AS-links. Next, we divide these 342 CFS-based x-connect records into different groups based on their alignment with our results. Table 23 shows this breakdown along the following different groups:

G1, Non-tenant AS: We disregard 3 AS-links and 3 CFS-based x-connects records from the obtained list since they are associated AS4323 that is not a tenant in the target facility.

G2, Matched x-Connects: From the provided list of CFS-based x-connect records, there are 43 (associated with 30 AS links) that our approach identifies with the same peering type and pins to the same target facility. If we relax the requirement of having similar peering type, the number of matched interconnects increases to 137 associated with 99 AS-links. The discovery of a different peering type for these 99 AS-links at the same facility suggests that the involved ASes shifted towards more public peering over time.

G3, Missing x-Connects: There are 202 reported CFS-based x-connect records (143 AS links) reported by CFP that are missing from our data. We divide these records into two subgroups: *G3.1, Targeted:* For 100 of these missing records (69 AS links), we indeed have performed, as part of our measurement campaign for this target facility, a localized traceroute by placing our source and destination in the corresponding tenant ASes but did not observe an interconnection. A careful examination of these missing 100 CFS-based x-connect records revealed that for 17 of them (9 AS links), our measurement indeed observe at least one IP-level interconnect between the networks, but our approach did not map it inside the target facility because at least one end of the interconnection is geo-located outside of LA. We argue that the remaining 83 CFS-based x-connect records (60 AS-links) are likely the result of using historical data and no longer reflect the more recent interconnectivity picture that was explored during the course of our study. *G3.2, Not Targeted:* There are 102 CFS-based x-connect records (77 AS-links) for which we

were unable to perform localized measurements and therefore do not have any reliable evidence to either confirm or dismiss their existence. To further examine these cases, we obtained from the authors of [115] the raw traceroutes that were responsible for 30% of these cases to be inferred by the CFS method. A close examination of these traceroutes produced the following results: *G3.2.1* For 73% of the 102 CFS-based x-connect records in question, none of the provided traceroute passes through an inter-AS IP segment where both sides are geo-located to LA by any IP-geo mapping tool. A possible explanation for this observation is the re-allocation of IP addresses. However, the large fraction of these cases suggests a possible error in how the CFS approach maps certain scenarios. *G3.2.2* For 14%, the CFS-based x-connect records are inferred from traceroutes that contain loops and should therefore not be considered for such inference [68]. *G3.2.3* This leaves 13% of the 102 CFS-based x-connect records (approximately 4% of all 342 consolidated CFS-based x-connect records) that are mapped by CFS but missing from our results. One possible explanation for this remaining discrepancy could be the inherently dynamic nature of interconnects at the target colo between the 10-month interval that separated the two mapping efforts. A second possible explanation is that the limited selection of VPs for our measurement campaigns could negatively impact the visibility of certain interconnects. However, this latter reason seems unlikely since many of the traceroutes that were used by CFP to infer these missing interconnects were launched from VPs that are geographically far from the target colo, e.g. Russia and Bangladesh.

Summary

This chapter proposes a methodology for identifying the x-connects that the tenants of a given colocation facility purchase from the colo provider to interconnect their networks. Using localized data plane measurements to minimize measurement

TABLE 23. The breakdown of the 342 reported x-connects (265 AS links) mapped to CoreSite-LA by CFS in comparison with BP's result at the same colo

	X-Connect	AS-Link
G1, Related to non-tenant ASes	3	3
G2, Matched peering	137	99
G2.1, Consistent type	43	30
G2.2, Different types	94	69
G3, Missing AS links	202	143
G3.1, Targeted	100	69
G3.2, Not Targeted	102	77
G3.2.1, Far-side IP is remote	73%	
G3.2.2, traceroute has a loop	14%	
G3.2.3, X-connect not observed	13%	

overhead, we employ a probabilistic framework in the form of a Markov Random Field graphical model. This model encodes our best understanding of the underlying router-level connectivity that is as consistent as possible with the comprehensive but necessarily limited view derived from the totality of our measurements. We apply a Belief Propagation algorithm for performing inference on our graphical model and illustrate our approach to accurately mapping or "pinning" x-connects to a facility in the context of commercial target colo facilities in three different cities. We validate our results exploiting limited available ground truth and compare them with relevant findings that were reported an independent recent study.

Our validation and comparison efforts highlight the advantage that comes with having two mostly complementary methodologies for providing more transparency in the ways networks interconnect with one another – the CFS approach developed in [115] and the approach presented in this chapter. It will be through cross-checking and cross-validating between these methods that advances in increasing our visibility into the geography (and parties to) peering interconnections (private and public) will happen. Thus, despite a number of remaining challenges that these complementary efforts have

revealed to date, the “grand challenge” in this area of mapping the interconnectivity in Equinix’s datacenters looms as a difficult but no longer impossible open problem.

CHAPTER VIII

SUMMARY AND FUTURE WORK

Summary

This thesis focuses on characterizing large-scale networked systems using measurement. Our target systems include various online social networks and the structure of the physical interconnections in todays Internet. Throughout our studies we are careful to revisit the measurement methodology, quality of the collected data and derived findings from the analysis of the measurements through the lens of *domain knowledge*. We also use domain knowledge to our advantage and refrain from collecting "big data" and processing it in the hope of finding insightful results. In this context, the methodologies proposed here are "targeted" rather than "opportunistic", that is, we are aware of the limitations and biases within the data collection process we use to perform measurements and answer specific questions about a system.

Future Work

The research presented in this thesis can be extended in several directions. Possible future work can be broadly divided based on the target systems under investigation in this thesis: *(i)* Social Networks, and *(ii)* Topology of the Internet. Following is a brief description of identified research avenues (see specific chapters for more details).

Graph Coarsening with Varying Length Random Walks

In Chapter III, we demonstrated how *dvr* values computed from short random walks of a certain length can be used as signal to group high degree nodes (core nodes) into

clusters that reside in different regions of a graph. As the results showed, the variation in the distribution of *dvr* captures a transient phenomenon before random walks mix in the graph. We are currently exploring the usage of different walk lengths for computing a *dvr* vector, as opposed to a single *dvr* value, which could result in identification of region cores at different random walk lengths. To do so, we first identify the cluster of nodes with similar *dvr* values using Gaussian Mixture Models (GMM) among high degree nodes. Fitted GMMs cluster the nodes by assigning each node to the multivariate normal components that maximize the component posterior probability given the set of all *dvr* values. We use *hard clustering* which assigns each node to exactly one cluster. Therefore, for each WL we compute one assignment of top nodes to clusters. We use "successive resilient clustering" to find groups of nodes that are always clustered together for WLs in a range. A *region core* is group of high degree nodes that are always assigned to the same cluster. Our evaluation of the primary results reveal that the identified *region cores* become more *pure* as more diverse walk lengths are included in the clustering.

Temporal Evolution of Elite Network

Our crawler for the Twitter elite network is capable of capturing one full snapshot of the 10K-ELITE every week. This provides a great opportunity to investigate the evolution of this important subgraph of the social network. A microscopic analysis of the elite networks will reveal how popular users gain or lose followers, while its macroscopic characterization at the community level helps identify the forces behind the evolution (birth, death, split, merge) of communities overtime [48]. Additionally, such investigation can help identify the internal or external events that lead to changes in the ranking of elites based on various measures of influence.

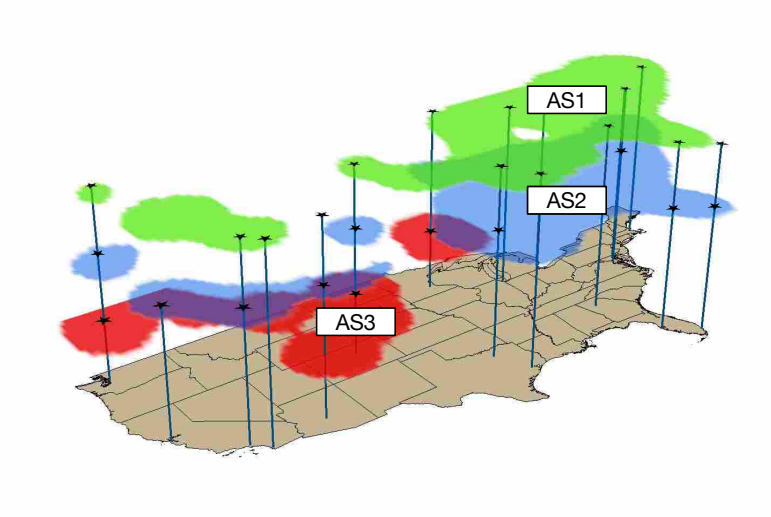

FIGURE 8.62. Internet topology map that encodes geographical coverage of network, number and location of network interconnects

City Level Mapping of Interconnections Between Networks' Points of Presence

Our solution to map x-connects inside a collocation facility can be used to geolocate more network interconnects at the granularity of "colocation marketplace". Indeed, the proposed targeted methodology in Chapter VII allows us to map the PoP-level topology of the Internet one colocation at a time. Despite the importance of building-level mapping of network interconnects, it is crucial to point out that the mapping does not even exist at the city-level. Thankfully, the tools and heuristics we have developed in combination with our proposed methodology provide a promising solution to this problem. Therefore, creating a city-level map of network interconnections is certainly a feasible future project. The existence of such a highly detailed map, in combination with recent advances in the research conducted in this area, such as the recently assembled repositories of publicly available maps of the physical infrastructure of different networks [160, 94], and research about elements of the physical Internet infrastructure with fixed geographic locations such as routers, PoPs, or long-haul fiber-

optic cables [95, 96], will bring us even closer to the ideal view of the Internet topology similar to the depiction in Figure 8.62.

APPENDIX

ALFReD: ACQUIRING LOCATION FROM REVERSE DNS

Extracting attributes such as location, role, and port technology from PTRs (reverse DNS names) is not a novel idea. Network operators and system administrators have long been using this information for debugging purposes.

The earliest work in this domain within the network research community is UnDNS by Spring et al. [244], which aims to automatically extract geo-information from the reserve DNS names. UnDNS uses regular expressions to reveal geo-information from a name. The main challenge of this approach lies in the wide variation in the name formats used by system administrators. The regular expressions should be compiled manually, which requires domain knowledge about the geography and location codes. To write rules that do not lead to erroneous results, the regular expressions have to be very specific in some cases (e.g. `los-angles`, `losangles`, `lax`, and `lsanca` all refer to *Los Angles* in PTR records used by different networks). Therefore, the task has to be done specifically for each AS, which leads to the need to write a large number of regular expressions. Naming formats and conventions may also change over time as networks expand, and some changes in the format will render the previously compiled regular expression useless. For instance, applying UnDNS to `ip-64-32-149-181.lax1.megapath.net` does not reveal the association of the name with *Los Angeles*, but can show that `ip-64-32-149-181.lax.megapath.net` refers to Los Angeles. Therefore, using AS specific PTR record parsing rule sets leads to a very high maintenance and expansion overhead, as the need for parsing PTR records assigned by new ASes arise, and as these ASes occasionally change their naming conventions.

Our mining tool for extracting information from PTR records is implemented in ALFReD (Acquiring Location From Reverse DNS). Our tool differs from UnDNS as we use a large dictionary of keywords that reveal relevant information from any reverse DNS name, regardless of the AS. We expand on the geolocation idea by also extracting port (interface) technologies (e.g. `fios` for *Fiber Optic Service*) and router role attributes (e.g. `gw` for *gateway*) from reverse DNS names. At its core, ALFReD is a parser that uses a few large dictionaries of location and network related keywords commonly used in PTR records to extract any relevant information. This approach is similar to the one taken by PathAudit [61, 62] which also relies on dictionaries. The main limitation of PathAudit, however, is its naive trie-based name parsing mechanism, in which a keyword in the dictionary can match any part of a PTR record. For instance, PathAudit returns `lax` as a relevant geo-hint in `ga`**`lax`**`y-capital-management-lp-iaf1070334.cu`. As opposed to a trie-based approach, we specifically search for meaningful segments inside the PTR records. DRoP [135, 136] is another PTR parsing tool that leveraged a dictionary-based mechanism. However, the usage of dictionaries in DRoP was limited to partly automating the regular expression inference, not to extract relevant information.

We next describe the parsing mechanism of ALFReD in Section A.1. We apply ALFReD on a large body of PTR records to show its strength in inferring information from names and compare it with its rival in Section A.2. It is worth noting that ALFReD is also available to the public through an online web-based interface [194].

ALFReD for Mining Attributes from PTR Records

Parsing Segments

We primarily search for meaningful *segments* inside a PTR record. To this end, we first identify the first and the second level domains in a PTR record. After

removing the domain (`lax1.cable-cyber.`**`verizon.net`**), we split the remainder string at non-alphabetic characters (such as numbers, dots and dashes). For instance, the list of segments extracted from `lax1.cable-cyber.verizon.net` is `['lax', 'cable', 'cybercable']`. These string segments are checked against a series of dictionaries to reveal any relevant embedded hints. Note that an exact match should exist between a segment and a term in one of our dictionaries. Going back to our previous example, `lax` matches with an entry in our *airport code* dictionary. Having manually examined a large number of PTR records, we observed that digits that trail each segment could carry additional information. To illustrate, consider `ge-0-.gw6.`**`pao1`**`.alter.net` and `te-1-.gw6.`**`pao3`**`.alter.net`; our hypothesis is that **`pao1`** and **`pao3`** refer to different points of presence (PoPs) in *Paolo Alto, CA*. To capture this detail, in addition to the dictionary keyword, ALFReD outputs the trailing digits in addition to the segment. Listing A.1 shows an sample output from ALFReD.

Listing A.1 An example output from ALFReD

```
{
 "name": "dataway-inc.edge8.sanjose1.level3.net",
 "city": [
  {
   "key": "sanjose",
   "segment": "sanjose1",
   "decode": "san jose,ca,us",
   "position": 1,
   "confidence": 100
  }
 ],
 "airport": [
  {
   "key": "inc",
   "segment": "inc",
   "decode": "yinchuan, china",
   "position": 3,
   "confidence": 100
  }
 ],
 "router": [
  {
   "key": "edge",
   "segment": "edge8",
   "decode": "edge router",
   "position": 2,
   "confidence": 100
  }
 ]
```

As the example shows, ALFReD finds all strings that could potentially reveal any information embedded in the name. As we see, `inc` is reported as an airport code although `sanjose` seems to be the correct location information embedded in this PTR record. We later in this chapter describe a few heuristics to identify the correct piece of location information embedded in a name. We now briefly explain the relevant dictionaries and the extracted information as follows:

Domain Name: We extract and report the top and the second-level domains (SLD). In most PTR records, this information corresponds to the two rightmost segments unless the the length of any of the last two segments is two characters (e.g. `co.uk` or `com.mx`). In such cases, the last three segments of the name are returned as the domain name (e.g. `bbc.co.uk`).

Interface Technology: We consider commonly used interface technology conventions from Cisco [73], Juniper [147] and Huawei [134] to populate a dictionary of commonly used terms that refer to port technologies. We also consider guidelines provided by NANOG [246] to improve this dictionary. Overall this dictionary includes 150 keywords. Few interface codes overlap with the geo location dictionaries, for instance, `wan` is conventionally used for "Wide Area Networks" and is also the airport code for "Waverney" airport in Australia, so extra care is necessary in inferring the correct information from these keywords. As a common strategy, ALFReD reports all possible hints and delegates any speculations to the user.

Router: ALFReD also reports network related keywords (e.g. "wireless", "host", "edge") which hint at the router's attribute [246]. We build a dictionary of these keywords totalling 58 entries. While this dictionary started as one that was built solely using domain knowledge and a manual inspection of names, it was later expanded using techniques explained later in the chapter.

Location Information: We have used a few separate dictionaries for extracting location information (geo hints) from a PTR record. Our first dictionary is 3-letter airport codes. We collected airport codes from `airportcodes.org` [1] which includes more than 3.5K airport codes. Second, we use CLLI codes. A CLLI code (Common Language Location Identifier) is used within the North American telecommunications industry to specify the location of a telecommunication equipment. We obtained a total of 22K 6-letter CLLI codes from `telcodata.us` [6]. Note that each city does not have a unique CLLI code, for instance 'STTLWA', 'STTMWA' and 'STTNWA' are all valid CLLI codes for *Seattle, WA*. We also observed the usage of many 4-letter CLLI codes. Hence, we added 11K 4-letter CLLI codes to this dictionary as well. Third, we check each segment against

city names obtained from `geonames.org` [4], but we only use the cities that have a population of more than $5\,000$. This dictionary added 57K cities.

Compound Segments

We noticed that some PTR records include clues that can not be extracted using our segment-based parsing scheme. For instance, cities that have two-part names or names with hyphens (such as Saint Louis, Los Angles, New York, San Jose, Dover-Foxcroft) can not be extracted with the proposed parsing method. To handle these cases, we include an additional dictionary of *compound* location keywords with less than 200 entries, whose elements are all longer 7 letters. Instead of looking for these keywords inside individual segments, we use a trie based string matching method to find the key anywhere in the name. The relatively long keywords and their small number ensure that our method does not suffer from the same issues that we reported in PathAudit.

Extending ALFReD

When applying ALFReD on a large body of PTR records, we realized that some strings frequently appear in PTR records. Further examination showed that some of these commonly used terms also contain relevant information but are not part of any dictionaries. For example, some of the commonly observed segments include: *fios*, *dial*, *dsl*, *ftas*, etc. In fact, via manual inspection we realized that `fios` stands for "FIber Optic Service" which is commonly used in Verizon PTR records, and `dsl` is short for "Digital Subscriber Line". Using the same technique, we also identified a list of approximately 100 city code names (e.g. `pitpa` for *Pittsburgh, Pa* and `lsnca` for *Los Angeles, CA*) that are commonly used in a few large networks including AT&T. As a result, we extended our dictionaries or created new ones to cover these frequently used keywords as well.

Heuristic for Resolving Conflicting Information

As shown before in Listing A.1, different segments of a name may hint at conflicting information. This issue is more problematic in the case of conflicting location information. For instance, due to the abundance of airport codes, a segment inside a name may match a code that does not reveal the location in reality (e.g. although `inc` is an airport code, it does not seem to reveal the correct location in `dataway-`**`inc`**`.edge8.sanjose1.level3.net`). We use three simple heuristics to identify the location information with the highest likelihood of correctness.

Overlapping Dictionaries: A key may exist in two different dictionaries. For instance, `bbr` could both refer to a *backbone router* or *Baillif Airport*. When a segment matches a key in two different dictionaries, we assign a lower confidence to it compared to the case when the key is only in one dictionary. The correct location code is most likely among the the keys with the highest confidence.

Key Length: If two location codes are found in a name, we first compare their length then and select the longer one. The rationale is that the likelihood of two strings randomly matching each other is inversely proportional to the strings' length.

Segment Position: In addition to the key itself, ALFReD also returns the position of the segment where the keyword is identified. Examining a large body of PTR records and observing naming patterns and conventions followed by operators [246, 241], we observed that keys that appear later in a PTR record likely reveal the location information. This heuristic is used as the last tie breaker to identify the correct location information.

ALFReD in Action

In this section we analyze the results from parsing a large set of PTR records using ALFReD. This analysis not only shows the functionality of ALFReD as an tool to extract

information from PTR records, but also allows us to see the frequency and the different type of information that is coded in PTR records by different administrators. We also use PathAudit [61, 62] and DRoP [135] to compare ALFReD with its rivals.

Mapping ASes Using ALFReD

In our first case study, we use ALFReD to reveal information in the PTR records assigned by one AS. Since our goal is to analyze and compare PTR records assigned by different ASes, we use the methodology similar to the one proposed by Ferguson et al. [105] to maximize the number of names recovered for each AS. However, we try to minimize the effort in searching for PTR records used by an AS as we explain the following: Instead of sweeping the entire IP space assigned to our target AS, we only focus on $/24$ prefixes that the AS uses for assigning IPs to network devises. To find these prefixes, we use CAIDA's ARK project dataset [51]. The dataset is collected as the result of CAIDA's large-scale traceroute-based measurements. We first identify all IPs observed in their measurements during September of 2015. We then map each IP to an AS number using Team Cymru's `whois` tool [250]. We finally include all $/24$ prefixes that contain the IPs that belong to our target ASes. We perform reverse DNS look up using `dig` command [140, 2] to scan all IPs in the selected prefixes of our target ASes.

We focus on four large ASes, namely AT&T, Level3, Cogent, and Verizon. We identified 157, 682, 404, and $35\,503$ prefixes in these networks respectively. Using the described `dig`-based reverse DNS look up method, we find 40K, 174K, 103K, and 9M PTR records in these prefixes respectively. Interestingly the domain name of these IPs does not always correspond with the PTR assigned to the same AS. Figure A.63 shows the domain names of IPs in three of these AS's IP space. In order to study the AS specific conventions and type of informations embedded in each AS we only focus on the PTR

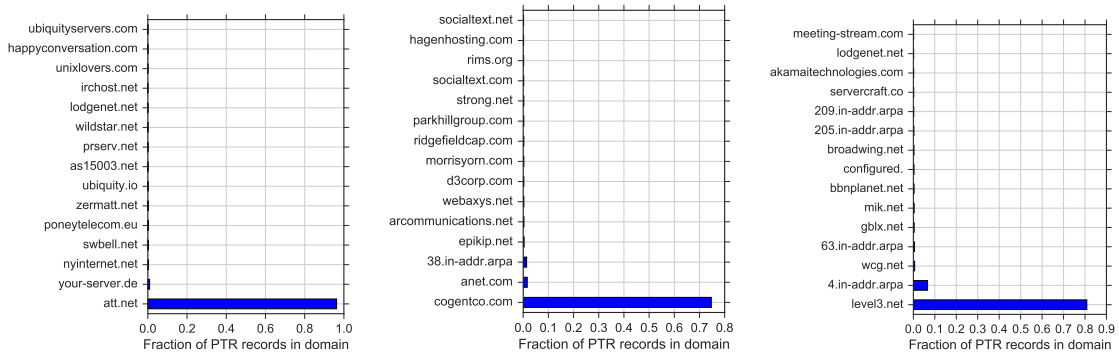

(a) AT&T (b) Cogent (c) Level3

FIGURE A.63. Frequent domains in AS's IP space

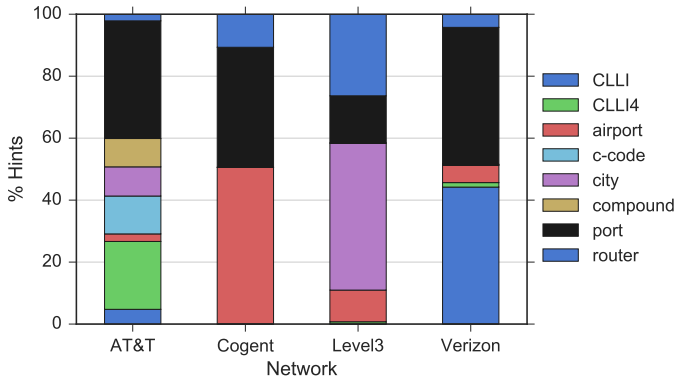

FIGURE A.64. The distribution of the amount of information recovered by ALFReD records whose domain name matches the AS name. These domain names are `att.net`, `level3.net`, `cogentco.com`, and `verizon-gni.net` for AT&T, Level3, Cogent, and Verizon respectively.

Information Obtained from PTR Records

Figure A.64 shows the type of information that ALFReD finds in PTR records of each target AS. In addition to the broad categories of information, the figure shows which location dictionary is commonly used for embedding location information in names. Figure A.64 reveals various interesting results of this experiment. *(i)* The prevalence of various types of information is different across PTR records in these networks.

(ii) Location information extracted from AT&T's PTR records come from various dictionaries, but the other networks seem to use conventions that strictly use certain types of keywords. *(iii)* A large amount of router role information can be inferred from names used in Level3. This fraction of router role information extracted from names in other networks is much less. *(iv)* The yield of different location dictionaries is AS dependent. While the usage of CLLI codes is frequent in Verizon, Cogent uses airport codes and Level3 prefers to use city names.

Mapping Footprint of ASes with ALFReD

We use the location information inferred from the PTR records of each network to find its geographical coverage. For comparison, we also use MaxMind IP geolocation dataset [184] and find the geo footprint of the target ASes using this dataset as well. Figure A.65 presents comparative views of these inferred geo-footprints using the two geolocation tools. As all the figures show, MaxMind only geolocates the IPs to the United States and does not provide a finer resolution for geolocation. However, ALFReD is able to geolocate the reverse DNS names of these IPs to specific cities in the United States. The plots reveal that all the target ASes have mostly similar coverage with large deployments along the coasts and also considerable IPs in the Midwest.

ALFReD vs. its Rivals

In this section we use ALFReD to infer the information from a pool of PTR records from various ASes. To this end, we use the PTR records provided by CAIDA's Ark project [8]. Due to the large scale of the measurement campaign and scheduling scheme of this project, this dataset contains names from all major ASes. We use this dataset to compare the location information extracted by ALFReD to those of DRoP and PathAudit.

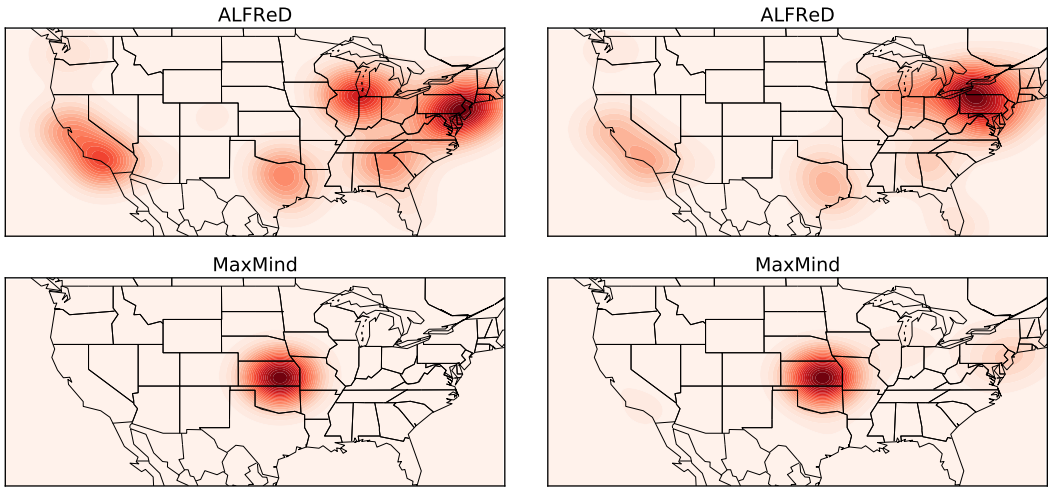

(a) AT&T

(b) Cogent

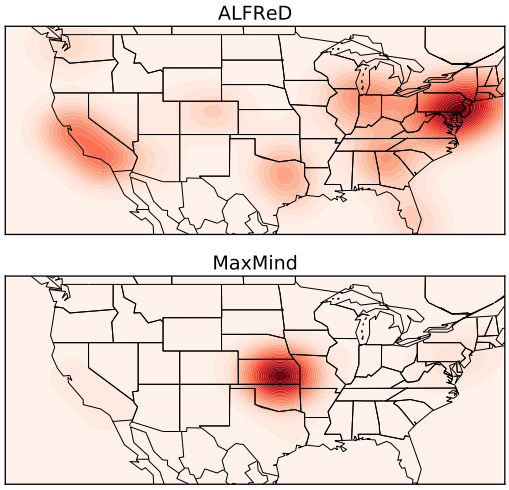

(c) Level3

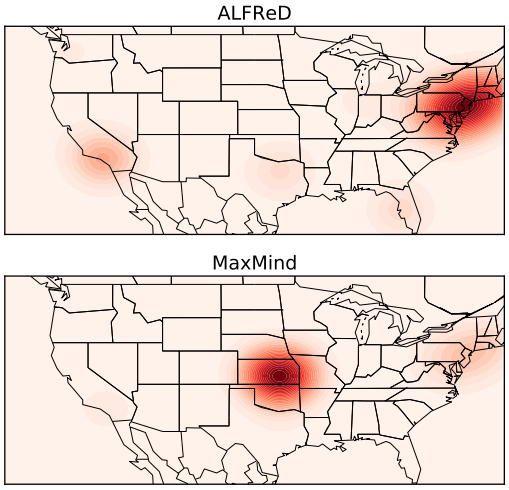

(d) Verizon

FIGURE A.65. Comparison of IP-geolocation using MaxMind (bottom) and DNS-geolocataion using ALFReD (top) for four target networks

Figure A.67 shows the coverage of these three parsing tools using a Venn diagram. While ALFReD is capable of extracting location information from 228K (22%) of the 1M PTR records obtained from CAIDA, this number is 112K (11%) and 5K (5%) for DRoP and PathAudit, respectively. These results clearly show that ALFReD is more capable of extracting location information from PTR records assigned by various ASes.

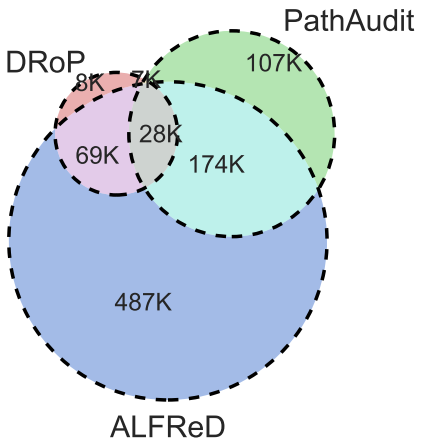

FIGURE A.66. Comparison of the number of PTR records that are parsed by each tool

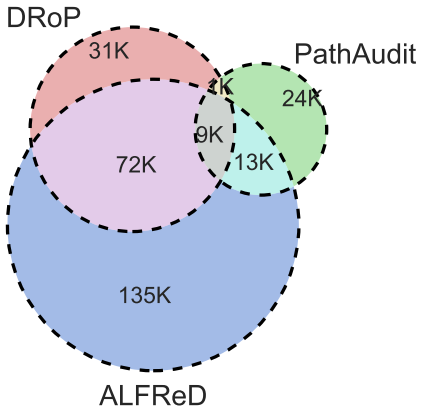

FIGURE A.67. Comparison of the number of PTR records that pack a location information according to each tool

We also examine the records that are parsed by DRoP and PathAudit but not ALFReD. Specifically, we check the geo-hints extracted by each tool. If these hints are correctly extracted by other tools, we can add them to ALFReD's dictionaries as well. Figure A.68 provides the number of times each geo-hint is extracted from all PTR records in this dataset. We make the following observations from these plots: *(i)* Many geo-hints extracted by DRoP do not seem to be keywords that are easily recognizable. Our manual examination of many of these character strings did not reveal any indication that the string could refer to a location. In the case of PathAudit, some of the extracted strings can be recognized (e.g. `pennsylvania`). Many of these strings are state names, and are ignored by ALFReD as a result of our city-level geolocation focus. Another issue with respect to PathAudit results is its parsing mechanism, which looks for dictionary keys anywhere in the PTR record. For instance PathAudit infers *reno* as a geo-hint from **reno**`vation.yourespressob1.com`, `tge1-7-1-1.g`**reno**`h1-rtr800.div.neo.rr.com` and `laco01-c1.core02.mtl-1250.fib`**reno**`ire.ca` which are obviously incorrect. *(ii)* Comparing the distribution of geo-hints extracted exclusively by ALFReD and those that

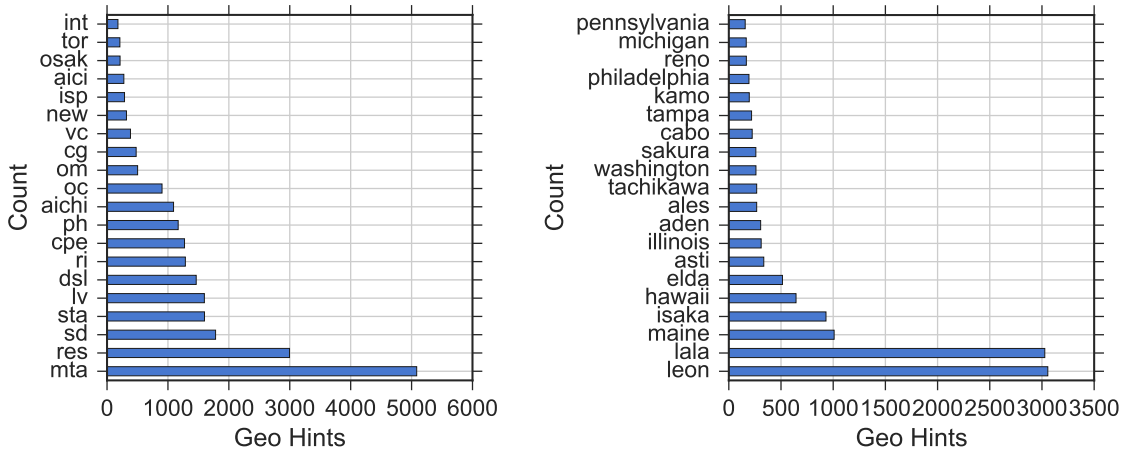

(a) Extracted by DRoP

(b) Extracted by PathAudit

FIGURE A.68. Distribution of geo-hints that ALFReD did not extract from PTR records it missed suggests that adding a few entries to its dictionaries can dramatically increase its coverage since the distributions in Figure A.68 are very skewed. Of course, we first need to establish that these strings correctly point to a location.

Summary

We presented ALFReD, a tool that automatically extracts relevant information from PTR records. ALFReD differs from other DNS parsing tools, as it uses various large dictionaries that reveal relevant information from DNS names. We explained how ALFReD addresses the shortcomings of its predecessors. ALFReD reports all extractable information, with a confidence level that shows what piece is most likely accurate. We also presented a few heuristics to resolve cases in which a name packs conflicting information.

REFERENCES CITED

[1] Airport Codes. https://www.airportcodes.org. Accessed: 2014-09-05.

[2] Domain Names - Implementation and Specification. https://www.ietf.org/rfc/rfc1035.txt. Accessed: 2014-09-16.

[3] Equinix Q1 2016 Earnings Conference Call. http://phx.corporate-ir.net/External.File?item=UGFyZW50SUQ9MzM2OTc1fENoaWxkSUQ9LTF8VHlwZT0z&t=1&cb=635979891794307751.

[4] GeoNames. https://www.geonames.org. Accessed: 2014-09-05.

[5] Sankey diagram. https://en.wikipedia.org/wiki/Sankey_diagram.

[6] Telcodata.us telecommunications database. https://www.telcodata.us. Accessed: 2014-09-05.

[7] Telx Cross Connects. http://www.telx.com/interconnection/.

[8] The CAIDA UCSD IPv4 Routed /24 DNS Names Dataset. http://www.caida.org/data/active/ipv4_dnsnames_dataset.xml. Accessed: 2014-09-09.

[9] RIPE RIS. https://www.ripe.net/data-tools/stats/ris/routing-information-service, 2011.

[10] A. Dhamdhere and C. Dovrolis. Twelve years in the evolution of the Internet ecosystem. *IEEE/ACM Transactions on Networking (ToN)*, 19(5), 2011.

[11] L. A. Adamic and N. Glance. The political blogosphere and the 2004 us election: divided they blog. In *Proc. of the workshop on Link discovery*. ACM, 2005.

[12] Advanced Network Technology Center. University of Oregon Route Views Project. http://www.routeviews.org, 2013.

[13] B. Ager, N. Chatzis, A. Feldmann, N. Sarrar, S. Uhlig, and W. Willinger. Anatomy of a large european IXP. In *Proc. of SIGCOMM*. ACM, 2012.

[14] R. Agrawal, B. Golshan, and E. Papalexakis. Homogeneity in web search results: Diagnosis and mitigation. Technical Report TR-2015-007, Data Insights Laboratories, San Jose, California, June 2015.

[15] R. Agrawal, B. Golshan, and E. Papalexakis. Overlap between google and bing web search results!: Twitter to the rescue? In *Proc. of COSN*. ACM, 2015.

[16] Y. Y. Ahn, S. Han, H. Kwak, S. Moon, and H. Jeong. Analysis of Topological Characteristics of Huge Online Social Networking Services. In *Proc. of WWW*. ACM, 2007.

[17] Akamai. EdgeScape Service Description. `http://uk.akamai.com/dl/brochures/edgescape_service_description.pdf`, March 2002.

[18] R. Albert and A.-L. Barabási. Statistical mechanics of complex networks. *Reviews of Modern Physics*, 74(1), 2002.

[19] R. Albert, H. Jeong, and A.-L. Barabási. Error and attack tolerance of complex networks. *Nature*, 406(6794), 2000.

[20] A. Alvarez-Socorro, G. Herrera-Almarza, and L. González-Díaz. Eigencentrality based on dissimilarity measures reveals central nodes in complex networks. *Scientific reports*, 5, 2015.

[21] L. A. N. Amaral, A. Scala, M. Barthelemy, and H. E. Stanley. Classes of small-world networks. *Proc. of NAS*, 97(21), 2000.

[22] R. Andersen, F. Chung, and K. Lang. Local graph partitioning using pagerank vectors. In *Proc. of Foundations of Computer Science (FOCS)*. IEEE, 2006.

[23] B. Augustin, X. Cuvellier, B. Orgogozo, F. Viger, T. Friedman, M. Latapy, C. Magnien, and R. Teixeira. Avoiding Traceroute Anomalies with Paris Traceroute. In *Proc. of IMC*. ACM SIGCOMM, 2006.

[24] B. Augustin, B. Krishnamurthy, and W. Willinger. IXPs: Mapped? In *Proc. of IMC*. ACM, 2009.

[25] C. Avin, Z. Lotker, and Y.-A. Pignolet. On the elite of social networks. *Personal Communication*, 2012.

[26] C. Avin, Z. Lotker, Y.-A. Pignolet, and I. Turkel. From caesar to twitter: an axiomatic approach to elites of social networks. *arXiv preprint arXiv:1111.3374*, 2011.

[27] K. Avrachenkov, N. Litvak, L. O. Prokhorenkova, and E. Suyargulova. Quick detection of high-degree entities in large directed networks. In *Proc. of ICDM*. IEEE, 2014.

[28] B. Eriksson, P. Barford and J. Sommers and R. Nowak. Inferring Unseen Components of the Internet Core. *Journal on Selected Areas in Communications, IEEE*, 29(9), 2011.

[29] L. Backstrom, P. Boldi, M. Rosa, J. Ugander, and S. Vigna. Four Degrees of Separation. *CoRR*, abs/1111.4570, 2011.

[30] E. Bakshy, J. M. Hofman, W. A. Mason, and D. J. Watts. Everyone's an influencer: quantifying influence on twitter. In *Proc. of WSDM*. ACM, 2011.

[31] E. Bakshy, J. M. Hofman, W. A. Mason, and D. J. Watts. Identifying influencers on twitter. In *Proc. of WSDM*. ACM, 2011.

[32] Balakrishnan Chandrasekaran and Georgios Smaragdakis and Arthur Berger and Matthew Luckie and Keung-Chi Ng. A Server-to-Server View of the Internet. In *Proc. of CoNEXT*. ACM, 2015.

[33] P. Barford, A. Bestavros, J. Byers, and M. Crovella. On the marginal utility of network topology measurements. In *Proc. of IMC*. ACM SIGCOMM, 2001.

[34] D. Barnes and B. Sakandar. *Cisco LAN switching fundamentals*. Cisco Press, 2004.

[35] T. Barnett. 2015 cisco vni complete forecast update: Key trends include mobility, m2m and multimedia content. `http://blogs.cisco.com/sp/2015-cisco-vni-complete-forecast-update-key-trends-include-mobility-m2m-and-multimedia-content`, 2015.

[36] M. Bastian, S. Heymann, M. Jacomy, et al. Gephi: An Open Source Software for Exploring and Manipulating Networks. AAAI, 2009.

[37] A. Bender, R. Sherwood, and N. Spring. Fixing ally's growing pains with velocity modeling. In *Proc. of IMC*. ACM SIGCOMM, 2008.

[38] F. Benevenuto, T. Rodrigues, M. Cha, and V. Almeida. Characterizing user behavior in online social networks. In *Proc. of IMC*. ACM SIGCOMM, 2009.

[39] R. Beverly, A. Berger, and G. G. Xie. Primitives for active Internet topology mapping: Toward high-frequency characterization. In *Proc. of IMC*. ACM SIGCOMM, 2010.

[40] V. D. Blondel, J.-L. Guillaume, R. Lambiotte, and E. Lefebvre. Fast unfolding of communities in large networks. *Journal of Statistical Mechanics: Theory and Experiment*, 2008(10), 2008.

[41] B. Bollobás. *Modern graph theory*, volume 184. Springer Science & Business Media, 2013.

[42] V. Bolotaeva and T. Cata. Marketing opportunities with social networks. *Journal of Internet Social Networking and Virtual Communities*, 2010, 2010.

[43] S. P. Borgatti. Identifying sets of key players in a social network. *Computational & Mathematical Organization Theory*, 12(1), 2006.

[44] A. Boutet, A. Kermarrec, E. Le Merrer, and A. Van Kempen. On the impact of users availability in osns. In *ACM SNS*, 2012.

[45] C. M. Bowman, P. B. Danzig, U. Manber, and M. F. Schwartz. Scalable Internet resource discovery: Research problems and approaches. *Communications of the ACM-Association for Computing Machinery-CACM*, 37(8), 1994.

[46] S. Brin and L. Page. The anatomy of a large-scale hypertextual web search engine. In *Proc. of WWW)*, 1998.

[47] S. Brin and L. Page. Reprint of: The anatomy of a large-scale hypertextual web search engine. *Computer Networks*, 56(18), 2012.

[48] P. Bródka, S. Saganowski, and P. Kazienko. Group evolution discovery in social networks. In *Advances in Social Networks Analysis and Mining (ASONAM)*. IEEE, 2011.

[49] R. Bush, O. Maennel, M. Roughan, and S. Uhlig. Internet optometry: assessing the broken glasses in Internet reachability. In *Proc. of IMC*. ACM SIGCOMM, 2009.

[50] X. Cai, J. Heidemann, B. Krishnamurthy, and W. Willinger. Towards an AS-to-organization Map. In *Proc. of IMC*. ACM SIGCOMM, 2010.

[51] CAIDA. Archipelago (Ark) Measurement Infrastructure. `http://www.caida.org/projects/ark/`.

[52] CAIDA. AS Rank: AS Ranking. `http://as-rank.caida.org/`.

[53] CAIDA. AS Relationships. `http://www.caida.org/data/as-relationships/`.

[54] CAIDA. Skitter. `http://www.caida.org/tools/measurement/skitter/`.

[55] G. Caldarelli. Scale-free networks: complex webs in nature and technology. *OUP Catalogue*, 2007.

[56] R. W. Callon. Use of OSI IS-IS for routing in TCP/IP and dual environments. rfc 1195: see online `http://tools.ietf.org/html/rfc1195`, 1990.

[57] R. Campigotto, J.-L. Guillaume, and M. Seifi. The power of consensus: random graphs have no communities. In *Proc. of ASONAM*. ACM, 2013.

[58] Q. Cao, M. Sirivianos, X. Yang, and T. Pregueiro. Aiding the Detection of Fake Accounts in Large Scale Social Online Services. In *Proc. of NSDI*, 2012.

[59] M. Cha, H. Haddadi, F. Benevenuto, and P. K. Gummadi. Measuring user influence in twitter: The million follower fallacy. AAAI, 2010.

[60] M. Cha, A. Mislove, and K. P. Gummadi. A measurement-driven analysis of information propagation in the flickr social network. In *Proc. of WWW*. ACM, 2009.

[61] J. Chabarek. PathAudit. `https://github.com/jc-wail/WAIL/tree/master/PathAudit`.

[62] J. Chabarek and P. Barford. What's in a name?: decoding router interface names. In *Proc. of IMC*. ACM SIGCOMM, 2013.

[63] H. Chang, S. Jamin, and W. Willinger. Inferring AS-level Internet topology from router-level path traces. In *ITCom*. International Society for Optics and Photonics, 2001.

[64] H. Chang, S. Jamin, and W. Willinger. Internet connectivity at the AS-level: an optimization-driven modeling approach. In *Proc. of the MoMeTools workshop*. ACM SIGCOMM, 2003.

[65] H. Chang, S. Jamin, and W. Willinger. To peer or not to peer: Modeling the evolution of the Internet's AS-level topology. *Ann Arbor*, 1001, 2006.

[66] N. Chatzis, G. Smaragdakis, J. Böttger, T. Krenc, and A. Feldmann. On the benefits of using a large IXP as an Internet vantage point. In *Proc. of IMC*. ACM SIGCOMM, 2013.

[67] N. Chatzis, G. Smaragdakis, A. Feldmann, and W. Willinger. There is more to IXPs than meets the eye. *ACM SIGCOMM Computer Communication Review*, 43(5), 2013.

[68] K. Chen, D. R. Choffnes, R. Potharaju, Y. Chen, F. E. Bustamante, D. Pei, and Y. Zhao. Where the sidewalk ends: Extending the Internet AS graph using traceroutes from P2P users. In *Proc. of CoNEXT*. ACM, 2009.

[69] W. Chen, Y. Huang, B. F. Ribeiro, K. Suh, H. Zhang, E. d. S. e Silva, J. Kurose, and D. Towsley. Exploiting the IPID field to infer network path and end-system characteristics. In *Proc. of the PAM*. Springer, 2005.

[70] D. Choi, J. Han, T. Chung, Y.-Y. Ahn, B.-G. Chun, and T. T. Kwon. Characterizing conversation patterns in reddit: From the perspectives of content properties and user participation behaviors. In *Proc. of COSN*. ACM, 2015.

[71] B. Chun, D. Culler, T. Roscoe, A. Bavier, L. Peterson, M. Wawrzoniak, and M. Bowman. Planetlab: an overlay testbed for broad-coverage services. *ACM SIGCOMM Computer Communication Review*, 2003.

[72] F. R. Chung. *Spectral Graph Theory*, volume 92. American Mathematical Soc., 1997.

[73] Cisco Systems. Configuring Router Interfaces. http://www.cisco.com/c/en/us/td/docs/security/security_management/cisco_security_manager/security_manager/4-1/user/guide/CSMUserGuide_wrapper/rtintf.pdf.

[74] A. Clauset, C. R. Shalizi, and M. E. Newman. Power-law distributions in empirical data. *SIAM review*, 51(4), 2009.

[75] P. Cogan, M. Andrews, M. Bradonjic, W. S. Kennedy, A. Sala, and G. Tucci. Reconstruction and analysis of twitter conversation graphs. In *Proc. of Workshop on HotSocial*. ACM, 2012.

[76] CoreSite. CoreSite Cross Connects. http://www.coresite.com/solutions/interconnection/cross-connects. Accessed: 2016-06-01.

[77] CoreSite. CoreSite: Investor Presentation, June 2016. http://phx.corporate-ir.net/External.File?item=UGFyZW50SUQ9NjM2NTEwfENoaWxkSUQ9MzQwOTY3fFR5cGU9MQ==&t=1.

[78] CoreSite. CoreSite SEC Filings 02/12/2016. http://www.coresite.com/investors/financial-reports/sec-filings.

[79] CoreSite. THE CORESITE OPEN CLOUD EXCHANGE - One Connection. Countless Cloud Options. http://www.coresite.com/solutions/cloud-services/open-cloud-exchange.

[80] W. de Donato, P. Marchetta, and A. Pescapé. A hands-on look at active probing using the IP prespecified timestamp option. In *Proc. of PAM*. Springer, 2012.

[81] Q. Deng and Y. Dai. How your friends influence you: Quantifying pairwise influences on twitter. In *Prof. of the CSC*. IEEE, 2012.

[82] A. Dhamdhere and C. Dovrolis. Ten years in the evolution of the Internet ecosystem. In *Proc. of IMC*. ACM SIGCOMM, 2008.

[83] I. S. Dhillon, Y. Guan, and B. Kulis. Kernel k-means: Spectral Clustering and Normalized Cuts. In *Proc. of SIGKDD*. ACM, 2004.

[84] I. S. Dhillon, Y. Guan, and B. Kulis. Weighted graph cuts without eigenvectors a multilevel approach. *IEEE Transactions on Pattern Analysis and Machine Intelligence (TPAMI)*, 29(11), 2007.

[85] G. Di Battista, M. Patrignani, and M. Pizzonia. Computing the types of the relationships between autonomous systems. In *Proc. of the INFOCOM*, volume 1. IEEE, 2003.

[86] R. Diestel. *Graph theory {graduate texts in mathematics; 173}*. Springer-Verlag Berlin and Heidelberg GmbH & amp, 2000.

[87] X. A. Dimitropoulos, D. V. Krioukov, and G. F. Riley. Revisiting Internet AS-level topology discovery. In *Proc. of PAM*. Springer, 2005.

[88] H. N. Djidjev. A Scalable Multilevel Algorithm for Graph Clustering and Community Structure Detection. In *Algorithms and Models for the Web-Graph*. Springer, 2008.

[89] G. W. Domhoff. *Who rules America?: power and politics, and social change*. McGraw-Hill Humanities, Social Sciences & World Languages, 2006.

[90] P. Domingos and M. Richardson. Mining the network value of customers. In *Proc. of SIGKDD*. ACM, 2001.

[91] B. Donnet and T. Friedman. Internet topology discovery: a survey. *Communications Surveys & Tutorials, IEEE*, 9(4), 2007.

[92] B. Donnet, M. Luckie, P. Mérindol, and J.-J. Pansiot. Revealing MPLS tunnels obscured from traceroute. *ACM SIGCOMM Computer Communication Review*, 42(2), 2012.

[93] B. Donnet, P. Raoult, T. Friedman, and M. Crovella. Deployment of an algorithm for large-scale topology discovery. *Journal on Selected Areas in Communications, IEEE*, 24(12), 2006.

[94] R. Durairajan, S. Ghosh, X. Tang, P. Barford, and B. Eriksson. Internet Atlas: a Geographic Database of the Internet. In *Proc. of the Workshop HotPlanet*. ACM, 2013.

[95] R. Durairajan, J. Sommers, and P. Barford. Layer 1-Informed Internet Topology Measurement. In *Proc. of IMC*, 2014.

[96] R. Durairajan, J. Sommers, W. Willinger, and P. Barford. InterTubes: A Study of the US Long-haul Fiber-optic Infrastructure. In *Proc. of the SIGCOMM*, 2015.

[97] D. Easley and J. Kleinberg. *Networks, crowds, and markets: Reasoning about a highly connected world*. Cambridge University Press, 2010.

[98] H. Electric. Hurricane Electric BGP Toolkit. `http://bgp.he.net/`.

[99] Equninix. Equinix Reports Fourth Quarter and Year-End 2015 Results. `http://www.equinix.com/company/news-and-events/press-releases/equinix-reports-fourth-quarter-2014-results/`.

[100] Equninix. Historical Quarterly and Year-End Results. http://investor.equinix.com/phoenix.zhtml?c=122662&p=quarterlyearnings.

[101] B. Eriksson, P. Barford, J. Sommers, and R. Nowak. DomainImpute: Inferring unseen components in the Internet. In *Proc. of INFOCOM*. IEEE, 2011.

[102] M. Faloutsos, P. Faloutsos, and C. Faloutsos. On power-law relationships of the Internet topology. 29(4), 1999.

[103] N. Feamster. Revealing Utilization at Internet Interconnection Points. *Available at SSRN 2756888*, 2016.

[104] D. Feldman and Y. Shavitt. Automatic large scale generation of Internet pop level maps. In *IEEE GLOBECOM 2008*. IEEE, 2008.

[105] A. D. Ferguson, J. Place, and R. Fonseca. Growth analysis of a large ISP. In *Proc. of IMC*. ACM SIGCOMM, 2013.

[106] D. Fitzgerald. Equinix Inc., the Internet's Biggest Landlord. http://www.wsj.com/articles/equinix-inc-the-internets-biggest-landlord-1414451918.

[107] S. Fortunato. Community detection in graphs. *Physics Reports*, 486(3), 2010.

[108] L. C. Freeman. A set of measures of centrality based on betweenness. *Sociometry*, 1977.

[109] T. M. Fruchterman and E. M. Reingold. Graph drawing by force-directed placement. *Software: Practice and experience*, 21(11), 1991.

[110] S. Gaito, M. Zignani, G. Rossi, A. Sala, X. Wang, H. Zheng, and B. Zhao. On the bursty evolution of online social networks. In *Proc. of KDD HotSocial Workshop*. ACM, 2012.

[111] J. Ganesh. Social network analysis reveals the alternative list of global power elite. http://www.datasciencecentral.com/profiles/blogs/the-alternative-list-of-global-power-elite,
2015.

[112] L. Gao. On inferring autonomous system relationships in the Internet. *IEEE/ACM Transactions on Networking (ToN)*, 9(6), 2001.

[113] D. Garcia, P. Mavrodiev, and F. Schweitzer. Social resilience in online communities: The autopsy of friendster. In *Proc. of COSN*. ACM, 2013.

[114] S. Garg, T. Gupta, N. Carlsson, and A. Mahanti. Evolution of an online social aggregation network: an empirical study. In *Proc. of IMC*. ACM SIGCOMM, 2009.

[115] V. Giotsas, G. Smaragdakis, B. Huffaker, M. Luckie, and k. claffy. Mapping Peering Interconnections to a Facility. In *Proc. of CoNEXT*. ACM, Dec 2015.

[116] V. Giotsas, S. Zhou, M. Luckie, et al. Inferring Multilateral Peering. In *Proc. of CoNEXT*. ACM, 2013.

[117] M. Gjoka, M. Kurant, C. Butts, and A. Markopoulou. Walking in facebook: A case study of unbiased sampling of osns. In *IEEE INFOCOM*, 2010.

[118] R. Gonzalez, R. Cuevas, R. Motamedi, R. Rejaie, and A. Cuevas. Google+ or google-?. dissecting the evolution of the new osn in its first year. Technical report available at: `http://www.it.uc3m.es/~rcuevas/techreports/g+TR2012.pdf`, Universidad Carlos III de Madrid, 2012.

[119] R. Gonzalez, R. Cuevas, R. Motamedi, R. Rejaie, and A. Cuevas. Google+ or google-?: dissecting the evolution of the new osn in its first year. In *Proc. of WWW*. International World Wide Web Conferences Steering Committee, 2013.

[120] R. Gonzalez, R. Cuevas, R. Motamedi, R. Rejaie, and A. Cuevas. Assessing the Evolution of Google+ in its First two Years. *IEEE/ACM Transactions on Networking (ToN)*, 2015.

[121] R. Govindan and A. Reddy. An analysis of Internet inter-domain topology and route stability. In *Proc. of the INFOCOM*, volume 2. IEEE, 1997.

[122] R. Govindan and H. Tangmunarunkit. Heuristics for Internet Map Discovery. In *INFOCOM*, volume 3. IEEE, 2000.

[123] Z. Govindarajulu. Rank correlation methods. *Technometrics*, 1992.

[124] B. Gueye, S. Uhlig, and S. Fdida. Investigating the imprecision of IP block-based geolocation. In *Proc. of PAM*. Springer, 2007.

[125] M. Gunes and K. Sarac. Resolving IP aliases in building traceroute-based Internet maps. *IEEE/ACM Transactions on Networking (ToN)*, 17(6), 2009.

[126] M. H. Gunes and K. Sarac. Analytical IP alias resolution. In *Communications, 2006. ICC'06. IEEE International Conference on*, volume 1. IEEE, 2006.

[127] L. Gyarmati and T. Trinh. Measuring user behavior in online social networks. *Network, IEEE*, 2010.

[128] J. Han, D. Choi, A. Choi, J. Choi, T. Chung, T. T. Kwon, J.-Y. Rha, C.-N. Chuah, et al. Sharing topics in pinterest: Understanding content creation and diffusion behaviors. In *Proc. of COSN*. ACM, 2015.

[129] S. Harenberg, G. Bello, L. Gjeltema, S. Ranshous, J. Harlalka, R. Seay, K. Padmanabhan, and N. Samatova. Community detection in large-scale networks: a survey and empirical evaluation. *Wiley Interdisciplinary Reviews: Comput. Stat.*, 6(6), 2014.

[130] T. Hashimoto, Y. Sun, and T. Jaakkola. From random walks to distances on unweighted graphs. In *Advances in Neural Information Processing Systems*, 2015.

[131] G. Haviland. Designing High-Availability Campus Networks, 2000.

[132] J. Hawkinson and T. Bates. Guidelines for creation, selection, and registration of an Autonomous System (AS). RFC 1930 (Best Current Practice), Avaiable online `http://www.ietf.org/rfc/rfc1930.txt`, March 1996. Updated by RFC 6996.

[133] Y. He, G. Siganos, M. Faloutsos, and S. Krishnamurthy. Lord of the links: a framework for discovering missing links in the Internet topology. *IEEE/ACM Transactions on Networking (ToN)*, 17(2), 2009.

[134] Huanetwork. The naming conventions of huawei ar routers. `http://www.huanetwork.com/blog/the-naming-conventions-of-huawei-ar-routers/`.

[135] B. Huffaker, M. Fomenkov, and k. claffy. DDec (BETA). http://ddec.caida.org/.

[136] B. Huffaker, M. Fomenkov, and k. claffy. DRoP:DNS-based Router Positioning. *ACM SIGCOMM Computer Communication Review*, 44(3), 2014.

[137] G. Huston. Interconnection, peering, and settlements. In *Proc. of the INET*, volume 9, 1999.

[138] Y. Hyun, A. Broido, and k. claffy. Traceroute and BGP AS Path Incongruities. Technical report, CAIDA, Mar 2003.

[139] Internet Routing Registry. Obtaining IRR Data. `ftp://ftp.radb.net/radb/dbase`, 2013.

[140] I. Internet Systems Consortium. Dig Manual Pages. https://ftp.isc.org/isc/bind9/cur/9.9/doc/arm/man.dig.html.

[141] IP2Location. IP2Location DB9, 2015. `http://www.ip2location.com/`, 2015.

[142] T. Isdal, M. Piatek, A. Krishnamurthy, and T. Anderson. Leveraging BitTorrent for end host measurements. In *Proc. of the PAM*. Springer, 2007.

[143] V. Jacobson. Traceroute. see source code: `ftp://ftp.ee.lbl.gov/traceroute.tar.gz`.

[144] R. Jain, D.-M. Chiu, and W. R. Hawe. *A quantitative measure of fairness and discrimination for resource allocation in shared computer system*. Eastern Research Laboratory, Digital Equipment Corporation, 1984.

[145] J. Jiang, C. Wilson, X. Wang, P. Huang, W. Sha, Y. Dai, and B. Y. Zhao. Understanding Latent Interactions in Online Social Networks. In *Proc. of IMC*. ACM SIGCOMM, 2010.

[146] D. Joanes and C. Gill. Comparing measures of sample skewness and kurtosis. *Journal of the Royal Statistical Society: Series D (The Statistician)*, 47(1), 1998.

[147] Juniper Systems, Inc. Interface naming overview. `http://www.juniper.net/techpubs/en_US/junos12.3/topics/concept/interfaces-interface-naming-overview.html`.

[148] S. Kairam, M. Brzozowski, D. Huffaker, and E. Chi. Talking in circles: Selective sharing in google+. In *Proc. of SIGCHI*. ACM, 2012.

[149] R. Kannan, S. Vempala, and A. Vetta. On clusterings: Good, bad and spectral. *Journal of the ACM (JACM)*, 51(3), 2004.

[150] G. Karypis and V. Kumar. METIS - Unstructured Graph Partitioning and Sparse Matrix Ordering System, Version 2.0. 1995.

[151] G. Karypis and V. Kumar. A Fast and High Quality Multilevel Scheme for Partitioning Irregular Graphs. *Journal on Scientific Computing*, 20(1), 1998.

[152] V. Katsenelson. How I Bought the Internet - and You Can Too. `http://www.institutionalinvestor.com/blogarticle/3310914/blog/how-i-bought-the-internetand-you-can-too.html#.VTl6IycVhBc`.

[153] E. Katz-Bassett, H. V. Madhyastha, V. K. Adhikari, C. Scott, J. Sherry, P. Van Wesep, T. E. Anderson, and A. Krishnamurthy. Reverse traceroute. In *NSDI*, volume 10, 2010.

[154] D. Kemp, J. Kleinber, and E. Tardos. Maximizing the spread of influence in a social network. In *Proc. of SIGKDD*, 2003.

[155] T. Kernen. traceroute.org. `http://www.traceroute.org`.

[156] K. Keys. iffinder. `http://www.caida.org/tools/measurement/iffinder/`.

[157] K. Keys, Y. Hyun, M. Luckie, and K. Claffy. Internet-scale IPv4 alias resolution with MIDAR. *IEEE/ACM Transactions on Networking (TON)*, 21(2), 2013.

[158] R. Kindermann, J. L. Snell, et al. *Markov random fields and their applications*, volume 1. American Mathematical Society Providence, RI, 1980.

[159] J. M. Kleinberg, R. Kumar, P. Raghavan, S. Rajagopalan, and A. S. Tomkins. The Web as a graph: measurements, models, and methods. In *Computing and combinatorics*. Springer, 1999.

[160] S. Knight, H. X. Nguyen, N. Falkner, R. Bowden, and M. Roughan. The Internet topology zoo. *Journal on Selected Areas in Communications, IEEE*, 29(9), 2011.

[161] B. Krishnamurthy, W. Willinger, P. Gill, and M. Arlitt. A Socratic method for validation of measurement-based networking research. *Computer Communications*, 34(1), 2011.

[162] R. Kumar, J. Novak, and A. Andtomkins. Structure and evolution of online social networks. In *Proc. of KDD*. ACM, 2006.

[163] H. Kwak, C. Lee, H. Park, and S. Moon. What is Twitter, a Social Network or a News Media? In *Proc. of WWW*. ACM, 2010.

[164] A. Lancichinetti and S. Fortunato. Community detection algorithms: a comparative analysis. *Physical review E*, 80(5), 2009.

[165] A. N. Langville and C. D. Meyer. *Google's PageRank and beyond: The science of search engine rankings*. Princeton University Press, 2011.

[166] S. Lattanzi and D. Sivakumar. Affiliation networks. In *Proc. of STOC*. ACM, 2009.

[167] W. E. Leland, M. S. Taqqu, W. Willinger, and D. V. Wilson. On the self-similar nature of Ethernet traffic. 23(4), 1993.

[168] J. Leskovec, J. Kleinberg, and C. Faloutsos. Graph evolution: Densification and shrinking diameters. *ACM Transactions on Knowledge Discovery from Data (TKDD)*, 1(1), 2007.

[169] J. Leskovec, K. J. Lang, A. Dasgupta, and M. W. Mahoney. Community structure in large networks: Natural cluster sizes and the absence of large well-defined clusters. *Internet Mathematics*, 6(1), 2009.

[170] S. Lloyd. Least squares quantization in pcm. *IEEE transactions on information theory*, (2), 1982.

[171] A. Lodhi, A. Dhamdhere, and C. Dovrolis. Analysis of peering strategy adoption by transit providers in the Internet. In *Proc. of the INFOCOM Workshops*, 2012.

[172] A. Lodhi, A. Dhamdhere, and C. Dovrolis. GENESIS: An agent-based model of interdomain network formation, traffic flow and economics. In *Proc. of the INFOCOM*. IEEE, 2012.

[173] L. Lovász. Random Walks on Graphs: A Survey. *Combinatorics, Paul erdos is eighty*, 2(1), 1993.

[174] D. Lowd and A. Rooshenas. The libra toolkit for probabilistic models. *Journal of Machine Learning Research*, 16, 2015.

[175] M. Luckie, A. Dhamdhere, D. Clark, B. Huffaker, et al. Challenges in Inferring Internet Interdomain Congestion. In *Proc. of IMC*, 2014.

[176] M. Luckie, Y. Hyun, and B. Huffaker. Traceroute Probe Method and Forward IP Path Inference. In *Proc. of IMC*. ACM SIGCOMM, 2008.

[177] H. V. Madhyastha, T. Isdal, M. Piatek, C. Dixon, T. Anderson, A. Krishnamurthy, and A. Venkataramani. iPlane: An information plane for distributed services. In *Proc. of OSDI*. USENIX, 2006.

[178] G. Magno, G. Comarela, D. Saez-Trumper, M. Cha, and V. Almeida. New Kid on the Block: Exploring the Google+ Social Graph. In *Proc. of IMC*. ACM SIGCOMM, 2012.

[179] P. Mahadevan, D. Krioukov, M. Fomenkov, X. Dimitropoulos, A. Vahdat, et al. The Internet AS-level topology: three data sources and one definitive metric. *ACM SIGCOMM Computer Communication Review*, 36(1), 2006.

[180] Z. M. Mao, R. Bush, T. G. Griffin, and M. Roughan. BGP Beacons. In *Proc. of IMC*. ACM SIGCOMM, 2003.

[181] Z. M. Mao, L. Qiu, J. Wang, and Y. Zhang. On AS-level path inference. In *ACM SIGMETRICS Performance Evaluation Review*, volume 33. ACM, 2005.

[182] Z. M. Mao, J. Rexford, J. Wang, and R. H. Katz. Towards an accurate AS-level traceroute tool. In *Proc. of the Conference on Applications, Technologies, Architectures, and Protocols for Computer Communications*. ACM, 2003.

[183] P. Marchetta, V. Persico, E. Katz-Bassett, and A. Pescapé. Dont trust traceroute (completely). In *Proc. of CoNEXT Student workshop*. ACM, 2013.

[184] MaxMind. Free World Cities Database. `https://www.maxmind.com/en/free-world-cities-database`. Accessed: 2015-12-01.

[185] MaxMind-LLC. GeoIP, 2016. `http://www.maxmind.com`, 2016.

[186] M. McPherson, L. Smith-Lovin, and J. M. Cook. Birds of a feather: Homophily in social networks. *Annual review of sociology*, 2001.

[187] P. Mérindol, V. Van den Schrieck, B. Donnet, O. Bonaventure, and J.-J. Pansiot. Quantifying ASes multiconnectivity using multicast information. In *Proc. of IMC*. AC SIGCOMMM, 2009.

[188] C. Metz. Interconnecting ISP networks. *Internet Computing, IEEE*, 5(2), 2001.

[189] D. L. Mills and H.-W. Braun. The NSFNET backbone network. 17(5), 1987.

[190] A. Mislove, H. S. Koppula, K. P. Gummadi, P. Druschel, and B. Bhattacharjee. Growth of the flickr social network. In *Proc. of WOSN*. ACM, 2008.

[191] A. Mislove, M. Marcon, K. P. Gummadi, P. Druschel, and B. Bhattacharjee. Measurement and Analysis of Online Social Networks. In *Proc. of IMC*. ACM, 2007.

[192] G. Moore. The structure of a national elite network. *American Sociological Review*, 1979.

[193] E. Mossel and S. Roch. On the submodularity of influence in social networks. In *Proc. of Symposium on Theory of Computing*. ACM, 2007.

[194] R. Motamedi and R. a. Rejaie. ALFReD – Acquiring Location From Reverse DNS. `atossa.cs.uoregon.edu:8080/alfred/`, 2015.

[195] J. Moy. OSPF version 2. rfc 2328: see online `http://tools.ietf.org/html/rfc2178`, 1997.

[196] W. Mühlbauer, A. Feldmann, O. Maennel, M. Roughan, and S. Uhlig. Building an as-topology model that captures route diversity. *ACM SIGCOMM Computer Communication Review*, 36(4), 2006.

[197] A. Nazir, S. Raza, and C.-N. Chuah. Unveiling facebook: a measurement study of social network based applications. In *Proc. IMC*. ACM, 2008.

[198] T. Nepusz, A. Petróczi, L. Négyessy, and F. Bazsó. Fuzzy communities and the concept of bridgeness in complex networks. *Physical Review E*, 77(1), 2008.

[199] M. Nerenberg, R. Motamedi, and R. Rejaie. Interactive Graph Coarsening by WalkAbout. Code available at: `http://onrg.cs.uoregon.edu/WalkAbout`, University of Oregon, 2014.

[200] M. E. Newman. The structure and function of complex networks. *SIAM review*, 45(2), 2003.

[201] M. E. Newman. Modularity and community structure in networks. *Proc. of NAS*, 103(23), 2006.

[202] R. Oliveira, D. Pei, W. Willinger, B. Zhang, and L. Zhang. The (in)completeness of the observed Internet AS-level structure. *IEEE/ACM Transactions on Networking (ToN)*, 2010.

[203] R. Oliveira, W. Willinger, and B. Zhang. Quantifying the completeness of the observed Internet AS-level structure. Technical report, UCLA, 080026, Sep 2008.

[204] R. V. Oliveira, D. Pei, W. Willinger, B. Zhang, and L. Zhang. In search of the elusive ground truth: the internet's as-level connectivity structure. In *ACM SIGMETRICS Performance Evaluation Review*, volume 36. ACM, 2008.

[205] R. V. Oliveira, B. Zhang, and L. Zhang. Observing the evolution of Internet AS topology. *ACM SIGCOMM Computer Communication Review*, 37(4), 2007.

[206] T. Opsahl, V. Colizza, P. Panzarasa, and J. J. Ramasco. Prominence and control: the weighted rich-club effect. *Physical review letters*, 101(16), 2008.

[207] L. Page, S. Brin, R. Motwani, and T. Winograd. The PageRank citation ranking: bringing order to the Web. 1999.

[208] J.-J. Pansiot and D. Grad. On routes and multicast trees in the Internet. *ACM SIGCOMM Computer Communication Review*, 28(1), 1998.

[209] J.-J. Pansiot, P. Mérindol, B. Donnet, and O. Bonaventure. Extracting intra-domain topology from mrinfo probing. In *Proc. of PAM*. Springer, 2010.

[210] V. Paxson and S. Floyd. Wide area traffic: the failure of Poisson modeling. *IEEE/ACM Transactions on Networking (ToN)*, 3(3), 1995.

[211] PeeringDB. Exchange Points List. `https://www.peeringdb.com/private/participant_list.php`, 2013.

[212] I. Poese, S. Uhlig, M. A. Kaafar, B. Donnet, and B. Gueye. IP geolocation databases: unreliable? *ACM SIGCOMM Computer Communication Review*, 41(2), 2011.

[213] P. Pons and M. Latapy. Computing communities in large networks using random walks. *Journal of Graph Algorithms and Applications*, 10(2), 2006.

[214] A. H. Rasti, N. Magharei, R. Rejaie, and W. Willinger. Eyeball ASes: from geography to connectivity. In *Proc. of IMC*. ACM SIGCOMM, 2010.

[215] A. H. Rasti, M. Torkjazi, R. Rejaie, N. Duffield, W. Willinger, and D. Stutzbach. Respondent-driven sampling for characterizing unstructured overlays. In *Proc. of the INFOCOM*. IEEE, 2009.

[216] G. Ravid and E. Currid-Halkett. The social structure of celebrity: an empirical network analysis of an elite population. *Celebrity Studies*, 4(2), 2013.

[217] R. Rejaie, M. Torkjazi, M. Valafar, and W. Willinger. Sizing Up Online Social Networks. *IEEE Network*, 2010.

[218] M. Richardson and P. Domingos. Mining knowledge-sharing sites for viral marketing. In *Proc. of SIGKDD*. ACM, 2002.

[219] N. RIPE. Routing registry consistency check reports. *http://www.ripe.net/projects/rrcc*, 2009.

[220] Y. Rochat. Closeness centrality extended to unconnected graphs: The harmonic centrality index. In *ASNA*, number EPFL-CONF-200525, 2009.

[221] E. M. Rogers. *Diffusion of innovations*. Simon and Schuster, 2010.

[222] M. Rosvall and C. Bergstrom. Maps of information flow reveal community structure in complex networks. In *Proc. of the NAS*. Citeseer, National Academy of Sciences, 2007.

[223] M. Roughan, W. Willinger, O. Maennel, D. Perouli, and R. Bush. 10 Lessons from 10 Years of Measuring and Modeling the Internets Autonomous Systems. *Selected Areas in Communications*, 2011.

[224] M. A. Sánchez, J. S. Otto, Z. S. Bischof, D. R. Choffnes, F. E. Bustamante, B. Krishnamurthy, and W. Willinger. Dasu: Pushing experiments to the Internet's edge. In *Proc. of NSDI*. USENIX, 2013.

[225] V. Satuluri and S. Parthasarathy. Scalable graph clustering using stochastic flows: applications to community discovery. In *Proc. of KDD*. ACM, 2009.

[226] S. Savage. Sting: A TCP-based Network Measurement Tool. In *Proc. of USITS*, volume 2. USENIX, 1999.

[227] D. Schiöberg, F. Schneider, H. Schiöberg, S. Schmid, S. Uhlig, and A. Feldmann. Tracing the birth of an osn: Social graph and profile analysis in google+. In *ACM WebSci*, 2012.

[228] F. Schneider, A. Feldmann, B. Krishnamurthy, and W. Willinger. Understanding online social network usage from a network perspective. In *Proc. of IMC*. ACM SIGCOMM, 2009.

[229] M. Seifi, I. Junier, J.-B. Rouquier, S. Iskrov, and J.-L. Guillaume. Stable community cores in complex networks. In *Complex Networks*. Springer, 2013.

[230] N. K. Sharma, S. Ghosh, F. Benevenuto, N. Ganguly, and K. Gummadi. Inferring who-is-who in the twitter social network. *ACM SIGCOMM Computer Communication Review*, 42(4), 2012.

[231] Y. Shavitt and E. Shir. DIMES: Let the Internet measure itself. *ACM SIGCOMM Computer Communication Review*, 35(5), 2005.

[232] Y. Shavitt and U. Weinsberg. Quantifying the importance of vantage points distribution in Internet topology measurements. In *INFOCOM, IEEE*. IEEE, 2009.

[233] Y. Shavitt and N. Zilberman. A structural approach for PoP geo-location. In *Proc. of the INFOCOM*. IEEE, 2010.

[234] Y. Shavitt and N. Zilberman. A geolocation databases study. *Journal on Selected Areas in Communications, IEEE*, 29(10), 2011.

[235] R. Sherwood, A. Bender, and N. Spring. Discarte: a disjunctive Internet cartographer. 38(4), 2008.

[236] R. Sherwood and N. Spring. Touring the Internet in a TCP sidecar. In *Proc. of IMC*. ACM SIGCOMM, 2006.

[237] R. Siamwalla, R. Sharma, and S. Keshav. Discovering Internet Topology. *Unpublished manuscript*, 1998.

[238] A. Singla, B. Chandrasekaran, P. Godfrey, and B. Maggs. The internet at the speed of light. In *Proc. of Hot Topics in Networks*. ACM, 2014.

[239] S. Siwpersad, B. Gueye, and S. Uhlig. Assessing the geographic resolution of exhaustive tabulation for geolocating internet hosts. In *Proc. of PAM*. Springer, 2008.

[240] S. Sobolevsky, R. Campari, A. Belyi, and C. Ratti. General optimization technique for high-quality community detection in complex networks. *Physical Review E*, 90(1), 2014.

[241] M. Solutions. A Proper Server Naming Scheme. `https://www.mnxsolutions.com/devops/a-proper-server-naming-scheme.html`. Accessed: 2014-09-05.

[242] J. Sommers, P. Barford, and B. Eriksson. On the prevalence and characteristics of MPLS deployments in the open Internet. In *Proc. of IMC*. ACM SIGCOMM, 2011.

[243] N. Spring, M. Dontcheva, M. Rodrig, and D. Wetherall. How to resolve IP aliases. Technical report, Univ. Michigan, UW CSE Tech. Rep, 2004.

[244] N. Spring, R. Mahajan, and D. Wetherall. Measuring isp topologies with rocketfuel. *ACM SIGCOMM Computer Communication Review*, 32(4), 2002.

[245] N. T. Spring, D. Wetherall, and T. E. Anderson. Scriptroute: A Public Internet Measurement Facility. In *Proc. of USITS*. USENIX, 2003.

[246] R. A. Steenbergen. A practical guide to (correctly) troubleshooting with traceroute. *North American Network Operators Group*, 2009.

[247] D. Strang and S. A. Soule. Diffusion in organizations and social movements: From hybrid corn to poison pills. *Annual review of sociology*, 1998.

[248] D. Stutzbach, R. Rejaie, N. Duffield, S. Sen, and W. Willinger. On unbiased sampling for unstructured peer-to-peer networks. *IEEE/ACM Transactions on Networking (TON)*, 17(2), 2009.

[249] D. Stutzbach, R. Rejaie, and S. Sen. Characterizing Unstructured Overlay Topologies in Modern P2P File-Sharing Systems. *IEEE/ACM Transactions on Networking (ToN)*, 16(2), 2008.

[250] Team Cymru. IP to ASN Mapping. `https://www.team-cymru.org/IP-ASN-mapping.html`.

[251] Telegeography. Colocation cross connect prices vary greatly between US, Europe. `https://www.telegeography.com/products/commsupdate/articles/2014/07/15/colocation-cross-connect-prices-vary-greatly-between-us-europe/`.

[252] Y. Tian, R. Dey, Y. Liu, and K. W. Ross. China's Internet: Topology mapping and geolocating. In *Proc. of INFOCOM*. IEEE, 2012.

[253] M. C. Toren. tcptraceroute: an implementation of traceroute using TCP SYN packets. man page, 2001, see source code: `http://michael.toren.net/code/tcptraceroute/`.

[254] M. Torkjazi, R. Rejaie, and W. Willinger. Hot today, gone tomorrow: on the migration of myspace users. In *Proc. of WOSN*. ACM, 2009.

[255] M. Tozal and K. Sarac. Tracenet: an Internet topology data collector. In *Proc. of IMC*. ACM SIGCOMM, 2010.

[256] M. E. Tozal and K. Sarac. Subnet level network topology mapping. In *Proc. of the IPCCC*. IEEE, 2011.

[257] J. Ugander, B. Karrer, L. Backstrom, and C. Marlow. The Anatomy of the Facebook Social Graph. *CoRR*, abs/1111.4503, 2011.

[258] M. Valafar, R. Rejaie, and W. Willinger. Beyond friendship graphs: a study of user interactions in flickr. In *Proc. of WOSN*. ACM, 2009.

[259] S. Van Dongen. A cluster algorithm for graphs. *Report-Information systems*, (10), 2000.

[260] S. M. Van Dongen. Graph clustering by flow simulation. 2001.

[261] F. Viégas, M. Wattenberg, J. Hebert, G. Borggaard, A. Cichowlas, J. Feinberg, J. Orwant, and C. Wren. Google+ ripples: a native visualization of information flow. In *Proc. of WWW*. ACM, 2013.

[262] B. Viswanath, M. A. Bashir, M. B. Zafar, S. Bouget, S. Guha, K. P. Gummadi, A. Kate, and A. Mislove. Strength in numbers: Robust tamper detection in crowd computations. In *Proc. of COSN*. ACM, 2015.

[263] B. Viswanath, A. Post, K. P. Gummadi, and A. Mislove. An Analysis of Social Network-Based Sybil Defenses. *ACM SIGCOMM Computer Communication Review*, 41(4), 2011.

[264] F. Wang and L. Gao. On inferring and characterizing Internet routing policies. In *Proc. of IMC*. ACM SIGCOMM, 2003.

[265] S. Wasserman and J. Galaskiewicz. *Advances in social network analysis: Research in the social and behavioral sciences*, volume 171. Sage Publications, 1994.

[266] D. J. Watts and S. H. Strogatz. Collective Dynamics of 'Small-World' Networks. *nature*, 393(6684), 1998.

[267] M. J. Welch, U. Schonfeld, D. He, and J. Cho. Topical semantics of twitter links. In *Proc. of the Conference on Web Seach and Data Mining (WSDM)*. ACM, 2011.

[268] S. White and P. Smyth. A Spectral Clustering Approach To Finding Communities in Graph. In *Proc. of SDM*, volume 5. SIAM, 2005.

[269] W. Willinger, D. Alderson, and J. C. Doyle. *Mathematics and the internet: A source of enormous confusion and great potential*. Defense Technical Information Center, 2009.

[270] W. Willinger, R. Rejaie, M. Torkjazi, M. Valafar, and M. Maggioni. Research on online social networks: time to face the real challenges. *Performance Evaluation Review*, 37(3), 2010.

[271] W. Willinger and M. Roughan. Internet Topology Research Redux. *ACM SIGCOMM eBook: Recent Advances in Networking*, 2013.

[272] S. Wu, J. M. Hofman, W. A. Mason, and D. J. Watts. Who says what to whom on twitter. In *Proc. of WWW*. ACM, 2011.

[273] J. Xia and L. Gao. On the evaluation of AS relationship inferences [Internet reachability/traffic flow applications]. In *Proc. of the GLOBECOM*, volume 3. IEEE, 2004.

[274] K. Xu, Z. Duan, Z.-L. Zhang, and J. Chandrashekar. On Properties of Internet Exchange Points and Their Impact on AS Topology and Relationship. In *Proc. of the ICRCICN*, volume 3042 of *LNCS*. 2004.

[275] Z. Xu, Y. Zhang, Y. Wu, and Q. Yang. Modeling user posting behavior on social media. In *ACM SIGIR*, 2012.

[276] J. Yang and J. Leskovec. Overlapping community detection at scale: a nonnegative matrix factorization approach. In *Proc. of WSDM*. ACM, 2013.

[277] B. Yao, R. Viswanathan, F. Chang, and D. Waddington. Topology inference in the presence of anonymous routers. In *In IEEE INFOCOM*, 2003.

[278] J. S. Yedidia, W. T. Freeman, and Y. Weiss. Understanding belief propagation and its generalizations. *Exploring artificial intelligence in the new millennium*, 8, 2003.

[279] K. Yoshida, Y. Kikuchi, M. Yamamoto, Y. Fujii, K. Nagami, I. Nakagawa, and H. Esaki. Inferring PoP-level ISP topology through end-to-end delay measurement. In *Proc. of the PAM*. Springer, 2009.

[280] B. Zhang, R. Liu, D. Massey, and L. Zhang. Collecting the Internet AS-level topology. *ACM SIGCOMM Computer Communication Review*, 35(1), 2005.

[281] M. Zhang, Y. Ruan, V. S. Pai, and J. Rexford. How DNS Misnaming Distorts Internet Topology Mapping. In *Proc. of the USENIX ATC, General Track*. USENIX, 2006.

[282] Y. Zhang, R. Oliveira, Y. Wang, S. Su, B. Zhang, J. Bi, H. Zhang, and L. Zhang. A framework to quantify the pitfalls of using traceroute in AS-level topology measurement. *Journal on Selected Areas in Communications, IEEE*, 29(9), 2011.

[283] Y. Zhang, H.-L. Zhang, and B.-X. Fang. A survey on Internet topology modeling. *Journal of Software*, 15(8), 2004.

[284] X. Zhao, A. Sala, C. Wilson, X. Wang, S. Gaito, H. Zheng, and B. Zhao. Multi-scale dynamics in a massive online social network. In *Proc. of IMC*. ACM SIGCOMM, 2012.

[285] S. Zhou and R. J. Mondragón. Accurately modeling the Internet topology. *Physical Review E*, 70(6), 2004.